UNIVERSITAT DE BARCELONA

Role of HDAC11 in muscle cell differentiation and regeneration

Paper de HDAC11 en la diferenciació i regeneració musculars

Yaiza Núñez Álvarez

UNIVERSITAT DE BARCELONA

FACULTAT DE FARMÀCIA I CIÈNCIES DE L'ALIMENTACIÓ

TESI DOCTORAL

Role of HDAC11 in muscle cell differentiation and regeneration

Paper de HDAC11 en la diferenciació i regeneració musculars

YAIZA NÚÑEZ ÁLVAREZ

BARCELONA, JUNY 2017

Programa de Doctorat en Biomedicina, Facultat de Farmàcia i Ciències de l'Alimentació.

Role of HDAC11 in muscle cell differentiation and regeneration

Paper de HDAC11 en la diferenciació i regeneració musculars

Memòria presentada per

Yaiza Núñez Álvarez

Per optar al títol de

Doctora per la Universitat de Barcelona

Tesi realitzada al Programa de Medicina Predictiva i Personalitzada del Càncer (PMPPC) a l'Institut de Recerca Germans Trias i Pujol (IGTP),

sota la direcció de

La Dra. **Mònica Suelves Esteban** i el Dr. **Miguel Á. Peinado Morales**

Dra. Mònica Suelves Esteban Dr. Miguel Á. Peinado Morales

Dra. Mònica Suelves Esteban (Tutora) Yaiza Núñez Álvarez (Doctoranda)

Barcelona, Juny de 2017.

If we knew what it was we were doing,
it would not be called research,
would it?

(Attributed to Albert Einstein)

ABSTRACT

HDAC11 is the newest member of the histone deacetylase (HDAC) family and one of the less studied. Its expression was described to be enriched in skeletal muscle tissues from the first moment of its discovery, yet now after 15 years, its roles in myogenesis remain unknown. We started this thesis by analyzing the expression changes of all HDAC's' members between proliferation and early differentiation conditions, which constitutes a crucial cell fate point in which cells have to decide whether to continue proliferating or enter to irreversible G0 arrest state to differentiate. With this analysis, we found HDAC11 as the HDAC family member the most upregulated in the skeletal muscle differentiation process. By CRISPR/Cas9 knock-in tagging of endogenous HDAC11, we show that HDAC11 protein levels are absent in proliferating cells and increased through differentiation. The silencing of HDAC11 in proliferation conditions is mediated, at least in part, by class I HDAC's deacetylation of MYOD. In differentiation conditions, acetylated MYOD and myogenin, the two master regulators of muscle differentiation, bind to HDAC11 promoter regions and trigger its expression.

HDAC11 deficient myoblasts did not present major alterations in cell proliferation or differentiation capacities but show reduced fusion ability. Genome-wide transcriptomic analysis of differentiating HDAC11 deficient myoblasts revealed an upregulation of genes involved in proliferation and a decreased expression of genes involved in muscle contraction, suggesting a delayed entry in G0 irreversible arrest state. Our ChIP results suggest that HDAC11 would mediate repression of proliferation related genes by deacetylation of H3 in their promoter regions. Moreover, HDAC11 expression is also highly expressed in additional G0 states, like in reversible arrested quiescent satellite cells.

In skeletal muscle tissues, HDAC11 is higher expressed in fast muscles than slow ones, especially in males. The analysis of HDAC11 deficient mice concludes that HDAC11 absence do not cause major alterations in muscle development, adult myofiber growth or fiber type composition in basal conditions. In regeneration conditions, HDAC11 deficient mice show advanced regeneration capacity at 7 days post injury, probably mediated at least in part, by an increased expression of Il-10 by HDAC11 deficient macrophages.

Finally, we show that HDAC11 upregulation through differentiation is conserved in human myoblast and its expression is reduced in rhabdomyosarcoma cells, which present impaired differentiation capabilities.

Altogether, our results place HDAC11 as a new epigenetic regulator in *in vitro* an *in vivo* myogenesis.

RESUM

HDAC11 és el membre més recentment descobert de la família de deacetilases d'histones (HDAC) i un dels menys estudiats. En el moment del seu descobriment es va veure que estava altament expressada en teixits de múscul esquelètic encara que després de 15 anys, les seves funcions en la miogènesi resten encara desconegudes.

Vam començar aquesta tesi analitzant els canvis d'expressió de tots els membres de la família HDAC entre les condicions de proliferació i diferenciació primerenca, un moment crucial on les cèl·lules han de decidir si continuen dividint-se o entren en l'estat d'aturada irreversible G0 per diferenciar-se. Amb aquesta anàlisi vam trobar HDAC11 com el membre de la família HDAC que augmentava més la seva expressió en aquest procés. Amb la tècnica d'enginyeria genètica CRISPR/Cas9 vam aconseguir inserir un epítop en el locus genòmic de HDAC11, que ens permeté demostrar que la proteïna HDAC11 està absent en condicions de proliferació i augmenta amb la diferenciació. El silenciament de l'expressió de HDAC11 durant la proliferació està mitjançada, almenys en part, per la deacetilació de MYOD per part de la classe I de HDACs. Durant la diferenciació, MYOD acetilat i miogenina, els dos reguladors responsables d'iniciar la diferenciació muscular, s'uneixen al promotor de HDAC11 i activen la seva expressió.

Els mioblasts deficients en HDAC11 no presenten greus alteracions en la proliferació cel·lular o en la seva capacitat de diferenciar-se però mostren una reduïda capacitat de fusió. L'estudi transcriptòmic a escala global de mioblasts deficients en HDAC11 va revelar una sobreexpressió de gens involucrats en la proliferació cel·lular i una reducció en l'expressió de gens amb funcions en la contracció muscular, suggerint una entrada més tardana en la fase G0 d'aturada irreversible. Els nostres resultats de ChIP suggereixen que HDAC11 podria intervindre en la repressió dels gens involucrats en la proliferació cel·lular mitjançant la deacetilació de les histones H3 dels seus promotors. A més, l'expressió d'HDAC11 també és alta en estats addicionals de G0 com l'arrest reversible de les cèl·lules satèl·lit quiescents.

En teixits de múscul esquelètic, HDAC11 està més expressada en músculs ràpids que lents, especialment en mascles. L'anàlisi de ratolins deficients en HDAC11 conclogué que l'absència de HDAC11 no causa greus alteracions en el desenvolupament muscular, el creixement de miofibres adultes o en la composició en tipus de fibres en condicions basals. Durant la regeneració muscular, els ratolins deficients en HDAC11 mostren un avanç en la seva capacitat de regeneració 7 dies després de la lesió, probablement mitjançat en part per un increment en l'expressió de Il-10 per part dels macròfags deficients en HDAC11.

Finalment, mostrem que l'augment d'expressió de HDAC11 està conservat en la diferenciació de mioblasts humans i que la seva expressió està reduïda en rabdomiosarcoma, patologia tumoral que presenta un impediment en la diferenciació muscular. En conjunt, els nostres resultats situen HDAC11 com un nou regulador epigenètic en la miogènesi *in vitro* i *in vivo*.

ACKNOWLEDGEMENTS

Quiero agradecer a mis jefes, el Dr. Miguel Ángel Peinado y la Dra. Mònica Suelves por haberme brindado la oportunidad de hacer el doctorado en su grupo. Gràcies als dos per haber tingut la porta sempre oberta per parlar, per apreciar les meves opinions i per la independència que m'han donat.

A la Dra. Pura Muñoz Cànoves y todo su laboratorio, especialmente a Vanesa, Susana, Laura, por toda la ayuda, reactivos y protocolos, y especialmente a Mercè, por enseñarme todo lo que sé sobre ratones, por toda tu paciencia y demostrarme que el trabajar con animales no está reñido con el respeto hacia ellos.

A todos los miembros del laboratorio del Dr. Alberto Pendás por acogerme tan calurosamente en Salamanca. A Laura, Natalia y especialmente a Alberto Tuñón por su impagable ayuda con los ratones.

Al servicio de genómica del PMPPC por su eficiencia y velocidad en hacer librerías y especialmente al Dr, Gabriel Rech por su implicación, rapidez con el análisis del RNA seq y por sus explicaciones para *dummies*.

Al servicio de citometria del IGTP, Marco y Gerard, por toda su ayuda y consejos con el FACS.

Al Dr. Eduard Gallardo, el Dr. Óscar Martínez Tirado, la Dra. Roser López, a la Dra. Miriam Ejarque y al Dr. Charles Keller, por haberme permitido colaborar con ellos y hacerme partícipe de sus trabajos.

A l'Agència de Gestió d'Ajuts Unversitaris i de Recerca (AGAUR) y al Ministerio de Educación, Cultura y Deporte de España, por proporcionarme la financiación necesaria para realizar esta tesis (FPU12/05668).

Recuerdo un seminario durante el máster en la UPF sobre el doctorado. Esperaba un compendio de consejos sobre cómo afrontar y sobrevivir a la tesis, tales como que hay que hacer cursos de bioinformática, hacer muchos back-ups, etc. Sin embargo, cuán grande fue mi sorpresa cuando el doctorando a punto de acabar centró la charla en la idea de no dejar a los amigos de lado aunque sea extremadamente fácil por el poco tiempo libre del que dispondríamos. Que nos sería mucho más útil, decía, un amigo y un café al lado para poder

seguir adelante que unos resultados asombrosos. Hoy, he de reconocer que he entendido el porqué de ese seminario.

He tenido la gran suerte de encontrar en nuestro "instituto del amor", no sólo muchos compañeros de trabajo, sino grandes personas, las cuales han hecho que en muchas ocasiones, hasta se me olvidara que estaba en el trabajo y no entre amigos.

En primer lugar, tengo que agradecer a Mar Muñoz, la incansable y ejemplar técnica de nuestro grupo. Gracias por tu entrega y pasión por tu trabajo. Por estar a las buenas y sobre todo a las malas. Por comprender a los estudiantes y por darnos siempre apoyo. Por enseñarme y por aconsejarme. Por emocionarte aún con los proyectos, ideas y experimentos, por no querer abandonar cuando no salen y buscar siempre mil y una alternativas. Por defender tus opiniones. Por no amilanarte nunca ante las montañas de trabajo. Por tu eficiencia y tu multitasking. Por escucharme siempre y, sobre todo, por contagiarme cada día con tu humor, tu pasión y tus ganas. Por hacer no solo fácil trabajar contigo, sino un placer. Todo lo que pueda enumerar aquí se quedaría corto para agradecer todo lo que has hecho por mí estos años, así que, sinceramente, gracias por toda la ayuda en el trabajo y en lo personal, por convertirte en una amiga además de una compañera.

Al Dr. Joaquin Custodio, por intentar siempre levantarme el ánimo con tus bromas ante las dificultades. Por ayudarme en los momentos de ausencia de proyecto, por tus discusiones científicas, por interesarte siempre por los demás. Por tus ideas innovadoras y tu forma de buscarte la vida, incansablemente proponiendo y formándote en técnicas nuevas. Gracias por ser para mí el ejemplo de cómo ser un buen doctorando.

Y los demás miembros del Peinado lab, Izaskun, Berta, y a los antiguos miembros, Raquel, Víctor, Mireia, Marta, Sergi, Anna Díez, Llorenç, mi expikachu Ruth y Dèlia. Gràcies sobretot a la Dra. Carrió per enseñar-me l'art de cultivar C2C12 i haver-me agafat de la mà en els primers passos d'aquesta etapa.

A Emili Cid, el postdoc que nunca tuve. Sin tu ayuda en clonajes, anticuerpos y proteínas creo que nunca habría hecho nada. Gracias por estar ahí siempre dispuesto a aconsejar, por transmitirme tantos y tantos conocimientos, por aguantar siempre mis dramas de todo tipo y por todas las risas y todos esos memorables ratos discotequeros en cultivos.

Thank you Miyako and Fumi for your support and the happiness you always irradiate.

Al Marcus lab, mi lab adoptivo y compañeros a la hora de comer. Gracias a todos los marcusitos: Vane, Sarah, Mélanija, Catherine, Anna, David, Julien e Iva; por toda la ayuda, plásmidos, reactivos, protocolos etc. infinitos, de estos años. A Vane, mi "mami" del centro. A Mél, por nuestras charlas sobre las C2C12 que no se diferenciaban. A Julien, por todas tus

bromas y por los mil viajes de coche. À Catherine, pour l'immense patience à m'écouter quand j'éssayais pour les exposées orals et pour tous nos caffes de filles. À Sarah, pour toutes ses blagues et son énorme support. A la Dra. Palau, por haber compartido con ella carrera, máster y doctorado, anécdotas, buenos y malos tiempos, y pese a eso continuar siempre tan mona conmigo. A Marcus, por sus consejos y discusiones científicas en un barco en el Senna y por demostrarme que el doctorado no es tan difícil como bajar una pared vertical de 15 m.
A Roberto. Mucho ha llovido y muchos volcanes hemos atravesado (literal y figuradamente incluyendo plots) desde aquel día que te expliqué mi proyecto dibujándolo en una servilleta de un bar. Gracias por los continuos consejos, por toda tu ayuda, el inmenso apoyo y el infinito troubleshooting bioinformático, sin nombrar todos los viajes terapéuticos a Canarias. Seguramente sin tus consejos, tus ánimos, llamadas y ayuda todo esto habría sido estadística significativamente mucho más difícil.
Al Maica lab (Anna, Sara, Pep, Érica, Jorge, y Jessica), gracias por vuestra alegría, por vuestras bromas, los vermuts y las risas frente a los problemas. A Jessica especialmente, por todas nuestras excursiones al "inserso" y por tus clases de ondas y disociación.
Al Serra lab: Edu, Meri, Carles, José Marcos, Inma (la técnica más sexy del universo), a Ernest, por nuestras charlas políticas en las comidas y sobre otras muchos temas. A Bernat, junto con Raquel, Anna y Roberto, por compartir aquellos inolvidables viajes a Lanzarote y Río Tinto y tantos Moogs.
A Gabrijela y Josep por su apoyo y amistad en los últimos momentos, por enseñarme que Badalona no es tan mala, por todas nuestras noches en el IMPPC y por su compañía en la oscuridad hacia el autobús de Mordor. Y no menos en lo profesional, por vuestros consejos, por compartir malos y buenos resultados y especialmente a Josep, por enseñarme la luz del FACS cuando el BrdU se negaba a funcionar.
A la Dra. Lightning por su frescura, su alegría, su amistad, su buen rollismo, su actitud ante la vida, sus helados y su casa en Canarias.
A Bárbara, por habernos hecho tan fácil la vida en el centro mientras teníamos el placer de contar con su presencia.
A los habitantes detrás de la puerta negra de Barad-dûr, los eficientes Jessica y Juan, al milagro de los móviles Adrià y a Jose Ponce, por haberme desbloqueado la contraseña una docena de veces, por tus bromas y por junto con el Corujo, el Couso y Roberto, las largas partidas y "el horror".
A Milagros, por ser tan especial y darme tanto cariño en el principio de los tiempos. A Irina, por su alegría al abrir la puerta del centro todos los fines de semana. A Oliver, por saludar

todas las mañanas con una sonrisa. A Antonia y Carol por sus charlas y la alegría que transmiten.
Als rutis, per donar-li sentit a la paraula "Campus", per les cerves…, dic, voley platja. A la dolça Irma, per ser com és; a les IGTPeias més mones, l'Anna Oliveira i la Iris, a la Marta i al Raül.
A los ratoncitos wild-type y knock-out de HDAC11.

Fuera del trabajo, también hay gente que me ha dado su apoyo incondicional, y con más mérito aún si cabe, por no entender muchas veces ni qué era una tesis, pero no por ello interesarse menos, así como por sacarme de casa en los malos y buenos momentos y por compartir sus sonrisas.
En primer lugar tengo que agradecer a mis dos compañeras de piso, Ana y Noela, por hacer de nuestras casas un hogar y una familia en Barcelona y por hacerme olvidar con su compañía, las vicisitudes del lab cada vez que entraba en casa.
Mi Ana, la Dra. Ana Gallego. Gracias por tantas llamadas, por tu apoyo, tus numerosos consejos, por ser un ejemplo a seguir, por tu multitasking, por nuestras cenas científicas, por nuestros increíbles 3 años de convivencia sin ninguna pelea, por aguantarme por las mañanas, por las fiestas y sobretodo, por haber estado siempre, siempre y siempre ahí. Al Jordi, pel seu suport (Nunca olvidaré la bronca que me echaste en Gracia: ¿pero cuándo narices vas a acabar este doctorado?), totes les festes (un cumpleaños con un donut del paki) i les que queden.
A Noela por todo el apoyo en los extenuantes momentos de escritura.
A Sergi Aldomà, por tragarte todos y cada uno de los rollos de mi tesis, por estar siempre ahí y ser un amigo incondicional como no hay muchos. Y por actitud ante la vida: "¡Vívelo!".
A muchos ex compañeros de laboratorio que me enseñaron lo divertido y agradable que puede ser trabajar, me dieron las ganas necesarias para emprender esta aventura, y han seguido allí después del tiempo aunque estén lejos, sobretodo, mis compis de fisio vegetal: Jean, Joan, Nati, Jann, Dulce, Rafa, Carla y Lily.
A las trinis, Belén, Ana, Laura y Mercedes, por nuestras comidas y sentadas pasilliles a través de los tiempos.
A mi madre, por haberme apoyado a venir a Barcelona y querer siempre que estudiásemos y diésemos lo mejor de nosotras y a Noelia.
A Cristina y Dani, pese a que Lleida "está muy lejos", mantener nuestra amistad como cuando estábamos en el instituto.

TABLE OF CONTENTS

LIST OF FIGURES

LIST OF TABLES

ABBREVIATIONS

aRMS: Alveolar rhabdomyosarcoma

bp: base pairs

BSA: Bovine serum albumin

Cas9: CRIPR associated protein 9

cDNA: complementary DNA

CN: central-nucleated

CpGi: CpG island

CRISPR: Clustered, regularly interspaced, short, palindromic repeats

CSA: cross-sectional area

CTX: cardiotoxin

D1, D2, D3: in C2C12 and MPC cultures, days of differentiation (1, 2 or 3)

DAPI: 4',6-diamino-2-phenylindole

DM: differentiation medium

DMD: Duchenne muscular dystrophy

DNA: deoxyribonucleic acid

DSB: Double-strand break

dpi: days post injury

DYSF: dysferlin

GM: growth medium

E1, E2, E3: In schematized gene representations, exon 1, 2 and so on.

ECM: Extracellular matrix

EDL: Extensor digitorum longus muscle

EDTA: ethylenediaminetetraacetic acid

EdU: 5'-ethynyl-2'-deoxyuridine

eRMS: Embryonal rhabdomyosarcoma

ESC: embryonic stem cell

F: forward oligonucleotide

FBS: Fetal bovine serum

FACS: Fluorescence-activated cell sorting

GC: gastrocnemius muscle

GFP: green fluorescent protein

HA: hemagglutinin epitope

HDAC: Histone deacetylase (common name, more appropriate called lysine deacetylase, KDAC)

FOXO1: Forkhead box protein O1 (traditionally known as FKHR)

H3ac: acetylation of histone H3 residues

HDR: Homology-directed repair

hpi: hours post injury

Il-10: Interleukin 10

IP: immunoprecipitation

kDa: kilodalton

KI: knock-in

KO: knock-out
LPS: lipopolysaccharide
M1: macrophages type 1, classically activated (pro-inflammatory)
M2: macrophages type 2, alternatively activated (anti-inflammatory)
MCK: muscle creatine kinase
mdx: C57BL mice model of DMD
MEF: Mouse embryonic fibroblast
MPC: muscle precursor cells
MRF: myogenic regulatory factor
MRF4: muscle-specific regulatory factor 4 (also known as Myf6)
MYF5: myogenic factor 5
MYOD: Myoblast determination protein
MYOG: myogenin
nt: nucleotide
o/n: overnight
OCT: Optimal cutting medium compound
P: proliferation
PAM: In type II CRISPR, 5'-NGG nucleotide sequence
Pan-HDACi: Non-specific, broad classes of histone deacetylases inhibitors
PAX3: Paired box protein 3
PAX7: Paired box protein 7
PBS: phosphate buffered saline
R: reverse oligonucleotide
rcf: relative centrifugal force
RT: room temperature
RMS: Rhabdomyosarcoma
SAHA: Suberoylanilide hydroxamic acid (Vorinostat)
SC: Satellite cell
SEM: Standard error of the mean
shRNA: Short-hairpin RNA
sgRNA: single guide RNA
sol: soleus muscle
ssODN: single-stranded oligo DNA nucleotide
TB: tibialis muscle
TF: transcription factor
TSA: Trichostatin A
TSS: Transcription start site
VPA: Valproic acid (Trapoxin)
v/v: volume/volume
WT: Wild-type
w/v: weight/volume

INTRODUCTION

1. The skeletal muscle

Skeletal muscle is the most abundant tissue of human lean mass and accounts approximately for the 40% of total body weight (Frontera & Ochala 2015). The human body has more than 600 muscles, which are mainly composed by terminally differentiated multinucleated cells named myofibers (Almada & Wagers 2016). Due to this particular morphology, specific names were created for their subcellular parts: sarcoplasm for the cytoplasm and sarcolemma for the myofiber membrane (Cooper 2000). Myofibers are disposed in parallel and surrounded by different layers of connective tissue, which attach the ensemble of myofibers through tendons to bones or another muscles (Gillies & Lieber 2012). The principal characteristics of the muscle structure are schematized in Figure 1.

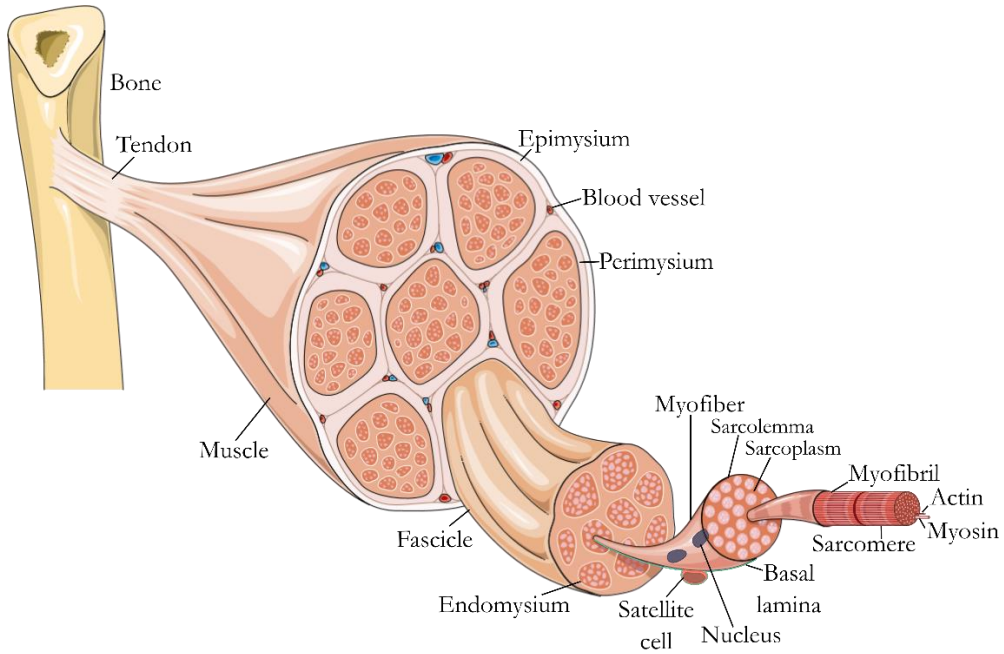

Figure 1. Structure and main parts of skeletal muscle. Adapted from (Servier 2017).

The specific and vital functions of skeletal muscle include breathing, execution of volunteer movements and locomotion, maintenance of tonus and posture, support for soft tissues, mastication and voluntary control of sphincters. It also helps to the maintenance of body temperature and serves as a reserve for nutrients in case of starvation. Recently, it has also been described an additional role of muscle in metabolism regulation through the secretion of muscle hormones and cytokines, the so called myokines (Schnyder & Handschin 2015).

Despite its appearance of quiescent tissue, skeletal muscle is a very active and plastic organ, which responds with changes in size and composition upon systemic stimuli (Matsakas & Patel 2009). Processes that stimulate muscle growth include contractile activity (endurance exercise and electrical stimulation), loading conditions like resistance training, the use of anabolic steroids, traumas and the endogenous levels of hormones like testosterone and thyroid hormones. Also pathological processes can induce muscle growth, like degenerative muscle diseases and rhabdomyosarcoma, a cancer type of cell muscle origin. On the contrary, conditions that result in muscle loss involve not only muscle pathologies like dystrophies, but systemic affectations like starvation, sepsis, diabetes, or renal failure; and its derived conditions, like bed resting or cachexia associated to cancer. Also the use of catabolic steroids, microgravity, and even natural processes like sedentarism and sarcopenia, the muscle wasting associated to aging, result in muscle weight loss (Braun & Gautel 2011; Zanou & Gailly 2013; Saclier et al. 2013).

There are two mainly mechanisms of response to these diverse endogenous and exogenous inputs. One, involves changes in muscle mass (named hypertrophy if increasing or atrophy if decreasing) and fiber type switch of terminally differentiated myofibers, the specialized cells of skeletal muscle (Ciciliot & Schiaffino 2010). The other, involves *de novo* incorporation of nuclei to the formed myofibers. In normal conditions, the number of nuclei of skeletal muscle is stable, and nuclei replacement occurs in a very low frequency (about 1-2% of nuclei per week). Therefore, the plasticity to adaptation changes to physiological stimuli are carry out principally through hypertrophia and atrophia mechanisms (Zanou & Gailly 2013). It is important to point out that changes in muscle mass and nuclei incorporation processes are not exclusory because in a myofiber, each nuclei controls a specific portion of the cytoplasmatic territory and an increase in cytoplasm volume could further be accompanied of the fusion of new nuclei (Gundersen et al. 2008). In this chapter we will discuss about hypertrophy and atrophy mechanisms and fiber type composition. *De novo* incorporation of nuclei to myofibers is exposed in Chapter 2, dedicated to "Myogenesis".

The principal components of muscle dry mass are proteins. Specifically, skeletal muscle contains from 50 to 75% of all body proteins and is responsible for the 30 to 50% of the whole body protein turnover. Therefore, adaptation changes of muscle will be mainly carry out through the balance of protein synthesis and degradation (Frontera & Ochala 2015).

Among the ensemble of the muscle proteome, not only its major proportion but also the responsible of the main function of skeletal muscle are contractile proteins.

1.1. Proteins involved in muscle contraction

Volunteer movements are not only indispensable in sport and physical activity but for an independent live of individuals. The high degree of specialization for this function is translated into the particular organization of the components of myofibers. Each cell contains hundreds of nuclei which are displaced to the periphery, pushed against to the cell membrane (van der Meer et al. 2011; Rahimov & Kunkel 2013). This leaves most part of sarcoplasm for containing mitochondria, sarcoplasmic reticulum, transverse tubules and mainly, for contractile proteins, responsible for the conversion of nutrient's energy into mechanical force. Contractile proteins are organized into myofibrils, which are constituted by myofilaments that are arranged into sarcomeres. Sarcomeres constitute the minimal muscular contracting unit and are structured in a dynamic and very highly organized protein network. Sarcomeres are present both in skeletal and cardiac muscles and its highly ordered structure and repetitive juxtaposition gives their cells a striated pattern when observed under a microscope. This observation was the origin of the common nomenclature of "striated muscles" used for both tissues, in contraposition to smooth muscle, that has no sarcomeres (Frontera & Ochala 2015; Gautel & Djinović-Carugo 2016).

The two most abundant myofilaments of sarcomeres are actin and myosin, which are disposed interdigitating and in parallel. Actin is a small (42 kDa) globular protein. The assembly of actin monomers forms microfilaments. Thin filaments of the sarcomere are formed by the coil of two microfilaments of actin. Muscle myosins, on the contrary, are a family of big (500 kDa) ATP-dependent motor proteins that constitute the thick filaments of sarcomeres. They consist of two identical heavy chains (MYHCs) and four myosin light chains (MLCs), two essential (ELC) and two regulatory ones (RLC). MYHCs contain a globular domain that bounds and hydrolyzes ATP and a α-helical tail that twist both proteins to form a dimer. They are the proteins responsible for force generation in contraction (Cooper 2000). MLC are divided into two classes, essential and regulatory or phosphorylable. They have both structural roles, involved in mechanical coupling and modulation of the ability of force and movement generation by MYHCs; and regulatory roles, as they have phosphorylable sites by calcium/calmodulin-dependent MLC kinases,

sensitive to calcium levels, that further modulate MYHC's contraction properties (Trybus 1994).

Besides contractile proteins, a large list of structural proteins constitute, align and maintain the sarcomere structure. Furthermore, sarcomeres include also proteins that shuttle between the nuclei and the sarcomeres, like the transcription factors CLOCK, LIM protein and MARPs, among others (Laing & Nowak 2005).

1.2. Types of muscles and fiber types

Not all muscles in the body are capable of exerting the same amount of force or sustaining it on time. What is more, another response to adaptation to different types of exercise, muscle innervation or hormone production, occurs through fiber type switch.
One of the main determinants of fiber type are myosins. As shown on Table 1, different isoforms of heavy (MHC) and light chains (MLC) exist. As the proteins responsible for force generation, depending on which type of myosin subunit is present in each sarcomere, the capacity of force generation will variate. Thanks to the availability of good antibodies, MYHCs detection is a relative easy method to assess fiber type composition in contraposition to other types of staining like pH sensitive ATPase or succinate dehydrogenase (Greising et al. 2013). In mammals, 11 genes encode for MYHCs. Five of them have a limited expression to specialized muscles, while the other six myosin heavy chain (MYH) genes are widely expressed in body muscles. For the skeletal muscles of trunk and limbs, their myosin expression defines four major fiber types: Type I fibers, which are slow twitch and contain MYHC-I, and Type II or fast fibers, that can be longer subdivided into Type IIA, IIB, IIX/D (fiber types IIX and IID have been considered to be equivalent). In addition to these pure fiber types, hybrid ones, expressing mixed types of myosins, also exist; I/IIA, IIA/IIX, IIX/A, IID/B and IIB/IID (Schiaffino & Reggiani 2011; Pette & Staron 2000).

Nonetheless, fiber type not only depends on myosins, but all compartments involved in muscle contraction are specialized on the type of contraction they exert, from specific isoform expression of sarcomeric proteins to the expression of metabolic genes that determine the source of ATP generation (Reggiani & Kronnie 2006; Drexler et al. 2012).

Protein	Gene	Expression in adult muscles
Myosin heavy chain (MYHC)		
MYHC-slow	*Myh7*	Slow I fibers & heart
MYHC-2A	*Myh2*	Fast 2A fibers
MYHC-2X	*Myh1*	Fast 2X fibers
MYHC-2B	*Myh4*	Fast 2B fibers
MYHC-emb*	*Myh3*	Extraocular, masticatory,
MYHC-neo*	*Myh8*	laryngeal and spindles muscles
MYHC-α	*Myh6*	Jaw muscles & heart
MYHC-EO	*Myh13*	Extraocular muscles
MYHC-slow/tonic	*Myh14* (*Myh7b*)	Extraocular muscles
MYHC-15	*Myh15*	Extraocular muscles
MYHC-M	*Myh16*	Jaw muscles
Myosin light chains (MLC)		
Essential MLCs		
MLC-1fast	*Myl1*	Fast muscles
MLC-3fast	*Myl1*	Fast muscles (2B>2A)
MLC-1emb/atrial*	*Myl4*	Atria
MLC-1sb	*Myl3*	Slow muscles & ventricles
MLC1-sa	*Myl6B*	Slow muscles
	Myl6	Non sarcomeric
Regulatory MLCs		
MLC-2fast	*Mylpf*	Fast muscles
MLC-2slow	*Myl2*	Slow muscles and ventricles

Table 1. Myosin proteins with their encoding genes and muscle type expression distribution in adult muscles. Adapted from (Schiaffino & Reggiani 2011; Schiaffino et al. 2015). *: Reexpressed in regenerating muscles.

The different composition in fiber types, stablishes the differentiation between muscle types. Pure slow muscles, like soleus, are red muscles phenotypically, due to a high presence of heme groups caused by its high degree of vascularization. Its main source of ATP generation is oxidative and for that, contain a high number of mitochondria. The type of contractions they produce, as their name indicates, are slow but long lasting, with a high capacity to fatigue resistance. On the contrary, fast muscles, like EDL or tibialis muscles, are visually whiter, due to its lower degree of irrigation. Their principal source of ATP generation is glycolysis so they contain a lesser number of mitochondria. They can exert fast, potent and short contractions, but are much sensitive to fatigue. Other muscles, present a mixture of fast and slow fibers and therefore, mixed combined contractile capacities, being mixed muscles, like gastrocnemius.

It has to be pointed out that these four types of myosin heavy chains are expressed on the adult. Fiber type composition is defined after birth following the transient expression of

embryonic, MYH3, and neonatal myosins, MYH8; and light chain myosin 4, MYL4 (indicated on Table 1). The expression of these myosins is recapitulated in regeneration (see "2.2.3. Postnatal myogenesis upon muscle injury: muscle regeneration") or *in vitro* differentiation systems like C2C12 (Schiaffino et al. 2015). In adults, fiber types are not permanently defined. Being muscle a very high plastic tissue, fiber types can switch through life, for example, in response to neuromuscular activity, overload, hormone expression, diseases like dystrophies or even aging (Pette & Staron 2000). As an example, aerobic exercise induces muscle hypertrophy and increased slow-oxidative fiber switch, whereas inactivity, aging or neuromuscular diseases can lead to a reduction in muscle size (atrophy) and an increase in fast-glycolytic fibers (Simmons et al. 2011). This type of muscle plasticity is key for physiological adaptation, and is mediated by enzymes sensitive to external signals, which are able to couple the environmental changes to changes in DNA expression. One of the best characterized examples among these enzymes are calcium/calmodulin kinases, which phosphorylate their substrates in a calcium dependent manner. Intense or repetitive contractions, trigger more frequently the release of Ca^{2+} from the sarcoplasmic reticulum. This, activates Ca^{2+}/calmodulin kinases to phosphorylate MLCs, modulating their contraction capacities, RYR1 receptors, increasing its opening probability; and calcineurin and class IIa HDACs, increasing the expression of slow fiber type and mitochondrial genes (Gehlert et al. 2015).

2. Myogenesis

The process of muscle formation, commonly named myogenesis, can be divided into two main phases, prenatal myogenesis for *de novo* formation of muscles during development, and adult myogenesis, which can be further subdivided into postnatal growth, maintenance of skeletal muscle mass and the extensive myogenesis triggered upon acute muscle damage. Most of the knowledge about myogenesis comes from the use of in *vitro* and *in vivo* animal models were specific knock-outs can be created or where muscle regeneration can be induced postnatally in non-vital muscles in a controlled and reproducible manner (Snijders et al. 2015). The distinct phases of myogenesis and the precursor cells they depend on are schematized in Figure 2.

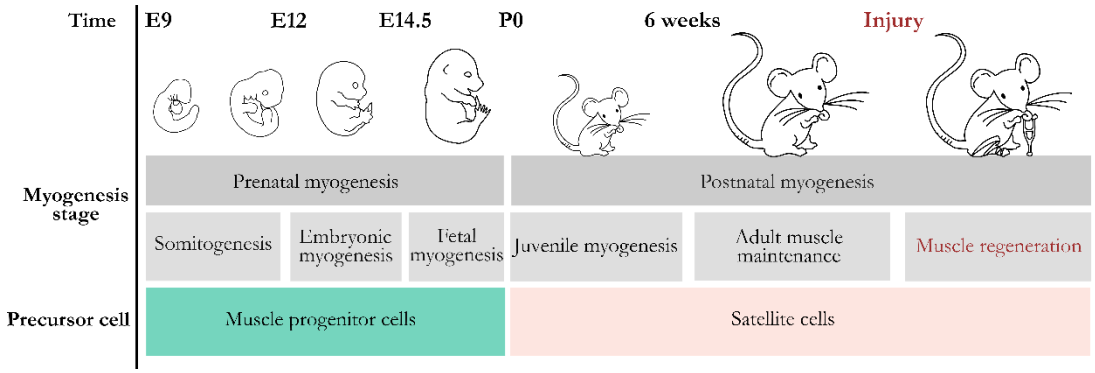

Figure 2. Myogenic stages in mice life. Muscle regeneration is not a life stage but a response to muscle damage and for this reason is colored in red. Adapted from (Relaix & Zammit 2012)

2.1. Prenatal myogenesis

All muscles, with exception of some head ones, are formed in the embryo from pluripotent cells of the dorsal portion of the somites called dermomyotome (Bentzinger et al. 2012). We will center on myogenesis of limb and trunk muscles. Noteworthy, despite the different lineages of origin, the expression of the MRF factors (see below) is common in the formation process of muscles of all origins. The differences between prenatal myogenesis of different muscle origins lie on the lineage-specific expression of additional transcription factors that create alternative networks of activation of the myogenic program (Rios & Marcelle 2009; Braun & Gautel 2011).

In response to Wnt and Sonic hedgehog signaling pathways, the muscle progenitors from the dermomyotome start to express the paired box transcription factors PAX3 and PAX7, which are required for the survival and establishment of the myogenic lineage (Sousa-

Victor et al. 2011; Relaix et al. 2005; Bharathy et al. 2013). The subsequent specification towards the myogenic lineage and the differentiation of these precursors to form the first differentiated skeletal muscle, the myotome, depend on the sequential activation of two families of transcription factors, the myogenic regulatory factors (MRF) and the myocyte enhancer factor 2 of MADS-box regulators (MEF2) (Yun & Wold 1996).

Myogenic regulatory factors (MRFs) belong to a family of DNA-binding proteins that contain a basic helix-loop-helix domain (bHLH) and has four members: MYF5, MYF6 (also named MRF4), MYOD and myogenin (MGN) (Braun & Gautel 2011). MRFs bind specifically to the consensus DNA motif 5'-CANNTG-3' called E-box, located in the promoters and enhancers of muscle-specific genes (Berkes & Tapscott 2005).

MADS (MCM1, Agamous, Deficiens, and SRF)-box regulators (MEF2) constitute a family of DNA-binding proteins that recognize A/T-rich elements located in regulatory regions of skeletal and cardiac structural muscle genes. In vertebrates, it is constituted by four members (MEF2A, MEF2B, MEF2C and MEF2D), which interact with MRF proteins and further activate the expression of differentiation genes, being essential for embryonic muscle differentiation (Sparrow et al. 1999; Black & Olson 1998).

The orchestrated expression of MRFs is nowadays well defined in a temporal manner through all the steps of myogenesis and is illustrated in Figure 3. In a first step, embryonic precursors commit into myogenic lineage cells. This process is driven by the expression of MYF5, MRF4 and MYOD (Berkes & Tapscott 2005). The ablation of these genes completely inhibits the formation of myoblasts, leaving progenitor cells multipotent and able to change their cell fate (Kassar-Duchossoy et al. 2004; Kablar et al. 2003; Braun & Arnold 1995). To a certain point, these three factors have redundant roles, because their specific knock-outs present muscles with only mild defects. On the contrary, MGN is absolutely required for embryonic muscle differentiation and no other protein has redundant or compensatory roles (Venuti et al. 1995; Knapp et al. 2006).
At late fetal stages, the aforementioned myogenic progenitors expressing PAX3 and PAX7, downregulate PAX3 (excluding some muscles like the diaphragm) and migrate in a position adjacent to the forming muscle fibers, between the primitive basal lamina and the myotome (Kuang & Rudnicki 2008; Yablonka-Reuveni 2011). This position is analogous to the future muscle stem cells' localization and these precursors have been proven to constitute

later on the adult muscle stem cell population (Relaix et al. 2005; Buckingham & Relaix 2015).

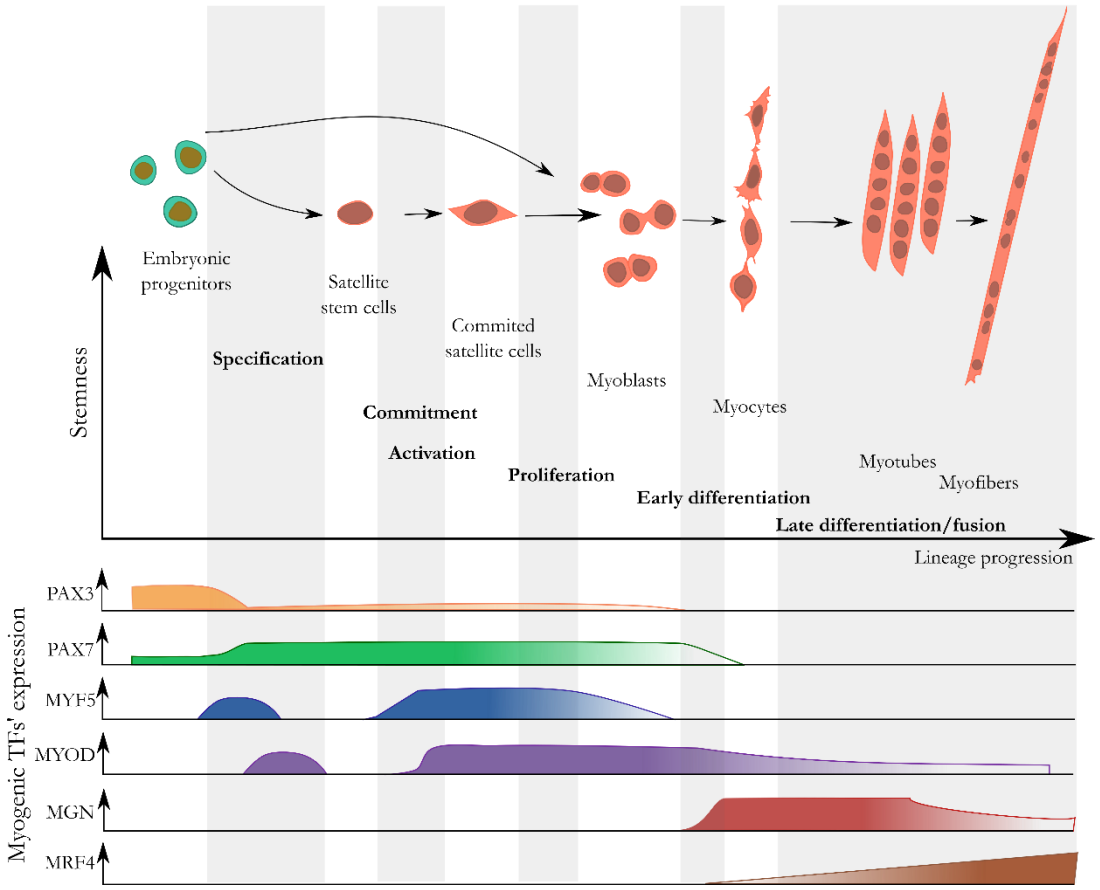

Figure 3. Temporal expression of myogenic transcription factors (TFs) that drive the different stages of prenatal myogenesis. Adapted from Bentzinger et al. 2012.

2.2. Postnatal myogenesis

While prenatal myogenesis relies on embryonic precursors, satellite cells are indispensable for most of postnatal processes. Satellite cells (SCs) where first identified by Alexander Mauro who gave them their name because of their peripheral location to myofibers, between the plasma membrane and the basal lamina (Mauro 1961). They are muscle-specific committed progenitors responsible for growth, maintenance, repair and regeneration of skeletal muscle (Relaix & Zammit 2012). Noteworthy, another cell types have been described to be able to contribute to these processes, like bone marrow cells, perycites, myoendothelial cells, side-population cells, and mesoangioblasts, among others (Tedesco et al. 2010). Nevertheless, the actual contribution to myogenesis of these precursors in healthy conditions is very low and definitely are not the main players in regeneration as SCs ablation results in complete failure of regeneration (Relaix & Zammit

2012). More research is currently needed to address the importance of the contribution of these other populations in healthy conditions and for these reasons, we will discuss only the role of SCs in postnatal myogenesis.

2.2.1. Juvenile myogenesis

The first three weeks of mouse life are characterized by an intense period of growth achieved both by increase in size of the fetal myofibers (hypertrophia) and by new formation or fusion of SCs. In this period of time, mice body weight can increase about 7 to 8 folds, half of them corresponding to muscle (Gokhin et al. 2008). Therefore, SCs, which are the responsible to incorporate the new nuclei needed, are very active at this stage. Up to 80% of SCs are proliferating at this time and in this moment they account for 30 % of total muscle nuclei (Hawke and Garry 2001). After this period of intense growth, adult muscles are formed and SCs enter in a quiescent state. Moreover, their number dramatically drops down to account for the 2 to 7% of nuclei within adult skeletal muscle (Halevy et al. 2004).

2.2.2. Adult muscle maintenance

As mentioned above, during adulthood, there is a very low turnover of myofiber nuclei and in normal conditions only small and focal damages are generated by muscle contraction and need to be repair (Ceafalan et al. 2014; Charge 2004). In these basal conditions, the majority of SCs are found in a quiescent state, which is reversible, as opposed to terminal post-mitotic quiescent state of nuclei within myofibers. Quiescence, also named G_0, is defined as a separated phase within cell cycle, characterized not only by a passive state of non-division, through down-regulation of cell cycle progression genes, but also an actively maintained state that involves inhibition of cell senescence, differentiation and apoptosis (Cheung et al. 2013). Morphologically, SCs present a high nuclear to cytoplasmatic volume ratio, few organelles and a small nuclear size characterized by high levels of heterochromatin. They have low transcriptional and metabolic activity, which is mainly glycolytic, to prevent reactive oxygen species that could induce damage and compromise genomic integrity (Brack & Rando 2012; Biressi & Rando 2010).

Despite its common location and appearance, satellite cells are not a homogenous population, not only at the level of embryonic origin as described, but also in their distribution. For example, slow myofibers contain more number of SCs than fast ones (Shefer et al. 2006; Keefe et al. 2015). Moreover, they present different proliferation rates,

ability to self-renew and engraftment, among others (Biressi & Rando 2010; Relaix & Zammit 2012; Kuang & Rudnicki 2008).

Traditionally SC isolation by cell sorting used a combination of positive and negative staining to surface antigens, as none marker is expressed specifically on SCs: positive selection for the adhesion proteins CD34 (only in mice) and α7-integrin and negative exclusion for Sca1 and CD45 (reviewed in: Ceafalan et al. 2014; Yablonka-Reuveni 2011). Noteworthy, PAX7, located in the nucleus, is widely accepted as a SC' marker because is a specific marker only expressed by SCs in the muscle and its expression is shared through different species (Kuang & Rudnicki 2008; Tedesco et al. 2010).

2.2.3. Postnatal myogenesis upon muscle injury: muscle regeneration

Intense muscle insults that imply the destruction of myofibers and the integrity of muscle architecture, trigger a very complex response of regeneration that involves the interplay of many cell types (Ceafalan et al. 2014). These insults, involve stimuli that cannot be overcome only by hypertrophy mechanisms, and that could be very diverse in origin: a sharp or blunt trauma derived from accidents, ischemia, exposure to extreme temperatures, toxic injuries like anesthetics or venoms, or diseases that induce muscle degeneration like dystrophies (Karalaki et al. 2009).

The processes that lead to the restauration of muscle histology could be divided in three main phases: a degeneration phase, a regeneration phase and a final phase of maturation and remodeling (Ciciliot & Schiaffino 2010). The timing of regeneration depends very much on the extent of the injury, but in general, it is estimated that the whole process could be completed in 3 to 4 weeks (Karalaki et al. 2009). First, we will describe strictly the processes depending on skeletal muscle stem cells. Second, we will briefly introduce the role of other cell types in the regeneration process.

Muscle stem cells depending processes during muscle regeneration

Degeneration phase

The degeneration phase starts immediately after the injury and takes places during the first days (Ceafalan et al. 2014; Laumonier & Menetrey 2016). It is triggered by the disruption of myofiber cell membranes, which increases cell permeability and causes the release of calcium and muscle proteins to the extracellular space and blood. The release of calcium activates proteases like calpains that further extend the damage, causing a rapid necrosis of

myofibers and, eventually, its apoptosis (Karalaki et al. 2009; Ceafalan et al. 2014; Ciciliot & Schiaffino 2010).

Regeneration phase

The regeneration phase starts with the activation of satellite cells (SCs). As mentioned, SC niche integrity is indispensable for the maintenance of SC quiescence. SC niche damage or removal of SC from it, causes its quickly activation and exit from quiescence.

The specific location of SCs, intimately close to myofibers, allows SCs for a rapid sensing of skeletal muscle integrity. The destruction of SCs' niche causes its quickly activation, which is further induced by the efflux of calcium ions from the degenerated myofibers, that is sensed by the calcitonin receptors (CALR) present in SCs (Montarras et al. 2013). Moreover, many secreted soluble factors, like FGF, HGF, NOS and inflammatory cytokines, can further activate SCs.

SCs become activated as early as 6 hours post injury (Mahdy et al. 2016) and are characterized by the expression of MYOD, which is indispensable for SCs activation, and, as in embryonic myogenesis, acts as a cell fate determinant factor (Megeney et al. 1996; Tajbakhsh 2009). Not in vane MYOD is considered as a master regulator of muscle, that is, one of the few genes that can trigger the expression of hundreds of genes involved in the complex program of cell differentiation (Davis et al. 1987).

Related with SCs activation, it was recently discovered that upon muscle injury, SCs located in a remote place (in the study, the contralateral limb of the one injured in the mice), enter in a different phase of quiescence named G_{alert}. This state is characterized by a slight increase in cell size, mitochondrial activity and ATP production. In this intermediate phase between quiescence and activation, cells can enter faster in cell cycle and shown enhanced regenerative capacity (Malam & Cohn 2014; Rodgers et al. 2014). This discover suggests a systemic response that prone SCs to activation in response to regeneration (Dumont et al. 2015)

After become activated, SCs reenter into cell cycle. SCs proliferation have two main purposes, one, is to give rise to the sufficient number of progenitors to replenish the damaged area, and the other, is to ensure the perpetuation of the SC pool through life. This double purpose is achieved by too kinds of division: the symmetric and the asymmetric division, which are the result of two principal events: the polarity of cell fate determinant proteins and their mitotic spindle orientation. The asymmetric apico-basal

division is performed by cells that have never expressed MYF5 and gives rise to two cell daughters, one that maintains MYOD and PAX7 expression, that will commit to differentiation; and the other that would downregulate MYOD while maintaining PAX7 expression, that will reenter into the quiescent state to maintain the SC pool (Kuang et al. 2009). In this division, it has also been observed a preferential segregation of chromatids in the daughter cells, being committed SCs the receptors of newly synthetized chromatids and quiescent SCs, the template ones (Rocheteau et al. 2012). The symmetric or planar division (parallel to the sarcolemma) gives rise to equivalent sister cells, either two SCs that will replenish the quiescent pool or two cycling SCs. The committed cells that upregulate MYOD, constitute the transient amplifying population of SCs and are known in this step as myoblasts or muscle proliferating cells (MPCs) (Brack & Rando 2012; Bentzinger et al. 2012). This proliferation step takes place during the firsts 2 to 5 days post injury (Ciciliot & Schiaffino 2010; Dumont et al. 2015).

After proliferating, SCs need to migrate from its niche to the damaged area. Migration is achieved through the secretion of protein metalloproteinases (MMP), like MMP2 and MMP9, which break up the collagen and proteoglycans of the basal lamina (Montarras et al. 2013).

Upon arrival to the damaged area, SCs will exit the cell cycle and start to differentiate. This process is genetically directed, as in embryonal myogenesis, by MRFs. Through this process, PAX7 will downregulate its expression, while the sequential expression of the different MRFs will regulate the differentiation process. The initiation of differentiation is driven by the expression of MYOG. The process is continued by the sequential expression of the late differentiation markers MCK and MRF4. Through the process of differentiation, myoblasts will maturate to myocytes, and finally will fuse between them to constitute the regenerating fibers. These fibers could be easily distinguished from mature myofibers because they have the nuclei centered in the middle of the cytoplasm and, as mentioned, express transiently, embryonic and neonatal myosin types (Schiaffino et al. 2015; Ciciliot & Schiaffino 2010). This SCs depending processes are illustrated in Figure 4.

Maturation and remodeling phase

The last step of muscle regeneration is the maturation of the newly formed myofibers and the remodeling of the regenerated muscle (Ciciliot & Schiaffino 2010).

From several rounds of myocyte fusion, regenerating myofibers will increase in diameter and finally maturate, replacing the expression of regenerating myosins and differentiation MRFs with the expression of fiber type specific adult myosins and specialized muscle proteins. At this point, the central nuclei from regenerating fibers will be displaced to the periphery to leave space for the contractile proteins (Casar et al. 2004).

The whole histological architecture of skeletal muscle needs to be also remodeled. The newly formed myofibers will be reinnervated by the motoneurons, the myotendinous connections will be reestablished and new capillaries will be formed. At the end of this process, skeletal muscles will not only look physically indistinguishable from non-injured ones, but will already have recovered its fully functional activity (Ciciliot & Schiaffino 2010; Karalaki et al. 2009).

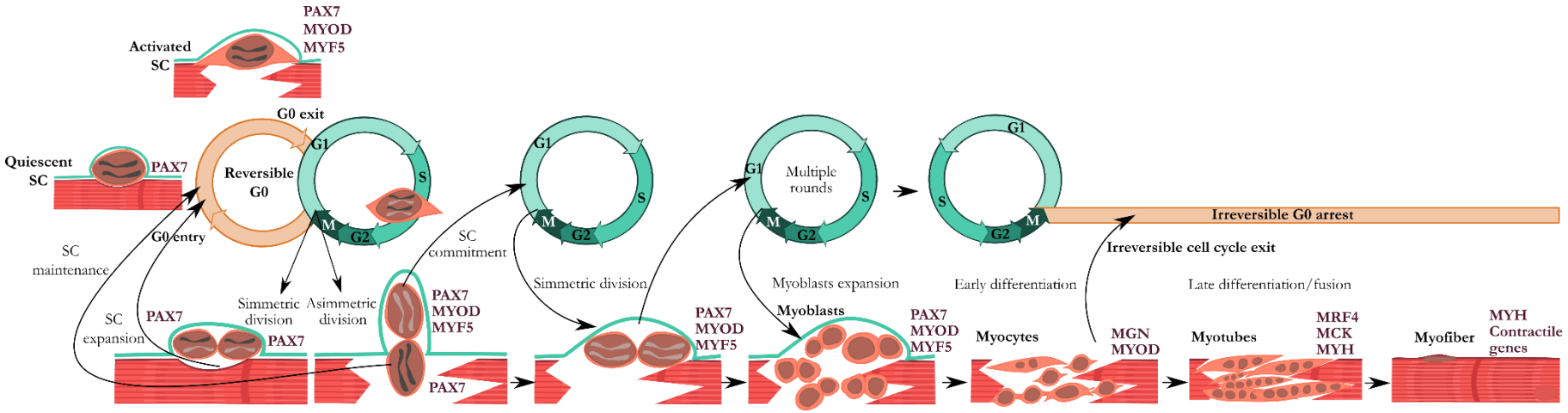

Figure 4. Satellite cells depending processes upon skeletal muscle injury. Satellite cells (SCs) are quiescent when located in their niche, between the sarcolemma (red) and the basal lamina (blue). SCs quiescent state is characterized by its reversibility. Once SCs get activated by extracellular stimuli like skeletal muscle injury, which causes disruption of their niche, they start to express the activation marker MYOD and the commitment MRF, MYF5. Once activated, they reenter to cell cycle, which can result in symmetric segregation of chromatid sisters, being the preferential division to expand the SCs' pool, or asymmetric, the preferred upon injury. Asymmetric division, generates a committed cell which has inherited the new synthetized chromatids and the expression of MRF activator factors, while the cell that has inherited the template chromatids, downregulates MYOD and reenters to G0 state to maintain the SC pool (new synthetized chromatids are painted in grey and template ones in black). The committed cell undergoes several rounds of cell divisions, that give rise to a sufficient number of myoblasts in the site of the injury, which will later on commit to differentiation and start to express myogenin (MGN), the early differentiation MRF. Cell differentiation causes the exit of cells from cell cycle and their entering in G0 irreversible arrest state. These post-mitotical cells will proceed to differentiation to finally fuse between them to replace the damage tissue and ultimately express contractile specialized proteins allowing the tissue to restore their contractile capacity. The markers that allow to monitor the regeneration process are indicated in purple. Image was created using data from: (Gayraud-Morel et al. 2012; Dumont et al. 2015; Almada & Wagers 2016; Brack & Rando 2012; Rumman et al. 2015).

One of the main differences in the environment where embryonal and postnatal myogenesis take place is the presence of immune system cells. While they are almost absent during prenatal myogenesis, in adult regeneration can exceed 100,000 cells/mm^3 (Tidball & Villalta 2010). For the sake of simplicity, muscle stem cells and inflammatory response processes are described here separately. However, it has to be pointed out that not only both processes occur at the same time, but exert a mutual interaction and influence, and that the two are indispensable for a proper muscle reconstruction (Chazaud et al. 2003; Tidball & Villalta 2010).

Immune system depending processes

Neutrophils are the first inflammatory cells that arrive to the injury, about 2 h after lesion, and reach its maximum concentration between 6 and 24 h. Its main function is to release proteolytic enzymes and reactive oxygen species that further increase the damage extension and help to activate SCs (Rigamonti et al. 2014; Tidball & Villalta 2010). Their number dramatically drops after 3-4 days after injury. After 2 days post injury, macrophages are the predominant inflammatory cells present in the lesion. The sources of macrophages are constituted by muscle-resident macrophages and monocytes that arrive through the bloodstream (Karalaki et al. 2009; Musarò 2014; Rigamonti et al. 2014).

Two main populations of macrophages exist: M1 or pro-inflammatory and M2 or anti-inflammatory macrophages (Rigamonti et al. 2014). Therefore, these two macrophage types are the simplified polarized extremes of a continuous spectrum of diverse functional macrophage activated states and in *in vivo* conditions also different intermediate phenotypes between these two populations coexist (Tidball 2017). These two main populations can be distinguished by their levels of expression of chemokine receptors and the profile of cytokines and molecules that they secrete (summarized in Table 2). M1 (also called classical activated macrophages) are the first population of macrophages that arrive to the injury place. They reach high levels between 24 and 48 h post injury. Its main roles are antigen presentation and the phagocytosis of muscle debris. Specifically on SCs, they stimulate its proliferation and inhibit their differentiation.

After 4 days of injury, M2 (alternatively activated macrophages) are the predominant macrophage type. They remain present in the injured tissue for at least 21 days (Novak et al. 2014). Opposing to M1 type, they promote tissue repair and stimulate SCs differentiation (Tidball & Villalta 2010).

M1	M2
Pro-inflammatory macrophages	Anti-inflammatory macrophages
$CD68^{high}$, $CD86^{high}$	$CD68^{low}$, $CD163^{high}$, $CD206^{high}$
Pro-inflammatory cytokines	**Anti-inflammatory cytokines**
iNOS, TNFα, Il-1β, Il-6, Il-12, CCL2	Arg-1, Il-10, TGFβ, IGF-1, MMP-9

Table 2. Cell surface markers that allow to distinguish between M1 and M2 macrophage populations and the main molecules they secrete. Adapted from: (Novak et al. 2014; Ceafalan et al. 2014).

It is still not clear whether M2 macrophages came from the transformation of M1 or if they originate from different cells (Schiaffino et al. 2016). What it is known is that when M2 response starts, M2 macrophages actively promote the deactivation of the M1 inflammatory response through the secretion of Il-10. Il-10 is not only expressed by M2 macrophages but by monocytes, dendritic cells, mast cells, neutrophils, eosinophils, natural killer cells, $CD4^+$ T cells, $CD8^+$cells and B cells. The role of Il-10 in limiting inflammatory processes is also present in the prevention of autoimmune pathologies (Engelhardt & Grimbacher 2014). In muscle regeneration, Il-10 ablation results in an extended M1 response and delayed muscle regeneration *in vivo* (Deng et al. 2012). In mdx mice (a model of DMD) Il-10 absence further increases muscle damage and reduces muscle strength while treatment of mice with Il-10 reduces M1 activation (Villalta et al. 2011). Moreover, i*n vitro* treatment of myoblasts with Il-10 increases myocyte fusion (Deng et al. 2012; Chazaud et al. 2009).

It is important to highlight that not only M2 response is crucial for injury healing. Proper regeneration requires both M1 and M2 responses occurring during the necessary and appropriate times. A fail in or a shorter M1 response, results in an incomplete clearing of the debris, while a chronic inflammatory response impedes the proper reconstruction of the tissue and leads to fibrotic deposition (Mann et al. 2011). The times at which each immune response type mainly occurs after acute muscle injury and the most abundant immune cells present at the lesion region are summarized in Figure 5.

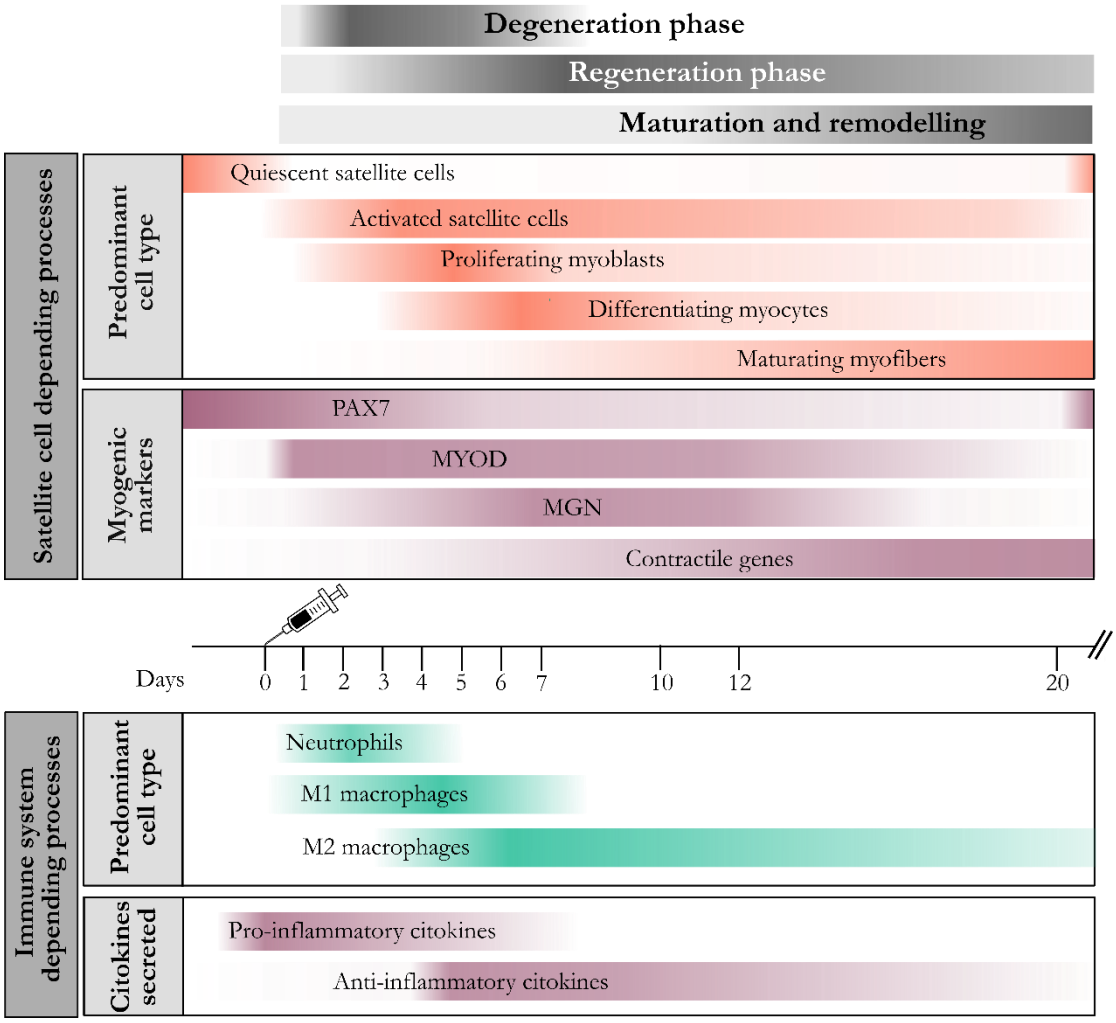

Figure 5. Temporal interaction between satellite cell's derived muscle precursors and immune cells after acute muscle injury. Figure was adapted from: (Shi & Garry 2006; Ciciliot & Schiaffino 2010; Musarò 2014; Tidball 2017).

In addition, not only skeletal and inflammatory processes are required for normal tissue reconstruction, but almost each cell type present in skeletal muscle has a role in the injury healing process. For instance, endothelial cells should rebuild blood vessels to supply nutrients and monocytes to repair the injury site, motoneurons should reestablish the innervation of the new created myofibers, providing electrical impulses indispensable for fully maturation of myofibers and fibroblasts should also proliferate and synthesize new extracellular matrix to reform the basal lamina that covers SCs (Ceafalan et al. 2014; Christov et al. 2007; Musarò 2014; Mann et al. 2011). Alterations in any of these processes can lead to the origin of many regeneration pathologies.

3. Epigenetics

The term epigenetics was first coined by Conrad Waddington in 1942 by adding the Greek prefix "epi-" (above) to the prevalent concept of "genetics" at the time, to refer to "the causal interactions between genes and their products, which bring the phenotype into being" (Waddington 1942). Since that moment, the concept of epigenetics has much evolved and many definitions have arisen. Intense debates about the current definition of the concept are still actively present on the field but one of the most accepted definition is from Dr. Russo and colleagues, who defined epigenetics as "the mitotically and/or meiotically heritable changes in gene function that cannot be explained by changes in DNA sequence" (Riggs et al. 1996; Tronick & Hunter 2016). In my opinion, this definition implies that cells which are not dividing in a particular moment, like satellite cells, or which will no longer divide, like myofibers, may not present epigenetic regulation, and that temporally restricted responses to non-sustained stimuli do not involve epigenetic mechanisms. For these reasons, I like more the definition proposed by Saade and Ogryzko, that consider epigenetic information "as the information that is required in order to specify the state of an organism in addition to genetic information (nucleotide sequence) and reaction norm" (Saade & Ogryzko 2014).

No matter the definition itself, one direct consequence of epigenetics is mammalian cell diversity. Each cell of a mammalian body has the same DNA information (excluding acquired mutations, viral DNA incorporation and putative retrotransposon movement), but each cell type expresses this DNA information on a particular and different way to give rise to the different kinds of cells present in the body (Shapiro 2014). Regarding the DNA molecule itself, each human cell has about 2 meters of DNA fitted in about 6 μm of nuclei diameter (Alberts et al. 2002). To achieve the fitting of such a large molecule in a so reduced volume, DNA has to be compacted at different levels. Moreover, this compactation has to be regulated and allow the access to the DNA sequence at the necessary moments to allow DNA transcription, replication and repair. The agents responsible to compact DNA in an adjustable manner are proteins which together with DNA constitute the chromatin that at the same time constitute the "canvas" and the "players" of epigenetics.

In the very first layer of condensation, DNA is wrapped around nucleosomes, which are composed by eight globular proteins named histones, two of each: H2A, H2B, H3 and

H4. Histone H1 is a linker histone that helps to pack neighboring nucleosomes together (Oberdoerffer & Sinclair 2007).

Histones are rich in lysine and arginine residues, which are positively charged, and through ionic interactions with the negative charge of phosphates each nucleosome wraps around 147 bp of DNA (Alberts et al. 2002). This first and intimate layer of DNA binding with histones and many other proteins, which possess DNA binding domains or protein domains to bind other DNA-associated proteins, constitute the first stratum of epigenetic regulation, and vastly the most studied one.

3.1. Epigenetic mechanisms

Epigenetic mechanisms can be divided into four groups: DNA modifications, histone modifications, histone variants and ATP-dependent remodeling proteins, which are schematized in Figure 6.

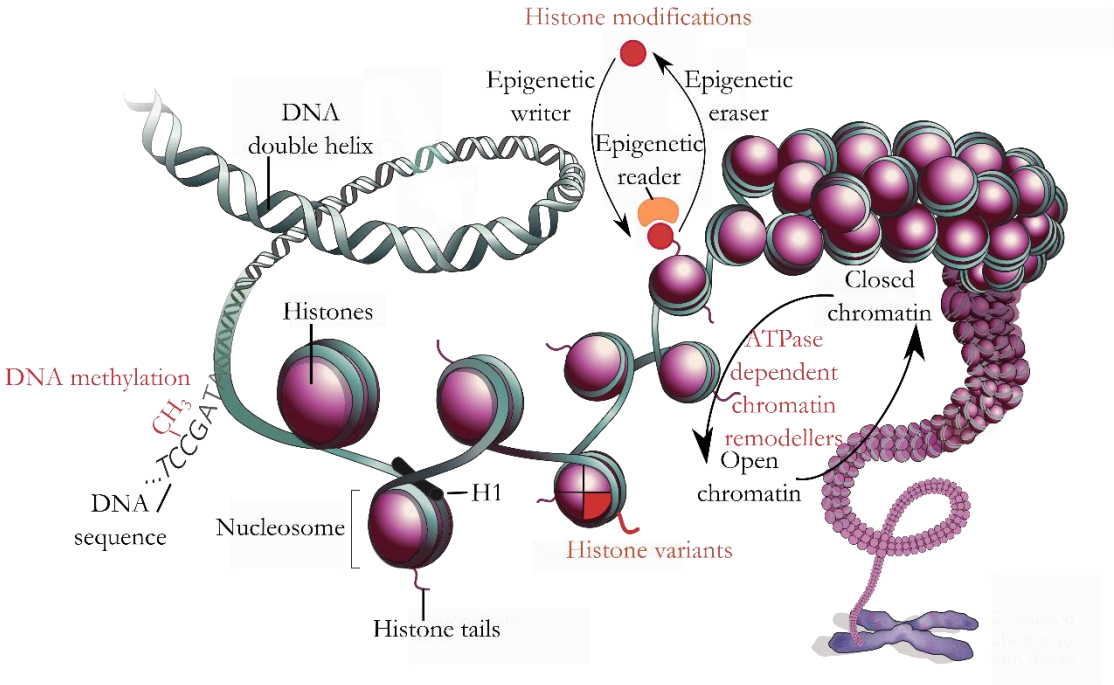

Figure 6. Epigenetic mechanisms. The four epigenetic mechanisms are indicated in red. Epigenetic mechanisms are based on the existence of epigenetic writers that deposit a specific mark, erasers, that are able to remove the mark, and readers, which recognize the mark and respond to this modification (represented for histone modifications). Modified from (Marx 2012).

3.1.1. DNA modifications

DNA methylation was the first epigenetic modification discovered in 1948 (Hotchkiss 1948) and therefore the most studied in normal and pathological processes. It consists on the addition of a methyl group (CH_3-) to the C5 position of cytosine residues when followed by guanines in the context of CpG dinucleotides. Overall, CpG dinucleotides are underrepresented in the human genome sequence as a result of the mutagenic potential of 5mC that can deaminate to thymine (Coulondre et al. 1978; Bird et al. 1985). Moreover, of the total of 28 million of CpG's present in human genomes, 60 to 80% of them are methylated. Only 10% of the CpG's are located in the so called CpG islands (CpGi), which are defined as short regions of about 1,000 bp on average, with a higher density of CpG dinucleotides than the statistically expected (Bird et al. 1985; Jones 2012). They are present in approximately the 70% of all vertebrate annotated gene promoters. This specific location in transcriptional regulatory regions confers them an important role in the control of gene expression (Saxonov et al. 2006; Jones 2012) and therefore are frequently unmethylated in normal conditions, allowing the expression of housekeeping, tissue specific and developmental regulatory genes (Deaton & Bird 2011).

DNA methylation is deposited on DNA by two *de novo* methyltransferases, DNMT3A and DNMT3B, and maintained after replication by DNMT1. DNA methylation can be erased passively or by DNA demethylases, which during the process of demethylation leave another different modifications attached to cytosines, among them, 5-hydroxymethylcytosine, 5-formylcytosine and 5-carboxylcytosine. Besides being a derivative of erasure of methylation, these modifications may have specific roles in DNA expression, not yet completely understood (Ngo et al. 2016).

Traditionally, DNA methylation has been seen as a long lasting repressing mechanism of gene expression. Indeed, DNA methylation controls allelic silencing in gene imprinting, X chromosome inactivation and silencing of repetitive elements (Jones 2012). The mechanisms by which DNA methylation exerts this repression are many, from the decrease of DNA flexibility (Ngo et al. 2016), to the physical impediment for the binding of methylation-sensitive transcription factors. Moreover, 5-methyl-cytosine can be further read by proteins containing domains that recognize and bind methyl cytosines, which also possess transcriptional repressor domains that can recruit additional repressive complexes like histone deacetylases or the Polycomb repressive complex (Jones 2012). Nevertheless, it is now accepted that methylation is not an initiating event in gene silencing, but acts to lock genes in an already present silent state (Jones 2012). However, the evidences of CpGi

methylation in gene repression are more associative than causative and the list of examples where CpGi methylation does not correlate with transcriptional repression grows each day (Doi et al., 2009; Ji et al., 2010).

Furthermore, the role of DNA methylation in gene regulation depends on the CpG genomic context. Beyond CpGi, that, as mentioned, are often demethylated in normal tissues, the up to 2 kb of sequence surrounding them, termed CpG shores, have been found to correlate more than CpGi with gene expression in a genome-wide manner (Irizarry et al. 2009). On enhancers, the regulatory gene regions situated at variable distances from promoters and that control gene expression in a cell specific manner; it has also been described that methylation can act as a repressor of their activity, although the mechanisms of this effects are still not clear (Jones 2012). Besides this regulatory genes, on gene bodies of dividing cells, on the contrary, CpG methylation is correlated with DNA transcription and in this case it may promote transcript elongation and the silencing of alternative promoters, present in the gene body (Moore et al. 2013; Jones 2012). Also, an additional role of DNA methylation in splicing control has been proposed (Maunakea et al. 2013).

The first evidence of the role of DNA methylation in skeletal muscle processes date as far as 1977, when Constantinides and colleagues treated non-muscle cells with the demethylating agent 5-azacytidine and observed their spontaneous transdifferentiation into myoblasts (Constantinides et al. 1977). Analysis of treated 10T1/2 fibroblasts identified MYOD as the transdifferentiation agent and demonstrated the same outcome when its DNA was transfected (Davis et al. 1987). Recently, it has been demonstrated that site specific demethylation of this enhancer by dCas9-Tet1 recombinant enzyme facilitates fibroblasts reprogramming into myoblasts (Liu et al. 2016).

During cell commitment and differentiation, globally, myogenic stem cells showed a gain of DNA methylation through differentiation, noteworthy, on developmental genes such as homeobox genes; while differentiation was also accompanied by a loss of DNA methylation in CpG-poor regions, such as occurs on contractile fiber genes (Carrió et al. 2015; Tsumagari et al. 2013).

3.1.2. Histone modifications

Histones are the closest bound proteins to DNA and, as a result, the first targets for protein epigenetic modification. The particular disposition of histones in the nucleosome leaves

their N-terminal domains protruding and susceptible for posttranslational modifications. Though, recent data also suggests the further possibility of modification of core histone residues to control DNA processes (Tessarz & Kouzarides 2014). Traditional known modifications, occur mostly on histone N-tails, and the list of known histone modifications is constantly growing and include at least histone methylation, acetylation, phosphorylation, ubiquitination, sumoylation, citrullination, ADP ribosylation, deamination, proline isomerization, crotonylation, propionylation, butyrylation, formylation, hydroxylation, O-GlnNAcylation and proteolysis (Falkenberg & Johnstone 2014; Sincennes et al. 2016). The abbreviation nomenclature of histone modifications refers, first, to the histone that is modified, followed by the single-letter code of the aminoacid affected, the type of modification and finally the number of modifications. For example, H3K27me3 makes reference to the tri-methylation modification of the 27th lysine of histone 3 (Carlberg & Molnár 2014).

Noteworthy, depending on the residue that is modified modifications can be:
- Compatible, if they involve two different residues. They may exert additive effects or confer different properties. For example, H3K4me3 and H3K9ac are found altogether in the promoters of transcribed genes being both positive marks of transcription; while when H3K4me3 is present together with H3K27me3, they mark bivalent domains of stem cells, where genes are repressed temporally until they are resolved being transcribed or repressed in the daughter differentiated cells as needed (Sincennes et al. 2016).
-Additive within the same aminoacid residue, with the same or different properties. As an example H3K9me1, H3K9me2 (both associated with gene transcription) and H3K9me3 (associated with gene repression).
- Incompatible, if different modifications, often possessing antagonic properties, are placed into the same residues. For example, the mentioned H3K9ac and H3K9me3.

Histone modifications inside the same nucleosome or within regions are not normally placed alone but a combination of them acts to define or modify the type of chromatin of each DNA domain. For example H3K9ac promotes H3K4me3 deposition (Seto & Yoshida 2014). A typical, but not the only one possible, distribution of histone marks in active promoters generally involves the presence surrounding the transcription start site of H3K4me3, H3K4me2, H3K4me1 and acetylated lysines, like H3K9ac; methylation of H3K79 at 5' of gene bodies and H3K36me3 at 3' of gene bodies. Inactive promoters

present low levels of all the mentioned marks and high levels of the repressive marks H3K27me3 or H3K9me3 and histone hypoacetylation (Illustrated on Figure 7).

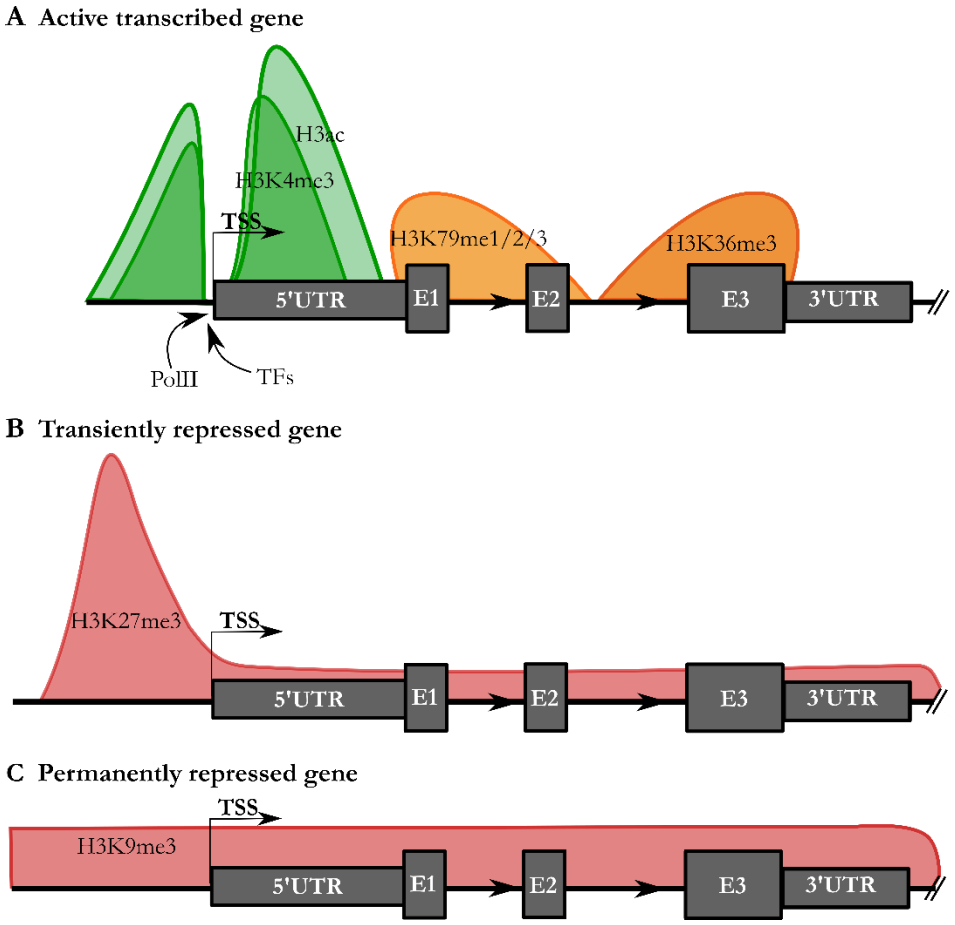

Figure 7. Distribution of histone modifications in transcriptional active and silence genes. Simplified representation of most known histone marks associated with active transcription (**A**) and inactive transcription corresponding to a transient repression state (**B**) or a constitutively silenced gene (**C**). Actively transcribed genes are characterized by the presence of H3K4me3 and histone acetylation in their promoter regions while in the gene body present marks deposited as a consequence of gene transcription. They also show polymerase (PolII) and transcription factors (TFs) bind to their promoter regions. Repressed genes are associated with the absence of the aforementioned marks and the presence of the transiently repressing mark H3K27me3 or the long-lasting repressing mark H3K9me3, typically present in constitutively heterochromatin regions. Image is an adaptation of (Barth & Imhof 2010; Kooistra & Helin 2012).

This combinatorial presence of histone marks suggested the formulation of the "histone code" hypothesis which mimicking the genetic code proposes that the combination of histone modifications present at a certain genomic locus determines the activity state of the underlying gene (Strahl & Allis 2000). In other words, it proposes that if we know the histone marks present on a gene, its transcriptional state could be predicted. This

hypothesis, although quite used, is a topic of debate and have many detractors. Some of the arguments against claim that we do still not know if histone marks are the result of cumulative events rather than a reflection of the actual state of the gene (Henikoff 2005; Barth & Imhof 2010) and that, moreover, they are not the best predictors of the gene transcriptional state (Corrales-Berjano et al. 2017).

3.1.3. Histone variants

Histones could not only be modified but exchanged by variants with different properties. This implies a higher reorganization of DNA packaging architecture more than the addition of covalent modifications As an example, the histone variant H1b contributes to repress MYOD promoter in undifferentiated myoblasts (Hansol et al. 2004) while H3.3 histone is recruited in differentiation conditions and contributes to MYOD active transcription (Harada et al. 2012; Sincennes et al. 2016).

3.1.4. ATPase-dependent chromatin remodeling complexes

Chromatin remodeling complexes make use of the energy released from ATP hydrolysis to disrupt DNA and nucleosome interactions, mediating the exchange of histone variants and nucleosome movement, destabilization or ejection (Han et al. 2011). This activity modulates nucleosome occupancy on the genes. A decreased nucleosome occupancy, measured frequently with DNAse hypersensitivity, is associated with regulatory regions of active transcribed genes, which allows the binding of transcription factors and RNA polymerase. On the contrary, tightly compacted genes, characterized by a higher chromosome occupancy and a decreased DNAse hypersensitivity, are associated with inactive transcription regions (Workman 2006). Skeletal muscle differentiation is not an exception, and for example, Forcales and colleagues, described that the SWI/SNF subunit BAF60C, interacts with regulatory regions of MYOD target genes, already in myoblasts, to facilitate its binding and the recruitment of the other subunits of SWI/SNF in differentiation to remodel the chromatin conformation of MYOD targets and allow its activation. Therefore, the knock-down of BAF60C results in an impaired binding of MYOD to its targets and reduced induction of them through differentiation (Forcales et al. 2011).

As mentioned, this four epigenetic mechanisms do not act alone, but in combination to shape the epigenetic landscape of the cells at each given moment. From the point of view of chromatin, epigenetic elements combination on mammalian genomes define two big territory types. The first one is assigned to "open" chromatin, named euchromatin, characteristic of actively transcribed genes, which present no methylation at the CpGi of their promoters, possess the positive histone marks associated with transcription, and a relative relaxed conformation permissive for transcription factor binding, RNA polymerase and remodeling protein complexes. On the contrary, silent transcriptional regions are located in heterochromatin regions, which can be further subdivided into facultative and constitutive heterochromatin territories. The facultative heterochromatin contains repressed genes at a moment but that have been activated in the past or that are susceptible of being activated latter on. They are characterized by negative associated histone marks and relative chromatin condensation. Constitutive heterochromatin, at its turn, possess the highest degree of condensation. It is characteristic of permanently silent regions that are repressed in an everlasting manner, locked by a high degree of DNA methylation and high levels of H3K9me3 histone mark, displaced to the periphery of the nucleus. It is found mainly at chromosomal centromeres and telomeres (Bannister & Kouzarides 2011).

3.2. Epigenetic alterations in myopathies

The mechanisms able to silence or disrupt the expression of the genes necessary for the proper function and identity maintenance of cells include both genetic mechanisms, accounting for point mutations, deletions, insertions, translocations and aberrant splicing patterns; and all the epigenetic mechanisms explained above (Moore et al. 2013). Disruption of any of these mechanisms could trigger or contribute to the development of human pathologies, including muscle diseases (Sharma et al. 2009).

3.2.1. Muscle dystrophies

Although congenital muscle dystrophies are mainly caused by heritable mutations, epigenetic aberrations have also been described to contribute to the onset or evolution of some muscle dystrophies. For example, Zhou and colleagues show that 55% of the cases of core myopathies studied displayed monoallelic instead of biallelic expression of RYR1

gene due to hypermethylation of one RYR1 allele (Zhou et al. 2006). Another study also corroborated the hypermethylation of RYR1 CpGi in minicore patients compared to healthy controls and also reported an increased HDAC4 and HDAC5 expression in these patients, which was also present in patients with nemaline myopathies (Rokach et al. 2015).

Another example of alterations in the DNA methylation patterns in myopathies is present in facioscapulohumeral muscular dystrophy (FSHD), a dominant autosomal myopathy. The aberrant hypomethylation of the D4Z4 macrosatellite repeat observed in patients affected by FSHD, causes a loss in the silencing of the transcription factor DUX4, encoded within the macrosatellite. The abnormal expression of DUX4 in myofibers causes cell death and atrophia, being a major cause of FSHD (Calandra et al. 2016; Daxinger et al. 2015).

In Duchenne muscular dystrophy (DMD), it has been identified that the generation of nitric oxid (NO) in response to extracellular signals by dystrophin associated complexes, altered in DMD, is decreased. This results in an aberrant constitutive activation of HDAC2 (Histone deacetylase 2), which results in a permanent inhibition of its nuclear regulated genes, that contributes to the progression of the pathology (Consalvi et al. 2011).

3.2.2. Rhabdomyosarcoma

Nowadays, it is widely accepted that in cancer both genetic and epigenetic events interplay between them to transform a normal cell into a tumoral one (Gilbert et al. 2004). The aberration of the epigenetic landscape in cancer is one of the best characterized among all human pathologies. Generalizing, human tumors present global DNA hypomethylation and local hypermethylation of CpGi compared to normal tissues, accompanied with a decrease on H4K16ac and histone acetylation dysregulation patterns (Timp et al. 2014; Fraga et al. 2005).

Rhabdomyosarcoma (RMS) is a type of cancer of muscle precursors cell origin that express myogenic factors but undergo an aberrant and partial differentiation. It is a rare cancer type that affects mostly children on the pediatric age but that can also appear in adolescents or adults (Keller & Guttridge 2013). They are two main types of rhabdomyosarcoma according to their histology and molecular characteristics:

- Embryonal rhabdomyosarcoma (eRMS) is the most frequent type (about 70% of all RMS cases). Affects mostly children under 10 years old and has a relative favorable prognosis. It is commonly localized in head and neck, genitourinary tract and retroperitoneum.
- Alveolar rhabdomyosarcoma (aRMS) accounts for the 30% of RMS cases and occurs mostly in adolescents. Its name comes from the observable alveoli structures that it forms, which resemble those from lungs. It is the most aggressive type and frequently has a very bad prognostic because of its high rate of metastasis already present at the moment of diagnosis. It is frequently localized in extremities and trunk and is characterized by the presence of a fusion gene that results of the translocation of the DNA-binding domain of PAX3 (80% of aRMS cases) or PAX7 (20% of aRMS cases) genes to the transactivation domain of FOXO1 (Cieśla et al. 2014; Hettmer et al. 2014; Marshall & Grosveld 2012).

Due to the low incidence of rhabdomyosarcoma and thus, the low amount of samples available to perform studies, epigenetic studies on this type of cancer are very limited. To circumvent this scarcity of samples, two main approaches have been generated by researchers. First, the derivation of *in vitro* cell lines from isolated tumors of patients and second, the generation of mouse knock-in models of aRMS that recapitulate the formation of the tumor *in vivo* by the expression of PAX3/7-FOXO1 oncogenes under the control of PAX3 or PAX7 promoters (Marshall & Grosveld 2012).
An important question in this field is why MYOD, which is expressed in RMS, is unable to activate their targets and trigger the muscle differentiation program instead of the uncontrolled proliferative state that rhabdomyosarcoma cells present. Tapscott and colleagues identified that in these cells MYOD is able to bind to their target sites, but has a poor activation potential towards them (Tapscott et al. 1993). Latter studies showed that this deficient capability of activation depended on the aberrant splicing of a protein, musculin, that competes with MYOD for E2 factors, which in normal conditions form heterodimers to activate MYOD targets (Yang et al. 2009). It was also identified that in aRMS cells, MYOD and SUV39 (H3K9me3 methyltransferase, KMT1A) are perpetually associated, even under differentiation conditions. In normal myoblasts, these two proteins dissociate upon differentiation conditions, but in aRMS are continuously bound, inducing the deposition of H3K9me3 on MYOG promoter and silencing its expression (Lee et al. 2011). In addition, and regarding MYOD modifications, it has been reported that P/CAF, an acetyl transferase that in normal conditions acetylates and activates MYOD upon differentiation, in aRMS cells preferentially acetylates and stabilizes PAX3-FOXO1

oncogene, inhibiting the MYOD differentiation capacity on these cells (Bharathy et al. 2016).

Other works, have focused particularly on the targets activated by the fusion oncoproteins in comparison to the activated by the normal non-translocated ones (Marshall & Grosveld 2012). In this direction, JARID2 (a Jumonji demethylase of dimethyl and trimethyl histone marks) was identified as a direct transcriptional target of PAX3-FOXO1. In aRMS cells, JARID2 associates with PRC2 Polycomb complex, increasing H3K27me3 on differentiation genes and promoting their silencing (Walters et al. 2014; Keller & Guttridge 2013).

Finally, it has to be mentioned the sole genome-wide epigenetic study on RMS to our knowledge, that identified the differential DNA methylation patterns on rhabdomyosarcoma cell lines, normal tissues and tumor samples. Mahoney and colleagues identified that over 1,900 CpGi were hypermethylated in RMS tumors compared to normal muscles. These CpGi controlled genes involved in tissue development, differentiation and oncogenesis. Moreover, they identified that eRMS and aRMS cell lines presented distinct DNA methylation patterns. Most notably, aRMS cell lines presented most frequently DNA hypermethylation events in Polycomb target genes than eRMS ones (Mahoney et al. 2012).

3.3. Targeting genetics versus epigenetics in myopathies

As mentioned above, each cell of an organism carries almost an identical and constant information (genetics), meanwhile the epigenetic information differs between cell types and is highly modifiable by environmental factors.

Muscle dystrophies are mainly caused by genetic mutations and therefore, the only way to correct them is to change the DNA sequence at least in the cells within the organs affected by the mutated protein. This process traditionally uses DNA nucleases as genetic modifiers, in particular, zinc-finger nucleases (ZFNs)7–10 and transcription activator–like effector nucleases (TALENs) (Ran et al. 2013). In addition, DNA modification, known as genome editing, constitutes an indispensable tool for researchers working with model organisms, to demonstrate how changes in the genotype affect the phenotype (Gaj 2014). For that, DNA recombinases like Cre–loxP system have been widely used besides the mentioned nucleases (Capecchi 2005).

A revolutionary discover in the field of genome editing has been recently produced with the description of CRISPR/Cas system. CRISPR (clustered, regularly interspaced, short,

palindromic repeats)/Cas (CRISPR-associated) systems are RNA-based bacterial defense mechanisms designed to recognize and eliminate foreign DNA from invading bacteriophages and plasmids. The type II CRISPR is the most currently used and the best one characterized and consists of a Cas endonuclease and a crRNA (CRISPR RNA array), that contains a guide RNA and a trans-activating crRNA (tracrRNA). The guide RNA (sgRNA) is composed by 20 nt that pair with the DNA target directly upstream of a 5'-NGG adjacent motif (PAM sequence). This sgRNA directs the Cas9 protein to their target site, where it makes a double strand break about 3 bp upstream of the PAM, within the sgRNA DNA paired sequence. The structure of crRNA and Cas9 binding to its targets is illustrated on Figure 8.

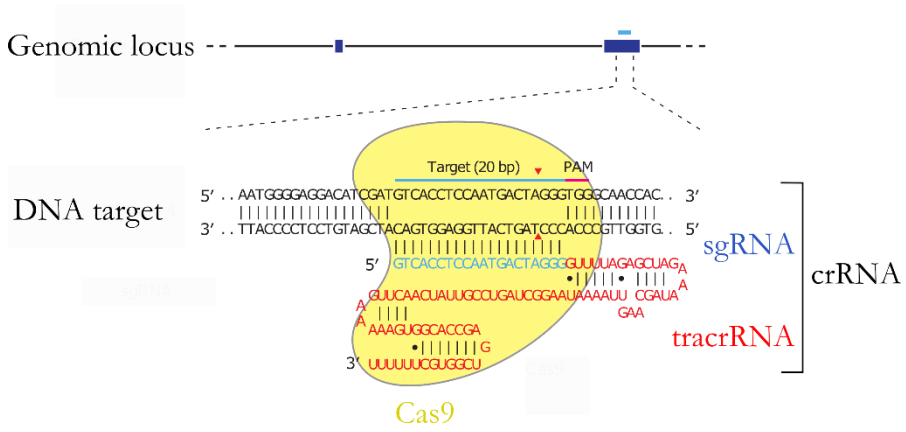

Figure 8. Representation of CRISPR/Cas9 editing components. In yellow is represented the Cas9 enzyme, which is guided to the DNA target sequence through specific pairing of the 20 nt conforming the sgRNA, in blue, which is attached to the scaffold RNA, in red, to form the tracrRNA. Cas9 will cleave DNA on the red triangles, generating a DSB about 3 bp upstream the PAM sequence (5'-NGG), represented in pink. Adapted from Ran et al. 2013.

After cleavage, the DSB can be repaired by two main pathways. The non-homologous end joining pathway consists on the religation of both DNA strands. It is the pathway most frequently triggered and is characterized by the appearance of deletion and insertion mutations in the site of religation. It is usually used by researchers to generate knock-outs as the deletions or insertions generated can change the frame of lecture of the gene affected and induce the use of premature stop codons. Also depending on the deletion size and its location, the resulting protein can be nonfunctional or non-stable. The other alternative DNA damage repair pathway is the homology-directed repair (HDR) pathway, which is the less frequently occurring one. It is a high-fidelity mechanism of repair that requires of

the existence of a complementary repair template. It is used by researchers to precisely introduce point mutations or small exogenous insertions within a sequence (Ran et al. 2013).

The quickly extension of the use of CRISPR system by researchers has been possible thanks to the availability of plasmids on public repositories, the excellent protocols available, the existence of dedicated resources for common questions and doubts and the relatively easy techniques required to obtain engineered cells. Moreover, compared with other endonucleases, CRISPR presents a system easier to design, more efficient and specific, that allows high throughput editing in all kinds of organisms (Ran et al. 2013).

CRISPR technology, has already been successfully used to cure leukemia in a child (Reardon 2015) and is currently undergoing their firsts clinical trials (Reardon 2014; Reardon 2016). Regarding muscle diseases, CRISPR has already been effectively applied to mdx mice model to edit germline cells (Long et al. 2014). The difficult to use it in patients is that instead of editing germline cells, all or at least a substantial part of the somatic cells of the affected organs have to be modified. Even if CRISPR techniques are capable of precisely edit DNA, they still require the use of a delivering vehicle for solid tissues that needs to be safe and that efficiently delivers the system to the nucleus. The use of viral and non-viral delivering particles are still being optimized (Munshi 2016; Wang et al. 2016).

Opposite to genetics, the characteristic of epigenetic mechanisms is that they could be modified by the use of epigenetic drugs. Epigenetic drugs target epigenetic enzymes responsible for the deposition or erasing of the corresponding marks. The first epigenetic drug approved by FDA was 5-Azacytidine (Vidaza) in 2004, and in 2006 its variant 5-aza-2'-deoxycytidine was also approved (Dacogen) (de Lera & Ganesan 2016). These two drugs are cytosine analogous, that are incorporated in the DNA instead of cytosine residues and they both inhibit DNA methyltransferases. The other epigenetic drugs approved for human treatment mediate its effect by inhibition of Histone deacetylases (HDAC) activities. HDAC enzymes and HDAC inhibitors (HDACi) will be specifically discussed on the next sections. Regarding myopathies, it was particularly remarkable the finding in 2006 that HDACi ameliorate the pathological phenotype of mdx mice (Minetti et al. 2006). This was an outstanding finding since DMD has no effective treatment or cure. Currently, the HDACi ITF2357 (givinostat), is in clinical trials for DMD (Bettica et al. 2016; Consalvi et al. 2013).

Regarding rhabdomyosarcoma, HDACi are not yet being used in patients but they are being used in the cancer types listed on Table 3. Nowadays, HDACi are considered very potent and promising drugs, as treatment with HDACi changes about 10% of gene expression of the cells, including genes controlling cell cycle and apoptosis, production of reactive oxygen species, angiogenesis and metastasis, and affecting also the acetylation levels of key proteins such as p53 (Seto & Yoshida 2014). They also have a role as immunomodulators and can be used in synergistically combinations with other cancer treatments. Understanding the specific functions of each HDAC in physiological processes may be key to determine not only the consequences of HDAC dysregulation in disease but also the adverse effects of HDACi when used for therapy (Seto & Yoshida 2014; Bolden et al. 2006).

For that, in the next sections we will specifically focus on HDAC family members and their functions, making a specific emphasis on muscle processes.

Compound name	**Commercial name**	**Year of approval**	**Disease**
5-azacytidine	Vidaza	2004	Myelodysplastic syndrome
5-aza-2'-deoxycytidine	Dacogen	2006	Myelodysplastic syndrome
SAHA	Vorinostat	2006	Cutaneous T-cell lymphoma
FK228	Romidepsin	2009	Cutaneous T-cell lymphoma
PXD101	Belinostat	2014	Peripheral T-cell lymphoma
LBH-589	Panobinostat	2015	Multiple myeloma
CS055	Chidamide	2015	Peripheral T-cell lymphoma
MS-275	Entinostat	Clinical trials	Non-small cell lung cancer, melanoma, ovarian and breast cancers.

Table 3. Epigenetic drugs approved for human therapy. Adapted from: (de Lera & Ganesan 2016)

4. Histone deacetylases

Histone acetylation was one of the first histone modifications discovered and therefore, is one of the most well studied (Seto & Yoshida 2014). It consists in the addition of an acetyl group to lysine residues of histones. The best known modification occurs on ε-lysine residues of the N terminal domain of histones, although acetylation in the core domain of histones have also been reported (Tessarz & Kouzarides 2014).

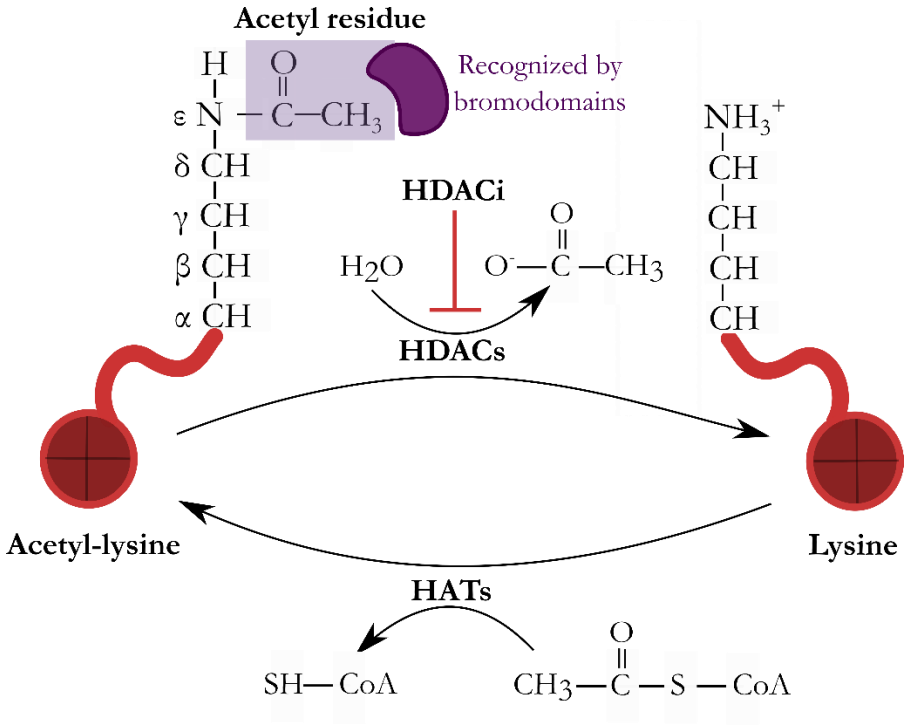

Figure 9. Mechanism of deacetylation by classical HDACs. Proteins like histones are frequently acetylated in ε position of lysine residues. This modification is reversible as histone deacetylases (HDACs) can catalyze the removal of the acetyl group releasing acetate. On the contrary, the acetylation reaction is carried out by histone acetyltransferases (HATs) which catalyze the transfer of the acetyl group from acetyl-coenzyme A. The acetyl group not only acts neutralizing the positive charge of the N lysine residue but can be recognized by bromodomain containing proteins. Adapted from: (Yang & Seto 2008; Yang et al. 2010).

Traditionally, acetylation has been seen as an activating mechanism of gene expression. The addition of the acetyl group to histones neutralizes the positive charge of the amino group, decreasing its electrostatic interaction with DNA and relaxing the chromatin structure (Workman & Kingston 1998). Moreover, acetylation modification itself can be read by bromodomain and tandem PHD domain containing proteins, that can further enhance gene expression (Yun et al. 2011). Therefore, recently, the first acetylation

modification with repressing properties has been described (Kaimori et al. 2016). This finding may indicate that acetylation depending mechanisms of gene expression could be more complex than previously thought and that perhaps, more modified residues remain to be discovered.

Histone acetylation is a dynamic modification that can be reversed by histone deacetylases (HDACs). HDACs were discovered in 1969 (Inoue & Fujimoto 1969) and its name comes from their capability to deacetylate histones, the proteins that were considered as their main targets (Dokmanovic et al. 2007). Nowadays, thousands of acetylation sites have been identified and the use of the more precise name "lysine deacetylases" (KADs) has been proposed to make reference to the widely number of substrates they can deacetylate (Falkenberg & Johnstone 2014; Choudhary et al. 2009). Notably, more than 3,600 acetylation sites have been identified on 1,750 proteins, not only directly regulating their functions but competing on the same residues with another modifications, like ubiquitination which promotes its degradation (Choudhary et al. 2009; Seto & Yoshida 2014). For all these important roles besides histone deacetylation, we agree that KDAC is a more appropriate nomenclature of this class of enzymes, but we will use from now on use the old terminology for being still the most widespread.

In mammals, 18 HDACs exist. They are divided into two families, the Zn^{2+} dependent or classical HDACs, and the nicotinamide adenine dinucleotide (NAD^{+}) dependent or sirtuins. Zn^{2+} dependent HDACs are divided into three classes, according to the homology of their catalytical domain to *Saccharomyces cerevisiae* HDACs. Class I HDACs are homologous to yeast RPD3 while class II HDACs share homology with yeast HDA1 (Grozinger et al. 1999). HDAC11 show both homology to class I and II HDACs, but neither enough to be classified in any of them, so a class IV was created to place it. The name of each HDAC member was given according to their moment of discovery, being HDAC1 the first discovered in 1996, and HDAC11 the last, in 2002 (Seto & Yoshida 2014). Class III is reserved for the aforementioned sirtuins which are homologous to the yeast Sir2. From now on, we will focus on classical HDACs, also named HDACs. Their classification and main structural characteristics are summarized on Figure 10.

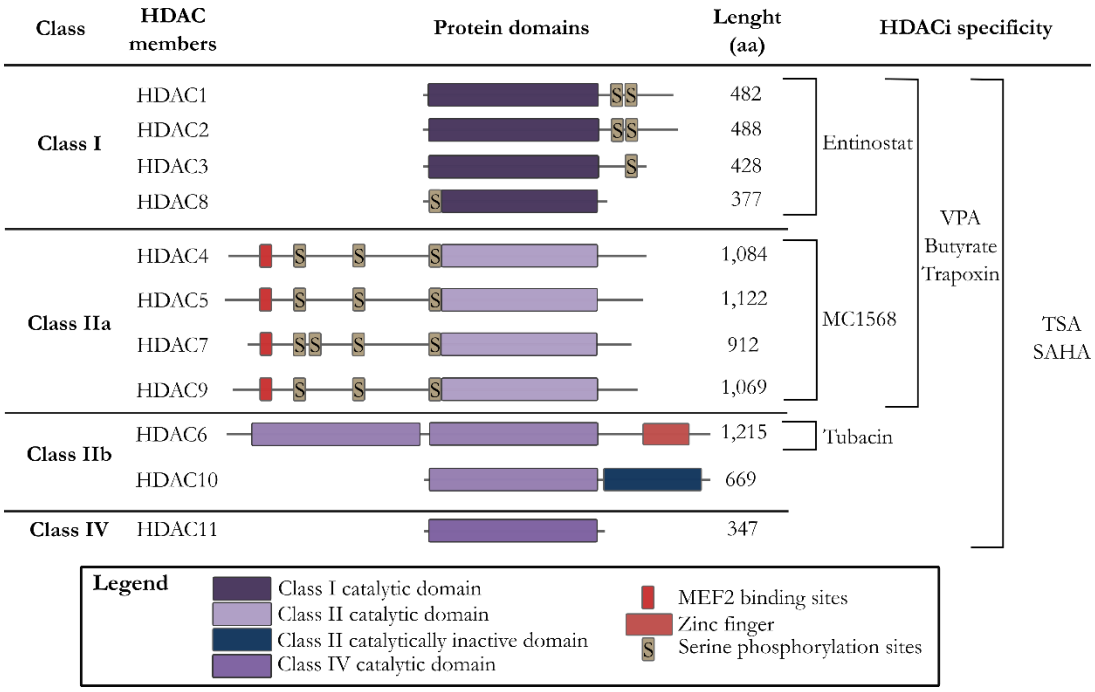

Figure 10. HDAC members' classification. Schematized are classical HDAC members with their principal protein domains, length and most used HDACi they are inhibited with. For HDACs with more than one isoform only the longest is represented for simplicity. Adapted from: (Bolden et al. 2006; Haberland, Montgomery, et al. 2009).

All HDACs were originated from a common ancestor dating to prokaryotes, which diverged and gave rise to the precursors of the three classes. The appearance of HDACs was before histone proteins, suggesting that their primary activity was not epigenetically related (Gregoretti et al. 2004). All HDACs share the same catalytic activity by which a zinc cation mediates the hydrolysis of the acetamide bond of the acetylated lysine (Seto & Yoshida 2014) (illustrated on Figure 9). Another common feature is that any HDAC possess any DNA binding domain in its coding sequence, thus, any common DNA binding motif has been identified for any HDAC. Moreover, most HDACs have been found to be poorly active when purified alone. These observations are explained by the fact that they exert their full activity by acting as a part of multiprotein complexes, which guide them to their specific substrates. This characteristic makes quite difficult the identification and attribution of their specific substrates to each HDAC. In addition, the variety of HDAC proteins suggest that up to a certain point, they may have compensatory roles and overlapping substrates (Seto & Yoshida 2014), at least among the ones that share greatest degrees of homology: HDAC1 and HDAC2, HDAC4 and HDAC5, and HDAC6 and HDAC10 (Haberland, Montgomery, et al. 2009).

4.1. HDAC classes. The differences beyond the homology

Besides the shared catalytical function of their common domains, HDACs have many structural, functional and biological differences. In this section, we will center in the structural characteristics of HDACs, while their functions, making special emphasis to skeletal muscle, will be discussed on the following sections.

Class I

Class I contains 4 members: HDAC1, 2, 3 and 8. As an oversimplification, class I members are considered to be mainly nuclear and obliquus (or expressed in many cell types), in contraposition to class II. Nevertheless, many works locate HDAC1 and 2 also in the cytoplasm of some cell types and in particular moments (Seto & Yoshida 2014). For example, HDAC1 in axonal degeneration (Kim & Casaccia 2010) and HDAC2 during terminal keratinocyte differentiation (Jung & Bakin 2008; Kelly & Cowley 2013).

Class I HDACs are the members which possess the highest activity towards histone substrates (Haberland, Montgomery, et al. 2009) and they control crucial cellular processes like cell survival and proliferation. Thus, their absence is often highly deleterious (Dokmanovic et al. 2007).

HDAC1 and HDAC2 share great homology and frequently show redundant roles (Montgomery et al. 2007). They share homology in their C-terminal tail, which contains tandem casein kinase-2 (CK2) phosphorylation sites, which should be phosphorilated to activate their HDAC activity (Yang & Seto 2008). HDAC1 and HDAC2 exert its function integrated in three protein repressive complexes: SIN3, nucleosome remodeling deacetylase (NuRD) and corepressor of RE1-silencing transcription factor (CoREST) (Seto & Yoshida 2014). These complexes interact with DNA sequence-specific transcription factors to repress transcription and cooperate with other chromatin modifiers to shape epigenetic programs (Yang & Seto 2008).

HDAC3 differs from its other class parterns because shuttles between the nucleus and the cytoplasm in a CRM1 (exportin) mediated pathway and has only one activating phosphorilation site. It acts in SMRT/NCoR repressive complexes (Yang & Yao 2011; Yang & Seto 2008).

HDAC8 is the most divergent HDAC of class I. It has only one phosphorilable site that when phosphorilated represses its activity (Yang & Seto 2008). Many of their partners have been discovered but by now it has been difficult to determine if they act as a cofactors or if are actually substrates (Wolfson et al. 2013).

Class II

Class II is further subdivided into 2 subclasses, IIa and IIb.

Class IIa

Class IIa is integrated by four members, HDAC4, HDAC5, HDAC7 and HDAC9. In contrast to class I and IIb enzymes, they are inactive towards acetylated residues, or at least, 1,000 folds less active than HDAC1. This loss of activity is due to the replacement of a conserved tyrosine of the HDAC catalytic domain, that acts as a transition-state stabilizer, by a histidine (Lahm et al. 2007). Therefore, they are found in a multiprotein complex containing HDAC3 and SMRT/N-CoR (silencing mediator for retinoid and thyroid receptor) in which HDAC3 is the enzyme responsible for the deacetylase activity of class IIa HDACs (Schuetz et al. 2008; Fischle et al. 2002).

Class IIa HDAC proteins are much bigger than Class I (1,000 aa on average) and contain additional regulatory domains in addition to their deacetylase motif, which is located in the C terminal end. They all share the following structural characteristics that mediate its repression activities and functions. The N-terminal domain is conserved in all IIa members and contains binding sites for MEF2 proteins, transcriptional corepressors like HP1, and the SUMO-conjugating enzyme Ubc9 (Simmons et al. 2011). In addition, they contain 3 phosphorylable sites by six groups of kinases: calcium/calmodulin-dependent protein kinase (CaMK), protein kinase D (PKD), microtubule affinity-regulating kinases, salt-inducible kinases, checkpoint kinase-1 and AMP-activated kinases (Seto & Yoshida 2014). The binding sites for MEF2 usually repress MEF2 mediated transcription in basal conditions, but when HDAC serines are phosphorylated by kinases, they are displaced from MEF2 binding and they are able to bind to the chaperone protein 14-3-3 and be exported from the nucleus to the cytoplasm.

All these docking binding sites, modifications and shuttling make class IIa susceptible of many regulatory mechanisms and moreover, sensitive to extracellular transmitted stimuli (Haberland, Montgomery, et al. 2009). Another layer of regulation within this class is tissue specific expression. Most abundantly, HDAC5 and HDAC9 are expressed in skeletal muscles, brain and heart. HDAC4 is expressed in brain and growth plates of the skeleton, and HDAC7 in endothelial cells and thymocytes.

HDAC9 constitutes a particular complex example of tissue specific protein expression and alternative splicing. Their different isoforms shown different subcellular and tissue specific

expression (Petrie et al. 2003). A particular spliced variant of HDAC9 lacks its catalytic domain and is named MEF2-interacting transcription repressor (MITR) or Histone deacetylase-related protein (HDRP). Surprisingly, MITR has the same repressive activity towards MEF2 than full length containing HDAC9, further indicating that the catalytic activity of class IIa HDACs is dispensable for their repressive activity (Haberland, Montgomery, et al. 2009).

Class IIb

Class IIb is integrated only by two members: HDAC6 and HDAC10. Both contain an additional catalytic domain to the HDAC domain, not found in any other HDAC, and they present a preferential cytoplasmatic location (Seto & Yoshida 2014).

HDAC6, in addition to its two HDAC catalytic domains, presents a C terminal zinc finger that can bind ubiquitin (Yang & Seto 2008). Is located mainly in the cytoplasm of cells, where it deacetylates the cytoskeletal proteins α-tubulin and cortactin, transmembrane proteins and chaperones (Haberland, Montgomery, et al. 2009).

The other class IIb member, HDAC10, has an N-terminal HDAC domain half of which is highly similar to the first deacetylase domain of HDAC6, while the C-terminal half is leucine rich (Yang & Seto 2008). It also contains a nuclear location signal and two putative retinoblastoma (Rb) binding domains, which suggest a role in cell cycle regulation (de Ruijter et al. 2003). It is only present in vertebrates and is one of the less studied HDACs (Yang & Seto 2008), being the only HDAC where none knock-out has been reported yet.

Class IV

HDAC11 is the sole member of Class IV. It was the latest discovered, identified by Basic Local Alignment Search tool by Lin Gao and colleagues (Gao et al. 2002). It is the smallest HDAC, and has only 347 aa both in mouse and human. The 90.2 % of its sequence corresponds to its HDAC domain, with a very small N and C terminal extensions. HDAC11 has not still being described as affected by any posttranslational modification. By now, it has not been identified in any of the multiprotein associated complexes described for the other HDACs, but it binds to HDAC6. Together with HDAC10, remain still the least understood HDAC members (Seto & Yoshida 2014; Gao et al. 2002).

4.2. HDAC inhibitors in myogenesis

The first experiments addressing the role of HDACs in myogenesis where made upon the discovery of HDAC inhibitors (HDACi). HDACi have constituted an invaluable tool in both demonstrating the deacetylation capacity of HDAC members and also to assess their biological functions. The specificity of the most used HDACi are illustrated in Figure 10.
Among HDACi, we can distinguish between:
- Pan-HDACi, which are non-specific and inhibit all HDAC classical classes (not sirtuins). The most used ones are Trichostatin (TSA) and Valproic acid (VPA).
- Class-specific HDACi: The most numerous class specific HDACi have been found for Class I HDACs. Among them, the most known are butyrate, suberoylanilide hydroxamic acid (SAHA, also known as vorinostat) and FK228 (romidepsin). There is also an HDACi specific for class IIa, MC1568. For classes IIb and IV, none specific inhibitor has been described yet.
- Selective HDACi: By now, there is only one, tubacin, which specifically inhibits HDAC6 (Gryder et al. 2012; Xu et al. 2007; Nebbioso et al. 2009). None other HDAC members have a selective HDACi.

4.2.1. HDACi in prenatal myogenesis

Due to the necessary use of animal model for these studies, there are few works using HDACi during prenatal myogenesis. It has also to be pointed out that the results observed differ depending on the moment of use of the HDACi and the moment of phenotypic inspection.
In *Xenopus* embryos, when thrichostatin (TSA) is applied before gastrulation, it inhibits MYOD transcription and muscle differentiation, indicating a necessary HDAC activity in the early steps of myogenesis for the induction of MYOD dependent lineage (Steinbac et al. 2000). On the contrary, when mouse embryos where treated latter on, during somitogenesis (E8.5 and killed on E9.5), showed more and larger somites with more H4ac present (Nervi et al. 2001). According to this result, both TSA and Valproic acid (VPA) treatment in mouse embryos at post implantation stages (E8.5) and killed at E10.5, resulted in a transient increase in the number of somites and a higher expression of endogenous muscle-specific genes whose expression was driven by MYOD, with also more H4ac present (Iezzi et al. 2002). An study with mouse pluripotent stem cells derived to muscle lineage also showed an enhanced formation of skeletal myocytes and an increase on H3K9ac and H3K14ac upon VPA treatment (Q. Li et al. 2014).

Taken together, these results indicate a role for HDAC members in embryonic myogenesis and cell specification.

4.2.2. HDACi and muscle cell proliferation and differentiation

The first study on the global acetylation levels changes between muscle proliferation and differentiation conditions was performed by Asp and colleagues. In this work, they shown that muscle differentiation occurs with a global decrease in histone acetylation levels, specifically in H3K9ac, H3K18ac and H4K12ac. Moreover, acetylation was the histone posttranslational modification studied that changed the most its levels between confluent myoblasts and purified myotubes differentiated for 4 days, while global changes on H3K4me3, H3K36me3 or H3K27me3 were not detected (Asp et al. 2011).

The works of many groups using different HDACi in muscle cell cultures and at different times of treatment, have provided very strong data regarding the importance of the acetylation levels, both in proliferation and differentiation states. Most notably, these studies have revealed the divergence of HDACi mediated effects depending on the moment of treatment (illustrated in Figure 11).

When HDACi are applied to myoblasts in proliferation conditions and afterwards they are removed from the media and the cells are switched to differentiation conditions, HDACi enhance muscle differentiation, cell fusion and increase myotube size. They also promote the expression of higher levels of the differentiation markers MEF2, MHC and MCK, although they decreased the expression of MYOG (Hagiwara et al. 2011; Iezzi et al. 2002). However, HDACi treatment does not cause spontaneous differentiation of cells if permissive conditions, like serum deprivation, are not present. Specifically on MHC enhancer, HDACi increase its acetylation levels but this effect is not sufficient to activate its expression in cycling conditions (Blau & Epstein 1979).

On the contrary, when HDACi are added in the differentiation medium deprived of serum, cells present a reversible inhibition of differentiation (Blau & Epstein 1979; Fiszman et al. 1980; Iezzi et al. 2002; Terranova et al. 2005). In these works, it is observed a reduced expression of the differentiation markers like creatine phosphokinase (CPK) acetylcholine-esterase, α-actin, acetyl-choline receptor protein (Blau & Epstein 1979), MYOD (Johnston et al. 1992), MYOG and MHC (Iezzi et al. 2002) and also apoptosis of cells (Iezzi et al. 2002).

Furthermore, if the HDACi is added when the cells have already started to differentiate, differentiation is not affected (Terranova et al. 2005). In this study, only MRF4 expression

was delayed, but an irreversible centromere clustering was observed, indicating that at early stages of muscle differentiation HDAC activity is crucial for establishment and maintenance of constitutive heterochromatin. (Terranova et al. 2005).

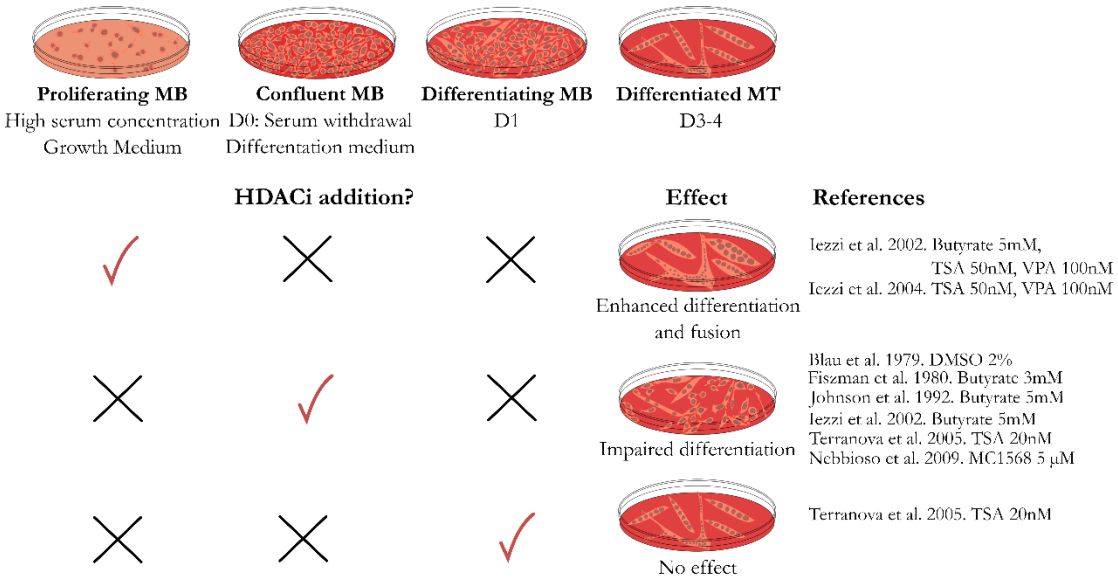

Figure 11. HDACi effects in muscle differentiation depend on the moment of treatment. On top is schematized a typical muscle differentiation *in vitro* time course from proliferating myoblasts which when reach high confluency levels and promoted by serum withdrawal from the medium start to differentiate and ultimately fuse. In the lower part are represented the effects mediated by the indicated HDACi treatments (Effect) at the corresponding moments of treatment (✓). ✗: Not HDACi present in the medium.

All these described studies were performed with Class I specific HDACi or pan-HDACi. An study using class IIa specific HDACi found reduced expression of MGN and α-MHC markers caused by decreased MEF2D expression and stabilization of HDAC4-HDAC3-MEF2D complex (Nebbioso et al. 2009). HDAC6 selective inhibition through tubacin treatment prior to differentiation and maintained through differentiation conditions also impaired MGN expression mediated by FAM65B protein down-regulation (Balasubramanian et al. 2014).

4.3. Functions of HDAC family members in myogenic processes

The generation of knock-out mice lacking HDAC genes has revealed specific functions for individual HDAC members during development and adulthood (Haberland, Montgomery, et al. 2009; Kim & Bae 2011). The most relevant HDAC phenotypes found by total deficient

mice generation are summarized in Table 4. Globally, the suppression of class I HDACs is more deleterious to mice survival than class II, which tend to control more tissue specific programs. HDAC6 (Y. Zhang et al. 2008) and HDAC11 (Villagra et al. 2009; Sahakian et al. 2017; Woods et al. 2017; Gutiérrez 2012) total deficient mice are the only ones with no phenotypes associated yet. Importantly, HDAC activities are involved in each step of myogenesis, although due to the lack of muscle conditional knock-outs and HDAC10 knock-out, probably more specific roles of HDACs in muscle processes remain to be discovered.

Specifically focusing on myogenesis, in general, it should be pointed out that while class I HDACs mainly act as repressors of MYOD dependent expression both during embryonic myogenesis (HDAC1 and HDAC2) (Cho et al. 2015; Ohkawa et al. 2006) and postnatal myogenesis (HDAC1) (Mal et al. 2001; Puri et al. 2001; Mal & Harter 2003); class II members mainly repress MEF2 dependent transcription, as indicated by their dedicated binding domain (Potthoff et al. 2007; Zhang et al. 2001; Lu et al. 2000; Haberland et al. 2007).
MYOD repression by HDAC1 is probably the best characterized mechanism of MRF regulation. In proliferating myoblasts, MYOD is expressed both at RNA and protein levels, but its differentiation capabilities are directly repressed by deacetylation, as deacetylated MYOD is not able to activate the transcription of its target genes (Mal et al. 2001; Mal & Harter 2003). HDAC1 is also present in proliferation conditions bound to differentiation genes regulatory regions, deacetylating histones of MYOG, MYH10 and MCK the promoters (Mal & Harter 2003), while HDAC2 represses MCK and DES promoters (Ohkawa et al. 2006). Differentiation signals like serum deprivation, induce downregulation of HDAC1 expression and dephosphorylation of pRb (phospho-retinoblastoma), that binds to HDAC1 displacing it from MYOD, that becomes available to be acetylated by P/CAF and form heterodimers with the E-proteins E2A, E2-2 or HEB, to activate the expression of differentiation genes (Puri et al. 2001; Mal et al. 2001; Lassar et al. 1991).

Class IIa HDACs HDAC4, HDAC5 and the catalytically defective MITR, act by direct repression of MEF2. In proliferating myoblasts, they are bound to MEF2 in the nucleus preventing the transcription of their promoters (Zhang et al. 2001; Lu et al. 2000) and allowing the recruitment of heterochromatin protein 1 (HP1), that methylates H3K9 of MEF2 target promoters, repressing them (Zhang, McKinsey & Olson 2002). Under differentiation conditions, class IIa HDACs are phosphorylated by calcium/calmodulin kinases and exported to the cytoplasm, causing its dissotiation from HP1 and releasing MEF2

to bind to p300/CBP and mediate the acetylation of their target genes involved in muscle differentiation and promoting their expression (Zhang, McKinsey & Olson 2002).

In this manner, HDAC members directly and epigenetically repress MRF action until differentiation stimuli trigger the differentiation program. Their control of myogenic expression explain the apparent paradoxical observation that MYOD is present in proliferation but do not activate their genes at this stage, even being expressed at the protein level and be already bound to its promoters (Weintraub 1993). Epigenetic control of differentiation also explains the sequential binding of MRFs to their binding sites. Even E-boxes present a common consensus sequence, MYOD activates early differentiation genes like MYOG in a first step, but also late ones like MCK later on. This temporal E-box activation by the binding of the same MRFs is explained by epigenetic mechanisms (Cho et al. 2015) like the local increase of H4 acetylated histones upon differentiation in the promoters of late differentiation genes (Cao et al. 2010) both by the downregulation of HDAC1 upon differentiation and the export of class IIa HDACs from the nucleus. Nevertheless, many mechanisms still remain to be elucidated, as the that the decrease in nuclear HDAC activity do not explain the aforementioned global decrease of histone acetylation observed during muscle differentiation, that remains to be clarified (Asp et al. 2011).

But myoblast differentiation it is not the only process that HDAC family members control. Class IIa HDACs, that are sensitive to external stimuli, have a key and redundant role between them to regulate fiber type composition in adult muscles (Potthoff et al. 2007).

Total knock-out	Phenotype	Related disease
HDAC1	Lethal at E9.5 with proliferation defects and retarded development (Lagger et al. 2002; Montgomery et al. 2007; Zupkovitz et al. 2010).	Muscle atrophy during nutrient deprivation and disuse (Beharry et al. 2014).
HDAC2	Controversial: lethal 24h after birth (Montgomery et al. 2007) and viable (Trivedi et al. 2007).	Cardiac malformations(Montgomery et al. 2007).
HDAC1 & HDAC2	Lethal 10 days after birth in 40% of offspring (Moresi et al. 2012).	Myopathy (Moresi et al. 2012).
HDAC3	Lethal at E9.5 with gastrulation defects (Montgomery et al. 2008).	Cardiac failure (Sun et al. 2011).
HDAC8	Perinatal lethality by skull malformations (Haberland, Mokalled, et al. 2009).	NO
HDAC4	Lethal before weaning (Vega et al. 2004).	Skeletal: chondrocyte hypertrophy and premature ossification (Vega et al. 2004).
HDAC5	NO. Viable (Chang et al. 2004).	Cardiac hypertrophy (Chang et al. 2004).
HDAC7	Lethal at E11 by loss of endothelial cell interactions and hemorrhage (Chang et al. 2006).	Vascular disorders (Chang et al. 2006).
HDAC9	Viable (Morrison & D'Mello 2008; Zhang, McKinsey, Chang, et al. 2002). Cardiac defects (Chang et al. 2004).	Cardiac (Zhang, McKinsey, Chang, et al. 2002).
HDAC6	NO. Viable (Y. Zhang et al. 2008).	NO
HDAC10	ND	ND
HDAC11	NO.(Villagra et al. 2009; Sahakian et al. 2017; Woods et al. 2017; Gutiérrez 2012).	NO

Table 4. Principal phenotypes of HDAC family members total knock-out mice. For the sake of simplicity only total and not conditional mice are indicated. NO: not observed. ND: Not described

5. HDAC11, the lone HDAC

As mentioned above, HDAC11 was the latest member of the HDAC family to be described. It is highly conserved from *C. elegans* and *D. melanogaster* to humans, with related proteins present in bacteria and plants (NCBI n.d.; Yang & Seto 2008). When HDAC11 was described, it was reported its preferential tissue expression in skeletal muscle, heart, brain, kidney and testis in humans, suggesting that it may have specific functions in this tissues (Gao et al. 2002). Regarding its HDAC activity, it seems that HDAC11 has intrinsic deacetylase capability as it has been described that is capable of deacetylate H4 peptides (Gao et al. 2002) and H3 and H4 lysine residues (Cheng et al. 2014; Kim et al. 2013; Liu et al. 2007; Villagra et al. 2009), albeit in contrast to the other HDAC members it has not been identified as a part of any known repressor complex.

Although HDAC11 was identified 15 years ago, very few data has been published regarding its functions. In this section it will be summarized what is known so far.

5.1. Cellular location of HDAC11

Distinct locations depending on the cell type studied have been reported for HDAC11 protein. In its first descriptive paper, it was shown that human HDAC11-Flag overexpressed in 293 human fibroblasts was exclusively nuclear (Gao et al. 2002). In mature monoaminergic and neuropeptidergic neurons, endogenous murine HDAC11 was observed in both the nucleus and cytoplasm of almost all neurons (Takase et al. 2013), while on specific mouse dentate gyrus neurons of the hippocampus, endogenous HDAC11 exhibited nuclear, perinuclear, and cytoplasmic localization (Watanabe et al. 2014). During murine optic nerve development, HDAC11 showed a curious distribution. In embryonic day 16, in astrocyte precursors, it was found predominantly in the cytoplasm. Five days after birth, in immature astrocytes and oligodendrocytes, HDAC11 was found both in the nucleus and the cytoplasm; and 30 days after birth, when the cells are mature, it was again only located in the cytoplasm, suggesting a nuclear control of differentiation only in immature cells (Tiwari et al. 2014).

In human T cells, endogenous HDAC11 was located both in the nucleus and the cytoplasm, concentrated in the perinuclear region (Joshi et al. 2013). Endogenous HDAC11 in resting $CD4^+$ T cells from a HIV-1^+ patient was exclusively cytoplasmatic (Keedy et al. 2009), while murine overexpressed Flag-HDAC11 in RAW264.7 mouse immortalized macrophages was localized mainly in cytoplasm but was also present in the nucleus (Cheng et al. 2014).

5.2. Tissue specific effects of HDAC11

As indicated on Table 4, the two generated total KO mice of HDAC11 are viable, fertile and do not present apparent phenotypic defects. None conditional or tissue specific KO mice have been reported.

For the aforementioned highly expressing HDAC11 tissues, the role of HDAC11 has only been addressed in three on them, and specifically, the most part of the works addressing HDAC11 distribution and roles published are in brain. In a comparative study of the expression levels of all HDAC members' expression in brain, HDAC11 was found as the most expressed HDAC by far. It was present in almost all brain regions, being in the Purkinje cells the only HDAC expressed. Notably, in the hippocampus, HDAC11 showed a high expression, suggesting a putative role in learning and memory (Broide et al. 2007; Takase et al. 2013). In addition, specifically on hippocampus region, the expression of HDAC11 was high in the dentate gyrus neurons (Liu et al. 2007), where overexpression of HDAC11 increases the length and the complexity of dendrites, and facilitates the maturation of postnatally born dentate granule neurons (Watanabe et al. 2014)

In developmental mouse brain, HDAC11 expression correlates with the maturation of oligodendrocytes and neurons (Liu et al. 2007). Specifically in oligodendrocyte development, HDAC11 favors their development and specific gene expression. Downregulation of HDAC11 expression in these cells, increases H3K9ac and H3K14ac globally and in the myelin basic protein (MBP) and proteolipid protein genes (PLP), both oligodendrocyte differentiation key genes, and reduces the morphological changes associated with oligodendrocyte development (Liu et al. 2009).

In kidney, the role of HDAC11 has been described in ischemia/reperfusion (I/R)-induced renal injury. It was previously noticed that male mice are more susceptible to renal ischemia/reperfusion induced injury than females due to testosterone production. Kim and colleagues revealed that the effect of testosterone in renal injury was mediated by downregulation of HDAC11 expression. The lack of HDAC11 activity in PAI-1 promoter, leads to an increase of H3 histone acetylation and expression of PAI-1. PAI-1 (Serpin1), is a serine protease inhibitor involved in fibrinolysis, inflammation and production of extracellular matrix proteins that when overexpressed, enhances the I/R-induced renal injury (Kim et al. 2013).

Regarding the function of HDAC11 in testis, HDAC11 knock-out were fertile and did not present alterations in meiosis, showing only an enhanced expression of olfactory receptors (Gutiérrez 2012, unpublised data).

Regarding heart and skeletal muscle tissues, none of them have been analyzed in detail in the knock-out mice yet.

In addition of these tissues, interestingly, they are several papers describing the role of HDAC11 in immune system cells. Most remarkable, a function for HDAC11 was reported in the repression of Il-10 promoter in antigen-presenting cells (APC), regulating T-cell activation and tolerance. Villagra and colleagues demonstrate that HDAC11 controls the acetylation state of H3 and H4 in the distal segment of Il-10 promoter in lipopolysaccharide (LPS) treated RAW264.7 immortalized macrophages, primary mouse macrophages and human APCs, repressing Il-10 when overexpressed. This effect is depending on its HDAC activity as overexpression of catalytically deficient HDAC11 cannot repress Il-10 expression (Villagra et al. 2009). In a latter work, the same group also shown that the control of Il-10 expression not only relies on HDAC11 activity but its association with HDAC6. Both HDACs are recruited to Il-10 promoter after LPS stimuli and HDAC6 presence is sufficient to promote Il-10 expression. When overexpressed, HDAC11 represses Il-10 expression, but when HDAC11 is not present or downregulated, the increased expression of Il-10 is dependent on HDAC6 activity (Cheng et al. 2014).
The promoter of Il-10 is not the only case where HDAC6 and HDAC11 have been reported to be bound together but it has also been described that both HDACs associate with the Vitamin D3 Receptor (VDR) to regulate the expression of MYC in normal prostate cells (Toropainen et al. 2010; Cheng et al. 2014). Further studies are needed to address the extent to which both HDACs participate together or separately in the regulation of gene promoters.
An additional article about Il-10 production unraveled an additional layer of control of Il-10 expression by miR-145, which through targeting HDAC11 promotes Il-10 expression (Lin et al. 2013). Notably, the modulation of mediated HDAC11 regulation of Il-10 expression may represent clinical benefits as in organ transplantation (Lai et al. 2011), allergies (Li et al. 2016), asthma (Zhang et al. 2015) and infections (Mukherjee et al. 2014).
In other immune system cells, T-cells, HDAC11 deficiency causes the overexpression of inflammatory cytokines (Woods et al. 2017).

5.3. HDAC11 and cell proliferation

Besides being described in differentiated cells and rarely colocalized with Ki67 positive cells in brain differentiation (Liu et al. 2007; Bagui et al. 2013), HDAC11 has also been described to participate in proliferation and cell cycle processes by direct deacetylation of bound proteins in gene promoters. Specifically, it was shown that HDAC11 binds to CTD1 and repress MCM loading to DNA replication origins in S phase (Wong et al. 2010). It also binds and deacetylates the dual phosphatase CDC25A, a key regulator of cell cycle progression. Briefly, DNA damage increases CDC25A acetylation, which triggers changes in cell cycle progression to allow DNA repair. Alteration in acetylation status can impair this control of cell cycle by CDC25A and lead to diseases like cancer (Lozada et al. 2016).

5.4. HDAC11 and cancer

The putative involvement of HDAC11 in cancer was first announced in its first describing paper, where the authors asses the expression of HDAC11 in normal and four cancer cell lines, finding HDAC11 present in all the cancer cell lines studied, and very notably, showing its highest expression in the rhabdomyosarcoma cell line Sjrh30 (Gao et al. 2002). Furthermore, several years after, it was pointed that the genomic location of HDAC11, the chromosomal band 3p25 in humans, presented chromosomal alterations in many cancer types, by frequency, lymphomas (83/300 cases), acute leukemia (78/300 cases), adenocarcinomas (41/300) and sarcomas (29/300) (Voelter-Mahlknecht et al. 2005), although it did not present mutations in pancreatic tumors (Lindberg et al. 2007), gastric and colorectal carcinomas with microsatellite instability (Song et al. 2010).

The most influential work in the role of HDAC11 in cancer came from Deubzer and colleagues who reported that HDAC11 is overexpressed in mixed lobular and ductal breast, hepatocellular and urothelial carcinomas. Most interestingly, they shown that HDAC11 downregulation or its catalytically inhibition, is sufficient to cause cell death and inhibit metabolic activity in many types of cancer cells, while non-affecting normal ones *in vitro* (Deubzer et al. 2013). This promising specific antitumoral effects observed would require for their therapeutically use the development of specific class IV inhibitors.

Besides these direct effects on tumoral cell processes, as in physiological responses, crucial roles for HDAC11 in organism immune response and tumor environment have been reported (Buglio et al. 2011; Sahakian et al. 2015).

As a summary, the main reported interacting proteins and promoters deacetylated by HDAC11 are indicated on Table 5. Particularly interesting is the study of Joshi and colleagues, who for the first time described an interactome of HDAC11. In this work they found that in human T-cells, HDAC11 binds to several components of SMN complex (SMN1, GEMIN3 and GEMIN4). SMN is a protein mutated in spinal muscular atrophy disease (SMN) and is associated in lymphoblasts with intron retaining in ATXN10 gene. They demonstrated that knock-down of HDAC11 also causes the retaining in this gene, indicating a functional role for HDAC11 in intron splicing (Joshi et al. 2013).

Interacting proteins	HDAC6 (Gao et al. 2002; Cheng et al. 2014; Watanabe et al. 2014), CDT1 (Wong et al. 2010), CDC20 (Watanabe et al. 2014), SMN1 (Joshi et al. 2013), GEMIN3 (Joshi et al. 2013), GEMIN4 (Joshi et al. 2013), DICER1 (Joshi et al. 2013), Vitamin D receptor (Liu et al. 2017).
Deacetylated proteins	BUBR1 (Watanabe et al. 2014), CDC25A(Lozada et al. 2016).
Bound promoters	MYC (Toropainen et al. 2010), tight junction proteins (Liu et al. 2017).
Deacetylated promoters	IL-10 (Villagra et al. 2009), PAI-1 (Kim et al. 2013), MBP and PLP (Liu et al. 2009).

Table 5. Overview of HDAC11 molecular actions.

MOTIVATION AND OBJECTIVES

To carry out their specific functions on muscle formation and maintenance, adult muscle progenitors, the satellite cells (SCs), undergo two crucial cell fate decisions. On the first one, they have to decide whether to remain quiescent to constitute the SC pool or to get activated to start amplifying the progenitor population that will form new muscle. On the second one, they have to decide whether to keep proliferating to give rise to more progenitors or to differentiate to become terminally functional muscle cells. These two cell fate decisions involve transitions to or from the cell cycle to a G0 quiescent state. The unravel of the mechanisms that control both cell cycle exit and entry are therefore key to understand and try to modulate physiological but also pathological conditions where differentiation and quiescence states are imbalanced, as in the case of muscle dystrophies and rhabdomyosarcoma tumors.

The role of histone deacetylation and HDACs in the control of the balance of these cellular states has already been demonstrated for some members of I and II HDAC classes while the functions of the other members remain unsolved. HDAC11, the newest member of the HDAC family, was reported to be enriched in adult skeletal muscle since the very first moment of its discover now 15 years ago, yet their specific functions in this tissue remain still unknown.

Motivated by these premises, the general objective of this thesis is to bring light to the roles of HDAC11 in skeletal muscle processes and functions.

To address this general objective we propose the following specific objectives:

1. To characterize the expression of HDAC family members in the transition from proliferation to skeletal muscle differentiation.

2. To evaluate the consequences of HDAC11 absence and overexpression in skeletal muscle proliferation and differentiation.

3. To determine the expression of HDAC11 in different skeletal muscle types and conditions.

4. To characterize the effects of HDAC11 deletion in different skeletal muscles of HDAC11 deficient mice in resting and regeneration conditions.

5. To address HDAC11 expression in human muscles in physiological and pathological conditions.

MATERIALS AND METHODS

Cell cultures

Cell lines

C2C12 cell line was kindly provided by Dr. Rita Perlingueiro (University of Minnesota, Minneapolis, USA). 293T cells were purchased from ATCC and Phoenix amphotropic cells were kindly provided by Dr. Maria José Barrero (Center of Regenerative Medicine in Barcelona) and Dr. Sonia V. Forcales (Program for Predictive and Personalized Medicine of Cancer, Germans Trias i Pujol Research Institute (IGTP)). E3 and E13 human primary myoblasts were provided by Dr. Eduard Gallardo (Hospital de la Santa Creu i Sant Pau, Universitat Autònoma de Barcelona). Rhabdomyosarcoma cell lines Rh4, Rh30, Rh31, CW9019 and A204 were kindly provided by Dr. Óscar Martínez Tirado and Dr. Roser López-Alemany (Sarcoma group, Bellvitge Biomedical Research Institute (IDIBELL)), Te671 was provided by Dr. Eduard Gallardo and Ruch-2 was given by Dr.Josep Roma (Translational research in child and adolescent cancer, Vall d'Hebron Research Institute).

Cell lines culture conditions

C2C12 were maintained in subconfluent densities (less than 60%) and subcultured each 2-3 days in growth medium (GM), composed by DMEM (Dubelcco's Modified Eagle's Medium, Ref. 11960085) supplemented with 10% of inactivated fetal bovine serum (FBS) (Ref. 10270106), 4 mM of L-glutamine (Ref. 25030024), 2 mM of pyruvate (Ref. 11360039) and 100 U/ml penicillin and 100 µg/ml streptomycin (Ref. 15140122). To induce cell differentiation, cells were trypsinized, counted and plated at confluent densities (12,346 cells/cm^2). 24h hours after plating, cells were washed with PBS 1X and the medium was changed by differentiation medium (DM), composed by DMEM 1X, 2% of Horse serum, 4mM of L-glutamine, 2mM of pyruvate, 100 U/ml of penicillin and 100 µg/ml streptomycin (all reagents were purchased from Gibco, LifeTechnologies).

Packaging 293T and Phoenix cells were maintained in subconfluent conditions subcultured each 2-3 days in DMEM (Dubelcco's Modified Eagle's Medium) supplemented with 10% of inactivated fetal bovine serum, 4mM of L-glutamine, 2mM of pyruvate, 100 U/ml of penicillin and 100 µg/ml streptomycin.

Human primary myoblasts were cultured at subconfluent densities in GM composed by 65% of DMEM 1X, 22% of M-199 (Medium 199 with Earle's BSS), 10% of inactivated fetal bovine serum, 1 µg/ml insulin, 2 mM glutamine, 100 U/ml penicillin, 100 µg/ml

streptomycin, 10 ng/ml epidermal growth factor, and 25 ng/ml fibroblast growth factor. To induce cell differentiation, myoblasts were plated at confluent densities and the medium was replaced by GM containing 2% FBS.

Human rhabdomyosarcoma cell lines were maintained in subconfluent conditions and subcultured each 2-3 days. The cell line types and culture media used are listed on Table 6.

Cell line	Rhabdomyosarcoma subtype	Fusion oncogene	Cell culture media
Rh4	aRMS	PAX3:FOXO1	RPMI + 10% FBS
Rh41	aRMS	PAX3:FOXO1	RPMI + 10% FBS
Rh30	aRMS	PAX3:FOXO1	RPMI + 10% FBS
CW9019	aRMS	PAX7:FOXO1	DMEM +10 % FBS
Rd	eRMS	None	DMEM +10 % FBS
A204	eRMS	None	DMEM +10 % FBS
Te671	eRMS	None	DMEM +10 % FBS
Ruch-2	eRMS	None	DMEM +10 % FBS

Table 6. List of human rhabdomyosarcoma cell lines used. Indicated are the cell lines used in this study, their subtype and the cell culture media used. All media listed were supplemented with **4** mM of L-glutamine, 2 mM of pyruvate, 100 U/ml of penicillin and 100 μg/ml streptomycin.

All cell lines indicated were maintained at 37ºC with 5% CO2. To store them, the cells were frozen in GM supplemented with 10% of DMSO and placed in cold Mr. Frosty™ (ThermoFisher) at -80ºC for 24h before storing them permanently in liquid nitrogen tanks.

Cell culture treatments

For selection of C2C12 overexpressing clones (shRNA's, overexpressing vectors and pLentiCRISPR v2), cells were cultured with GM supplemented with 3 μg/ml of puromycin dihydrochloride (P8833, Sigma-Aldrich). After this selection period, selected cells were maintained in 0.5 μg/ml of puromycin concentration in GM or DM.

HDACi treatments. C2C12 cells were treated in GM or DM for 24 h with 50 nM Trichostatin A *Streptomyces* sp. (TSA) (Ref. T8552, Sigma-Aldrich) or 10 mM Valproic acid (VPA) (Ref. P4543, Sigma-Aldrich), concentrations at which no cell toxicity was previously described (Iezzi et al. 2002).

HDAC11 knockdown using shRNA constructs

shRNA vector

Empty pLKO was kindly provided by Dr. Marcus Buschbeck's laboratory (Josep Carreras leukemia research Institute (IJC)). Their map and main functional elements are illustrated on Figure 12.

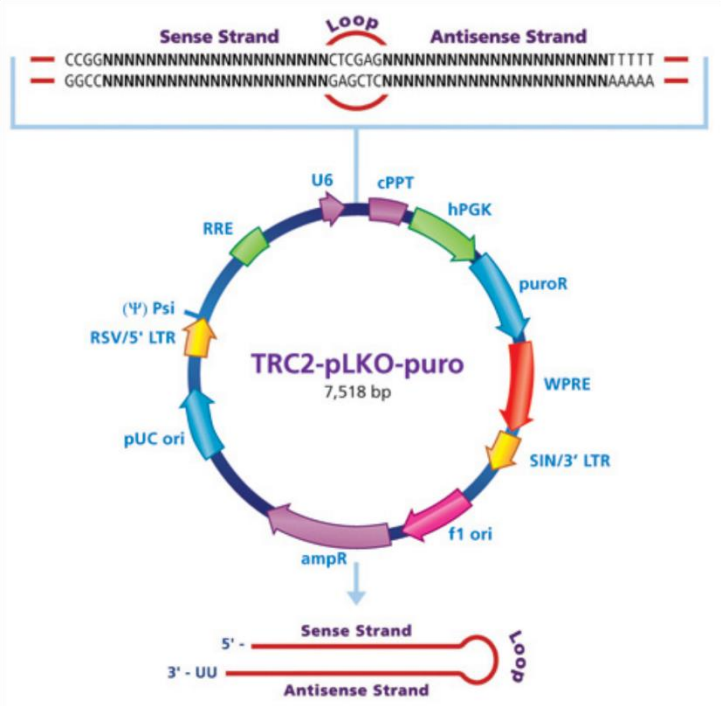

Figure 12. TRC2-pLKO vector map. Schematic representation of pLKO functional elements, shRNA cloning location and the corresponding shRNA structure obtained. Abbreviations: ampR: ampicillin resistance for bacterial selection, pUC ori: origin of replication, RSV/5' LTR: 5' long terminal repeat, Psi: RNA packaging signal, RRE: Rev response element, U6: RNA transcription promoter, cPPT: central polypurine track, hPGK: human phosphoglycerate kinase eukaryotic promoter, puroR: puromycin resistance gene for mammalian transduction selection, WPRE: Woodchuck hepatitis post-transcriptional regulatory element, SIN/3'LTR: 3' self-inactivating long terminal repeat, f1 ori: f1 origin of replication. Image was modified from: http://www.sigmaaldrich.com/life-science/functional-genomics-and-rnai/shrna/library-information/vector-map.html.

The shRNA sequences used are listed on Table 7. The shRNA's 01, 02, 03, 74 and 11 were directly purchased from Sigma-Aldrich as bacterial glycerol transformed plasmids cloned in pLKO TRC version 2 (MISSION shRNA library). The glycerol stocks were defrost and an aliquot was grown in 500 µl of lysogeny broth (LB) without antibiotics for 30 min at 37ºC with shacking. Then, 50 µl were plated onto LB agar plates with ampicillin 50 µg/ml and incubated o/n at 37ºC. The next day, a single colony was selected for each plasmid. Plasmid integrity and identities were checked by electrophoresis in 1% agarose gels stained

with ethidium bromide of the circular plasmid and 200 ng aliquots digested with 20 U of BamHI (Ref. R0136S, New England Biolabs Inc.) in NEB buffer 3 (Ref. B7203S, New England Biolabs) supplemented with 100 μg/ml of BSA.

shRNA name	Working name	Sequence (5'->3')	Targeted region
TRCN0000339501	01	CCGGTGGTCCGAGCCCATGATATACCTCG AGGTATATCATGGGCTCGGACCATTTTTG	CDS HDAC11 (ENSMUSE00000423267)
TRCN0000339502	02	CCGGGAAGCGCACAGCCCGTATTATCTCG AGATAATACGGGCTGTGCGCTTCTTTTTG	CDS HDAC11 (ENSMUSE00000423267)
TRCN0000339503	03	CCGGCATGGGTGACAAGCGAGTATACTC GAGTATACTCGCTTGTCACCCATGTTTTTG	CDS HDAC11 (ENSMUSE00001216372)
TRCN0000339574	74	CCGGAGAGTCGTTTGCTGTTCATATCTCG AGATATGAACAGCAAACGACTCTTTTTTG	3' UTR HDAC11
TRCN0000377111	11	CCGGTTGGCTTACTTCCTCACTTTACTCGA GTAAAGTGAGGAAGTAAGCCAATTTTTG	3' UTR HDAC11
TRCN0000039224	24	CCGGGCCACCATCATTGATCTCGATCTCG AGATCGAGATCAATGATGGTGGCTTTTTG	CDS (ENSMUSE00001279263)
TRCN0000039225	25	CCGGCCATGATATACCCATCCTCATCTCGA GATGAGGATGGGTATATCATGGTTTTTG	CDS (ENSMUSE00000423267)
TRCN0000039228	28	CCGGGCGCTATCTCAACGAGCTGAACTCG AGTTCAGCTCGTTGAGATAGCGCTTTTTG	CDS (ENSMUSE00001222983)
SHC002		CCGGCAACAAGATGAAGAGCACCAACTCG AGTTGGTGCTCTTCATCTTGTTGTTTTTG	Turbo-GFP (Non-mammalian targeting)

Table 7. Sequences and targeting regions of the shRNA's used. Underlined are marked the corresponding sense and antisense siRNA sequences. CDS: coding sequences. Working name: name used in this manuscript. Packaging psPax2 and envelope CMV-VSVG coding plasmids were kindly provided by Dr. Maria José Barrero (Center of Regenerative Medicine in Barcelona).

shRNA cloning

As any shRNA from the library of commercial shRNA's mentioned above provided satisfactory downregulation levels, we decided to select other shRNA sequences that had been already published: shRNA_24 (Cheng et al. 2014; Kagey et al. 2010), shRNA_25 (Watanabe et al. 2014; Kagey et al. 2010; Villagra et al. 2009) and shRNA_28 (Watanabe et al. 2014; Kagey et al. 2010; Villagra et al. 2009).

The corresponding siRNA sense and antisense sequences incorporating 5' and 3' ends to anneal to digested pLKO vector, were purchased as oligonucleotides from Life technologies (Invitrogen) desalted and using 50 nM as a synthesis scale. Upon arrival, they were dissolved in nuclease-free sterile water up to 100 μM to make the stock solution and

these solutions were further dissolved to make working solutions at 20 µM. The protocol for cloning the siRNA's into pLKO vector was obtained from Addgene (https://www.addgene.org/tools/protocols/plko/). Briefly, 5 µl of each pair of oligonucleotides were mixed with 5 µl of 10X NEB buffer 2 (Ref. B7002S, New England Biolabd Inc.) and 35 µl of water and annealed by incubating at 37ºC for 30 min, denaturalizing at 95ºC at 5 min and cooling down by decreasing 5ºC per minute until 25ºC in a PCR thermocycler. These annealed nucleotides (2 µl of the mix) were ligated with 20 ng of previously digested vector pLKO with AgeI and EcoRI enzymes using 400 cohesive end units (1 µl) of T4 DNA ligase (Ref. M0202L, New England Biolabs Inc.) in a final volume of 20 µl by incubating at 16ºC o/n. A reaction with only the digested dephosphorylated vector without the insert was included as a control of plasmid religation. 10 µl of these ligation reactions were transformed into 50 µl of DH5α competent cells (custom made at PMPPC central services) by incubating the cells with the ligation reactions on ice for 30 min, heat shock at 42ºC for 45 seconds, 5 minutes on ice and grown at 37ºC for 1 h with Super Optimal Broth (SOC) medium without antibiotics. The cells were then plated into LB plates containing ampicillin selection and incubated o/n at 37ºC. Single colonies were transferred to 3 ml of LB with ampicillin (Ref. 171254, Merck) and grown o/n at 37ºC with shacking. The next day, the plasmids were purified using GenElute™ Plasmid Miniprep Kit (Ref. PLN70, Sigma-Aldrich) and 1 µg of each was digested with XhoI (Ref. ER0691, ThermoFisher) or EcoRI (Ref. 11175084001, Roche) and BamHI (ER0641, ThermoFisher) (AgeI restriction site is destroyed after cloning and the insert cannot be released). The plasmids with the expected digestion patterns for shRNA insertion were sequenced using pLKO_F primer (5' CAAGGCTGTTAGAGAGATAATTGGA 3') at GATC Biotech service and verified sequences were used to generate lentiviral particles.

Lentivirus generation

293T cell line (an immortalized human kidney embryonic cell line expressing large antigen T) was platted at D0 ($2.5x10^6$ cells in 100 mm plates) to be at a confluence of approximately 80% at D1. At this moment, cells were transfected by $CaPO_4$ method. For that and for each condition, 10 µg of the corresponding shRNA vector were combined with 3 µg of CMV-VSV-G vector, 8 µg of psPAX2 and 62 µl of 2M $CaCl_2$ in a final volume of 500 µl with water. Then, 500 µl of 2x HEPES-buffered saline (HBS) were added dropwise with briefly vortexing. The obtained mix was incubated at RT for 5 min and then added

dropwise to 293T cells, which were incubated o/n at 37ºC and 5% CO_2. In all transfection experiments was included a positive transfection control (pLVHTM-GFP, kindly provided by Dr. Marcus Buschbeck's lab). The next day, GFP of the control plate was observed on a fluorescent microscope and if the number of positive GFP cells was acceptable, the media of the shRNA transfected plates was changed and they were incubated for additionally 48 h to allow lentiviral particle generation. After this time (72 h after transfection), the media of the plates was collected and filtered using 0.45 µm polysulfonate filters (Ref. 514-0074, VWR) to remove cellular debris.

Lentiviral transduction of C2C12 cells

The day before infection, 24,000 cells were plated into 100 mm plates (436 cells /cm^2). This density was experimentally set up as the cell confluency that allow to maintain the highest number of C2C12 cells for 3 days without reaching cell confluency. The day of infection, the cell medium was removed and replaced with 5 ml of 293T filtered media and 5 ml of fresh media. 8 µg/ml of polybrene (hexadimethrine bromide, Ref. H9268, Sigma Aldrich), were added to enhance transduction efficiency. The cells were incubated o/n and the next day the supernatant was discarded.

Generation of stable expressing shRNA cells

To generate stable expressing shRNA cell lines, the transduced pools were selected with puromycin as described on "Cell culture treatments". A no transduced plate was included to assess the moment when resistant cells were selected. shRNA downregulation efficiencies were assessed by qPCR.

Overexpression of HDAC11

Overexpression vector

Empty pMSCV-puro-Flag (murine stem cell virus plasmid) and pMSCV-puro-HA retroviral overexpression vector were kindly provided by Dr. Maria José Barrero (Center of Regenerative Medicine in Barcelona). Their maps and main functional elements are illustrated on Figure 13.

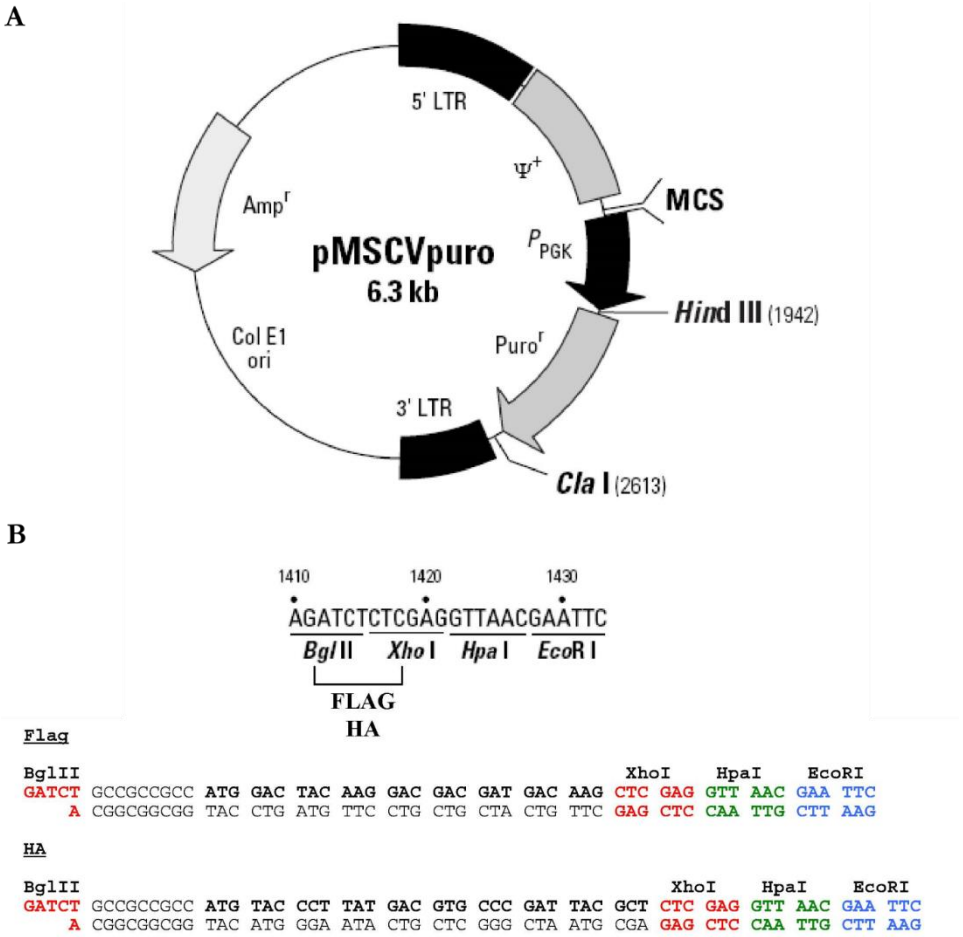

Figure 13. pMSCV overexpression transfer plasmid vector map. A Schematic representation of pMSCV vector functional elements. Abbreviations: Col E1 ori: origin of replication, Amp^r: ampicillin resistance gene for bacterial selection, 5'LTR: 5' long terminal repeat, Ψ^+: retroviral psi packaging element, MCS: multiple cloning site, P_{PGK}: phosphoglycerate kinase promoter, $Puro^r$: puromycin resistance gene for eukaryotic selection 3' LTR: 3' long terminal repeat. **B** Multiple cloning site detailed sequence of flag and HA tags inserted sequences preceded by the first initiating ATG triplet. Immediately before ATG is indicated the Kozak sequence (5' GCCGCCGCC 3'). The image was modified from: http://www.yrgene.com/documents/vector/utf-8zh-cnpt3303-5.pdf.

Overexpression constructs generation

HDAC11 cDNA was amplified from day 4 differentiating murine primary myoblasts cDNA prepared as indicated on "cDNA retrotranscription" using as primers F: 5' CCG CTCGAG GGC ATGCCTCACGCAACACAGCT 3' (the sequence corresponds to 3 nt to allow cut close to DNA ends, a XhoI restriction site, a glycine coding triplet and the 5' HDAC11 sequence) and R: 5' C GAATTC TCA AGGCACAGCACAGGAAAGCAGGG 3' (the sequence corresponds to 1 nt to allow cut close to DNA ends, an EcoRI restriction site, the stop codon and the 3' HDAC11

complementary sequence) and Phusion High Fidelity polymerase (Ref. E385HT, ThermoFisher Scientific) with the following PCR conditions: 98ºC for 30 seconds, 25 cycles of 98ºC for 8 seconds and 72ºC for 30 seconds, and a final step of amplification at 72ºC for 10 min. The PCR product was ran into 2% agarose gel stained with ethidium bromide to verify amplicon size. Eight 20 µl PCR reactions were pooled and purified using JETQuick columns (Ref. 410250, Genomed) following the manufacturer's protocol. The purified insert and vector were cut with XhoI (Ref. ER0691, ThermoFisher) and EcoRI (Ref. 11175084001, Roche) in 2 X Tango buffer (Ref. BY5, ThermoFisher) o/n at 37ºC followed by enzyme inactivation at 80ºC for 20 minutes. The cut plasmid was purified from the uncut fraction by electrophoresis in 1% agarose gel and excision. After purification from agarose using NucleoSpin Gel and PCR Clean-up (Ref. 22740609.5, Cultek) the vector was then dephosphorylated to prevent religation using of FastAP™ thermosensitive alkaline phosphatase (Ref. EF0654, Thermo Scientific) at 37ºC for 15 min, followed by 85ºC for 15 min of inactivation. Plasmid and insert were ligated in a ratio 1 vector : 10 insert molar ratios using T4 DNA ligase (Ref. M0202L, New England Biolabs Inc.) at 16ºC o/n. The next day, 10 µl of the ligation were transformed into DH5α competent cells as described for shRNA cloning. Transformed colonies were validated by insert release upon digestion with XhoI and EcoRI and sequencing of the plasmid using pMSCV_F primer: 5' TCGTTCGACCCCGCCTCGATC 3'. The necessary amount of vector was generated using PureLink HiPure Plasmid Filter Maxiprep Kit. (Ref. K210017, Thermo Fisher).

To obtain HDAC11 tagged with HA in C-terminal, pMSCV-Flag-HDAC11 was used as a template and the insert was amplified using as a F primer 5' CG AGATCT ATGCCTCACGCAACACAGCT 3' (the sequence corresponds to 2 nt to allow enzyme cut close to DNA ends, BglII restriction site and 5' HDAC11 sequence) and R 5' CGAATTCTCAAGGCACAGCACAGGAAAGCAGGG 3' (the sequence corresponds to 1 nt to cut close to DNA ends, the stop codon, the HA sequence, the EcoRI restriction site and 3' HDAC11 complementary sequence). The amplification conditions were the same than for Flag-HDAC11. Empty pMSCV-Flag was digested with BglII and EcoRI to remove the cloned tag. The digested insert and plasmid were ligated and checked as indicated for pMSCV-Flag-HDAC11.

Generation of retrovirus

Phoenix cell line (an immortalized human kidney embryonic cell line expressing 4070A envelope) was platted at D0 ($2.5x10^6$ cells in 100 mm plates) to be at a confluence of approximately 80% at D1. At this moment, cells were transfected by $CaPO_4$ method. For that and for each condition, 10 µg of pMSCV-HDAC11 were combined with 62 µl of 2M $CaCl_2$ in a final volume of 500 µl with water. Then, 500 µl of 2x HEPES-buffered saline (HBS) were added dropwise with briefly vortexing. The obtained mix was incubated at RT for 5 min and in the meanwhile 293T media was replaced by media without antibiotics. After the incubation, the mix was added dropwise to 293T cells, which were incubated o/n at 37ºC and 5% CO_2. In all transfection experiments was included a positive transfection control (pRS-GFP, kindly provided by Dr. Marcus Buschbeck's lab). The next day, GFP of the control plate was observed on a fluorescent microscope and if the number of positive GFP cells was acceptable, the media of the transfected plates was changed and they were incubated for 48 h to allow retroviral particle generation. After this time (72 h after transfection), the media of the plates were collected and filtered using 0.45 µm polysulfonate filters (Ref. 514-0074, VWR) to remove cellular debris.

Retroviral transduction of C2C12 cells

The retroviral transduction and selection of HDAC11 overexpressing cells was performed as indicated for lentiviral infection.

Primary myoblasts

Muscle bulk preparation

First, mice muscles not used for histology or RNA/protein extraction (quadriceps and upper back-legs, upper legs, abdominal and back legs muscles) were dissected and maintained in 50 ml falcons with DMEM 1X supplemented with penicillin/streptomycin on ice (all washes were performed with this medium). Then, they were placed into Petri's dishes on ice and bones and adipose tissue were removed as much as possible. Muscles were chopped using scissors and blades and minced muscles were collected and placed again in falcons with 40 ml of cold DMEM. Minced muscles were allowed to sediment for 5 minutes on ice and then the medium with the floating fat pieces was removed. Then, 10 ml of 0.08% Collagenase D (Ref. 11088882001, Roche Diagnostics) and 0.125% Trypsin

solution (Ref. 210234, Roche Diagnostics) were added to the minced muscles and were then incubated for 25 min at 37ºC in a shacking water bath to allow muscle digestion. After the digestion, tubes were centrifuged at 50 rcf for 5 min at 4ºC. The supernatant was recovered and placed in a new tube with 5 ml of FBS to quench trypsin and on ice to stop collagenase D. The pellet was resuspended again with 10 ml of Collagenase D and Trypsin solution and this process was repeated up to 4 digestions, when only tendons and small bones remained.

To isolate mononucleated cells, the pooled supernatants recovered were filtered successively through 100 and 70 μm strainers (Ref. 08-771-19 and 08-771-2, Falcon BD) to remove tendons and undigested pieces of muscle. The filtered suspensions were centrifuged for 10 min, at 50 rcf and 4ºC. The supernatant was recovered and the pellet was resuspended and centrifuged again to recover more cells. The supernatants were centrifuged to recover the cells for 15 min at 350 rcf and 4ºC. The supernatant was discarded and the cells were washed with 40 ml and spun again. The resulting pellet was resuspended in 3 ml of 1/10 v/v erythrocyte lysis buffer and incubated at darkness on ice for 10 min. The lysate was filtered through 40 μm filter and spun for 15 min at 350 rcf and 4ºC. The pellet of cells was counted in a Neubauer chamber and the cells were frozen in 90% of FBS + 10% DMSO in a cold Mr. Frosty™ and kept at -80ºC until FACS sorting.

Antibody staining for satellite cell isolation by FACS sorting

Cells were thaw at 37ºC in a water bath. DMSO was removed by diluting with 12 ml of F-10 medium with 20% FBS and 100 U/ml penicillin and 100 μg/ml streptomycin and spun at 300 rcf for 5 min at RT. Cells were resuspended in FACS buffer (PBS + 1% FBS), in a ratio of 100 μl: 10^6 cells on ice and incubated for 30 min on ice with the indicated amounts of antibodies against the cell surface markers listed in Table 8.

After the incubation, cells were washed in FACS buffer, resuspended in 1 ml of FACS buffer again and stained 1/1,000 with DAPI to exclude death cells. Cells were sorted using a FACS Aria II at CRG/UPF FACS unit. SC population was selected to be $DAPI^-$, $CD34^+$, $\alpha7\text{-integrin}^+$, $CD45^-$ and $Sca\text{-}1^-$ (Pasut et al. 2013). To check SC identity, PAX7 expression was checked by immunochemistry. For that, for each animal 500 cells were directly spread onto SuperFrost®Plus microscope slides (Ref. 631-0108, VWR) and fixed with 4% PFA (Ref. 8.1875.0100, Merck) for 10 min at RT, washed twice with PBS and stored in PBS containing 0.001% sodium azide at 4ºC until processing. The rest of cells were collected and plated in collagen-coated plates.

Assess of SC identity by immunofluorescence

To check that the isolated populations by FACS consist on quiescent SC cells, SC were stained with antibodies against PAX7 and MYOD. For that, the cells were permeabilized with 0.5% Triton-X in PBS for 10 min followed by three washes with PBS 1X. Then, unspecific interactions were blocked with 10% v/v goat serum and 10% FBS for 30 min at RT. Then, the sections were stained o/n at 4ºC with α-PAX7 concentrate 1:10 (Developmental Studies Hybridoma Bank (DSHB), University of Iowa) and 1:50 MYOD (clone 5.8A, Dako) in 3% BSA. Next day, they were performed two washes for 3 min with 0.1 % Tween PBS, followed by incubation for 30 min at darkness and RT with 1/250 v/v Alexa red 568 α-mouse IgG1(γ) (Ref. A-21124, ThermoFisher) and 1/250 v/v Alexa green 488 α-rabbit (H+L) (Ref. A-11008, ThermoFisher). Sections were then washed twice for 3 min with 0.1 % Tween PBS 1x and mounted with Vectashield mounting medium with DAPI (Ref. 53826, Palex Medical S.A.).

Antibody	Manufacturer	Species	Amount used $10^{\wedge 6}$ cells	Comments
Alexa Fluor® 647 anti-CD34, clone RAM34	BD Biosciences	Rat	$3x10^{-3}$ µg	Positive SC selection
PE/anti-α7-integrin	AbLab	Rat	$1x10^{-3}$ µg	Positive SC selection
PE/Cy7 anti-CD45	Biolegend	Rat	$1x10^{-3}$ µg	Negative SC selection
PE/Cy7 anti-Sca-1	Biolegend	Rat	$1x10^{-3}$ µg	Negative SC selection

Table 8. List of antibodies used for FACS sorting of satellite cells.

Primary myoblast culture

Primary isolated myoblasts from WT and KO genotypes were maintained at subconfluent conditions in growth medium (GM), composed by Ham's F-10 (Ref. 22390025, Gibco), 20% v/v inactivated FBS, 4 mM of L-glutamine, 2 mM of pyruvate, 100 U/ml of penicillin and 100 µg/ml streptomycin (all reagents were purchased from Gibco, LifeTechnologies). Media was supplemented with 1/10,000 v/v of basic fibroblast growth factor (Ref. 100-18B, Prepotech. After FACS isolation, cells were plated in 6 well plates and then successively subcultured to 60 mm and 100 mm plates every 2-3 days. All culture plates

were previously coated with rat tail collagen I (Ref. 354236, Corning, Becton and Dickinson). Coating solution was prepared by dissolution of the collagen to a final concentration of 0.05 mg/ml with water containing 0.02N acetic acid glacial previously filtered through 10 μm Stericup-VP (Ref. SCVPU02RE, Merck-Millipore). Coating was performed by incubating the plates with a sufficient volume of coating solution to cover them (10 ml in 10 mm plates) for 2h to o/n at 37ºC. After coating, coating solution was reused and coated plates were washed twice with PBS 1X and used directly or stored dried at RT.

To differentiate the cells, the necessary amount of plates were washed twice with PBS, trypsinized and counted and seeded at a confluency of 26,600 cells/cm^2 with GM in matrigel basement membrane matrix coated plates. Next day, GM was removed, the plates were washed with PBS 1X and media was replaced by differentiation medium, with the same composition than for C2C12 and without adding any additional factors. Matrigel coating solution was prepared by dissolving matrigel (Ref. 354234, Corning, Becton and Dickinson) at a working concentration of 0.2 mg/ml in cold Hams F-10 media. This solution was directly used to cover the plates from 1h to o/n at 37ºC. After that time, the coating solution was discarded and the plates were washed twice with Hams F-10 media and directly used or stored at 4ºC.

For all experiments, primary myoblasts cultures were used until passage 15.

Proliferation assays

Growth curves

At day 0 subconfluent MPC's cultures were trypsinized, counted at least in duplicate independent dilutions using the automated cell counter Countess™ (Invitrogen) and Eve™ cell counting slides (NanoEntek) (data window: 9-25 μm, 75% circularity). 200,000 cells were plated in cell culture Petri dishes (Nunc™ 150350, 100x15mm (ThermoFisher) coated with collagen in proliferation medium at a density of 3,527 cells/cm^2. This density was determined in pilot experiments to allow cell growth for 3 days in subconfluent conditions. At day 1, 2 and 3 after plating, the cells were counted as described for day 0. For each time point one different plate was included, the cells were no replated after counting. For each primary culture at least two independent experiments were performed.

EdU incorporation and propidium iodide staining for cell flow cytometry analysis

Proliferating cells were counted and plated as for growth curve experiments. Medium was changed 24h after plating, and the cells were incubated in growth medium with 20 μM of 5-ethynyl-2-deoxyuridine (EdU) for 2 hours. Click-iT® EdU Alexa Fluor 488 Flow Cytometry assay kit (ThermoFisher, C10425) was used for EdU detection. Protocol was performed according to the manufacturer instructions, including a final step of propidium iodide staining to label DNA content. After the last saponin-based permeabilization and wash, the pellets were resuspended in 100 μl of analysis solution (500 μg/μl of propidium iodide (Ref. P4170, Sigma-Aldrich), 38mM of sodium citrate (Ref. C8532, Sigma-Aldrich) and 0.3 μg/μl of Ribonuclease A, incubated for 30 min at 37ºC and immediately analyzed using Fortessa cytometer at the Cytometer service of the Trias i Pujol Research Institute (IGTP, Badalona).

G0 cell cycle arrest induction by methylcellulose induced loss of cell anchorage

The protocol was performed as described on (Sambasivan et al. 2008; Sachidanandan et al. 2002). Briefly, subconfluent C2C12 cultures were trypsinized, counted and resuspended in 1.3% methyl cellulose 4,000 centipoise (Ref. M0512, Sigma-Aldrich) in GM at a concentration of 10^5 cells /ml (10^7 in 10 ml). Cells were maintained at 37ºC and 5% CO2 in these suspensions for 48 h. To recovery the cells, the suspensions were washed with 10 ml of PBS pre-heated at 37ºC followed by centrifugation at 2,500 rpm for 20 min. Then, the pellets were washed three times with 40 ml of PBS followed by centrifugation at 1,500 rpm for 10 min. After the last pellet, the cells were counted, pelleted or plated to monitor cell cycle entry.

Reserve cell separation by trypsinization

Primary myoblasts cultures were differentiated to D3 as described. To separate reserve cells, the plates were washed three times with modified PBS 1X containing divalent cations (8 g/L NaCl, 0.2 g/L KCl, 1.15 g/L Na_2HPO_4, 0.2 g/L KH_2PO_4, 0.13 g/L $CaCl_2x2H_2O$, 0.1 g/L $MgCl_2x6H_2O$). Then, the cells were treated with 0.025% v/v Trypsin without EDTA (Ref. 15090-046, Gibco) in PBS with cations for 15 min or until all myotubes are detached by visual inspection under a microscope. The plates were then extensively rinsed

with PBS containing cations to remove myotubes which were recovered in a falcon and spun to get purified myotubes fraction. Reserve cells that remain now attached to the plate were recovered by conventional trypsinization.

Cell differentiation analysis

To determine cell differentiation analysis cells were fixed directly on the plates with 4% paraformaldehyde (Ref. 8.1875.0100, Merck) for 10 min at RT followed by 2 washes with PBS. Then, internal peroxidases were blocked by incubation for 30 min with 3% H_2O_2 (Hydrogen peroxide solution 30% w/w in H_2O, Ref. H1009, Sigma-Aldrich) and washed twice with PBS for 3 min each. To block unspecific staining, cells were incubated with 10% BSA 10% FBS in PBS for 1h at RT and incubated for 1 h 67667at RT with F1.652 hybridoma in blocking buffer (kindly provided by Dr. Marcus Bushbeck lab). Three washes for 5 min each were performed with 0.1 % Tween PBS, followed by incubation for 20 min at RT with 1/250 v/v secondary biotinylated α-mouse Dako IgG in blocking solution (the same as before) followed by three washes for 5 min with 0.1 % Tween PBS 1x. The staining was developed by incubation with 0.6% 3,3'-diaminobenzidine in PBS under a microscope until brown coloration was clearly observed.

Cell differentiation index was calculated as the number of eMHC positive cells / total number of cells. The number of nuclei per myotube was estimated by counting the number of nuclei in the cells containing 3 or more nuclei / number of these cells. All measures were performed with ImageJ 1.48v (NIH, USA).

Bisulphite analysis

Bisulphite analysis is the gold standard technique to assess the methylation state at a single base resolution level of DNA. Sodium bisulphite treatment of single stranded DNA results in specific sulphonation of unmethylated cytosines versus modified ones (methylated and hydroxymethylated). A following step of hydrolysis and alkaline treatment results into the conversion of unmethylated cytosines into uracil, leaving the modified ones as cytosines and allowing the quantification of methylation (Clark et al. 2006)

DNA extraction

Cells were pelleted by centrifugation at 300 rcf for 5 min. The pellet was next resuspended

in 300 µl of urea lysis buffer (48% w/v urea, 300mM NaCl, 15mM EDTA, 10mM Tris pH8, 2% SDS) and incubated with 0.2 mg/ml of proteinase K and 1.3 mg/ml RNAse A for 2 h at 56ºC. DNA was purified by phenol/chloroform extraction and precipitated afterwards in absolute ethanol in the presence of 0.4 M of sodium acetate. The pellet was washed twice in ethanol 70% and finally resuspended in TE buffer. DNA purity was checked and quantified by NanoDrop (Thermo Scientific). A 100 ng aliquot was run on 1% agarose gel stained with ethidium bromide for 1h at 100mV to check DNA integrity.

Bisulphite conversion

Bisulphite conversion was performed using 400 ng of DNA with EZ DNA Methylation-Gold™ Kit (ZymoResearch, Orange, CA USA) according to manufacturer's instruction. Converted DNA was eluted in 40 µl of water.

Direct bisulphite sequencing

Bisulphite sequencing was performed following (Clark et al. 2006) procedure. PCR amplification was first performed starting with 1 µl of bisulphite-treated DNA by conventional PCR method in a final volume of 12.5 µl, in duplicate with the primers listed in Tables 9 and 10. These PCR products were directly used as a template for a nested PCR with conventional PCR method. The nested PCR was performed one reaction per PCR product of the previous reaction in a final volume of 12.5 µl. Primers were designed using MethPrimer (Li & Dahiya 2002). Previously, PCR conditions were set up at least with two independent samples by testing different combinations of temperatures of annealing of the external and internal PCR's and different dilutions of the external PCR. The amplicons generated were then checked by DNA electrophoresis in 2% agarose stained with ethidium bromide and the duplicate samples were pooled. The PCR products were cleaned of unincorporated primers and nucleotides by incubating 5µl of each pooled samples with 10 U of Exonuclease I and 1 U of FastAP™ thermosensitive alkaline phosphatase (Ref. EF0654, Thermo Scientific) at 37ºC for 15 min, followed by 85ºC for 15 min of inactivation. The purified products were checked again by DNA electrophoresis as described, and sequenced with the internal reverse primer at GATC Biotech service. Internal reverse primer was determined to be better than the forward one by a first pilot sequencing because it allows the sequencing of more CG dinucleotides than the forward one.

Primer name	Sequence (5'->3')	Annealing temperature (ºC)	Amplicon lenght (bp)
External_F	GTTATAGATGGTATAGGAATGTAGGG	56/58	422
External_R	AAATCCCCAAAACCCATACTTAACC	56/58	
Internal_F	TAGGAAAGAATATATAGTTGGGTTGG	56	383
Internal_R	CCCAAAACCCATACTTAACCCCAC	56	

Table 9. Primers used to study murine HDAC11 CpGi methylation by bisulphite PCR amplification and Sanger sequencing analysis

Region	Primer name	Sequence (5'->3')	Annealing temperature (ºC)	Amplicon lenght (bp)
1	Ext_F	ATTGTTTTTTGATTTTTTGGATTTG	58/60	433
	Ext_R	ATAATAACTTTAAACAAATTACTTC		
	Int_F	ATTGTTTTTTGATTTTTTGGATTTG	66	419
	Int_R	CAAATTACTTCAACCTTCTAATCCTTC		
2	Ext_F	AGATGTAGATATGAAGGATT	46/48	440
	Ext_R	AAATAAACTAAACCAAACCC		
	Int_F	ATAGAAGGATTAGAAGGTTGA	51	304
	Int_R	CCATCCAAACAAAAACAACTAA		
3	Ext_F	TGTTTATTTTTTAGGGTTGTTGTGAG	58/60	382
	Ext_R	CAAAAAAAACCTTCCATACCTTTTA		
	Int_F	TAAGTAGTTGTTGTTGAGGGGTTTT	60	293
	Int_R	AAAAATTAATCACTTTACCCCATTTT		

Table 10. Primers used to study human HDAC11 methylation by bisulphite PCR amplification and Sanger sequencing analysis.

Estimation of DNA methylation

The received sequences were analyzed using FinchTV (Version 1.4.0., Geospiza Inc.). Knowing that during PCR amplification, uracils are amplified as thymines whereas methylcytosines remain cytosines, for a given CG dinucleotide, the percentage of methylation was estimated by comparing the height of the corresponding C and T peaks

on the raw sequence (G and A if sequencing with the reverse primer). The results were represented using Methylation plotter (http://maplab.imppc.org/methylation_plotter/; Mallona et al. 2014).

mRNA expression analysis

RNA extraction

Different methods for RNA extraction were used depending on the type and amount of samples.

For cell line's pellets, RNA extraction was performed using PureLink™ RNA Mini Kit (Ref. 12183018A, Ambion, Life Technologies), including On-Column PureLink® DNase treatment. The protocol was performed according to manufacturer instructions.

For tissues, the same procedure was followed, including a homogenization step with TissueRuptor (Qiagen). Briefly, tissue was homogenized on ice until no fragments were found by visual inspection. As muscle tissue is very rich in proteins and extracellular material, a preclearing centrifugation at 16,100 rcf during 10 min at 4ºC was included to remove insoluble material. Supernatant was processed as for cell pellets lysate. RNA concentration and purity was quantified using Nanodrop (Thermo Scientific), and integrity was checked by observation of 28S and 18S ribosomic bands on 1% agarose gel electrophoresis stained with ethidium bromide.

For cells directly isolated by FACS (low number of cells), RNA was extracted using RNeasy Micro Kit (Ref. 74004, Qiagen) according to manufacturer instructions and including on-column DNAse treatment. RNA was eluted with 10 µl of water and in this case the retrotranscription reaction was directly performed with all the eluted volume.

cDNA retrotranscription

Working dilutions at the same concentrations (60 ng/µl) were performed from the obtained RNAs. The concentration of these dilutions were quantified twice. Unless indicated, 500 ng of each working dilution were brought to 11 µl with water and mixed with 150 ng of random hexamer primers and 10 pmols of dNTP's mix. The mix was incubated at 65ºC for 5 min and 1 min at 4ºC. Then, 4 µl of First-Strand buffer, 1 µl of 0.1M DTT, 1 µl of RNaseOUT™ Recombinant RNase Inhibitor and 200 U of SuperScript™ III were added, to a final volume of 20 µl. Two negative controls were included each time: a negative control without RNA and another without

retrotranscriptase. First-strand cDNA was synthetized in a PCR Thermocycler with the following program: 5 min at 25ºC, 60 min at 50ºC, 15 min at 70ºC and hold at 4ºC until permanent storage at -20ºC.

qPCR analysis

RNA expression levels were analyzed using the quantitative Real-Time PCR technique in the LightCycler®480 (Roche Diagnostics Corporation) platform. Retrotranscribed cDNA was diluted 1/10 v/v with water and reactions were performed in technical triplicates. Each reaction contained 1 µl of 10 µM forward primer, 1 µl of 10 µM reverse primer, 2 µl of water, 5 µl of Fast Start DNA Master SYBR®Green I mix (Roche Diagnostics Corporation) and 1 µl of sample, in a final volume of 10 µl.

Three reference genes were used at least for each experiment and their number was increased up to five when necessary. The best(s) reference genes were selected for each condition using RefFinder tool (http://fulxie.0fees.us/?type=reference).

Primer efficiencies were calculated by extracting fluorescence raw data and using Chainy (http:// http://maplab.imppc.org/chainy/; Mallona et al. 2017)), a tool designed in the lab, that calculates the amplification efficiencies per well. The efficiency was calculated using and the Cp D2 2nd derivative method, and the averages of the wells included for the analysis were used on LightCycler software to perform the relative quantification analysis to the selected reference genes.

Primers were designed using Real Time PCR Tool from IDT Technologies (http://eu.idtdna.com/scitools/Applications/RealTimePCR/) within exons flanking one intron to avoid possible DNA interference and taking into account primer properties (GC content, melting temperature, self-dimer and hetero-dimer formation). Specificity of primer amplification was evaluated *in silico* using "Primer-search, ePCR" tool of Primer design and search tool (http://bisearch.enzim.hu/, Arányi et al. 2006; Tusnády et al. 2005), Primer3 (http://bioinfo.ut.ee/primer3-0.4.0/primer3/(Koressaar & Remm 2007; Untergasser et al. 2012)) and "In-Silico PCR" tool from UCSC Genome browser (genome assembly mm9, http://genome.ucsc.edu/). Selected primers were purchased from Life technologies (Invitrogen) desalted and using 50 nM as a synthesis scale. Upon arrival, they were dissolved in nuclease-free, sterile water to 100 µM to make the stock solution and these solutions were further dissolved to make working solutions at 10 µM. All of them were stored at -20 ºC.

To set up annealing temperatures and times of each pair of the primers, control cDNA's of expressing cells in each case were used at different concentrations and both Ct variation and melting peaks were taken into account. When only one peak in the melting dissociation curve was observed, 1 µl of the PCR products was ran with 1 µl of loading DNA buffer 2 X on 2% agarose gels stained with ethidium bromide for 20 min at 160 mV to check if the size of the obtained amplicons coincided with the expected ones. Amplicon identity was confirmed when necessary by conventional Sanger sequence as described above for bisulphite products. The primers used in this work are listed on Tables 11 and 12.

Gene name	F (5'->3')	R (5'->3')	Amplicon lenght (bp)
HDAC members			
HDAC11	ttacaaccgccacatctacc	gacattcctctccaccttctc	118
HDAC1	tgaggaggaccctgacaaac	accaccttctccctcctcat	100
HDAC2	catggtgatggtgttgagga	tcatgggaaaattgacagca	151
HDAC3	cgacgctgaagagagaggtc	tttccttgtcgttgtcatgg	92
HDAC4	ttctgaagcctgcgtgtc	ggcattgggtctctgatgtag	82
HDAC5	ggtttgatgctgttgaaggac	agatggcggtcaagtcatg	150
HDAC6	cctagatgtgtcccaaccttg	tgttcagaggcttcatggtg	132
HDAC7	catctgtgatgcctcggag	cagccccagtatttcctgtg	150
HDAC8	accgaatccagcaaatcctc	cagtcacaaattccacaaaccg	149
HDAC9	cgttcatgtagcaatggaagg	gagactgagggtgtaatggaac	131
HDAC10	ttgtgtaccacgaggacatg	ctcacaagctgacaaacacag	149
Myogenic genes			
PAX7	caggagactgcgtccatccg	ccgaacttgattctgagcac	219
MYOD	gccgcctgagcaaagtgaatg	cagcggtccaggtgcgtagaag	192
MYF5	gccatccgctacattgagag	acagggctgttacattcagg	143
MGN	ggtgtgtaagaggaagtctgtg	taggcgctcaatgtactggat	182
MCK	aggcatggcccgagac	agatcacgcgaaggtggtc	101
MYH3	aaaaggccatcactgacgc	cagctctctgatccgtgtctc	200
MYH8	aacagaaacgcaatgctgagg	tcgcctgtaatttgtccacca	135
MYH1	ccaaagccaacagtgaagtg	tggcgttcacagcttctac	144
MYH2	tcaggcttcaggatttggtg	ggatcttgcggaacttggatag	114
MYH4	caaaagcaaagggaagagcag	agcagagttcagacttgtcag	84
MYH7	aatgcagagtcagtgaaggg	tcttcctgtcttcctctgtct	82
Quiescence gene			
CalR	agtgaagtctgcgttcctga	gcgctctaatggcacttacc	94
RNA-seq validation			
KI67	ttgcaaaattgaagtcaaagagc	tcaatgatggttattatgtctcc	132
ADCYAP1R1	aaatgagtcttccccaggttg	tgagatggtccttgtgagctg	149
DYNAP	ggagtccttactgttcaacgg	tggatgtggcaactagacaag	147
SCN9A	agcacagttgataaccctctg	aaactttccctttcccggag	148
TNFSF11	aggctcatggttggatgtg	gaggacagagtgactttatggg	114

KCNN4	attccgatcacattcctgacc	tgttgaactccagcttccg	148
AURKA	gccccttggaacagtctatag	ctctggcttaatgtctctgtgg	142
AURKB	agggagaactgaagattgcag	cccgatgcaccatagatctac	149
PCNA	gggtgaagttttctgcaagtg	gtacctcagagcaaacgttagg	137
PVALB	ctggacaaagacaaaagtggc	gacaagtctctggcatctgag	86
TRDN	aagactccaaagatgtcccac	aacccatagccattgtaccc	133
ATP1A2	aaatccccttcaactccacc	gatctccttgccctgtacc	146
MYL2	agccttcacaatcatggacc	aagttaattggacctggagcc	144
RYR3	ggagggtgttctatgaagctg	gtagtggcctgtggtaagatg	143
MYOM1	accgaggaaaagataagagcag	cagacaaaggagtatagccgg	148
MYOM2	atcttagccatgagtcgtgtg	agctgaccttcatttcctctg	121
MYOM3	agagtcgctttcagtggttc	ctctgtagactccctggttttc	123
TTN	cagcggaaagtacacaattaagg	cactgctcgttttcaataccac	122
TCAP	tgagctgccaagtgtctg	ggtctcatgcctctgtgtatc	134
TMOD1	gccctgaaagagaactcctatg	ccagagatgaagttggactcc	143
ACTN3	gagaagggctatgaggattgg	tcgtagtcgtgctggtttaac	146
RYR1	tccgcaccatcctttcatc	cgtcctcatcttcgctcttg	144
DYSF	agatggacgatgctgtgatg	cactgagggttagctgtcttc	148
CCNA2	gtccttgcttttgacttggc	acgggtcagcatctatcaaac	139
CCNF	agcgacagaaaggtggatatg	ttcccttccagtccaagttg	149
CCNB2	cctcagaacaccaaagtaccag	ccttcatggagacatcctcag	148
CXCL12	actccaaactgtgcccttc	aagctttctccaggtactcttg	106
Citokines			
CD68	caaagcttctgctgtggaaat	gactggtcacggttgcaag	140
CCL2	ggtcttcagcacctttgaatg	attaaggcatcacagtccgag	145
IL6	gaacaacgatgatgcacttgc	cttcatgtactccaggtagctatggt	154
IL12	cgcagcacttcagaatcaca	tctcccacaggaggtttctg	129
Arg1	caatgaagagctggctggtgt	gtgtgagcatccacccaaatg	153
Il-10	caaggagcatttgaattccc	ggccttgtagacaccttggtc	157
Splicing			
USPL1(1/2)	gagttcgggtccactgtatg	ggcaaaccatttccaatcttcag	60
HIF3A(3/7)	gggtttcgtcatggtactcac	cgtcttgaagttcctcttggtc	65
KCNG4(2/3)	caccatgcccgacttcag	accacgaagatgtaatagcact	72
COL5A1(62/63)	tgaacagatgaagcgaccac	gcagtagactttgaaggagtcc	148
Reference genes			
TBP1	gggagaatcatggaccagaa	ccgtaaggcatcattggact	113
GAPDH	actcccactcttccaccttc	tcttgctcagtgtccttgc	271
RLP	gaggaagtataactggagtgcc	tcttgggtttcggcgttg	131
SDHA	agtgcgggtcgatgagtatgat	tatgaggggaaacgcaggtaag	176
18S	ttgacggaagggcaccaccag	gcaccaccacccacggaatcg	150

Table 11. Primer sequences used for mouse qPCR analysis of mRNA expression. All primer annealing temperatures was 66ºC.

Gene name	F (5'->3')	R (5'->3')	Amplicon lenght (bp)
HDAC11	gtttctgtttgagcgtgtgg	ggtagatgtggcggttgtag	140
MYOD	gctccaactgctccgac	tgtgagagctgcattcgc	144
MYOG	gtgccatccagtacatcgag	tgcactggagttcagcg	126
Reference genes			
PUM1	cggtcgtcctgaggataaaa	cgtacgtgaggcgtgagtaa	121
TBP	gtggggagctgtgatgtgaa	tgctctgactttagcacctgt	182
RPO	ttcattgtgggagcagac	cagcagtttctccagagc	156

Table 12. Primer sequences used for human qPCR analysis of mRNA expression. All primer annealing temperatures was 66ºC.

Genome-wide expression analysis

Microarray

For proliferating and differentiating myoblasts expression analysis, previous data generated in the lab was considered (Carrió et al. 2015). Briefly, Mouse 8x60K one color microarray (Agilent Technologies) was used. Gene expression differences with log_2fold change>1.2 and with a false discovery rate (FDR) <0.01 were considered statistically changing.

For quiescence and activation satellite cell expression analysis, also previous data generated in the lab was used (Carrió 2015). Quiescent satellite cells were isolated from muscles from three 6-to 8-week- old Pax7Cre^{-} /YFP mice generated by Bosnakovski and collaborators (Bosnakovski *et al.,* 2008) and kindly provided by Dr. Pura Muñoz-Cánoves (UPF, Barcelona). The extraction of muscle mononuclear cells was performed as explained in the previous sections and the satellite cells population (cells expressing yellow fluorescent protein) was sorted by fluorescence-activated cell sorting (FACS) and directly frozen. Alike, *in vivo* activated satellite cells were isolated from Pax7/YFP^{+} mice 6 and 72 h after CTX injury by FACS sorting. Intramuscular injection of 300 µl of 10^{-5} M CTX (Latoxan) was performed in the quadriceps muscle of the mice (Suelves *et al*., 2007) by Dr. Vanesa Ruiz and Mercè Jardí (P. Muñoz-Cánoves Lab, UPF, Barcelona). This concentration and volume were chosen to ensure maximum degeneration of the myofibers.

RNA-seq

For transcriptomic analysis of D1 differentiating WT and KO myoblasts, RNA was extracted as described using PureLink™ RNA Mini Kit (Ambion, Life Technologies), including On-Column PureLink® DNase treatment.

RNA-seq library preparation

Library preparation was performed by Dr.Raquel Pluvinet at the High Content Genomics and Bioinformatics Unit of the Germans Trias I Pujol Research Institute (IGTP). RNA integrity was assessed by Bioanalyzer nano 6000 assay. All samples had RNA integrity number (RIN) values between 8 and 9.4. Stranded mRNA sequencing libraries were generated with the NEBNext® Ultra™ Directional RNA Library Prep Kit for Illumina starting from 100 ng of total RNA subjected to oligo-dT capture with the NEBNext Poly(A) mRNA Magnetic Isolation Module. Libraries obtained had an average size range between 344 and 424 bp as determined by Bioanalyzer DNA 1000 assay. Libraries were quantified by qPCR with the KAPA library quantification kit for Illumina GA. Sequencing was performed at the Genomics Unit of the Center for Genomic Regulation (CRG) on an Illumina HiSeq2500 sequencer using TruSeq v4 chemistry to generate between 46 and 62 million 2x50 bp paired end reads per sample.

RNA-seq data analysis

Bioinformatics and statistical analysis was performed by Dr.Gabriel Rech and Dr.Lauro Sumoy at the High Content Genomics and Bioinformatics Unit of the IGTP. Raw sequencing data was assessed for quality with FastQC (http://www.bioinformatics.babraham.ac.uk/projects/fastqc; Andrews 2010) and quality based trimming was performed using Trimmomatic (http://www.usadellab.org/cms/?page=trimmomatic; Bolger et al. 2014). Trimmed reads were aligned to the mouse reference genome (Ensembl release 85, Mus_musculus.GRCm38.dna.primary_assembly) with Tophat v2.0.8 (http://ccb.jhu.edu/software/tophat/index.shtml, Trapnell et al. 2009), which uses Bowtie v2 (http://bowtie-bio.sourceforge.net/bowtie2/index.shtml). The resulting BAM files were further analyzed using the QualiMap software (http://qualimap.bioinfo.cipf.es/; García-Alcalde et al. 2012). Aligned reads were counted using FeatureCounts (Liao et al. 2014) based on annotation at the gene, transcripts and exon level. Differential gene expression analysis between WT and KO mice was performed with the DESeq2 R package (Love et al. 2014) with p value correction adjusting for multiple testing by the false discovery rate (FDR) method of Benjamini and Hochberg.

Functional enrichment was assessed with several different tools. First, gene ontology enrichment analysis was performed using the GOrilla web server (http://cbl-gorilla.cs.technion.ac.il/; (Eden et al. 2009)) on the top significant upregulated and downregulated genes after applying a cutoff of an absolute fold change larger than 1.2 and

adjusted p-value under 0.05. We also used Enrichr (http://amp.pharm.mssm.edu/Enrichr/, Chen et al. 2013, Kuleshov et al. 2016) to search for further functional enrichment. We then used the same gene lists as input for the compareCluster function in clusterProfiler (Yu et al. 2012) and the Pathview (Luo & Brouwer 2013) packages in the R statistical programming environment to graphically depict individual gene expression in enriched KEGG pathways. Finally we performed gene set enrichment analysis (using the GSEA software, (Subramanian et al. 2005) on preranked log2ratio data using the weighted statistic option to explore the following MaSigDB geneset collections: C2 ('cgp', curated literature genesets from cellular and genetic perturbation, and 'cp' canonical gene pathways including KEGG, REACTOME, SA,PID,), C3 (miRNA, for miRNA targets, and 'tft', transcription factors), C5 (gene ontology) and C7 (immunological gene sets). For GSEA analysis we converted mouse symbols to the closest human orthologues using the MART tool in ENSEMBL and reducing the list such that a gene with several orthologues passed the log_2ratio value to al hits and log_2ratio values of several genes with a common orthologue were averaged.

Protein expression analysis

Total protein extraction

For cell pellets, cells were washed with cold PBS 1X and scrapped on ice. Pellets were obtained by centrifuging at 300 rcf for 5 min at 4ºC and stored at -80ºC until processing. Pellets were resuspended on radioimmunoprecipitation assay buffer (RIPA), containing, 150 mM NaCl, 1% Triton X-100, 0.5% deoxycholate, 0.1% SDS and 50 mM Tris pH, and supplemented with fresh protease inhibitors (Table 13). The amount of RIPA was proportional to the volume of pellet obtained (for a 10 mm plate about 50 µl of RIPA were used). The pellets were pipetted with RIPA intensively and cell lysis was allowed for 30 min on ice, followed by 30 min of centrifugation at 16,000 rcf at 4ºC, to remove insoluble particles.

For tissue fragments, tissues were cut on dry ice and immediately resuspended on RIPA buffer prepared as for cell pellets, followed by homogenization with TissueRuptor (Qiagen) on ice. Then, lysis was allowed to proceed for 30 min and after that lysates were passed trough 26 GA syringes several times to reduce viscosity. After the lysis, the extracts were centrifuged at 16,000 rcf for 30 min to remove insoluble particles.

Protease inhibitor	Working concentration	Proteases inhibited
Aprotinin	2 µg/ml	Trypsin, chymotrypsin, plasmin
PMSF	30 mM	Serine, cysteine proteases
Sodium orthovanadate	1 mM	Tyrosine phosphatases
Sodium fluoride (NaF)	5 mM	Serine/threonine phosphatases
Pepstatin A	2 µg/ml	Aspartic proteases

Table 13. Protease inhibitors used for WB sample preparation. Source: Abcam (http://www.abcam.com/protocols/sample-preparation-for-western-blot)

Nuclear and cytoplasmatic separation analysis

Nuclear and cytoplasmatic fractions were separated using NE-PER® Nuclear and Cytoplasmic Extraction Reagents (Ref. 78833) according to manufacturer's instructions.

Protein quantification

Protein extracts were quantified by the BCA method (BCA™ protein assay reagent A, #23223; BCA™ protein assay reagent B, #23224, PIERCE). Briefly, 49 parts of reagent A were mixed with 1 part of reagent B in a sufficient amount for the total number of samples, using 200 µl per sample and 10 µl of protein extract per well. The quantification was performed on transparent 96 well plates with flat base (Ref. 82.1581, Sarsted), including 9 dilutions of known concentration of purified bovine serum albumine (BSA) (Ref. A-7906, Sigma-Aldrich, USA) on water (10, 5, 2.5, 1.25, 0.625, 0.313, 0.156, 0.078 and 0.039 µg/µl), water and the corresponding protein lysis buffers in each case as blanks. The mixtures were incubated for 30 min at 37ºC and the final point absorbance was read at 562 nm on a Spectramax 340 PC spectrophotometer with the software version SoftMax Pro 5.3. (Molecular Devices, USA). Concentrations were calculated by extracting of read absorbances with the corresponding blank wells. The calibration curve was calculated with the standards and applied to calculate samples' concentrations according to Lambert-Beer law.

Protein separation and Western blot detection

For each sample, 40 to 50 µg of protein extract were used. Samples were diluted up to the same volume with water and mixed with 5X Laemli buffer (LB) containing β-mercaptoethanol to a final 1X concentration (final 1X LB concentrations: 25% v/v glycerol, 2% w/v SDS, 0.01% w/v bromophenol blue and 5% v/v β-mercaptoethanol) and boiled for 5 minutes at 95ºC in a thermoblock. Samples were cold down to RT, spun and immediately load into SDS-acrylamide gels or stored at 4ºC until use.

Samples were separated using 8% sodium dodecyl sulphate polyacrylamide gels (SDS-PAGE) except for histone detection were a percentage of 15% was used on the bottom of the gels, and a percentage of 8% on the top to separate bigger proteins, followed by the stacking gel. Gels were prepared using Bio-Rad Mini-protean Tetra System, with 1.5 mm spacer glass plates (Ref. 1653312, Bio-Rad). Detailed gel composition is supplied on Table 14. The Precision Plus Protein™ All Blue Prestained protein standard (Cat. 161-0373, Bio-Rad) was included each time to estimate the approximate weight of migrating proteins. Gels were ran in 1X running buffer (25 mM Tris, 192 mM glycine and 3.5 mM SDS) at 100 mV until proteins have been concentrated on stacking gel and then at 150 V until the migrating bromophenol had reach the bottom plates.

After electrophoresis, gels were transferred to 0.45 µm Immobilon® polyvinylidene difluoride membranes (Ref. IPH00010, Millipore), previously hydrated with methanol and washed with distilled water (Ref. 1060092500, Merck), for 1 h at 100 V or o/n at 35 V at 4 ºC (Transfer buffer 1X: 20 mM Tris, 154 mM glycine and 20% methanol).

Transfer was checked by Ponceau S (0.5% w/v Ponceau S, 1% v/v glacial acetic acid in water) staining of membranes and cut to incubate different antibodies. Blocking was performed for 45 min with 5% non-fat milk in 0.1% Tween TBS. All antibodies were incubated in the same

blocking buffer in the conditions listed on Table 15. After incubation, 3 washes with 0.1% Tween TBS 1X (248 mM Tris, 1.37 M NaCl and 26.83 mM KCl, pH:8) for 10 min each were performed, and then the corresponding horseradish peroxidase-conjugated (HRP) secondary antibody was applied for 45 min. After 5 washes for 5 min each, membranes were developed by incubation for 5 min with Luminata™ Classico Western HRP substrate (Ref. WBLUC0100, Millipore) for histones and tubulin detection or Luminata™ Crescendo Western HRP substrate (Ref. WBLUR0100, Millipore) for all other antibodies. Luminescent signals was exposed to High performance chemiluminiscence ECL films (Ref. 28906837, Amersham, GE Healthcare Life Sciences), processed after exposure using

an automatic film processor (Ref. FPM 100A, Fujifilm).

% acrylamide	**3 (Stacking)**	**8**	**15**
Reagents			
Tris 1.5 M (pH 8.8)	-	2.5 ml	2.5 ml
Tris 0.5 M (pH 6.8)	1.25 ml	-	-
30% acrylamide/bis-acrylamide solution (37.5:1) (Ref. 161-0158, Bio-Rad)	1 ml	2.67 ml	5 ml
10% SDS	50 µl	100 µl	100 µl
Distilled H_2O	2.59 ml	4.67 ml	2.34 ml
10% ammonium persulfate (APS)	20 µl	40 µl	40 µl
N,N,N',N'-tetramethylethylenediamine (TEMED) (Ref. T7024, Sigma-Aldrich)	10 µl	20 µl	20 µl
Final volume	5 ml	10 ml	10 ml

Table 14. SDS-PAGE gel composition used according to acrylamide percentages. Tris and SDS solutions were made at common services of PMPPC institute.

Antibody	Source	Catalogue ID	Clonality	Working concentration	Raised species	MW (kDa)
α-HDAC11	Sigma-Aldrich	H4539	Polyclonal	6 µg/ml	Rabbit	39
	Abcam	ab18973	Polyclonal	2.5 µg/ml	Rabbit	
α-PAX7	Developmental Studies Hybridoma Bank	-	Hybridoma	1:200	Mouse	57 (observed 65)
α-MYOD1	Santa Cruz	M-318 (sc-760)	Polyclonal	1:200 (1 µg/ml)	Rabbit	45
α-MGN	Developmental Studies Hybridoma Bank	F5D	Hybridoma	1:50	Mouse	Predicted 24, observed 34
α-MHC	Developmental Studies Hybridoma Bank	MF20	Monoclonal	1:250	Mouse	223
α-H3 ac	Upstate-Millipore	06-599	Polyclonal	1:10,000	Rabbit	17
Tag antibodies						

α-FLAG clone M2	Sigma-Aldrich	F1804	Monoclonal	1:3,000	Mouse	-
α-HA tag	Abcam	ab9110	Polyclonal	1:4000	Mouse	-
Loading controls						
α-TATA binding protein	Abcam	ab818	Monoclonal	1:2,000	Mouse	37
α-Tubulin CloneB-5-1-2	Sigma	T6074	Monoclonal	1:10,000	Mouse	50
Secondary antibodies						
α-mouse IgG HRP	Dako		Polyclonal	1 : 10,000	-	-
α-rabbit IgG-HRP	Dako	P0448	Polyclonal	1 : 4,000	-	-

Table 15. Antibodies used for western blot detection.

Mass spectrometry identification after acrylamide gel excision

The samples were run on SDS-PAGE gels as explained for Western Blot anaylis. Instead of proceeding to transfer the proteins into membranes, gels were stained with Coomassie Blue 1X (10% v/v acetic acid, 10% v/v 2-propanol and 0.1% w/v coomassie blue) for 10 min and destanined with Coomassie destaining (10% v/v acetic acid, 10% v/v 2-propanol) until the washes were clear and the bands identifiable. Interesting regions of the gel at the molecular weights indicated were excised from the gel using clean scalpels and placed into clean eppendorfs. The samples were sent and processed at the Proteomics Unit from Centre for Gene Regulation (CRG). Briefly, samples were digested with trypsin. The 80% of each sample was injected in an Orbitrap XL with a Short method (30 min gradient). To avoid carry over, BSA runs were added between samples. BSA controls were included both in the digestion and LCMS/MS analysis for quality control. The data was searched using an internal version of the search algorithm Mascot (http://www.matrixscience.com/) against a *Mus musculus* data base (SP_mouse July 2013). The analysis of the generated data was performed with Proteome discoverer v 1.4 filtering the peptides using 1% FDR.

HDAC11 immunofluorescence

C2C12 were grown onto glass coverslips and fixed with 3.7% formaldehyde for 10 min at the indicated points followed by two washes twice with PBS and blocking of unspecific interactions for 30 min with 5% horse serum and 1% BSA in 0.25% Triton X-100. Then, they were incubated for 1h at RT with 2% horse serum and 1% BSA with HDAC11

antibodies (1:50 v/v ab18973 or 1:25 v/v H4539) or 1:500 α-Flag F1804. Three washes of 5 min each with PBS containing 0.2% Tween-20 were performed and then they were incubated for 45 min at RT with 1/350 v/v α-rabbit Alexa green IgG (L+H) (Ref. A110470, Invitrogen) or α-mouse Alexa 488. Then, three washes with PBS 0.2% Tween were performed and finally coverslips were mounted with Vectashield mounting medium with DAPI (Ref. 53826, Palex Medical S.A.).

Co-immunoprecipitation

Cell plates at the indicated points of differentiation were washed with PBS, scrapped on ice and pelleted at 300 rcf for 5 min at 4ºC. Cells were washed again with cold PBS and pelleted again. Cell pellets were resuspended in Co-IP lysis buffer (25 mM TrisHCl pH 7.5, 150 mM NaCl, 1% NP-40, 1 mM EDTA, 5% glycerol), supplemented with protease inhibitors to a final concentration of 2 µg/ml of aprotinin, 30 mM PMSF, 1 mM sodium orthovanadate, 5mM NaF and 2 µg/ml of pepstatin. Lysis was performed for 30 min at 4ºC in rotation. Lysates were then passed trough 26 GA syringes several times to reduce viscosity. After the lysis, the extracts were centrifuged at 16,000 rcf for 30 min to remove insoluble particles. The extracts were quantified using BCA as explained. An aliquot corresponding to 100 µg was saved for posterior analysis as "Input" fraction. For each co-immunoprecipitation, 1 mg of protein and 25 µl (0.25 mg) of Pierce™ α-HA magnetic beads containing α-HA IgG1 monoclonal mouse antibody were used, in a final volume of 100 µl (filled up with Co-IP lysis buffer supplemented with protease inhibitors, when needed). According to manufacturer instructions, first, the beads were washed with 175 µl of cold PBS containing 0.05% Tween-20 (PBS-T), gently resuspended by tapping to mix, and placed into a magnetic stand to remove the supernatant. After another wash with 1ml of PBS-T, the extracts were added to the beads, and incubated together for 7 h to o/n at 4ºC in tube rotators. Then, the extracts were removed and saved for analysis as an "Unbound fraction" and the beads were transferred to another eppendorf and washed twice with 1 ml of Co-IP lysis buffer for 5 min, twice with 1ml for 5min also of a more astringent washing buffer containing PBS with 1% Tween-20 and 500 mM NaCl, and twice with 1ml of PBS for 5min to remove detergents and salts. For WB analysis, proteins were changed of eppendorf again and eluted with 50 µl of SDS-PAGE buffer without DTT or β-mercaptoethanol to prevent antibody dissociation from the beads (4% w/v SDS, 0.2% w/v bromophenol blue, 20% v/v glycerol). The beads were incubated with SDS-PAGE

buffer for 5min at 92ºC with shacking. Finally, the beads were removed using a magnetic platform and 10 µl of 1M DTT were added to a final concentration of 200 mM. Eluted inmunoprecipitations were subjected to Western blot analysis as described previously.

Mass spectrometry analysis

For mass spectrometry analysis, the Co-IP was performed as described until the elution step. Instead of that, samples were digested, desalted, precipitated and dried according to the Proteomics Unit protocol from the Centre for Genomic regulation (CRG). Briefly, beads were washed three times with 500 µl of 200 mM ammonium bicarbonate buffer (ABC). Then, they were resuspended in 60 µl of 6M urea and 200 mM ABC and disulfide bonds were reduced by incubation at 37ºC for 1h with shaking, in the presence of 10 mM dithiothreitol. After that, free sulfhydryl groups of cysteins were alkylated by incubation of the previous mix with 20 mM iodoacetamide for 30 min with shaking, at RT and darkness. After alkylation, samples were diluted to decrease urea concentration with 280 µl of 200 mM ABC. Then, samples were digested by o/n incubation with 1 µg of sequencing grade modified porcine Trypsin (Ref. V511A, Promega) per sample, at 37ºC with shaking. Next day, the beads were removed using a magnetic rack and the supernatant was kept. The digestion was stopped by acidification with 20 µl of 100% formic acid. C18 stage tips (UltraMicroSpin Columns, Ref. SUM SS18V, The Nest Group) were used for sample desalting. First, columns were conditioned with 400 µl of Methanol (Ref. 1060092500, Merck), followed by centrifugation at 100 rcf for 5 min. Then, they were equilibrated by addition of 300 µl of 5% formic acid and centrifugation at 100 rcf for 5 min. This step was repeated twice and the collector eppendorf was changed. After equilibration, the sample was loaded onto columns and centrifuged at 100 rcf for 10 min. Then, columns were washed twice with 300 µl of 5% formic acid and centrifuged at 100 rcf for 5 min. After eppendorf change, samples were eluted by addition of 300 µl of 50% acetonitrile, 5% formic acid and centrifuged at 100 rcf for 5 min. The elution step was repeated twice. Finally, solvents were evaporated by centrifugation in vacuum conditions at 45ºC for 2h in a miVac concentrator (Ref. DNA-23050-B00, Genevac Ltd, UK). Unless indicated, reagents were provided by the Proteomics Unit (CRG). Dried samples were processed by the Label-free quantitation method.

Chromatin immunoprecipitation (ChIP)

Cells were seeded at confluency 6,452 cells/cm^2 (10^6 cells/15 mm cell culture dishes) and grown on GM for three days when it was replaced with DM (moment in which the cells have reachen confluency). The cells were differentiated for 24 h and two plates were used per point while an aliquot to perform expression analysis was separated.

For ChIP analysis, cells were cross-linked by adding 1% formaldehyde for 10 min at RT with shacking (540.4 µl of 37% formaldehyde 37%, Ref. K41839403, Merck to each 150 mm culture dish containing 20 ml of differentiation media). After 10 minutes, unreacted formaldehyde was quenched by adding fresh glycine at a final concentration of 125 mM (1250 µl from 2M glycine freshly prepared with 1.5 g glycine (Ref. 68790, Sigma) to 10 ml of water). The plates were incubated for 5 min at RT with shacking. The media was then discarded and the plates were washed twice on ice with PBS 1X containing protease inhibitors (cOmplete, Mini Protease inhibitor cocktail, Ref. 11836153001, Sigma-Aldrich). Then, the cells were scrapped with PBS and protease inhibitors on ice and collected onto 15 ml falcons followed by centrifugation at 1500 rpm for 5 min at 4ºC to obtain the pellet. The supernatant was discarded and the pellet was stored at -80ºC until processing. MagnaChIP A/G kit was used (Ref. 17-10086, Millipore). To share the DNA, the pellets were defrost on ice and resuspended in 500 µl of cell lysis buffer containing protease inhibitors (1mM PMSF, 1ug/ml aprotinin and 1ug/ml pepstatin) and incubated on ice for 15 min with vortex each 5 min. The nuclei were recovered by centrifugation at 800 rcf for 5min at 4ºC, the supernatant was discarded and the pellet were resuspended on 500 µl of pre-warmed nuclear lysis buffer (to dissolve SDS) containing protease inhibitors. The nuclei were immediately sonicated in 15 ml falcon tubes with 10 ml tube holders (Ref. B01200012, Diagenode) in a Bioruptor (Diagenode) with high settings on in 4 cycles of 30 s on/ 30 s off. Each cycle, the water bath temperature was check and the water was replaced with ice cold water containing crushed ice. The sonication conditions were previously set up. After sonication, the samples were stored at 4ºC and the sonication efficiency was checked. For that, an aliquot of 20 µl was taken from each sample, diluted with 90 µl TE buffer and reverse cross-linked by incubation at 65ºC with shacking for 1 h. After this time, DNA was purified using JETQuick columns (Ref. 410250, Genomed) following manufacturer protocol. DNA was eluted with 20 µl of water heat at 65ºC and the recovered DNA was ran into 1% agarose gels stained with ethidium bromide for 1h to check that sheared DNA was between 500-200 bp long. On the meanwhile, another aliquot of the sonicated samples was diluted 1:10 and 1:20 v/v with water and the DNA

concentration was calculated with Nanodrop as described.

For each immunoprecipitation reaction (IP), 50 µg of shared chromatin were diluted 10 folds with dilution buffer and mixed with 20 µl Magna ChIP™ Protein A+G Magnetic Beads (Ref. 16-663, Merck-Millipore) and the corresponding amounts of antibodies listed on Table 16. The same amounts of normal IgG of the specie in which the antibodies were raised were used as controls. For one IP reaction per sample condition, 5 µl of the diluted chromatin were saved as "Input control". The samples with the beads and the antibodies were incubated o/n at 4ºC and in rotation.

Antibody	Amount per IP	Reference	Supplier	Specie
α-H3	10 µl	1791	Abcam	Rabbit
α -panH3ac	5 µg	06-599	Upstate-Millipore	Rabbit
α -H3K9ac	5 µg	07-352	Millipore	Rabbit
IgG	5 µg			Rabbit

Table 16. List of antibodies used for ChIP.

After 16 h, the supernatant was discarded from the beads using a magnetic rack, and they were washed at 4ºC once with 500 µl of low salt buffer, once with 50 µl of high salt buffer, 500 µl of LiCl buffer and twice with 500 µl of TE buffer. Between washes, the beads were incubated for 5 min at 4ºC with rotation. After the washes, the beads and the inputs were eluted with 100 µl elution buffer and 1 µl of 10 mg/ml proteinase K per sample at 65ºC with shacking for 2 h followed by 10 min at 95ºC. The samples were cold to RT, the beads were removed and the supernatant was purified using JETQuick columns following the manufacture's protocol. The DNA was eluted on 50 µl of water. The samples were quantified by qPCR as explained in "qPCR analysis" using directly 1µl of eluted DNA per reaction and the reactions were performed in technical triplicates with the primer pairs listed on Table 17. The efficiencies were extracted with Chainy as for cDNA expression quantification but the normalization was performed using an Excel template.

Briefly, the histone marks values were always normalized by input and total H3. For input normalization, the ΔCp was calculated by extracting the average value Cp of the histone marks to the average Cp value of the corresponding input and the normalized ratio was calculated using the formula Efficieny ^(-ΔCp). For H3 normalization the procedure was the same substituting the average of Cp of the input with the average Cp of H3.

Name	F (5'->3')	R (5'->3')	Amplicon lenght	Genomic location	Relative position to TSS	Comments
ChIP controls						
ACTB1 promoter	tcgctctctcgtggctagta	ggaatgtggctgcaaagagt	152	chr5:143668149-143668300	(+255:+104)	Positive control H3K9ac
Gene desert Chr6	ctggacgtgtggatgttgtc	cctcctgcttacacctcagc	51	chr6:120258781-120258831	ND	Negative control H3K9ac
Targets RNA-seq						
DYNAP_1	agagtacccacctgctctgc	cccaggatggttagaaagca	74	chr18:70403969-70404042	(+270:+197)	
DYNAP_2	ccaaggcattggtttgagta	cagactcgtgaaaacgtacctg	63	chr18:70403441-70403503	(+798:+736)	
KCNN4	ctgctggagcaggagaagag	cccaggaaccacaacatctc	101	chr7:25155507-25155607	(+226:+326)	
AURKA_1	cccattcccacaagaaccta	aaacggatagggaaggctgt	125	chr2:172195801-172195925	(+206:+82)*	(+225:+101)
AURKA_2	actcccgttcatccacagac	gggatccagaccatcagcta	134	chr2:172195669-172195802	(+338:+205)*	(+354:+224)
AURKB_1	gagcgcctagtggcgtag	gatagcgggcacgtggat	104	chr11:68859194-68859297	(+50:+153)	
AURKB_2	tcgctgttgtttccctctct	taccgtctttgagccgtagg	103	chr11:68859411-68859513	(+267:+369)	
PCNA	cacctggtgaggttcacg	tcgtctcacgtctcctggt	101	chr2:132078549-132078649	(+368:+268)	

Table 17. List of primers used for qPCR ChIP analysis. The annealing temperature for all the primers was 64ºC. *: AURKA gene has 2 TSS, for isoforms 201 and 002 (Ensembl) the relative position is indicated. The relative positions with respect to isoform 001 are the indicated in comments.

CRISPR-Cas 9 knock-in

CRISPR vector and sgRNA cloning

LentiCRIRPR v2 one-vector system (Ref. 52961, Addgene) was directly purchased from Addgene (gift from Feng Zhang). In Figure 14 are indicated its vector map and detailed the elements for genome editing.

The sgRNA sequences were designed using CRISPR design (http://crispr.mit.edu/, Zhang lab). Three sgRNA's were selected to test their efficiencies. They were purchased as oligonucleotides to Invitrogen using 50nM scale synthesis and desalted. The sequences are indicated on Table 18. The cloning was performed as described in http://genome-engineering.org/gecko/wp-content/uploads/2013/12/lentiCRISPRv2-and-lentiGuide-oligo-cloning-protocol.pdf and (Ran et al. 2013). Briefly, lentiCRISPR v2 vector was digested with BsmBI enzyme. The products were ran into 1% agarose gels and the vector was cut from the gel leaving in the gel the 2 kb filler. The cut vector was extracted from the gel using NucleoSpin Gel and PCR Clean-up (Ref. 22740609.5, Cultek) and

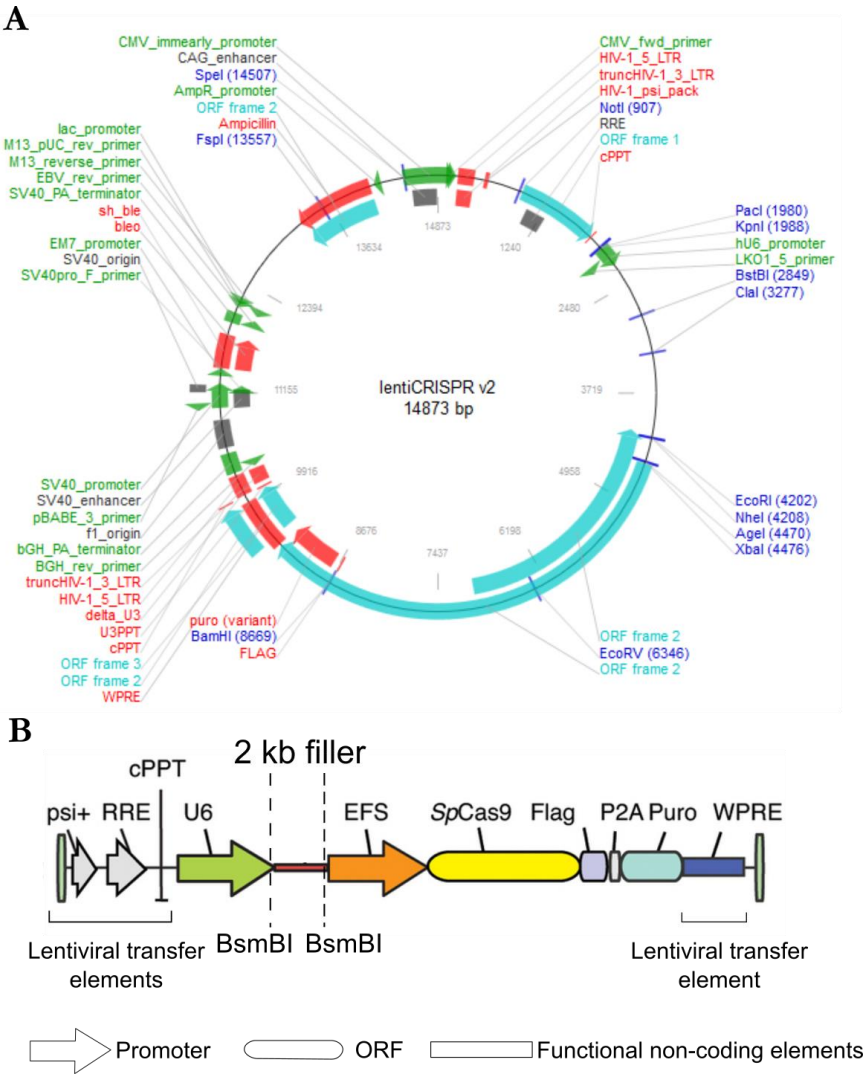

Figure 14. LentiCRISPRv2 vector map. A Complete map for lentiCRISPR v2 (the image was modified from https://www.addgene.org/52961/). **B** Detailed elements important for genome engineering. These include the elements that allow lentiviral transfer to the cell: psi: packaging signal, RRE: reverse response element, cPPT: central polypurine track and WPRE: Woodchuck hepatitis virus post-transcriptional regulatory element; and the elements that allow the simultaneous expression of the sgRNA: U6 promoter for sgRNA expression (note that the vector comes with 2 kb DNA filler that needs to be removed by BsmBI restriction which generates the restriction sites to clone the sgRNA. Included also but not represented after the 2nd BsmBI restriction site is the invariant sequence for sgRNA scaffold that will direct the sgRNA); and the elements to express Cas9 protein: EFS: elongation factor 1α short promoter, *Sp*Cas9: *Streptococcus pyogenes* Cas 9 protein ORF tagged with a flag (Flag) epitope, P2A: 2A self-cleaving peptide and Puro: puromycin selection marker. The image was modified from (Sanjana et al. 2014).

dephosphorylated to prevent religation using of FastAP™ thermosensitive alkaline phosphatase (Ref. EF0654, Thermo Scientific) at 37ºC for 15 min, followed by 85ºC for

15 min of inactivation. In the meanwhile, the sgRNA were resuspended with PCR water to 100 µM stock solution and each pair of oligonucleotides were hybridized and cloned into lentiCRISPR as described for shRNA cloning. Finally, the ligated constructs were transformed into Stbl3 competent cells by heat shock and sgRNA insertion was verified using the following custom designed primers: lentiCRISPR_v2_F: 5' GAGGGCCTATTTCCCATGAT 3', lentiCRISPR_v2_R: 5' CGGTGCCACTTTTTCAAGTT 3'.

	Sequence F (5'->3')	Sequence R (5'->3')
1	CACCGTGGTACAGCTGTGTTGCGTG	AAACCACGCAACACAGCTGTACCAC
2	CACCGCGAGTTCTGTGCCGAGACGC	AAACGCGTCTCGGCACAGAACTCGC
3	CACCGAGCAACAAACACAGGCGGGT	AAACACCCGCCTGTGTTTGTTGCTC

Table 18. sgRNA sequences used for CRISPR knock-in. Underlined are the sgRNA sequences. The non-underlined regions correspond to BsmBI overhangs.

ssODN repair template sequences

The ssODN were manually designed taking into account Zhang lab's recommendations. For that, about 80 bp flanking the cut point were used as homology arms. For HA taq insertion, the 5' tac cca tac gat gtt cca gat tac gct 3' sequence was used but to facilitate clone screening a mutation on the first tac triplet (taT) was introduced (Paix et al. 2014). ssODN's were directly purchased from IDT as 4 nM ultramer oligos non-PAGE purified and resuspended with H_2O sterile water upon arrival at a working concentration of 10 µM. The complete sequences are listed on Table 19.

Name	Sequence (5'->3')	
ssODN_1 (196 nt)	ggtgtgagtggggaggggaacactgctttccacaaggaggctgttgtccatatgtgtgtctcttttgcacg ttgaaggtacccataTgatgttccagattacgctcctcaTgcCacacagctgtaccagcatgtaccaga gaaacgctggcccatcgtgtactcaccacgttacaacatcaccttcatgggcctgg	▲
ssODN_2 (180 nt)	gaagcgcacagcccgtattatcgccgactccatcctcaacttgcatgacctggggctcattgggcctgag tttccTtgcgtctcggcacagaactcgggcatccccctgctttcctgtgctgtgcctggctacccataTg atgttccagattacgcttgacggctactcacagaacattg	*

ssODN_	ccccctgctttcctgtgctgtgcctggctacccataTgatgttccagattacgcttgacggctactcacag	*
3 (175 nt)	aacattgtcatacctgccccccacccatccacccgTcTacccgcctgtgtttgttgctgtgaagaca	
	gctgccagtgagtgtggaggggcaggaagagcagg	

Table 19. CRISPR sgRNA sequences. Legend: In lower letters are included the cannonical sequences and upper letters correspond to mutations introduced. The introduced mutations encode for the same aminoacid with similar codon usage efficiencies. Red: HA taq. Upper letter base was mutated from tac to taT to introduce a NdeI restriction enzyme site to facilitate clone screening. Purple: exons. Underlined: sgRNA. Gray: PAM sequence. ▲ Note that as the PAM sequence (which is located in the reverse complementary sense) cannot be inactivated by mutation without changing the aminoacid that encodes (proline) and this is located in the coding sequence (2nd exon), two silent mutations were introduced in the sgRNA instead. * In the ssODN located at the 3' of HDAC11 a glycine (ggc) was introduced.

Nucleofection of C2C12

To avoid having constitutively active Cas9 and genomic unstable clones minimizing the off-target events, the vector containing CRISPR-Cas9 was expressed transiently instead of using lentivirus. As C2C12 cell line it is quite a difficult cell line to transfect (with Lipofectamine reagents less than 5% of the cells were transfected), nucleofection was selected to introduce both CRISPR vector and ssODN. A test nucleofecting only with pmaxGFP® Vector was performed obtaining 25% of cells GFP$^+$ 24h post nucleofection (Figure 15).

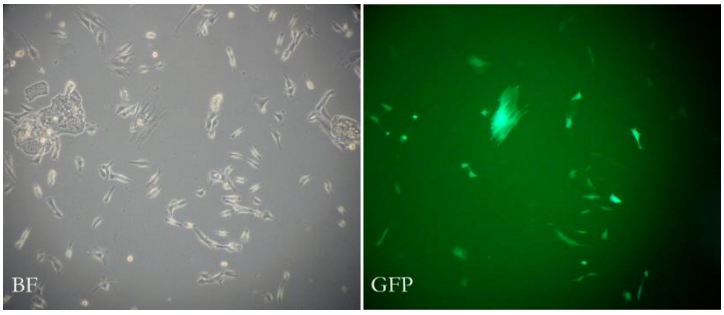

Figure 15. Nucleofection efficiency of C2C12 cells. Bright film (BF) and fluorescence (GFP) microscopy images C2C12 cells after 24h of nucleofection.

As described by the manufacturer to nucleofect this cell line, Amaxa™ Cell line Nucleofector™ Kit V (Ref. VACA-1003, Lonza, Amaxa GmbH, Germany) was used. C2C12 was amplified in subconfluent conditions to have the estimate amount of cells needed the day of nucleofection. First, the supplement was added to the nucleofector solution in a ratio of 1:4.5 according to manufacturer instructions and both were heat to RT. Then, C2C12 cell plates were trypsinized and counted. 10^6 cells for each condition were spun down at 300 rcf for 5min. The supernatant was discarded and the pellet was resuspended in 100 µl of Nucleofector solution and carefully transferred to the cuvettes avoiding bubble formation. For each nucleofection condition (one condition for each

sgRNA and their corresponding ssODN) they were added 2.5 μg of Lenti CRIRPR v2 with the corresponding sgRNA cloned and 5 μl of 10 μM of the matching ssODN. An additional 10^6 cell pellet was nucleofect only with 2 μg of pmaxGFP® Vector (included in Nucleofector kit V) as a control of nucleofection. The cuvettes containing the mix were inserted into a Nucleofector II device (Ref., Lonza), where the program B-032 was ran. After nucleofection, 500 μl of medium were added and the cells were carefully transferred to previously prepared plates with pre-warmed GM. Next day, the nucleofection efficiency was assessed by checking the GFP expressing control cells and to select the cells that had incorporated the vector, puromycin was added to the media to a final concentration of 3 μg/ml for 72 h. After that time, the cells were maintained in GM until clonal isolation was performed. A representative population of each pool of cells (3 in total corresponding to the 3 nucleofections) together with a sample from WT cells, were separated to assess knock-in efficieny.

Clonal isolation of C2C12

Clonal isolation was repeated twice, once by performing serial dilutions and once with single plating by FACS sorting.

For serial dilutions, the cells were counted as explained with cell counter CountessTM (Invitrogen) and EveTM cell counting slides (NanoEntek) (data window: 9-25μm, 75% circularity). Then, 100,000 cells were diluted in 10 ml of GM to make a concentration of 10,000 cells/ml. This solution was successively diluted to 1,000 cells/ml, 100 cells/ml and finally to 10 cells/ml (1cell/100 μl). With this final working solution, several 96 well plates were filled with 1 cell/well concentration or 0.5 cells/well per condition. The wells were inspected daily to select those ones which had only included 1 cell/well and these ones were successively amplified to 24 well, 12 well and 6 well avoiding cell contact.

For FACS sorting isolation, the cells were trypsinized and 10^6 cells were pelleted, resuspended in 1 ml of GM and brought to the Cytometer service of IGTP. The cells were sorted in a FACSAriaII and plated onto 96 well plates prefilled with half of the final volume (50 μl) with prewarmed media. In this case, all the wells contained 1 cell in the middle of the well and only viable clones were selected and also inspected daily to avoid cell contact.

Efficiency of HA incorporation in pools and screening of positive knock-in clones

DNA extraction of cell pools and clones was performed as explained in "Bisulphite

analysis, DNA extraction", adding 1 µl of glycerol as a carrier (Ref. 10901393001, Sigma-Aldrich). As the number of screened clones was quite high, some clones (n=38) where tested by PCR without performing the DNA extraction directly by aspirating the cell media, adding 50 µl of TE to the cell wells and freezing them directly in the plates at -80ºC and then refreezing them at 37ºC (two cycles) to break them. 5 µl of these supernatants where directly used for PCR analysis. The efficiency of this method was 79% by control PCR amplification (30/38 clones).

The clones were screened by three different methods. In each case, oligonucleotides flanking the engineered region were designed to amplify the region to modify using Primer3 (http://bioinfo.ut.ee/primer3-0.4.0/primer3/(Koressaar & Remm 2007; Untergasser et al. 2012)). The oligonucleotide sequences, PCR conditions and amplicon lengths are listed on Table 20.

As the difference of PCR lengths were no longer enough to unequivocally determine HA insertion, a nucleotide from the canonical HA sequence was mutated to introduce an NdeI restriction site to assess HA incorporation, as described. For that, for clone screening, as Phusion GC buffer is compatible with the restriction enzyme, 0.5 µl (5 U) NdeI 10U/µl were added directly to each PCR reaction (Ref. ER0581, Thermo Fisher Scientific) and incubated at 37ºC o/n.

A

Name	F (5'->3')	R (5'->3')	Length (bp) WT	KI
5'_UTR	AGCCGCTGTTAGGACTGTGT	GAAGGCAGTAGGCAGTCTGG	523	550
HA_F	CATATGATGTTCCAGATTACGC	5'_UTR_R	0	372
HA_R	5'UTR_F	GCGTAATCTGGAACATCATATG	0	200
3'_UTR	CTGTCTTCCCACAGGGCATT	GCCTCCCAATCCATACCAGG	728	758

B

Reagent volumes	**1x (µl)**
Buffer GC 5x	2
dNTPs 5 mM	0.4
F 20uM	0.25
R 20uM	0.25
Phusion taq (2U/ul)	0.1
H_2O	6
Sample	1
Vf	10

Temperature (ºC)	Time	Number of cycles
98	30 s	1
98	10 s	30
64	20 s	
72	30 s	
72	5 min	1
16	∞	1

Table 20. Primers used for CRISPR validation. A Primer sequences and expected amplicon lengths. **B** PCR reaction mix per 1 sample and thermocycler program (all pairs have the same mix and amplification conditions). The PCR's were performed with Phusion High Fidelity polymerase (Ref. E385HT, ThermoFisher Scientific).

For sgRNA's 2 and 3, the corresponding restriction products were ran into 2% agarose gels stained with ethidium bromide as described. For sgRNA 1, as the diagnostic band was only 37 bp length, the restriction products were ran into 8% acrylamide gels using Bio-Rad Mini-protean TetraSystem, with 1.5 mm spacer glass plates (Ref. 1653312, BioRad) and stained after ran using ethidium bromide. The composition for a 8% acrylamide gel is indicated in Table 21.

Reagent	Volume (µl) for one gel
TBE 5X	2,000
Acrylamide 40%	2,000
H_2O distilled	6,000
AMPS 10%	150
TEMED (Ref. 761, Iberlabo S.L.)	20
Vf	10,000

Table 21. Reagents used for one 8% DNA acrylamide gel.

To further confirm PCR insertion, a F and a R oligonucleotides were designed directly into the HA sequence to be used with the mentioned primers surrounding the edited region with the purpose to get amplification only if HA tag was incorporated. The conditions of these PCR's are also listed on Table 20.

Positive clones by these three methods of screening were sequenced to check HA incorporation. To perform sequence on both chromosomal copies of HDAC11, the products obtained by PCR were cloned into pGEM-T easy vector system (Ref. A1360, Promega) to transform them into competent bacteria that would incorporate only one copy of amplified DNA and that when grown in agar plates can be easily clonally separated. For that purpose, first, as Phusion taq gives blunt ends, a previous step of 3' A tailing was performed. NEB NExt dA-Tailing Module was used (Ref. 174E6053S, New England Biolabs Inc.). Briefly, two PCR reactions were pooled for each clone (Vf=20 µl) and purified using JETQuick columns (Ref. 410250, Genomed) following manufacturer instructions. For reaction, 16.8 µl of the purified amplification product were mixed with 2 µl of 10X dA tailing buffer and 1.2 µl of Klenow fragment and incubated for 1h at 37ºC. Then, the A-tailed product was ligated with pGEM-T. For that, 1.5 µl of the tailed product were incubated with 0.5 µl pGEM-T vector (25 ng), 0.5 µl T4 DNA ligase (3 Weiss Units/µl) and 2.5 µl of 2X buffer at 4ºC o/n. The next day, the ligated product was transformed into DH5α competent cells that were grown overnight. The next day, single colonies were selected and resuspended in 15 µl of water and the amplicon incorporation was check by colony PCR (Table 22). Two µl of each reaction were ran into 2% agarose gels as described. The colonies that had incorporated the PCR amplicon where sequenced

at GATC services after Exosap purification as described (at least 10 sequences for each selected clone).

Reagent volumes	**1x (µl)**
Buffer 10X	1.25
dNTPs 1 mM	1.25
M13 F 20µM	0.5
M13 R 20µM	0.5
Taq (5U/µl)	0.1
H_2O	6.9
Resuspended colony	2
Vf	10

Temperature (ºC)	Time	Number of cycles
95º	10 min	1
95º	30 s	30
68º	60 s	
72º	90 s	
72º	5 min	1
16º	∞	1

Table 22. Colony PCR amplification conditions for pGEM-T amplicon insertion screening. Taq DNA Polymerase (Ref. 11418432001, Roche).

Mice

Generation and maintenance of HDAC11 total KO mice

HDAC11 total KO animals were generated by Dr. Cristina Gutiérrez-Caballero at Dr. Alberto Pendás laboratory in CSIC-USAL (Salamanca) by crossing mice carrying loxP sites flanking the exon 3 of HDAC11 (ENSMUSE00001222983, chr6:91,109,155-91,109,255, mm9), with mice expressing CRE recombinase under the control of SOX2 promoter. The floxing of loxP sites causes a deletion of 923 bp that excises exon 3 and part of flanking introns and that originates a stop codon in exon 4 that results in a HDAC11 truncated protein of 59 aa instead of 349 aa (Gutiérrez 2012).

HDAC11 KO animals were obtained from intercrossing heterozygote mice. WT littermates were used as controls. Mice were maintained in CSIC-USAL animal facilities in cages separated by genotype in *ad libitum* conditions of food and water.

Genotyping conditions

At the very end of this PhD thesis, WT and KO mice were brought to Barcelona and kept at the IGTP animal facility. To genotype the animals here, one set of oligonucleotides were designed flanking the deletion region. The primer sequences and amplicon lengths obtained are listed on Table 23. PCR were performed using Phusion High Fidelity polymerase (Ref. E385HT, ThermoFisher Scientific) as detailed on Table 21 with 66ºC and 30" s annealing conditions.

		Amplicon lengths (bp)	
F (5'->3')	R (5'->3')	WT	KO
ggaaaggcactttcacttgc	accaaccacacagcccata	1104	181

Table 23. Primers used for HDAC11 mice genotyping and amplicon lengths obtained.

Cardiotoxin injection

Three months old adult mice were used for cardiotoxin experiments. Mice were anesthetized by intraperitoneally injection of tribromoethanol (Avertin®). After checking the anesthesia, mice back legs were shaved and disinfected with ethanol. Gastrocnemius and tibialis were injected intramuscularly using a Hamilton syringe and needles (Ref. 7803-07, Hamilton) with 50 µl of cardiotoxin (CTX) (Ref., L8102, Latoxan) in each muscle (200 µl in total per animal corresponding to the two GC and two TB muscles) at a concentration of 10 µM, resuspended in water. After the procedure, the injection points were disinfected with povidone-iodine (Betadine®, MEDA Pharma). During the injection procedure and recovery from the anesthesia, the animals were kept on electric blanket at 37ºC.

Sacrifice, extraction and processing of organs

Three months old mice were sacrificed by cervical dislocation. Legs were shaved and dissected to extract the selected muscles. Brain and hearth organs of selected mice were also extracted for analysis and placed into perforated eppendorfs that were immediately frozen in liquid nitrogen and stored at -80 ºC until RNA and protein extraction.

Muscles were dissected and transversally cut separating 1/3 of the muscle for protein and RNA extraction and 2/3 parts for histology analysis. Pieces for protein and RNA extraction were placed into perforated eppendorfs and immediately frozen on liquid nitrogen. Pieces for histology were placed on disposable base molds and embedded with OCT medium (Ref. 00411243, Q path, VWR) avoiding bubble formation. Pieces were frozen on liquid nitrogen-cold isopentane and then kept at -80ºC until processing.

Histology and stain

OCT blocks were equilibrated prior to cut for 15 min in a Cryostat (Leica CM 1950) chamber set at -22 ºC. Then, they were trimmed to remove OCT excess and expose the whole face to cut at 20 µm and finally cut with a fine setting of 10 µm with the anti-roll plate on. Selected tissue sections were collected by direct transfer to SuperFrost®Plus

microscope slides (Ref. 631-0108, VWR). Slides were dried at RT for 30 min and then stored until processing at -80 ºC.

For morphological analysis, muscle sections were stained with hematoxylin and eosin. First, slides were defrosted and equilibrated to RT for 15 min. Then, they were fixed for 12 min with 4% paraformaldehyde (Ref. 8187150100, Merck) at RT, followed by three washes with PBS. Slides were then immersed for 3 min in Harris hematoxylin (Ref. HHS32, Sigma-Aldrich) diluted 1:3 with distilled water and filtered at the moment, followed by intensive washes with tap water. Sections were then immersed 5 times in acid alcohol (80% ethanol 0.1% HCl), followed by washing in distilled water for 1 min. Then, they were plunged in 70% ethanol 3 times, followed by staining in eosin Y alcoholic solution (Ref. HT110132, Sigma Aldrich) for 5 min and washes with distilled water until they were clear. After staining, sections were dehydrated by sequential immersion in 70% ethanol for 1 min, 96% ethanol for 1 min, 96% ethanol for 1min, 96% ethanol: xylene (1:1) for 5 min, xylene for 2 min and a final immersion in xylene for 2 min. All ethanol solutions were made with (Ref. 1070172511, Merck). The slides were immediately mounted with DPX (Ref. 44581, Sigma-Aldrich) and covered with glass coverslips (Ref. BBAD02400600#S1, 24 x 60 mm, Menzel-Gläser, ThermoFisher). Preparations were allow drying o/n before observation. Photos were taken with a Leica DMI 6000 B microscope, connected to a Leica DFC420 color camera at different augments using Leica Application Suite (LAS).

Fiber cross-sectional area was calculated using freehand selections tool of the public available ImageJ software 1.48v version (Wayne Rasband, National Institutes of Health, USA). The number of myofibers per area was calculated using cell counter plugin.

Inmunohistochemistry

To stain regenerating fibers, injured muscle sections at the indicated time points of recovery were stained with α-embryonic myosin heavy chain (eMHC) antibody. For that, muscle sections were defrost and equilibrated at RT for 15 min. Then, the slides were labeled surrounding the sections regions with a hydrophobic Dako Pen (Ref. S2002, Dako) and sections were hydrated by washing with PBS 1X. Internal cellular peroxidases were blocked by incubation with 3% H_2O_2 in PBS for 30 min (Hydrogen peroxide solution 30% w/w in H_2O, Ref. H1009, Sigma-Aldrich) and then washed twice with PBS for 3 min each. M.O.M. Ig blocking reagent (3.6 % in PBS) was used to block unspecific staining for 1h at RT (Ref. PK-220, Vector laboratories). Then, they were washed twice with PBS for 3 min

and incubated for 1 h at RT with F1.652 hybridoma (kindly provided by Dr. Marcus Buschbeck lab). Two washes for 3 min were performed with 0.1 % Tween PBS, followed by incubation for 20 min at RT with 1/250 v/v secondary biotinylated α-mouse IgG in diluent solution constituted by 8 % v/v M.O.M. protein concentrate (Ref. PK-220, Vector laboratories) in PBS 1x. Sections were then washed twice for 3 min with 0.1 % Tween PBS 1x, followed by incubation for 15 min at RT with ABC (avidin/biotin) solution (3.6% A reagent, 3.6% B reagent in PBS 1x, mixed and incubated for 30 min prior use) (Ref. PK-220, Vector laboratories). Two washes were performed for 3 min with 0.1 % Tween and finally, the staining was developed by incubation with 0.6% 3,3'-diaminobenzidine in PBS under a microscope until brown coloration was clearly observed.

To stain activated SCs at 6 hpi, injured muscle sections were defrost and equilibrated at RT for 15 min. Then, the slides were labeled surrounding the sections with a hydrophobic Dako Pen (Ref. S2002, Dako) and sections were hydrated by washing with PBS 1X. Then, they were permeabilized with 0.1% Triton-X in PBS for 20 min followed by three washes with PBS 1X. Unspecific interactions were blocked by incubation with M.O.M. Ig blocking reagent (3.6 % in PBS 0.001% Triton-X) for 1h at RT (Ref. PK-220, Vector laboratories) followed by incubation with 5% BSA for 1 h more. Then, the sections were stained o/n at 4ºC with α-PAX7 concentrate 1:10 (Developmental Studies Hybridoma Bank (DSHB), University of Iowa) and 1:50 MYOD (clone 5.8A, Dako in 3% BSA. Next day, they were performed two washes for 3 min with 0.1 % Tween PBS, followed by incubation for 30 min at darkness and RT with 1/400 v/v Alexa red 568 α-mouse IgG1(γ) (Ref. A-21124, ThermoFisher) and 1/400 v/v Alexa green 488 α-rabbit (H+L) (Ref. A-11008, ThermoFisher). Sections were then washed twice for 3 min with 0.1 % Tween PBS 1x and mounted with Vectashield mounting medium with DAPI (Ref. 53826, Palex Medical S.A.).

Inflammatory cell isolation by FACS

To isolate inflammatory cells the point of 4 dpi and tibialis and gastrocnemius muscles were selected. Five WT and 3 KO animals were injured as described in "Carditoxin injection". One back leg was processed for histology and RNA and protein extraction and the other was handled as for muscle bulk preparation only using one injured tibialis and gastrocnemius per mice. This cell extracts where frozen as described until FACS sorting.

Antibody staining for inflammatory cells isolation by FACS sorting

Cells were thaw at 37ºC in a water bath. DMSO was removed by diluting with 12 ml of F-10 medium with 20% FBS and 100 U/ml penicillin and 100 µg/ml streptomycin and spun at 300 rcf for 5 min at RT. Cells were resuspended in FACS buffer (PBS +2.5% FBS), in a ratio of 100 µl: 10^6 cells on ice and incubated for 15 min on ice with 1 µg per 10^6 cells of α-mouse CD16/32 (Ref. 553142, BD Pharmigen) to block non-specific interactions. Then, the antibodies listed on Table 24 were added to the mix and incubated for 30 min on ice at darkness. After the incubation, cells were washed in FACS buffer and centrifuged at 900 rcf for 5 min. The supernatants were then discarded and the pellets were resuspended in 1 ml of FACS buffer containing 1/1000 v/v DAPI to exclude death cells. Cells were sorted using a FACS Aria II at CRG/UPF FACS unit and collected in eppendorfs containing 75 µl of RLT buffer with fresh 1% β-mercaptoethanol and 4 ng/µl of polyA-RNA carrier, vortex to lysate the cells and stored at -80ºC until RNA extraction. RNA was extracted using RNAeasy®Micro kit (Ref. 74004, Qiagen) with DNAse treatment following the manufacturer's instructions.

Antibody	Manufacturer	Reference	Specie	Amount used for 10^6 cells
APC CD11b clone M1/70	BD Pharmigen	553312	Rat	0.1 µg
APC Cy7 F4/80	Biolegend	123118	Rat	0.1 µg
PE Ly-6C clone AL-21	BD Pharmigen	560592	Rat	0.1 µg
FITC CD45 clone 30-F11	BD Pharmigen	553079	Rat	0.1 µg

Table 24. Antibodies used for FACS sorting of immune inflammatory cells.

.

RESULTS

1. Characterization of HDAC family members' expression during muscle differentiation

Satellite cells (SCs) isolated from adult mice muscles are the most physiologically primary source to study muscle proliferation and differentiation processes *ex vivo*. Once extracted from their niche, SCs loss their quiescent state, get activated and when maintained in subconfluent conditions and high serum containing media, they undergo several rounds of proliferation and give raise to daughter cells that are commonly called muscle precursor cells (MPCs). These conditions allow the study of cell proliferation processes and the amplification of the original population necessary to carry out many further studies. On the contrary, cell contact and serum deprivation promote the differentiation of MPCs towards muscle terminal cells, allowing the study of muscle differentiation processes (Figure 16 A). Taking advantage of this system, we started this study with a microarray expression dataset previously generated and validated in our lab that explored the expression changes occurring through muscle cell differentiation in three independent time courses of isolated satellite cells from mice that were amplified and differentiated *ex vivo* (Carrió et al. 2015). Considering the many precedent works that evidenced the role of protein deacetylation in the muscle proliferation and differentiation processes and taking into account that the expression of all HDAC members had not been entirely elucidated in this system, we decided to evaluate HDAC members' expression changes at the onset of muscle cell differentiation. We focused specifically in the transition from proliferating (P) towards day 1 (D1) differentiating cells as it is an early time point were crucial expression changes occur. At this point, cells have to exit from the cell cycle by repressing the expression of genes that promote cell proliferation and start to express differentiation genes that will commit them to become the functional specialized muscle cells or myotubes that can be already seen in this cultures as early as day 3 of differentiation.

As can be observed in Figure 16 B, only three HDAC members changed statistically its expression between these two conditions: HDAC7, which was downregulated at D1; and HDAC9 and HDAC11, which were upregulated. None member of the sirtuin family changed its expression in this transition so we decided to continue our studies with classical HDACs. As HDAC7 and HDAC9 expression changes had already been reported in this process (Dressel et al. 2001; Haberland et al. 2007), HDAC11 rapidly caught our attention for being the HDAC member that changed the most its expression at the onset of muscle differentiation.

A

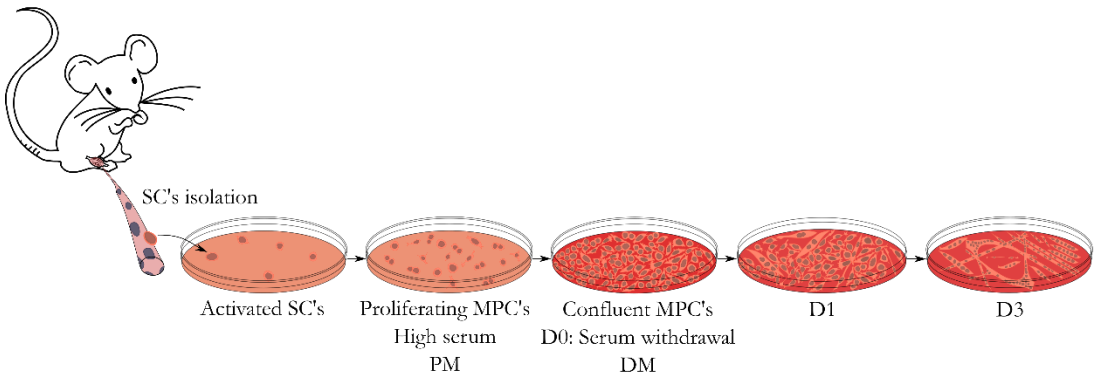

B

log₂ratio (D1/P)	Gene name	FC(D1/P)	P adj val
	HDAC1	-1.02	0.9695
	HDAC2	1.29	0.4615
	HDAC3	-1.07	0.9220
	HDAC8	-1.38	0.5599
	HDAC4	-1.38	0.3770
	HDAC5	1.18	0.6257
	HDAC7	**-2.38**	**0.0002**
	HDAC9	**3.69**	**0.0002**
	HDAC6	-1.42	0.1247
	HDAC10	-1.31	0.1171
	HDAC11	**4.76**	**0.0001**

log₂ratio (D1/P)	Gene name	FC(D1/P)	P adjval
	SIRT1	1.31	0.7942
	SIRT2	1.67	0.2281
	SIRT3	-1.38	0.4359
	SIRT4	-1.03	0.9568
	SIRT4	1.15	0.7071
	SIRT5	1.19	0.6949
	SIRT6	-1.36	0.4615

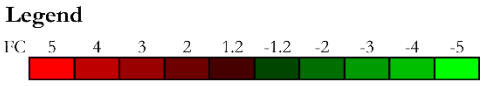

Figure 16. HDAC family members' expression changes between day 1 of differentiation (D1) and proliferating (P) MPCs by microarray expression analysis. A Scheme of the steps followed to study muscle proliferation and differentiation processes *ex-vivo*. SCs can be isolated from muscles by muscle bulk extraction. These cells, when plated in proliferation medium containing high serum (PM), get activated and start to proliferate giving rise to an amplification population, the muscle precursor cells (MPCs). These conditions allow the study of muscle proliferation processes. At high cell confluences and promoted by serum withdrawal from the medium (DM), MPCs start to differentiate, change their morphology and fuse between them originating myotubes. **B** In the left part are shown classical HDAC' members organized by classes and in the right part are shown class III sirtuin members. For each HDAC gene it is indicated its fold change expression (FC), calculated by dividing the average value of three biological independent replicates at day 1 of differentiation (D1) by the average value obtained in the matching samples at proliferation (P). To facilitate visual comparison the log_2FC value has been assigned to a color scale (Legend). P values were adjusted for multiple testing and in bold are highlighted the genes whose expression change was statistically significant. For the genes represented by more than one probe in the microarray platform, representative probes are indicated.

To validate our results and have a whole picture of classical HDACs expression through muscle differentiation, we decided to quantify their expression levels in four different independent MPCs cell lines at three time points, P, D1 and D3 of differentiation (Figure 17 B). As observed in Figure 17 C, the most expressed members of class I were HDAC1 and HDAC3. While HDAC1 is downregulated through differentiation, HDAC3 expression increases at the late differentiation point. HDAC2 was not detected at any point and HDAC8 expression levels remain low and unchanged. Among class IIa members, HDAC4, HDAC5 and HDAC9 get upregulated at late differentiation points while HDAC7 expression progressively decreases through differentiation. Class IIb members expression remain invariant in this process. Class IV member expression increases at day 1 and remains expressed at day 3. HDAC11 is the only member whose expression changes specifically at the onset of differentiation (FC: 4.48, p val: 0.046) although HDAC9 also shares an upregulation change at this point although to a lesser extent (FC: 3.89, p val: 0.021). For this reason and because nothing was known about HDAC11 in this process, we decided to go further with HDAC11 analysis in muscle differentiation.

Figure 17. Classical HDAC members' expression through *ex-vivo* muscle differentiation. A Pictures of a representative time course of differentiation illustrating the typical morphological changes occurring through MPC's differentiation. From left to right, proliferating MPC's at low confluence (P) are characterized by their round shape and small size. When they are plated at high confluences and deprived of serum from the media, MPC's start to change their morphology and acquire flattener shapes at day 1 of differentiation (D1). By day 3 of differentiation (D3) MPC's morphology has dramatically change, with the appearance of both flattened structures and big aggregates containing dozens of nuclei formed by sequential fusion of MPC's that correspond to myotubes. **B** Classical markers that allow to monitor the muscle differentiation process. From left to right are shown, Ki67, a wide use cell proliferation marker, expressed in cycling MPC's and silenced through differentiation; myogenin (MGN) an early muscle differentiation marker expressed at early points of cell differentiation, and muscle creatine kinase (MCK), a late differentiation marker highly expressed in differentiated cells. Markers expression was determined by qPCR and data was normalized to TBP1 reference gene's expression. Data correspond to the average value of at least three biological independent experiments. Error bars represent ± SEM. **C** Classical HDAC members' relative expression was determined by qPCR and is relative to TBP1 in the same four biologically independent differentiation time courses as B. Paired t-test with two tails was applied to assess statistical significance. *: p val <0.05; **: p val < 0.01. ND: not detected.

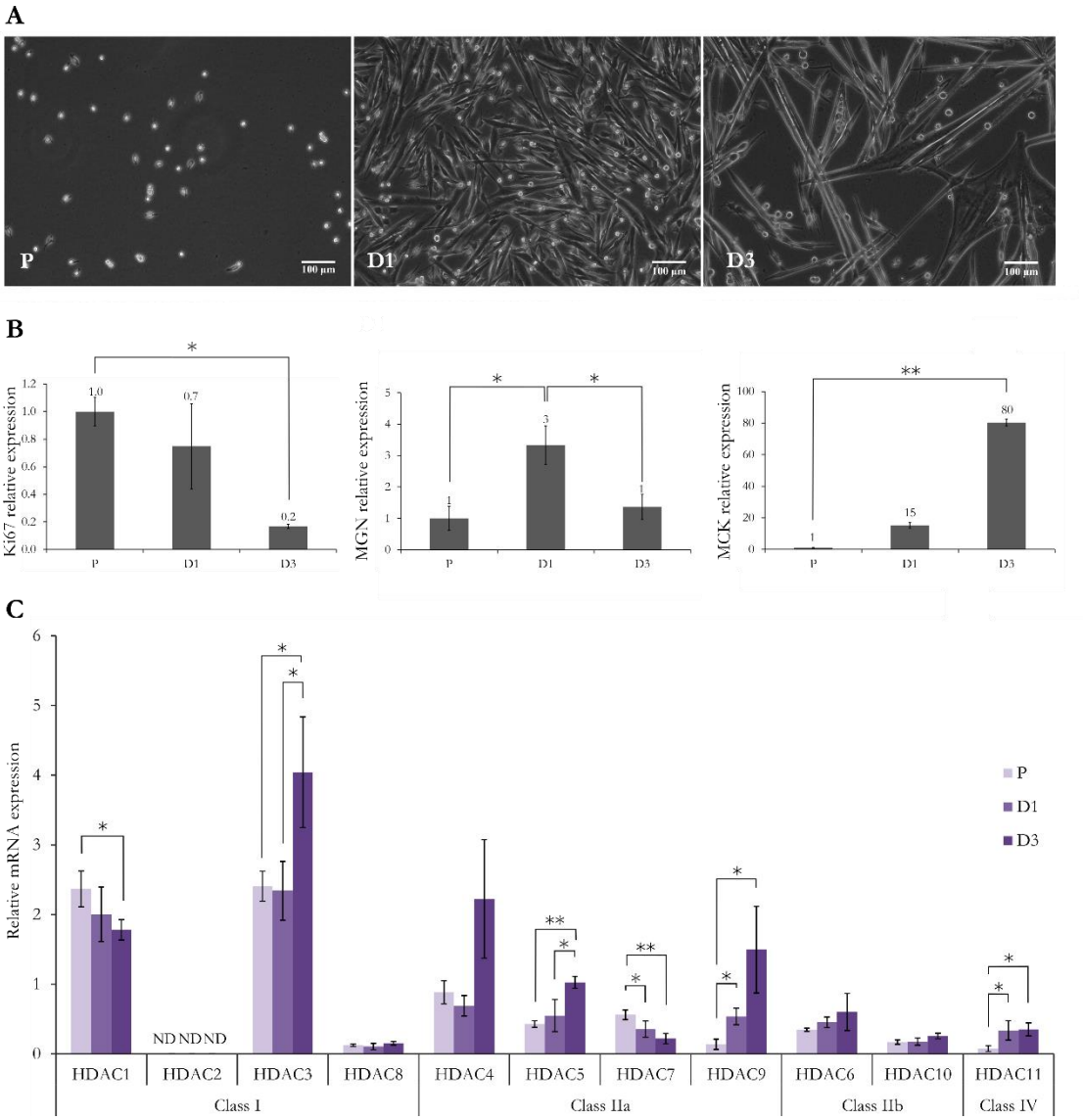

Focusing on HDAC11, we next wondered if its increase in mRNA levels reach its higher levels at D1 of differentiation or if its upregulation occurs even at earlier points. For that, we performed a new time course with the same four MPC's at earlier points of differentiation. As illustrated on Figure 18, the increase on HDAC11 expression starts already at 12h after serum withdrawal although the highest levels are reached at D1 of differentiation.

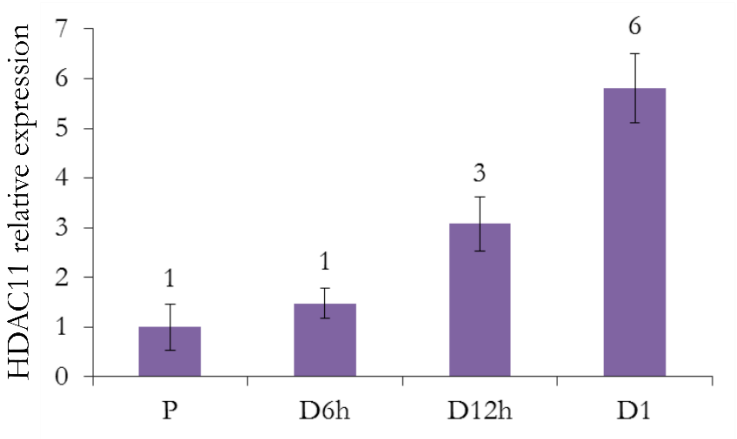

Figure 18. HDAC11 expression in early muscle differentiation points. Values correspond to the average expression of HDAC11 of four biological replicates relative to TBP1 reference gene, in proliferating cells (P), cells harvested after 6h (D6h), 12h (D12h) and 24h (D1) after changing to differentiation conditions. Error bars correspond to SEM.

2. Characterization of HDAC11 expression in *in vitro* skeletal muscle differentiation

2.1. Validation of HDAC11 expression in C2C12 cell line

We next wanted to extend our observations to another skeletal muscle differentiation system, C2C12, an immortalized cell line derived from mouse myoblasts, the most used in *in vitro* muscle differentiation studies (Yaffe & Saxel 1977). Working with C2C12 has the advantage to be a system easier to work with than primary myoblasts as it requires less growth factors in the cell culture media and does not need to pretreat the cell culture plates. To confirm that our observations were reproduced in this system, we performed analogous differentiation time courses than for MPC's. As observed on Figure 19 C, HDAC11 is also upregulated through muscle differentiation in this cell line.

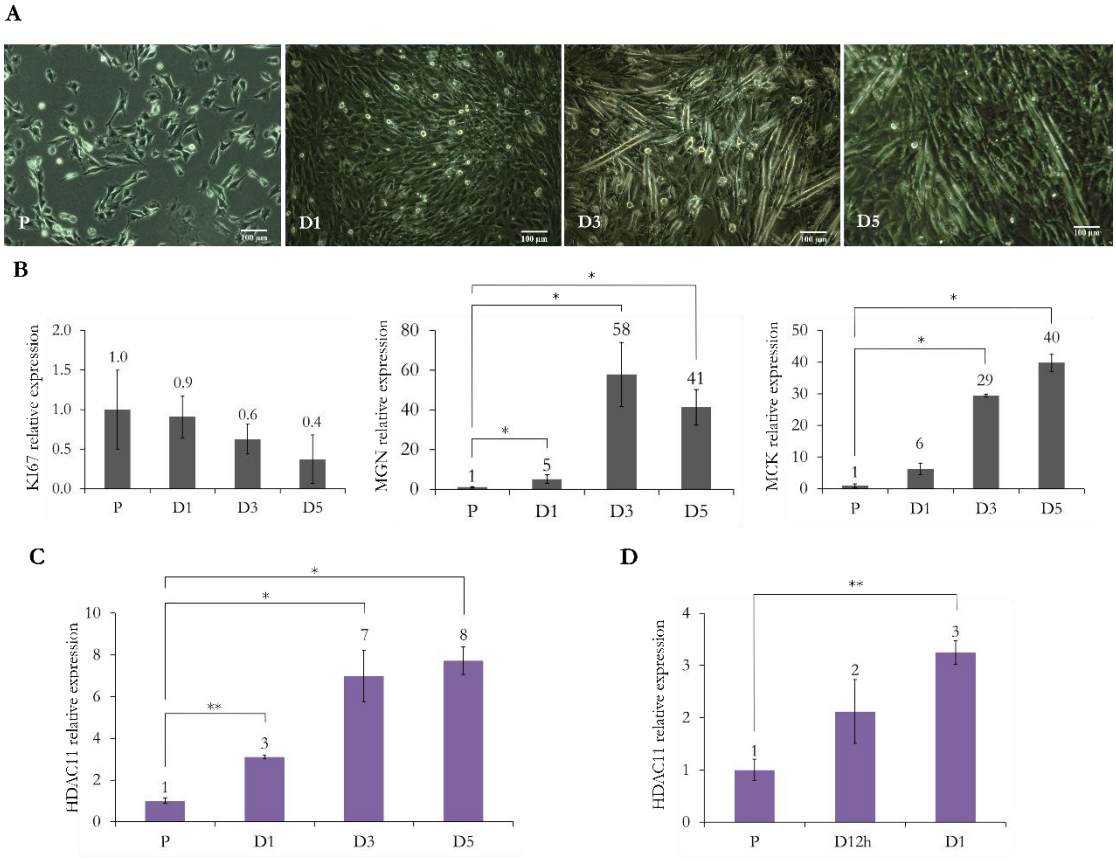

Figure 19. HDAC11 expression is upregulated through muscle differentiation in C2C12 cell line. A Microscopy images of C2C12 cells at the indicated time points showing morphological changes occurring through cell differentiation. C2C12 cells grow as proliferating cells (P) at subconfluent conditions. When plated at high confluences and deprived of serum from the media (D1), they start to differentiate and fuse between them. Multinucleated myotubes are visible already by day 3 of differentiation (D3). Further on, these myotubes increase in size as can be seen at day 5 of differentiation (D5). **B** qPCR quantification of the

markers that allow to monitor the muscle differentiation process. KI67 is a widely used cell proliferation marker that is highly expressed in proliferating cells and is downregulated through differentiation. Myogenin (MGN) is used as an early differentiation marker and myosin creatine kinase (MCK) as a late differentiation marker expressed in myotubes. Indicated are the average values of the mentioned genes normalized to TBP1 reference gene. Values correspond to the average of at least three independent biological replicates ± SEM. **C** and **D** HDAC11 qPCR quantification in the aforementioned time courses of differentiation (C) and early differentiation time courses (D). Values indicate the average expression value of HDAC11 normalized by TBP1 ± SEM. Paired t-test with two tails was applied to assess statistical significance. *: pval<0.05. **< 0.001.

As C2C12 has been widely used as a model to study muscle processes *in vitro*, many public data are available for this cell line. Thanks to the accessibility to public expression data from ENCODE of a RNA-seq experiment of C2C12 differentiation (Wold 2012), we decided to validate our results in this independent external time course and with another mRNA quantification system. As observed on Figure 20, in proliferating C2C12 HDAC11 mRNA levels are very low compared with the levels presented at 2.5 days of differentiation. We included two biological replicates of skeletal muscle in the analysis to assess the expression levels of HDAC11 in terminal differentiated cells, which are even lower than in proliferating cells, suggesting that HDAC11 expression is specific of early differentiating cells.

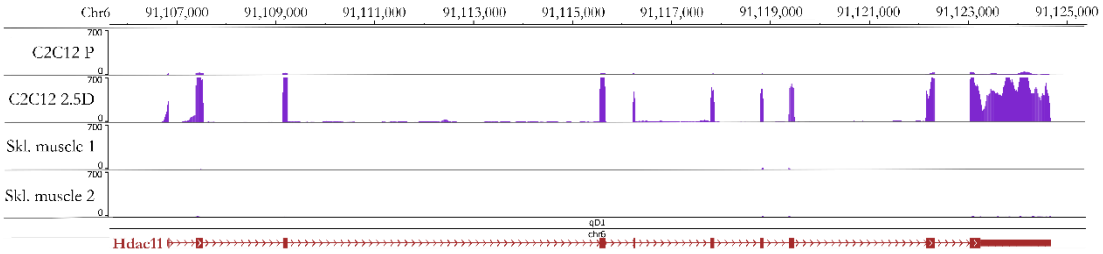

Figure 20. HDAC11 is highly expressed at early differentiation points through the muscle differentiation process. ENCODE RNA-seq expression levels of HDAC11 in C2C12 cell line. Indicated is the genomic location (mm9 genome assembly) of HDAC11 gene with the following tracks (Raw signal): C2C12 proliferating (P), differentiating at day 2.5 (D2.5) and two samples of adult skeletal muscle (Skl. muscle) (Wold 2012). The tracks were visualized using WashU Epigenome Browser browser v40.6 mm9 (Zhou & Wang 2002) (http://epigenomegateway.wustl.edu/browser/).

2.2. Epigenetic mechanisms regulating HDAC11 expression

Being observed this specific pattern of HDAC11 expression, we were interested in investigating the mechanisms that maintained HDAC11 expression repressed in proliferation conditions and the ones that trigger its expression at the onset of muscle differentiation. As HDAC11 contains a CpG island (CpGi) in its promoter region, we wondered if its expression could be repressed in proliferation conditions by DNA methylation of the CpG dinucleotides present in its CpGi. For that, we analyzed by PCR followed by bisulphite sequencing, the gold standard method to analyze DNA methylation, a region spanning about 200 bp of its CpGi. As observed in Figure 21, the cytosines present in HDAC11 CpGi were already completely unmethylated in proliferative myoblasts and their methylation levels did not change in differentiated cells, excluding DNA methylation of HDAC11 promoter region as the responsible mechanism of the variation in mRNA levels observed.

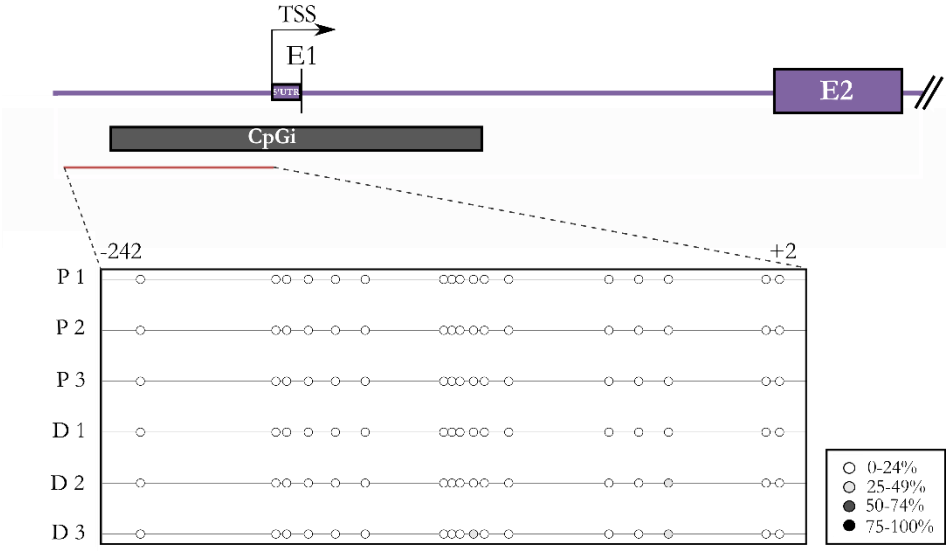

Figure 21. HDAC11 is not repressed by CpGi methylation in proliferating conditions. Scheme of HDAC11 genomic locus. The box adjacent to TSS correspond to 5'UTR and the bigger boxes correspond to exons. The region analyzed by bisulphite sequencing is indicated in a red line. Each dot within the box represents a cytosine of a CpG dinucleotide and their relative separation are proportional to their genomic position. The color indicates the percentage of methylation, as indicated on the legend. The numbers above the dot box correspond to the relative position of the first and last cytosines analyzed to HDAC11 TSS. Lines correspond to three independent C2C12 proliferating cells (P) and three day 3 differentiated isolated myotubes (D).

We next wondered if the histone modification marks present in HDAC11 regulatory regions could explain the aforementioned HDAC11 expression changes. For that, we took advantage of ENCODE data (Wold 2012), focusing this time in the available histone marks tracks present in HDAC11 locus in proliferation and differentiation conditions.

As shown on Figure 22, the histone marks positively associated with gene expression H3K4me3 and H3ac, both located around the TSS, are already present in proliferating cells. H3K4me3 is already present in proliferating myoblasts although its levels increase in differentiating cells while H3ac is present in both states at similar levels. At their turn, the marks deposited as a consequence of transcription, H3K79me2 and H3K36me3, are both absent in P and increase in differentiating cells. H3K79me2 increases at 5' of gene body and H3K36me3 at 3' of gene body, where they are usually located. H3K27me3 levels, a mark associated with repressed chromatin states, are very low and did not change between both conditions.

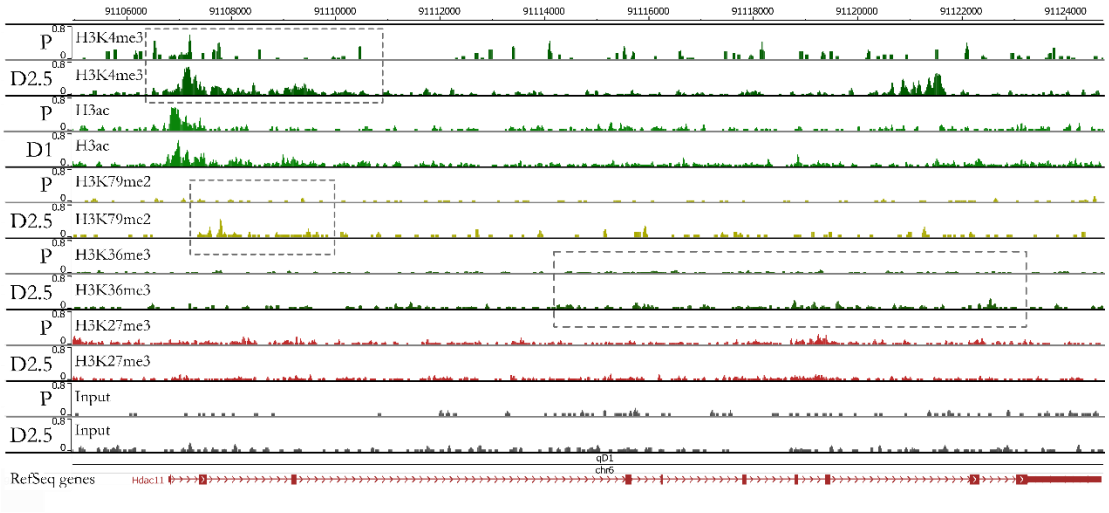

Figure 22. ChIP-seq tracks of ENCODE histone modifications' profiles in C2C12 differentiating cells. Positively associated with gene expression marks are colored in different shades of green and the repressive mark H3K27me3, associated with gene repression, is colored in red. Inputs are shown as controls in grey. P: C2C12 proliferating cells, D2.5: C2C12 after 2.5 days of differentiation (Wold 2012). The bigwig tracks were visualized with WashU Epigenome Browser v40.6 mm9 (Zhou & Wang 2002) (http://epigenomegateway.wustl.edu/browser/).

These results indicate that the increase in HDAC11 mRNA levels observed in differentiating cells are a result of increased gene transcription (evidenced by the increase of H3K4me3, H3K79me2 and H3K36me3 marks). However, the chromatin states in both conditions seemed permissive for HDAC11 gene expression, evidenced by the presence of permissive chromatin marks and the absence of repressive ones, thus evidencing that HDAC11 silencing in proliferation conditions is not mediated by different histone modification patterns or CpGi methylation.

To continue exploring the mechanisms that would keep HDAC11 expression repressed in proliferation conditions even when epigenetic mechanisms are permissive for transcription, we decided to consider if HDAC11 induction is triggered by some transcription factor binding to its promoter. Knowing that MRFs are the drivers of muscle cell differentiation and thatHDAC11 expression coincides with the onset of this process, we decided to ascertain whether MRFs were bound to HDAC11 promoter region in differentiating cells.

2.3. The increase of HDAC11 expression in early muscle differentiation is induced by MRFs binding

Thanks to the public availability of transcription factor binding data from ENCODE in the same samples used for RNA-seq expression (Wold 2012), we investigated whether the increase on HDAC11 expression coincided with the binding to its promoter region of any activator transcription factor. As observed on Figure 23 A, MYOD is bound to HDAC11 promoter region with a peak at D1 and day D2.5 of differentiation. Further on, its binding decreases in intensity. MYOG, at its turn, starts to bind also at D1 but the peak of most intense binding is observed latter on, at D2.5 of differentiation. Then, at day 7 of differentiation its binding decreases as in the case of MYOD.

MRFs do not bind alone to their target sites in the DNA but form heterodimers with E-proteins of the bHLH subfamily (Cao et al. 2010). For this reason, we included in the analysis TCF3 (commonly known as E2A or E12/E47) and TCF12 (commonly known as HEB) track profiles and, as can be observed, this two E-proteins also bind to HDAC11 promoter in coinciding regions with MRFs. Moreover, we checked for the presence of E boxes in the proximal promoter of HDAC11 (1,000 bp upstream the TSS) and we found three E boxes in this region, presenting the consensus sequence for MYOD/MYOG binding (5'CASCTG3', S=G/C (Cao et al. 2006; Cao et al. 2010)): GACATG, GACCTG, GAGTG. These observations indicate that MRF binding could be responsible of HDAC11 expression at the onset of differentiation.

To ascertain whether MYOD presence could induce HDAC11 expression, we had access to some pellets of mouse embryonic fibroblasts (MEFs) double knock-out for MYOD and MYF5 stably transduced with MYOD cDNA fused to an estrogen receptor binding domain whose expression was induced by β-estradiol addition and allowed to differentiate for 4 days thanks to Dr. Patrizzia Pessina in Dr. Pura Muñoz laboratory (Universitat

Pompeu Fabra). As observed in Figure 23 B, we observed that HDAC11 expression is triggered by MYOD expression in differentiation conditions.

To broaden our observations, we analyzed the data generated by Cao and colleagues in a similar and more complete experiment in which they used the MYOD and MYF5 double knock-out MEFs, stably transduced with a vector encoding for MYOD cDNA fused to an estrogen receptor hormone binding domain (Cao et al. 2006). To separate MYOD and MGN targets, they added or not β-estradiol to the media to induce or not MYOD expression or they transduced the aforementioned cells with a plasmid encoding for MGN cDNA with the presence of β-estradiol (to have both MYOD and MGN expressed) or not (to have only MGN). In Figure 23 C are shown the normalized values for HDAC11 probe intensity values of their microarray results (GSE3858). As observed, in proliferation conditions neither MYOD nor MGN trigger the upregulation of HDAC11 expression. At 12 h of differentiation, where MYOD and MGN targets could be separated (from D1 the expression of MYOD activates endogenous MGN expression and cannot be distinguished), it can be observed that the highest levels of HDAC11 upregulation are reached by combined MYOD and MGN activation. So on, at latter points of differentiation, the highest upregulation levels of HDAC11 are also reached by combined MRF's expression. Thus indicate that both MYOD and MGN are necessary to fully activate HDAC11 expression.

With these observations we concluded that the expression of HDAC11 in differentiation conditions increases upon MYOD and MGN binding to its promoter.

Figure 23. HDAC11 expression in differentiating cells is induced by MRF's binding to its promoter. **A** ChIP-seq binding profiles of MYOD and MYOG MRF's and the E-proteins TCF3 and TCF12 at the indicated points of differentiation. The bigwig tracks were visualized using WashU Epigenome Browser browser v40.6 mm9 (Zhou & Wang 2002) (http://epigenomegateway.wustl.edu/browser/). **B** qPCR expression analysis of MYOD and MYF5 double KO MEFs stably transfected with an inducible vector expressing MYOD cDNA under the control of a fused estrogen receptor binding domain. Indicated are the obtained values in proliferation and differentiation conditions of MEFs transduced with the aforementioned vector with or without β-estradiol. Data correspond only to one replicate. Samples were provided by Dr. Patrizzia Pessina (Dr. Pura Muñoz's laboratory). **C** HDAC11 1454803_a_at probe intensity values in a microarray normalized data (GSE3858) from MEFs double knockout for MYOD and MYF5 (EMPTY) stably expressing MYOD fused to an estrogen receptor hormone binding domain. MYOD was induced in all cases by β-estradiol addition to the cell culture media and MGN was induced by cDNA transduction of the mentioned cells at D12h ("& MGN" or "MGN") or by indirect activation of endogenous MGN by MYOD ("(MGN)"). In each condition, the three bars values correspond to three biological replicates (Cao et al. 2006).

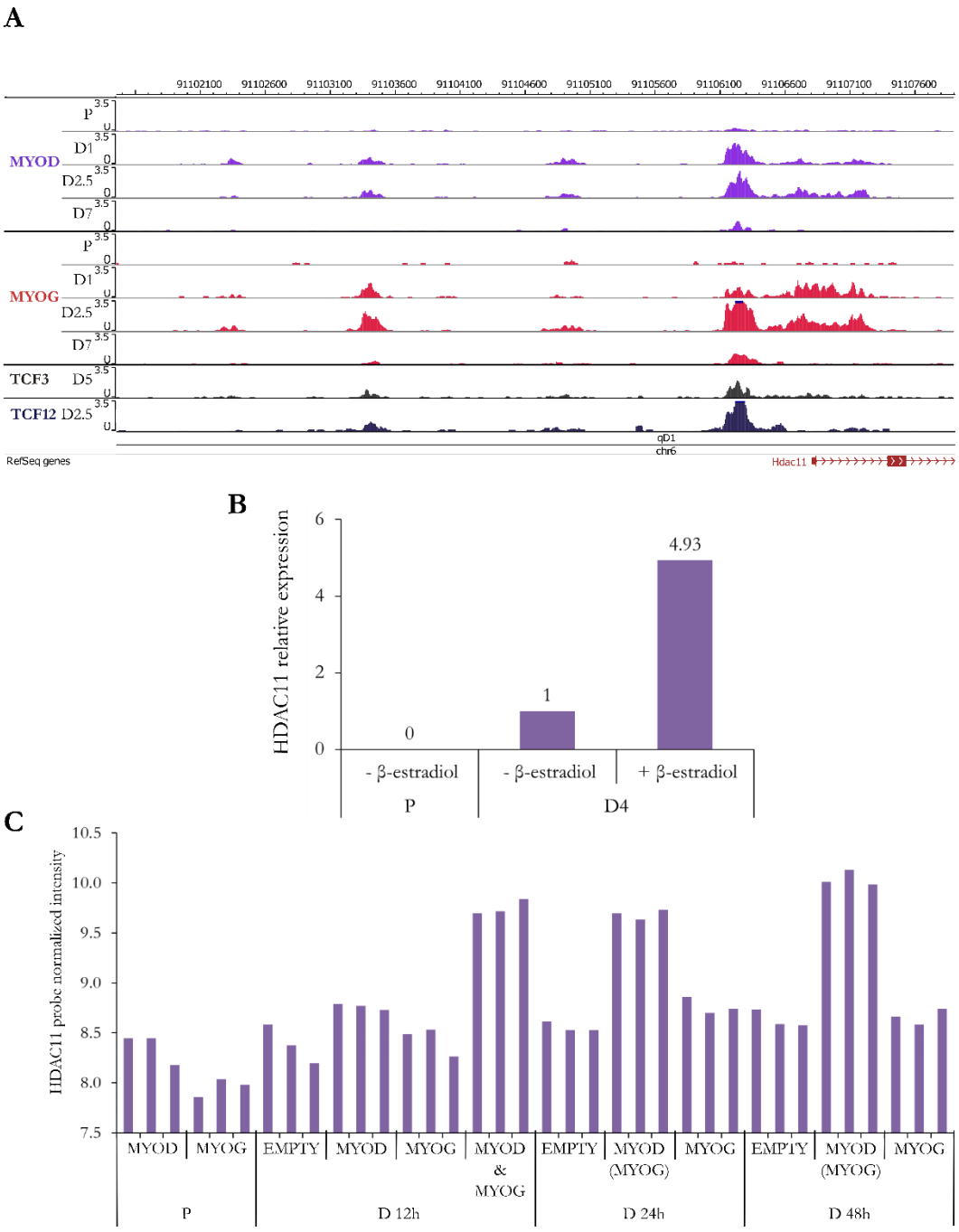

MYOD is present at the protein level already in proliferating myoblasts but cannot exert its transactivation activity because it is maintained inactive by HDAC1 deacetylation on three conserved arginines (Mal et al. 2001). With this information, we analyzed another public dataset in which using the same double MYOD and MYF5 KO MEFs, they transduced WT MYOD under the control of an estrogen hormone receptor or non-acetylable MYOD in which lysine residues 99, 102 and 104 had been mutated to arginines (GSE6487) (Di Padova et al. 2007). As observed on Figure 24 A, non-acetylable MYOD cannot activate HDAC11 up to the same levels as WT MYOD.

To further explore this acetylation mediated capacity of MYOD to induce HDAC11 expression, we treated C2C12 cells in proliferation conditions with the HDAC inhibitors (HDACi) TSA (non-specific HDACi,) and VPA (class I specific HDACi) (Figure 24 B) and analyzed HDAC11 induction at D0 and D1 of differentiation. As observed in Figure 24 D, inhibition of deacetylation results in analogous HDAC11 induction as day 1 of differentiation both in VPA and TSA treatments, concluding that HDAC11 is maintained repressed in proliferation conditions by class I HDAC mediated deacetylation of MYOD. The treatment with HDACi at day 0 and analysis at D1, when the differentiation program had already been triggered, did not further influence HDAC11 expression.

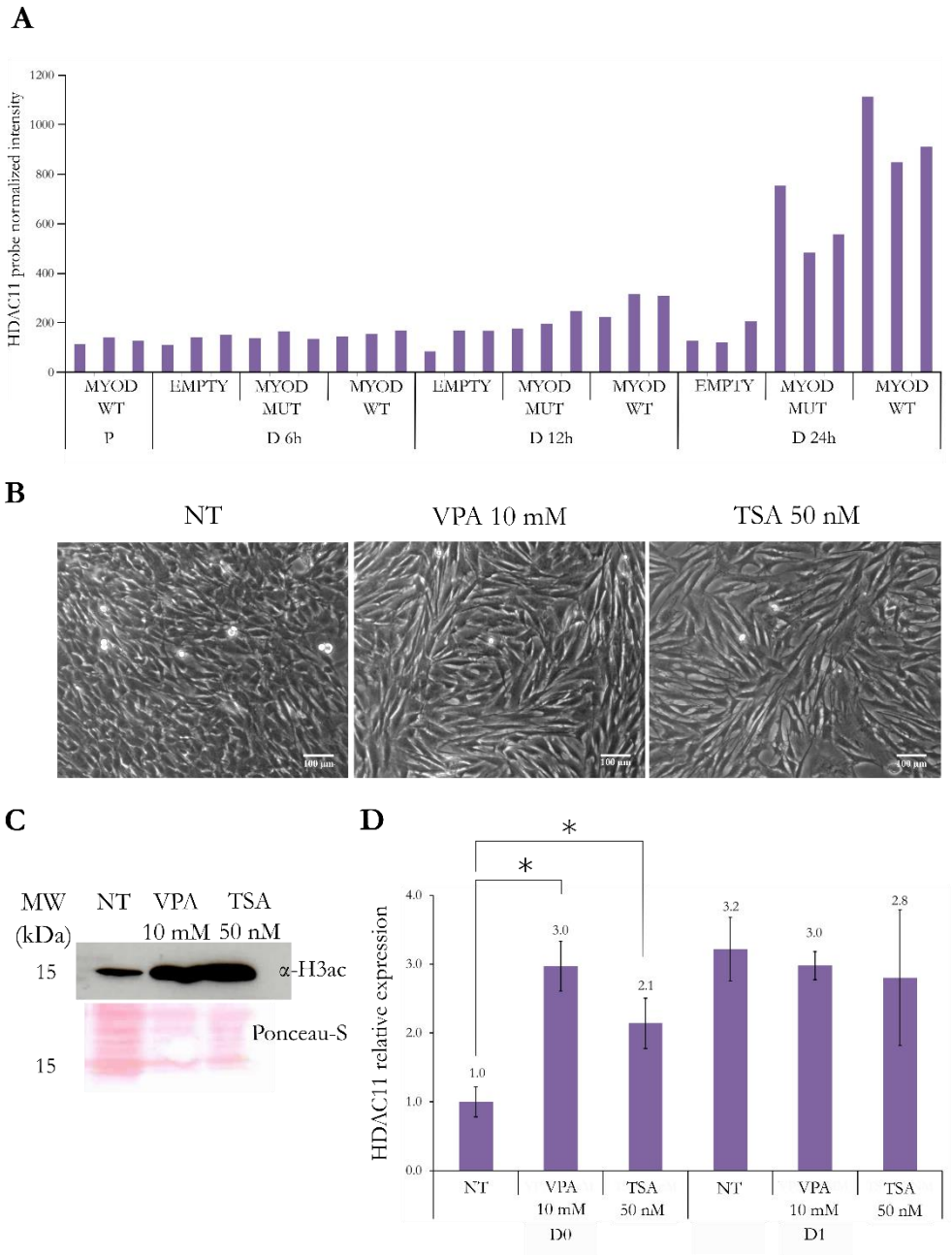

Figure 24. HDACi treatment in proliferation induces HDAC11 expression. A 1454803_at HDAC11 probe intensity values in a microarray normalized dataset (GSE6487 from MEF's double knockout for MYOD and MYF5 (EMPTY) stably expressing WT MYOD or mutated (MUT) fused to an estrogen receptor hormone binding domain. Mutated MYOD harbors three mutations in conserved arginines 99, 102 and 104 that impede its activation by acetylation. MYOD was induced in all cases by β-estradiol addition to the cell culture media. In each condition, the three bars values correspond to three biological replicates (Di Padova et al. 2007). **B** Representative microscopy images illustrating the morphological changes induced by HDACi treatment in proliferation conditions after 24h of treatment. Cells were plated in proliferation conditions at a density to reach confluence at D0. As observed, non-treated (NT) cells are mostly round and did not present any particular spatial disposition, while cells treated with VPA and TSA presented elongated and speculated shapes and are disposed aligned while containing less proliferating cells (round and brilliant), all indicatives of cell cycle arrest induction. **C** Western blot check of H3 acetylation increasing upon HDACi treatments. Cell pellets from cell treatments in B were lysed directly with 1.2X Laemli buffer and ran into 15% acrylamide gels. The corresponding membranes were incubated with α-H3 ac antibody (Ref. 06-599, Upstate-Millipore). Ponceau S staining of transferred membranes is shown as control. **D** HDAC11 qPCR quantification analysis upon HDACi treatment. Left: C2C12 treated cells in proliferation for 24h and harvested at D0 (labelled as D0). Right: C2C12 treated at D0 and harvested at D1 of differentiation (labelled as D1). Data represents the average values of HDAC11 normalized to TBP1 expression ± SD of four biological independent experiments. *: pval <0.05, paired t-test two tails.

2.4. Pan-HDAC inhibitors further impaired myogenic differentiation compared with specific class I HDACi

As reviewed in the introduction, several previous published studies have already demonstrated that the treatment of myoblast cultures with HDACi at the moment of performing serum withdrawal resulted in a complete abrogation of muscle differentiation. Therefore, all these treatments were centered in pan-HDACi (broad class inhibition, non-specific) or class I specific inhibition. As a target of MYOD and MYOG, which are in the top of the cascade that triggers cell differentiation and activate all downstream factors involved in differentiation, we wondered if HDAC11 was involved in muscle cell differentiation. For that, we performed an initial approach by inhibiting HDAC11 at the onset of cell differentiation. Although no specific commercial HDAC11 inhibitors exist, we took advantage of the specificity of existing HDACi. For that, we treated C2C12 at the moment of performing serum withdrawal (D0) with the pan-HDACi TSA (inhibits class I and IV HDACs) and the specific class I inhibitor valproic acid (VPA) (Lozada et al. 2016). As it is currently accepted that class II HDACs are catalytically inactive and exert its deacetylation capabilities though class I HDAC recruitment, we assumed that the

differential behavior between TSA and VPA would be due to differential HDAC11 inhibition. In Figure 25 are shown representative images of these HDACi treatments at day 3 and 5 of differentiation. As observed, both HDACi impaired myotube formation but TSA resulted in a further impaired myotube formation with less and smaller myotubes than upon class I specific VPA treatment.

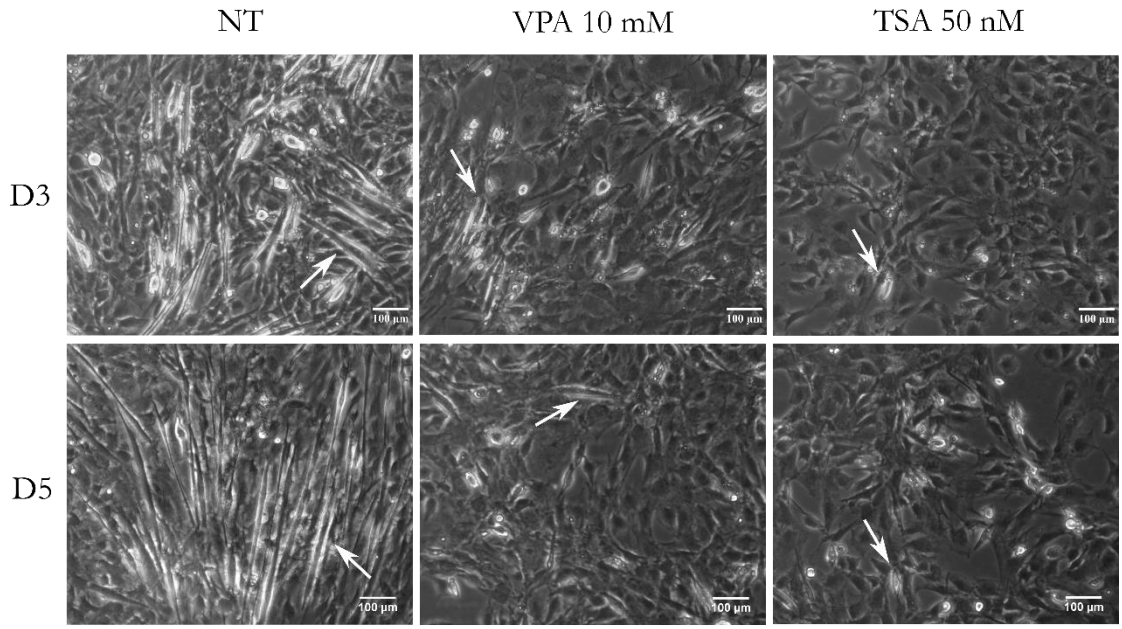

Figure 25. Treatment with the pan-HDACi TSA at the onset of cell differentiation results in a higher impairment in myotube formation than class I specific VPA HDACi. Microscopy images of C2C12 cells at day 3 and 5 of differentiation treated for 24h with the HDACi VPA (Valproic acid) or TSA (Trichostatin) at the moment of performing serum withdrawal. HDACi doses were used as in (Iezzi et al. 2002). Arrows point myotubes.

With this preliminary observation, we hypothesized that the enhanced differentiation inhibition exerted by the pan-HDACi TSA compared with the class I specific inhibitor VPA could be due to HDAC11 inhibition, which might be involved in cell differentiation and myotube formation. This first evidence of HDAC11 function in muscle differentiation made us continue exploring HDAC11 roles in myogenesis.

2.5. Attempts on endogenous HDAC11 protein detection through muscle differentiation

To determine whether the observed increase on HDAC11 mRNA expression at days 1 and 3 of differentiation was accompanied with an increase in HDAC11 protein levels, we tested in a first attempt α-HDAC11 rabbit polyclonal antibody ab18973, as it had already

been used for western blot detection of endogenous HDAC11 protein in brain mouse tissues in a previous publication (Liu et al. 2007). Antibody concentrations of 1.5 and 2.5 μg/ml were tested as recommended, in both total and nuclear extracts of Jurkat and mouse intestine lysates, both positive controls suggested by the manufacturer, applying different sensitivity detection methods and using both total and nuclear protein extraction methods in different amounts as samples. Unfortunately, we were not able to detect a band that matched the expected theoretical weight of HDAC11 (39 kDa).

Then, we tried a custom antibody made by rabbit immunization with purified murine HDAC11 peptide by our collaborators in CSIC-USAL (Dr. Alberto Pendás) with the same negative results. Afterwards, we tested a second commercial antibody, Sigma H4539, which gave a very clean and clear signal of only two bands, one that could match the expected 39 kDa band and another higher than 50 kDa, both consistently and repetitively detected in several differentiation time courses of primary myoblasts and C2C12 cells. Nevertheless, the band of 39 kDa did not change though differentiation as mRNA levels did in the matching samples, whereas the 50 kDa band increased at D1 and D3 of differentiation. Given this consistent results and the absence of studies of posttranslational modifications and because indeed by bioinformatics prediction programs we observed that HDAC11 could be putatively modified, we hypothesized that we could be detecting HDAC11 with a higher weight due to the presence of some posttranslational modifications. To test that, we performed gel excision of both putative bands from total and nuclear primary myoblasts extracts ran into 8% acrylamide gels stained with Coomassie blue. The proteins were extracted from the bands and digested as explained on "Material and methods" section and sequenced by MALDI-TOF at UPF proteomics service. Unfortunately, none peptide of HDAC11 was detected in any of the bands suggesting that or the protein was low expressed or that it could not be detected by this method. We also tried a prior enrichment of the extracts by immunoprecipitation starting with 500 μg of total protein with 5 μg of H5439 and ab18973 antibodies with the same negative results.

3. Analysis of HDAC11 functions in C2C12 cells

3.1. HDAC11 is located both in nucleus and cytoplasm of HDAC11 overexpressing C2C12 cells

Given our problems to detect endogenous HDAC11 with the available antibodies, we decided to continue the study of HDAC11 protein with constitutively expressed tagged HDAC11. For that, we cloned HDAC11 as described in "Materials and methods" section and overexpressed it tagged independently in N-terminal with a flag epitope and in the C terminal with an HA to ascertain that tag location did not interfere with HDAC11 location. As observed on Figure 26 A by immunofluorescence against flag epitope, HDAC11 was located both in nucleus and cytoplasm of C2C12 proliferating cells. As expected, the overexpressed protein was recognized both by immunofluorescence and western blot detection by the antibodies against HDAC11 previously described, further indicating that the endogenous protein was not recognized by an issue of protein abundance. The immunofluorescence results with both commercial antibodies against HDAC11, located the protein also both in nucleus and cytoplasm as the flag epitope.

Figure 26. HDAC11 is located both in nucleus and cytoplasm of C2C12 overexpressing HDAC11 proliferating cells. A Western blot images showing HDAC11 overexpression validation. For each sample they were ran in parallel 20 μg of total RIPA protein extracts into 10% acrylamide gels. The corresponding membranes were incubated with the indicated antibodies. α-Flag and α-H5439 films correspond to 10 seconds expositions with Luminata Crescendo HRP substrate (Ref. WBLUR0100, Millipore) while ab18973 correspond to overnight exposition of the membrane with the same substrate. **B** Representative microscopy images of immunofluorescence against Flag and HDAC11 in HDAC11 overexpressing cells (pMSCV-Flag-HDAC11).

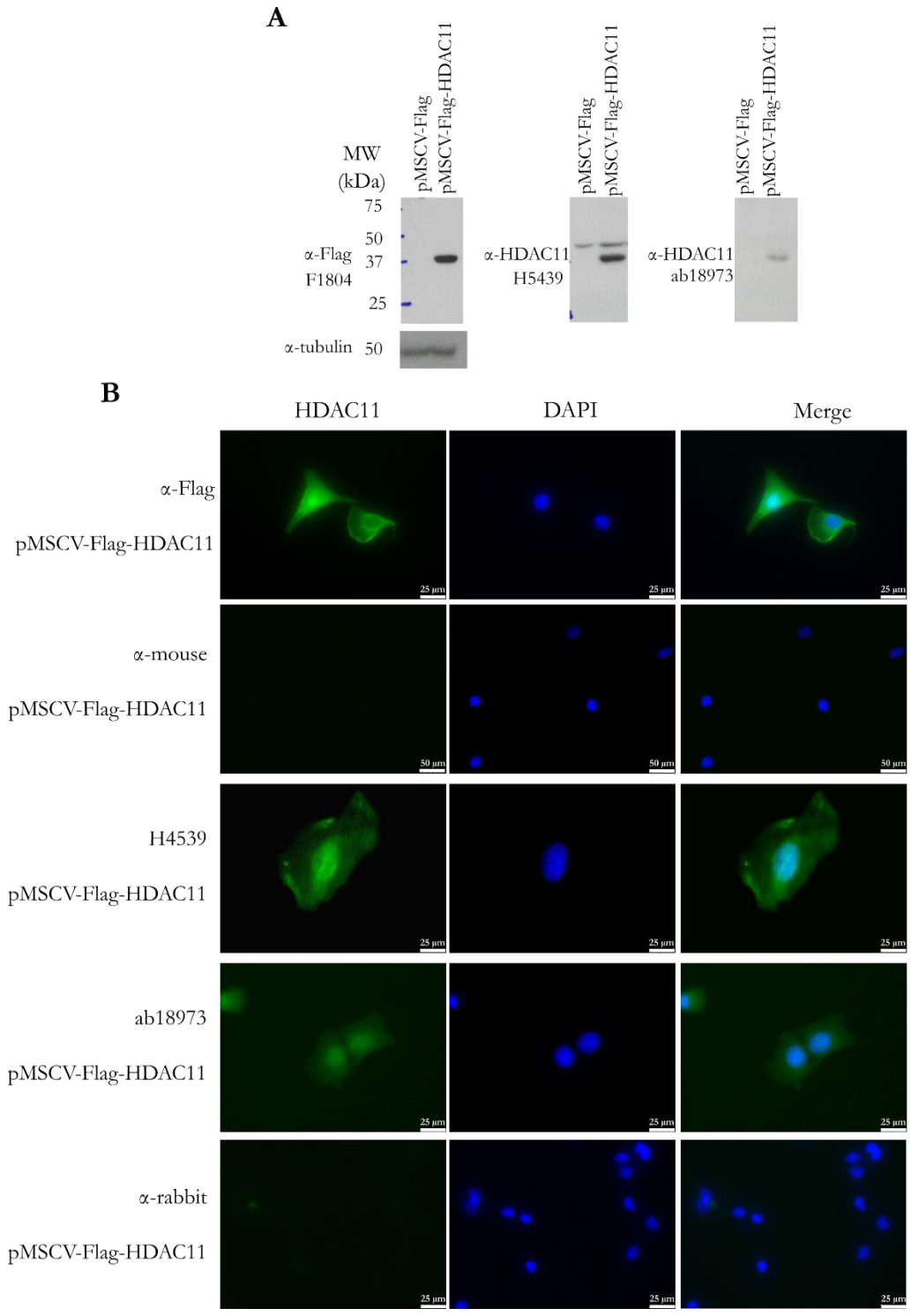

We next investigated the location of HDAC11 in differentiation conditions with the tagged protein in both terminal ends and we obtained the same results both by immunofluorescence and western blot against the compartment enriched fractions indicating that overexpressed HDAC11 is located in nucleus and cytoplasm both in proliferating and differentiating conditions (Figure 27).

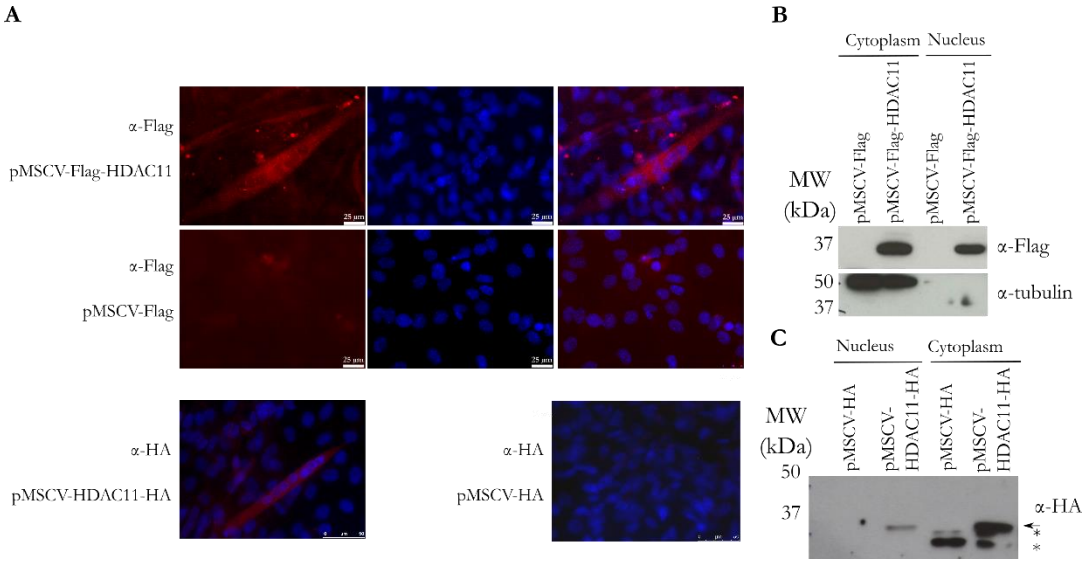

Figure 27. HDAC11 is located both in nucleus and cytoplasm of C2C12 overexpressing HDAC11 differentiated cells. A Representative microscopy images of immunofluorescence against Flag and HA epitopes in empty overexpressing cells (pMSCV) and HDAC11 (pMSCV-Flag-HDAC11 and pMSCV-HDAC11-HA) day 3 differentiated cells. **B** and **C** Western blot images showing HDAC11 location in cytoplasmatic and nuclear enriched extracts at day 1 of differentiation with α-Flag antibody (B) and proliferating and day 1 differentiating cells with α-HA antibody (C). *: Unspecific band (lower). See Supplementary Figure 2 for more details.

3.2. HDAC11 overexpression does not affect cell proliferation and differentiation but facilitates muscle fusion

At the morphologically level, HDAC11 overexpressing cells did not present any distinctive trait and look identical than empty vector overexpressing ones (Figure 28 A). As HDAC11 is low expressed in proliferation conditions, we wanted to investigate if the ectopic overexpression of HDAC11 in proliferating myoblasts interfered with cell proliferation. For that, we performed growth curves of empty and overexpressing HDAC11 C2C12 cells. As observed on Figure 28 B, the proliferation ratio of HDAC11 overexpressing cells was not different from the empty ones, discarding that HDAC11 overexpression interferes with cell proliferation.

Figure 28. HDAC11 overexpressing cells did not present differences in their morphological traits or cell proliferation rates. A 10X bright film microscopy images showing C2C12 transduced with retrovirus containing an empty vector (pMSCV-HA) or overexpressing HDAC11 (pMSCV-HDAC11-HA). No differences in cell morphology were observed. **B** Growth curves for pMSCV empty vector and pMSCV-HDAC11-HA overexpressing cells. At D0, 26,000 cells were seeded in 6 well plates and counted in technical replicates three times each 24 h until they reach confluency. Values represent the average values of three independent experiments ± SD.

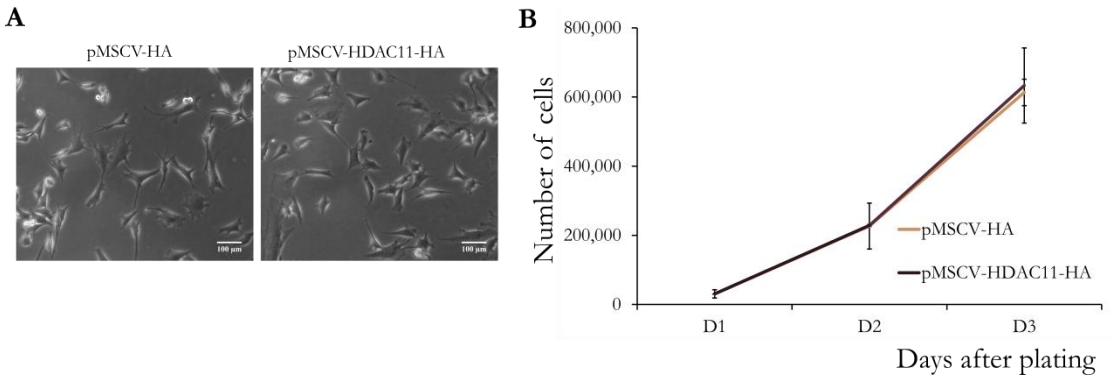

Next, we tested whether HDAC11 overexpression could initiate the differentiation program by platting together the cells at a confluent density but without performing serum deprivation medium change. In that conditions, we did not observe spontaneous cell differentiation indicating that HDAC11 overexpression is not sufficient to trigger the myogenic differentiation program if the conditions are not permissive (data not shown).

Finally, we investigated if HDAC11 overexpression could affect the cell differentiation capacity when differentiation conditions are permissive. For that, we platted the same amounts of confluent cells as described above, we performed serum deprivation when reached confluence and analyzed the levels of classical differentiation markers by qPCR at days 1 and 3 of differentiation. As observed in Figure 29 A, no statistical differences were observed both in the early differentiation marker myogenin (MGN) and the latte one myosin creatine kinase (MCK), although a certain increase is observed in HDAC11 overexpressing cells. To further assess differentiation and fusion capacity of HDAC11 overexpressing cells, we performed immunostaining against embryonic myosin heavy chain (eMHC), which is expressed in differentiating cells, in order to visualize differentiating cells and myotubes. As shown on Figure 29 B, we did not observe differences in the number of $eMHC^+$ cells present per area, but when we quantified the number of nuclei per myotube, defined as those cells containing three or more nuclei, it was observed a higher number of nuclei in HDAC11 overexpressing cells at day 5 of differentiation, suggesting that HDAC11 overexpressing cells present an increase in their fusion capacity.

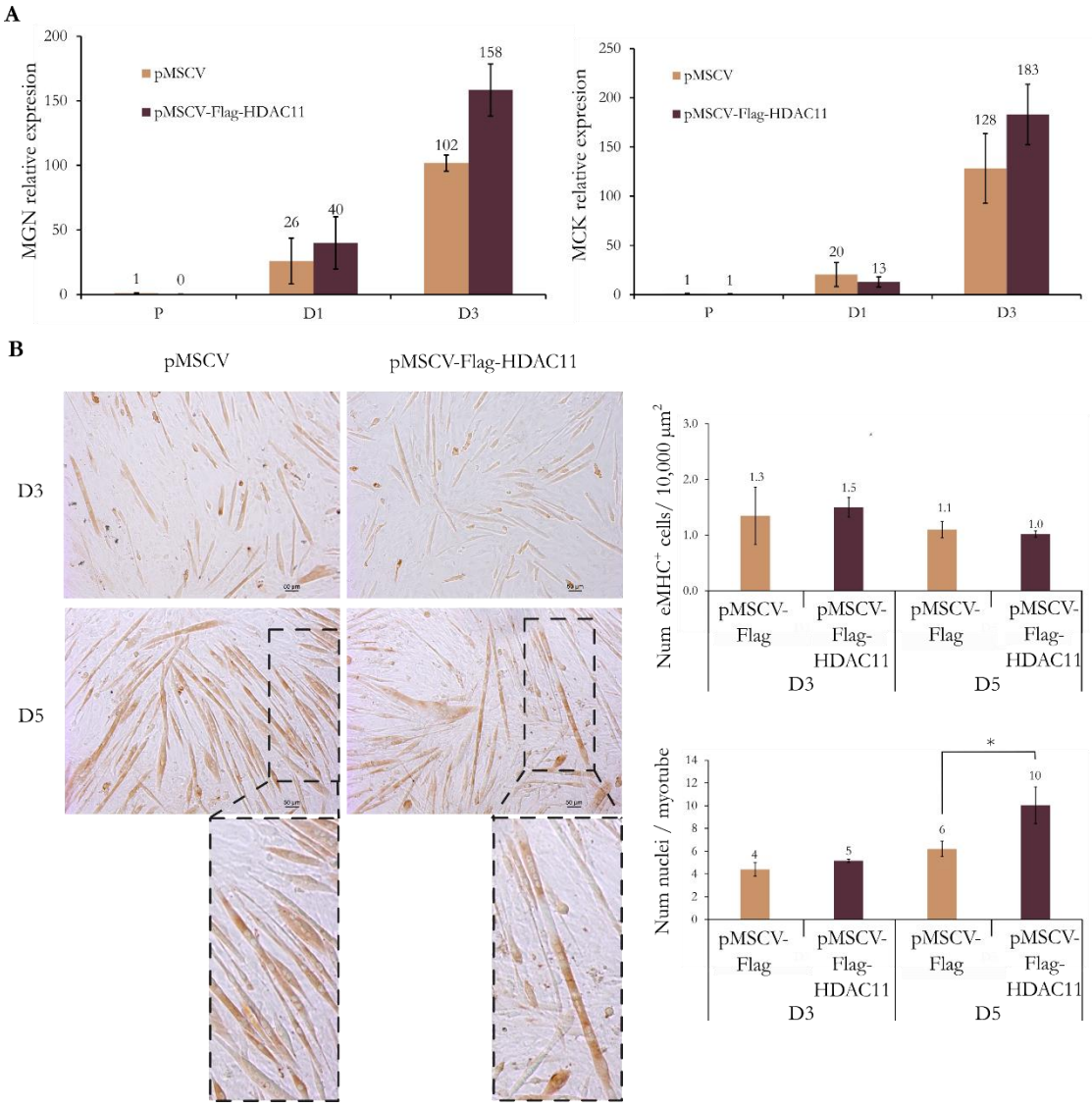

Figure 29. Overexpressing HDAC11 C2C12 cells did not present different expression of muscle differentiation markers but shown increased fusion capacity at D5. A qPCR expression of muscle differentiation markers at the indicated time points. Values represent the average data of three independent experiments ± SEM. **B** Left panel: Representative images of eMHC stained overexpressing empty vector (pMSCV-Flag) or HDAC11 (pMSCV-Flag-HDAC11) differentiating cells. A detail of a representative myotube in each case is shown to appreciate the number of nuclei per myotube (dashed lines). Right: quantification of the number of positive eMHC cells per area and the number of nuclei per myotube. Data correspond to the average value of three independent experiments ± SEM At least four random images at 10 X were counted for each condition.

4. CRISPR/Cas9 HA tagging of the endogenous locus of HDAC11

As our attempts to detect the endogenous levels of HDAC11 had been unsuccessful, we decided to use the novel and powerful CRISPR/Cas9 technique to tag the endogenous locus of HDAC11 as an alternative to detect its protein expression levels bypassing the use of antibodies against HDAC11. For that, we decided to use a hemagglutinin (HA) epitope as it is an immunogenic tag with many verified commercial antibodies available. The basis of this technique is that the cells transfected with CRISPR/Cas9 protein and driven by a sgRNA sequence, will specifically introduce a double strand break (DSB) in the neighbour of the sgRNA, specifically about 3 nt from the PAM sequence. This double strand break can be repair, if there is a homology template available, by the homology-directed repair system (HDR), introducing in the endogenous DNA sequence the editing elements available in the repair template. As illustrated in Figure 30 A, we decided to design the sgRNA's at the N-ter (sgRNA 1) and C-ter (sgRNA's 2 and 3) domains of the protein, locations where we had already checked by overexpression that tagging did not interfere with the protein location. We decided to use ssODN (single stranded oligonucleotides) as repair templates rather than plasmid donors because they can be generated faster and work more efficiently for small insertions (Cong & Addgene 2013). Both sgRNA's and ssODN designs were performed following the recommendations of Zhang's laboratory (Ran et al. 2013; Cong & Addgene 2013).

To assess HA incorporation, three methods were designed (Figure 30 B). The first one, consisted in the amplification by PCR of the regions flanking the locus to modify (red arrows and boxes in Figure 30 B). As HA length is small (27nt) and the differences of amplicon lengths are difficult to be seen by electrophoresis, a second method of validation was incorporated, consisting on a mutation in the "tac" consensus codon of the HA tag sequence to "taT" to generate a NdeI restriction site. Consequently, the digestion of the previously generated amplicons is performed only if HA has been incorporated. The third method consisted also in the amplification of the region to modify but using as a forward or reverse primers (with the aforementioned ones) one of a pair directly located directly in the HA sequence so the resulted amplicons are produced only if HA had been incorporated (orange arrows and boxes, Figure 30 B).

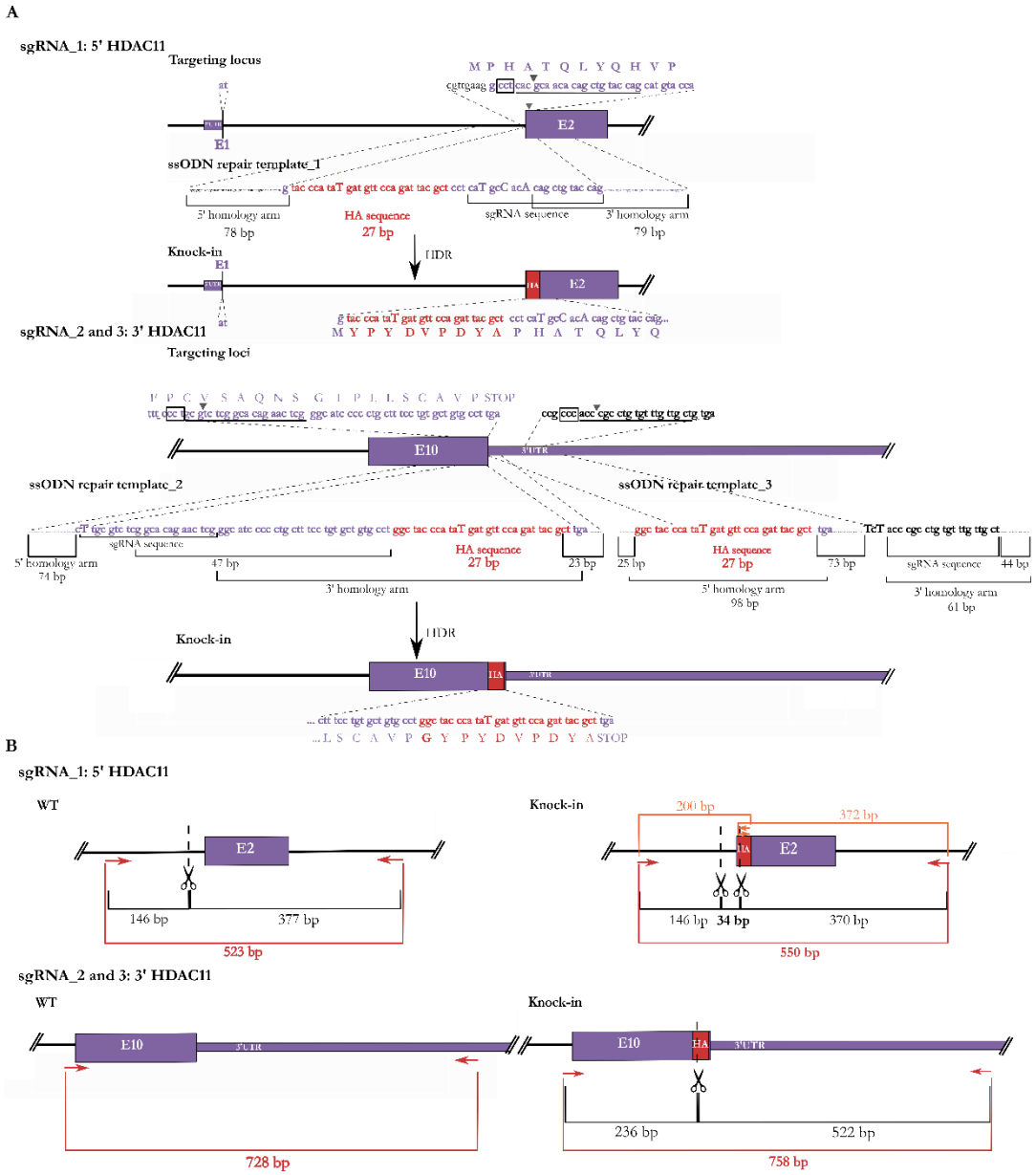

Figure 30. Targeting and validation strategies to tag HDAC11 locus by CRISPR/Cas9 knock-in technique. A Schematic illustration of the strategies to insert an HA tag in the genomic locus of HDAC11. In the upper rectangle is shown the strategy for sgRNA_1, which targets the second exon (E2) of HDAC11. The sgRNA_2 and 3 target the last exon (E10). In both cases, the first illustration (Targeting locus) represents the WT genomic locus targeted. Underlined are indicated the location of sgRNA targeting sequences. The triangles indicate the cut positions of Cas9, 3 nt upstream the PAM sequence (grey square), in each case. Note that the PAM sequence 5'-NGG 3' is located in all cases in the complementary strand of the represented. In violet are colored the coding nucleotides and in black the non-coding from intron 1 (sgRNA_1) or 3'UTR (sgRNA's 2 and 3). In the middle part (ssODN repair template) are indicated the ssODN sequences used for each sgRNA with the homology arms locations and sizes indicated and HA sequences (in red) to integrate. Upper letters correspond to mutations introduced to prevent ssODN cut by Cas9 (in the sgRNA sequence for sgRNA_1 or PAM sequences for sgRNA's 2 and 3) and to introduce a NdeI restriction site in HA tag sequence (red). In sgRNA's 2 and 3

a codon coding for glycine was introduced upstream the HA tag as was used in overexpressed HDAC11-HA. In the bottom (Knock-in) are represented the expected knock-in sequences to be obtained after a perfect homology directed recombination event (HDR). **B** Validation strategies for sgRNA's pools and clones. The validation of KI was performed by three different methods. First, a pair of primers flanking the insertion points were designed (red arrows). As indicated, the amplicon length are 27 bp (sgRNA_1) or 30 bp (sgRNA's 2 & 3) longer if HA is inserted. As these differences of amplicon lengths are not very evident to be seen by gel electrophoresis, the obtained amplicons (red) were digested with NdeI enzyme. As the sequence of the introduced HA was mutated to generate a NdeI restriction site (A) the insertion of HA digests the amplicon only if the HA had been incorporated (note that for sgRNA_1 a endogenous NdeI site is already present in the targeted region so the diagnostic band to be seen is 34 bp long). As a third method of validation, a pair of primers directly aligning on HA sequence (orange arrows) were design to get amplification products only if HA tag had been incorporated.

The process followed to perform CRISPR KI and all the possible genotype outcomes are represented on Figure 31. After checking of nucleofection by control GFP expression ("Materials and methods" section) only the cells that had incorporated the vector containing Cas9 protein and the corresponding sgRNA were selected by puromycin treatment. To decide which sgRNA was the most efficient, the modified regions were amplified as explained. In Figure 32 A are shown the amplicons for the indicated pools and wild-type samples. As observed here, the difference of size amplicons was not evident by gel electrophoresis (maybe due to the low efficiency of editing in the pools). For that, a higher amount of DNA (pooled from several PCR amplification reactions) was digested. Taking into account that HDR pathway occurs at very low rates and considering the worst scenario of HDR efficiency as occurring in 0.5% of the cells (Maruyama et al. 2016; Mali et al. 2013), we digested a minimum of 3 μg of pooled DNA assuming that the minimum amount of DNA to be detected by ethidium bromide visualization was 15 ng.

Figure 31. HDAC11 HA knock-in editing steps. Scheme of the process followed to obtain CRISPR HA tagged HDAC11. First, C2C12 cells were nucleofected in three different conditions corresponding to the three combinations of sgRNA's and ssODN's. The next day, puromycin was added for 72h to the medium to select those cells that had incorporated the vector from those not nucleofected or that had only incorporated the ssODN. The obtained pools were amplified until having a sufficient cell number and then were tested for HA incorporation to select which sgRNA was the most efficient. Of this selected sgRNA, clonal lines were isolated by serial dilution and after expansion for 15-20 days, the clones were screened to select those that had incorporated the HA tag in the desired position (biallelic or monoallelic knock-in's) from those that had not been edited or presented off-target editing.

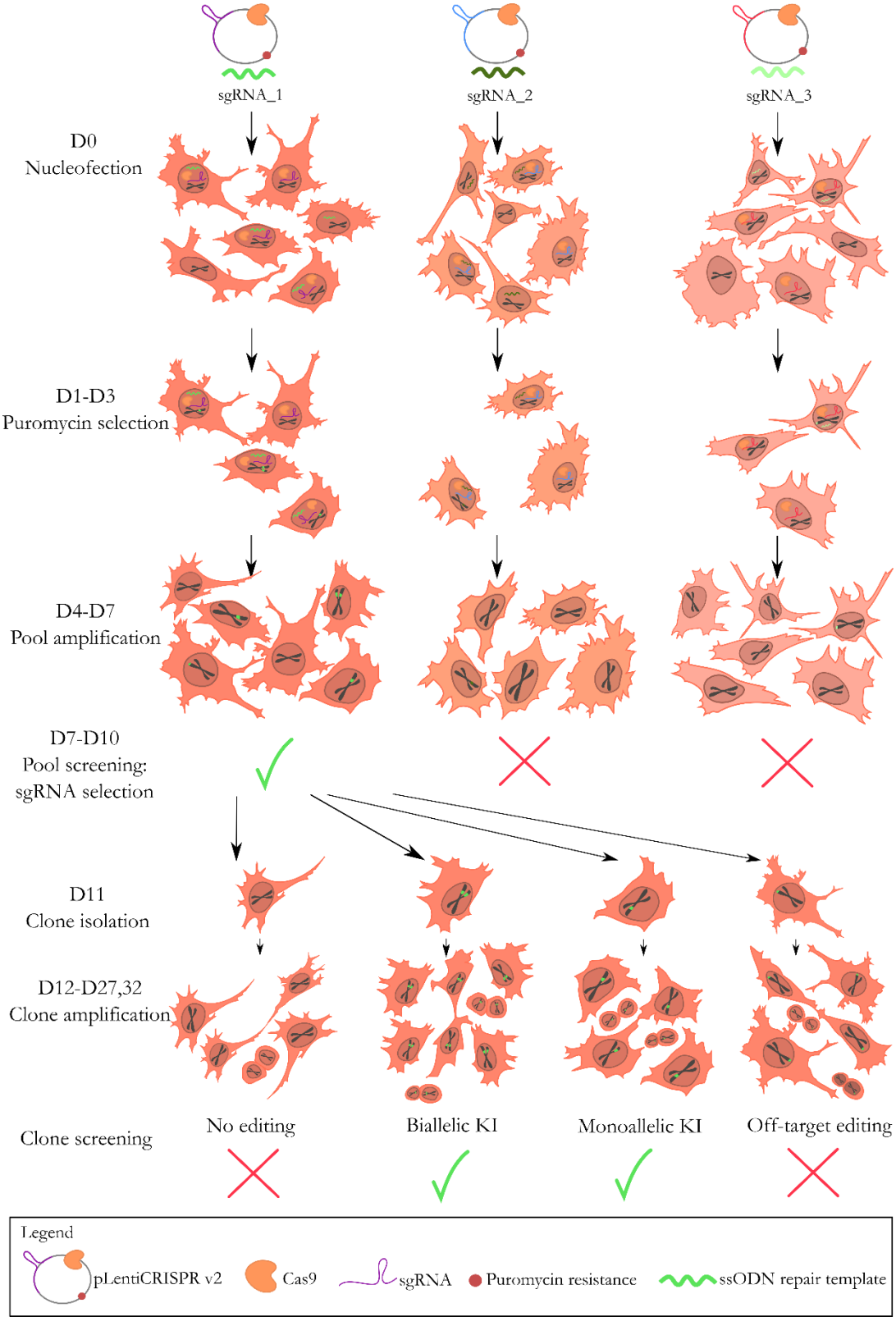

As observed on Figure 32 B, sgRNA2 showed the expected digestion bands, so we screened 30 derived clones but none of them was positive for KI editing. sgRNA3 did not shown the expected bands so it was discarded (13 already derived clones were also screened

but none was either positive). On the contrary, the digestion of sgRNA_1 pooled amplicons showed the expected diagnostic band about 34 bp (Figure 32 C). The amplification of DNA from this sgRNA_1 pool with the two pairs of primers designed directly on the HA sequence to integrate gave the expected amplicon weights (Figure 32 D) so these two positive validation strategies made us select this sgRNA for further clone screening. A total of 219 clones were screened by the three indicated methods. The summary is shown in Table 25.

	Total screened clones	Positive clones*	KI efficiency	Clones validated by sequencing	
				Monoallelic KI	Biallelic KI
sgRNA_1	219	13	6%	6	0
sgRNA_2	30	0	0	0	0
sgRNA_3	13	0	0	0	0

Table 25. CRISPR sgRNA KI efficiencies obtained by clone screening. * Screened by three methods: PCR amplification followed by NdeI restriction, PCR amplification with HA forward primer and PCR with HA reverse primer. Of these clones, only selected ones were validated by sequencing.

Figure 32. CRISPR KI pool validations. A PCR amplification bands of the corresponding sgRNA's pools and WT control samples. In each case one PCR reaction prepared as described in "Materials and methods" starting with 25 ng of template was directly run (Undig) or digested with NdeI (Dig) in 2% agarose gel stained with ethidium bromide. For sgRNA_1, the bands observed correspond to the digestion of the endogenous restriction site. The band of 34 bp is not visible by electrophoresis in agarose. For none sgRNA's is observed an increase in their amplicon weights, so several PCR's were pooled and 3 μg of the purified products for sgRNA_2 and WT and 7 μg for sgRNA_3, were digested with NdeI (**B**). As observed, for sgRNA_2 two bands could be compatible with KI generation (marked with arrows, the expected sizes are 522 and 236 bp) but not for sgRNA_3, that was discarded. **C** Pooled PCR's (about 10 μg per condition) digested with NdeI and ran into 8% acrylamide gel stained with ethidium bromide after run. The first lane of each condition represents the 95% of the digested sample and the second lane the 5%. As shown, they are visible both the bands from endogenous NdeI restriction site (146 and 377 bp) and also the 34 bp expected from KI editing of sgRNA_1. **D** PCR amplification of the previous PCR amplicons with the primers directly annealing on HA. Left: 5'UTR_F and HA_R primers. Right: HA_F and 'UTR_R (the gel was cut because included other irrelevant samples). MW: Molecular weight ladder. 1: GeneRuler 100 bp DNA ladder (Ref.SM0241, Thermo Scientific). 2: GeneRuler 1kb Plus DNA ladder

(SM1331, Tamar Laboratory Supplies. 3: GeneRuler 50 bp DNA ladder (Ref. SM0371, Thermo Scientific). 4: Low molecular weight DNA ladder (Ref. N32336, Biolabs).

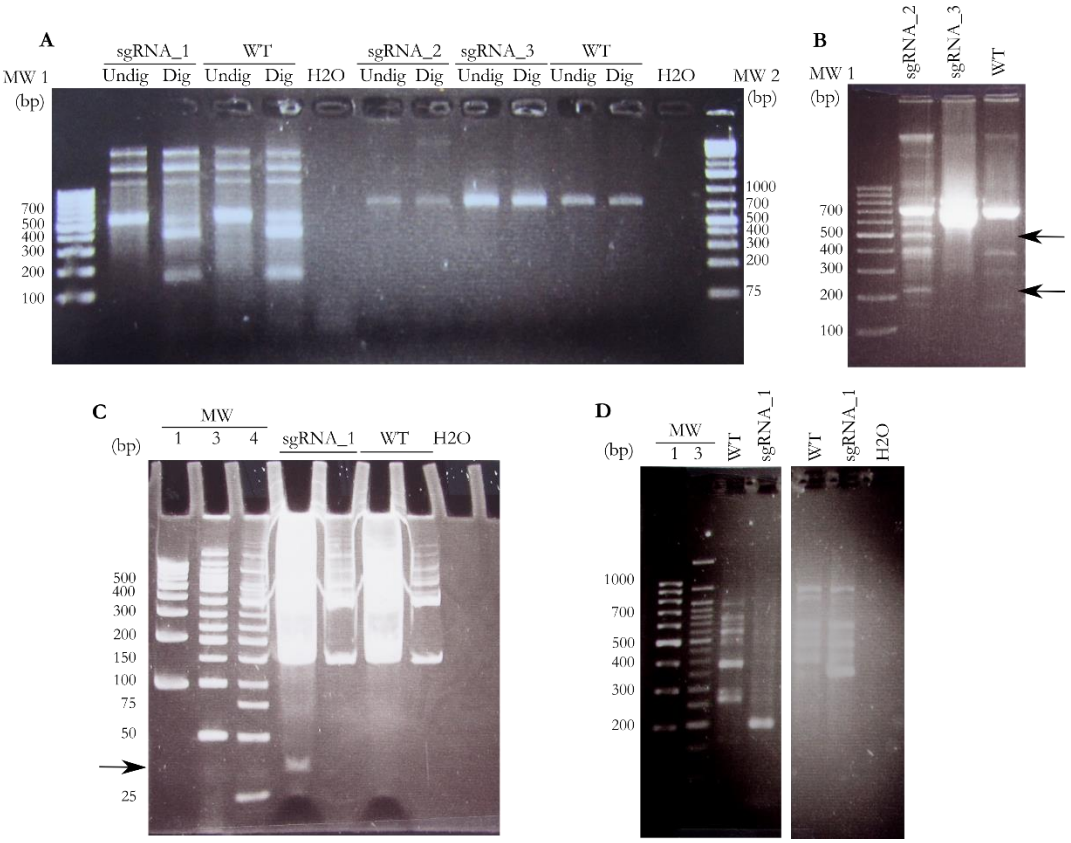

In Figure 33 are shown the validation results for the positive clone (clone 19) that was latter on checked by western blot analysis. In Figure 33 A is shown the identification of clone 19 as a KI edited evidenced by the appearance of the 34 bp expected band. All the other clones in the gel analysis resulted negative. To further validate clone 19, PCR amplification was performed with the primers directly annealing with the HA inserted sequence (Figure 33 B). In Figure 33 C is shown the edited sequence of clone 19 that was edited only in one chromosome, as the clones sequenced from the PCR amplicons contained both edited and not edited copies.

In Supplementary Figure 1 are shown some other positive clones obtained and their process of validation. As the number of clones obtained was sufficient to continue the experiments, not all clones where further validated. Moreover, some clones showing only faint amplification bands (as clone 17 from Figure 33 A and clones 5 and 47 from Supplementary Figure 1) were not further tested. Also, not all the obtained clones were sequenced by cost and time issues, so probably the efficiency of KI integration for sgRNA_1 is slightly higher than the 6% stringently calculated. Furthermore, the screening of more clones of sgRNA_2, as gave the expected NdeI restriction pattern, could also had

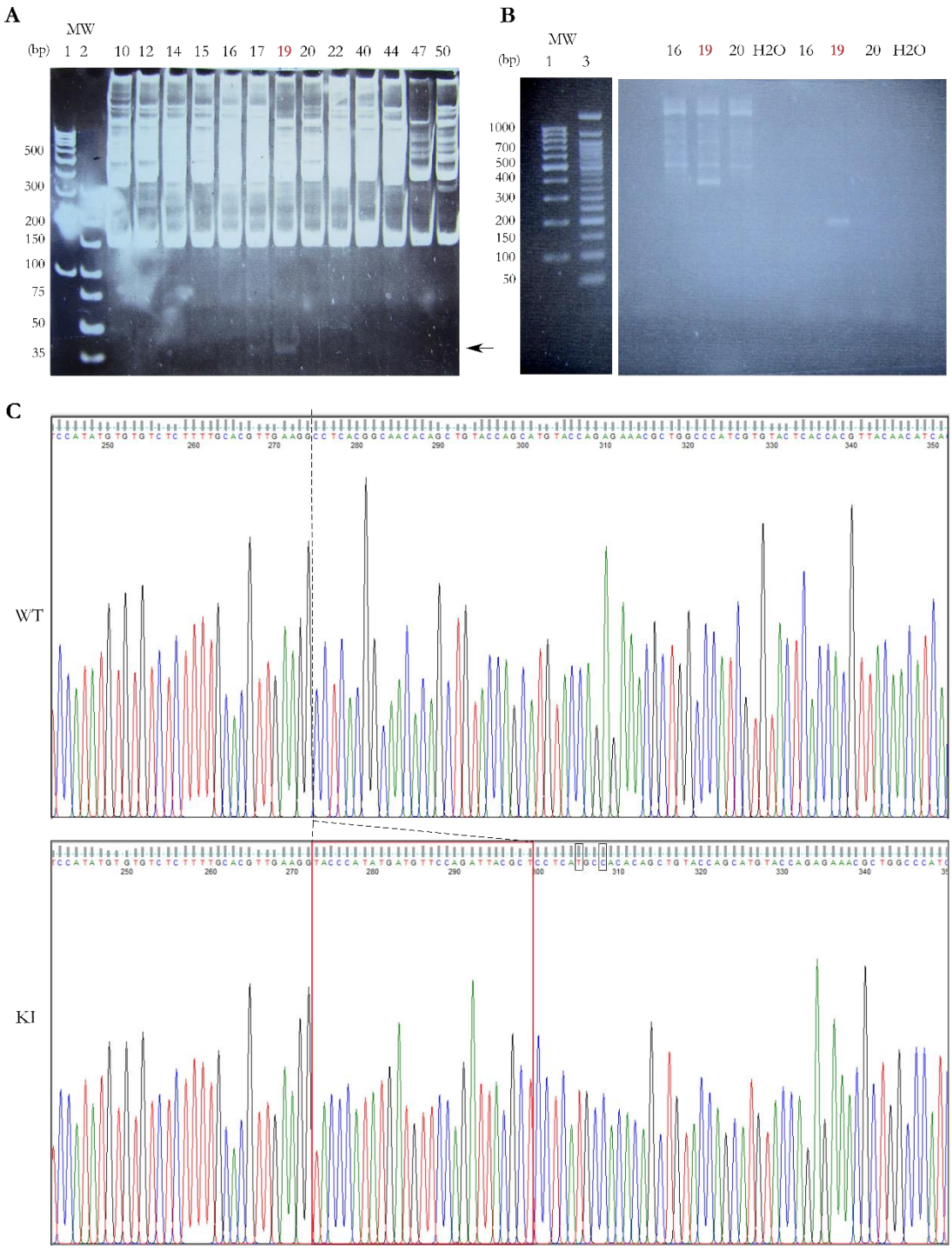

Figure 33. Clone 19 CRISPR KI validation. A Clone screening identification of clone 19 as KI edited. Restriction products from NdeI digestion were ran into 8% acrylamide gel. Indicated with an arrow is the expected 34 bp band indicative of KI editing. **B** PCR validation of KI editing with primers annealing to the inserted HA sequence. The left three lanes correspond to the amplification products with HA_F and 5'_UTR_R (expected band 372 bp). The next lanes in the right correspond to the amplification product with 5'UTR_F and HA_R (expected band 200 bp). Clones 16 and 20 were included as negative controls that did not present a 34 bp band in acrylamide gel in A. Gel was cut because irrelevant samples were ran between the ladders and the samples. MW: Molecular weight ladder. 1: GeneRuler 100 bp DNA ladder (Ref.SM0241, Thermo Scientific). 2: GeneRuler ultra low range DNA ladder (Ref. SM1211, ThermoFisher).

3: GeneRuler 50 bp DNA ladder (Ref. SM0371, Thermo Scientific). **C** Electropherograms showing HDAC11 locus in C2C12 WT and KI edited clone 19. In a red box is marked the HA sequence inserted in knock-in edited clone 19. In black boxes are indicted the silent mutations introduced to avoid cut of ssODN by Cas9.

led to positive ones but as our goal was to obtain at least one positive to detect HDAC11 endogenous protein, we did not continue with the screening.

We decided to continue our studies with clone 19 and we performed several differentiation time courses, but unfortunately, the only detected band resulted to be an unspecific one detected also in overexpressing empty pMSCV-HA C2C12 and WT cells (Figure 34 A). For this reason, we decided to increase the amount of protein analyzed. As 100 µg is almost the loading limit in western blot technique, we set up the immunoprecipitation conditions with overexpressing pMSCV-HDAC11-HA (Supplementary Figure 2 B). With these conditions, we examined clone 19 at day 1 of differentiation (the point with the highest HDAC11 RNA expression) and we observed a mild band that coincided with HDAC11-HA (Supplementary Figure 2 C). To increase sensitivity, we increased 2,000 folds the amount of immunoprecipitated protein to 10 mg and we performed HDAC11 detection in pooled points of time courses of differentiation. As observed on Figure 34 B, endogenous HDAC11 HA KI tagged protein is detected at day 1 and 3 of differentiation and is not observed in proliferation conditions. The detection of HDAC11 only in differentiation conditions matches the upregulation of HDAC11 RNA expression in muscle cell differentiation.

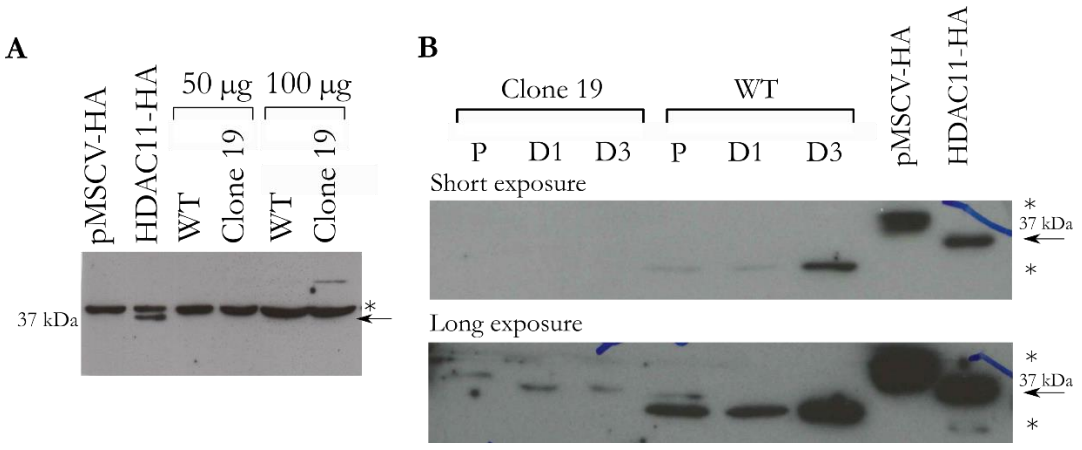

Figure 34. Endogenous CRISPR HA tagged HDAC11 is detected in differentiating C2C12 but not in proliferation conditions. A Endogenous tagged HDAC11 was not detected by western blot

detection in monoallelic edited clone 19. Western blot showing C2C12 constitutively expressing an HA empty vector and overexpressed HDAC11-HA (50 μg each) as controls. As observed, even with high amounts of loaded protein, HA is not detected in clone 19 KI at day 1 of differentiation. Proteins were extracted with RIPA buffer and ran into 8% acrylamide gel. Membrane was incubated with α-HA clone 11 (Ref. 901515, Biolegend, kindly provided by Dr. Buschbeck's lab). The detection was perform with two HA antibodies as with both an unspecific band (*) appeared very near to the specific one (data not shown for ab91110). **B** Western blot detection of endogenous HDAC11-HA after immunoprecipitation. All samples were immunoprecipitated starting with 10 mg of total protein. All the immunoprecipitated elution was ran into 8% acrylamide gel and detected with α-HA (Ref. ab91110, Abcam). As indicated, in empty vector and in clone 19 proliferation (P) appears an unspecific band (marked with an asterisk) not detected in the overexpressed immunoprecipitated protein or differentiating clone 19. This band seems to appear only at high amounts of precipitated protein as when the immunoprecipitation is performed with 500 μg of total starting protein it is not observed (Supplementary Figure 2 C).

5. Analysis of HDAC11 functions in HDAC11 wild type and deficient primary myoblasts

At the moment we were experiencing problems with the antibody detection of endogenous HDAC11, we became aware that Dr. Alberto Pendás laboratory (CSIC-USAL, Salamanca) had generated a HDAC11 total deficient mice (Gutiérrez 2012, unpublished). We therefore initiated a collaboration with this group in order to address the role of HDAC11 in *in vivo* myogenesis.

5.1. Establishment of primary cultures derived from wild-type and HDAC11 deficient myoblasts

First of all, we isolated satellite cells (SCs) from 6 female HDAC11 wild-type (WT) and 5 female deficient (KO) mice as described on "Material and methods" by muscle bulk isolation of muscles from the back, forelimbs and quadriceps, followed by FACS sorting. Representative plots of the gating conditions for FACS SC isolation are shown on Figure 35 A. At the moment of cell sorting, 500 sorted SC's of each animal were placed onto coverslips to verify the identity of the isolated SC's (P6) by immunochemistry. As shown on Figure 35 C, sorted cells expressed the SC marker PAX7 and lack MYOD staining, confirming their identity as SCs and showing that at the point of isolation they were still on a quiescent state. We also determined the percentage of isolated SCs with respect to the total number of alive sorted cells (P3) and as shown on Figure 35 B, we found no differences in the number of SC between both genotypes, indicating that HDAC11 deficient mice did not present an alteration in SC numbers.

Isolated SCs, were activated by platting and kept in proliferation conditions as indicated to amplify the starting cultures to have a sufficient number of them to perform experiments.

Figure 35. HDAC11 KO mice did not present alterations in the number or quiescence state of their SC. A FACS sorting strategy for SC isolation. Representative FACS plots and gating schemes to isolate mononucleated SC from heterogeneous populations of muscle extracts. First, cells were separated from aggregates and debris using forward scatter (FSC) and side scatter (SSC) parameters. Living cells, no stained with DAPI (Pacific blue, P3), were subsequently selected by negative staining with CD45 and Sca-1 antibodies (to exclude hematopoietic and endothelial and intersticial cells, respectively) and finally SCs were selected by double staining with α-7 integrin (PE-A) and CD34 (APC-A) (both cell surface antigens expressed by SCs) to obtain P6 population which was platted to obtain primary myoblasts cultures from HDAC11 WT and KO mice. **B** Average percentages of isolated SC versus the total number of living cells were calculated

by dividing P6 number of events (SCs) by P3 number of events (living cells). Bars represent the average values of 6 WT and 5 KO ± SEM. **C** Immunofluorescence of representative WT and KO directly isolated SCs by FACS, showing positive staining for PAX7 SC marker and negative staining for MYOD as marker of SC activation, indicating that isolated cells correspond to SCs and that both genotypes present SC in a quiescent state.

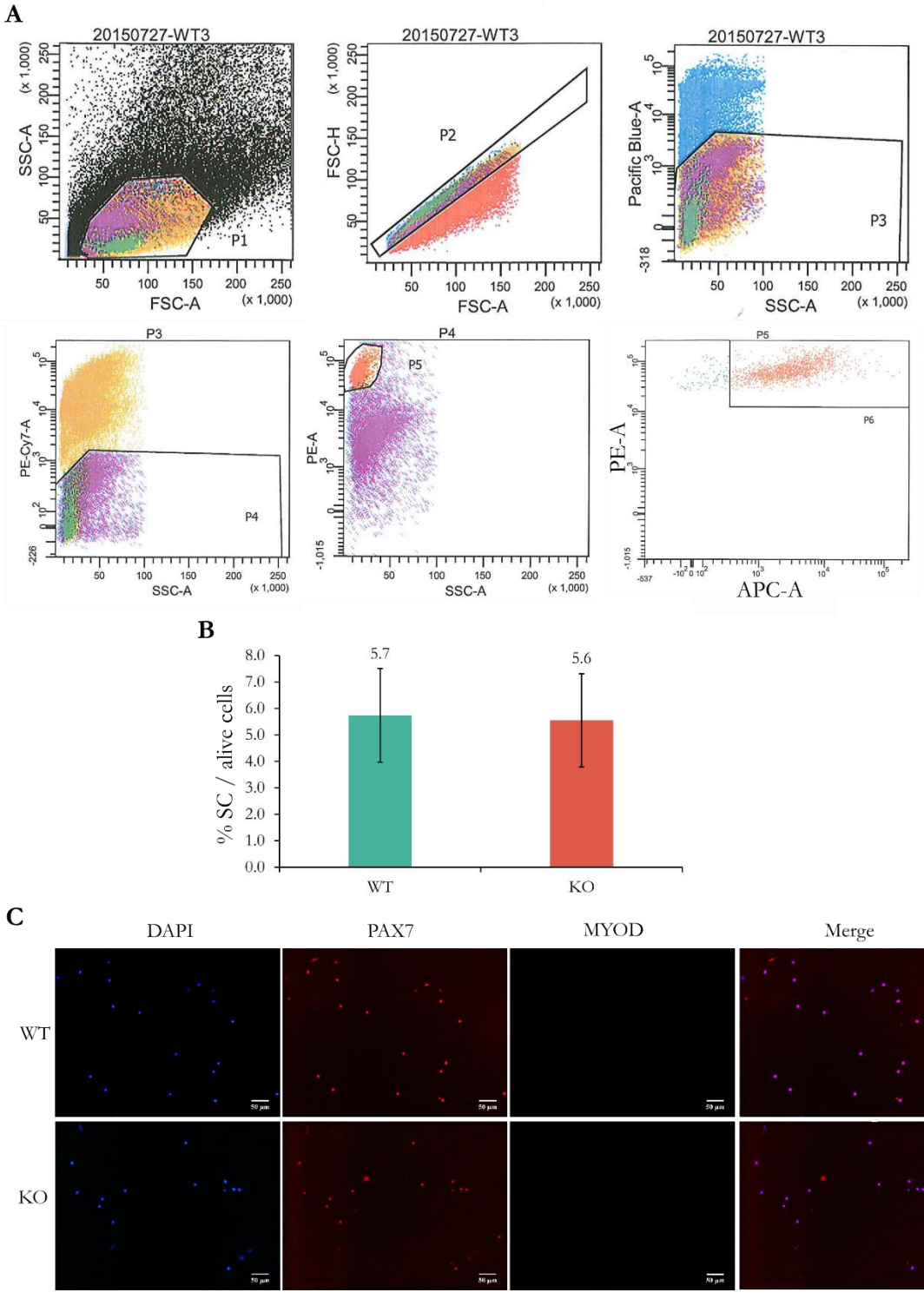

5.2. HDAC11 deficient myoblasts do not present alterations in cell proliferation

We first investigated whether primary isolated myoblast cultures presented differences in its proliferative capacity comparing growth curves. For that, we previously set up the confluency of 3,527 cells/mm^2 as an optimal density that gave a sufficient and reliable number of cells to count at all time points and that also allowed cell number monitoring for three days, moment at which cells started to reach confluency. As observed on Figure 36 A, the proliferation rates of HDAC11 deficient MPCs were not different than wild-type ones. To go into more detail, we quantified the percentage of cells present in S phase by EdU incorporation (Figure 36 B) and we performed cell cycle analysis of the same proliferating cells (Figure 36 C). We did not observe a difference on the number of cells present on S phase both by EdU staining and propidium iodide incorporation but the number of HDAC11 deficient cells presented in G2/M phase was modestly higher (pval<0.05). Altogether, these results suggest that HDAC11 deficient myoblasts did not present major alterations in cell proliferation.

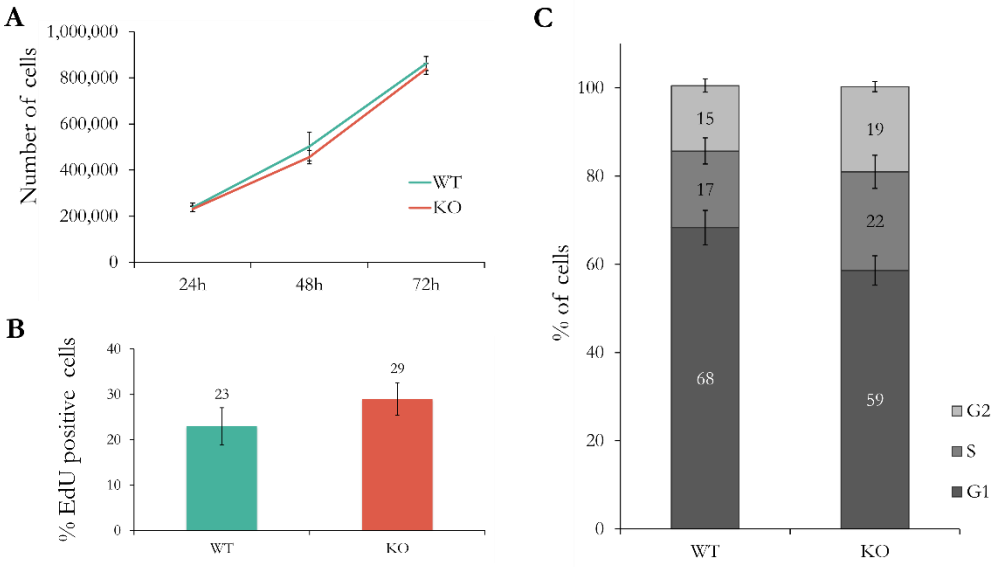

Figure 36. HDAC11 deficient myoblasts did not present alterations in cell proliferation. A Growth curves of three WT and three KO MPC's. 200,000 cells for each condition were seeded in 100 mm plates and counted each 24h. Values represent the average value of counts at each time point ± SD. **B** Percentage of stained EdU cells by FACS analysis in proliferating MPCs. Data represent the average of 5 WT and 5 KO ± SEM. **C** Percentage of cell distribution in cell cycle phases of proliferating MPCs by FACS analysis after EdU staining. Data represent the average of 5 WT and 5 KO ± SEM.

5.3. HDAC11 deficient myoblasts do not present major alterations in cell differentiation but showed reduced fusion capabilities

In the next step, we wondered if HDAC11 deficient myoblasts presented defects in cell differentiation. For that, we plated the same number of cells per animal and condition at a confluent density of 2,660 cells/cm^2 (250,000 cells in 6 well plates) and we performed serum deprivation the next day to induce cell differentiation. The levels of expression of the classical differentiation markers were quantified at the indicated points (Figure 37 A) by qPCR as described, not observing major differences between both genotypes.

To further assess differentiation and fusion capacities of HDAC11 deficient myoblasts, we performed eMHC staining in differentiating cells. As shown on Figure 37 B, the differentiation index of WT and KO myoblasts was not different at any point, which goes in agreement with qPCR MGN quantification, suggesting that HDAC11 KO cells have not a defect in their differentiation capability. Regarding cell fusion, HDAC11 deficient myoblasts present a reduced fusion index and number of nuclei per myotube at day 2 of differentiation.

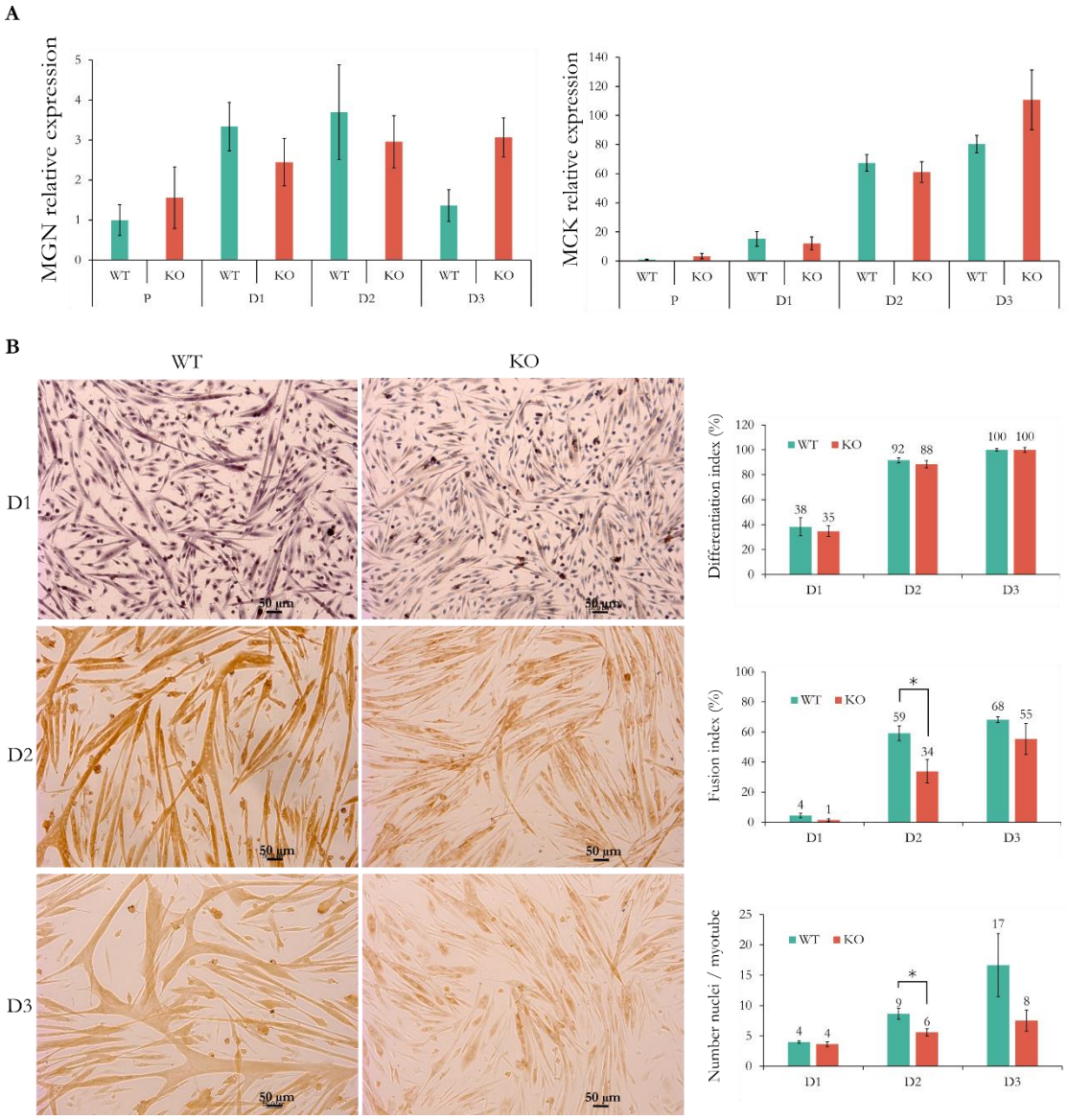

Figure 37. HDAC11 deficient myoblasts did not present differences in cell differentiation but present reduced fusion capabilities. A qPCR quantification of myogenin (MGN) and muscle creatine kinase (MCK) in 4 WT and 5 KO ± SEM. **B** Left panel: Bright film microscopy images of representative WT and KO time courses of differentiation stained with eMHC. At day 1, hematoxylin staining was also performed after eMHC to help in the visualization of nuclei. Right panel: Quantification of the differentiation index (number of eMHC$^+$ nuclei/number of total nuclei), fusion index (number of nuclei is myotubes / number of total nuclei) and number of nuclei per myotube. Myotubes were considered as those cells with 3 or more nuclei. Data represent the average of at least three independent differentiation MPC's ± SEM. *: p val<0.05, two tails t-test.

5.4. Transcriptomic analysis of differentiating HDAC11 KO myoblasts

We next sought to determine the specific effects of HDAC11 in myoblast differentiation at the molecular level. For that, we decided to perform RNA-seq transcriptomic analysis of myoblasts at day 1 of differentiation, as it was the moment were HDAC11 was upregulated the highest through differentiation (Figure 18). For that, and as we had a considerable number of samples and independent time courses of differentiation, 4 WT and 4 KO myoblasts were chosen for the analysis in an unbiased way based on the RNA integrity number (RIN) of the extracted samples. Unsupervised clustering and principal component analysis revealed one set of 4 pairs of samples as having outlier behavior. These were subsequently excluded from the analysis.

After performing differential expression analysis of the remaining samples and setting as a cut-off a p adj value <0.05, a total of 918 genes were found differentially expressed between both conditions, 609 corresponding to genes overexpressed in KO MPC's versus WT and 309 overexpressed in WT compared to KO. In Figure 38 differentially expressed genes are represented in a Volcano plot with the names of the most changing genes indicated.

To perform data mining of both sets of genes, we selected the most changing ones in both conditions setting as a threshold a p adj val <0.05 and a FC restriction >2 in absolute value, which corresponded to 416 genes overexpressed in KO myoblasts and 213 genes overexpressed in WT ones. The complete list of these genes is presented in Supplementary Table 1. GO analysis was also performed with the complete list of genes in each case without FC restrictions obtaining the same GO terms. The complete list of genes was also analyzed using GSEA enrichment finding the same categories and processes.

Figure 38. Volcano plot representation of differentially expressed genes at D1 differentiating WT and KO myoblasts. For the analysis, all genes with at least 5 mapping reads in one sample were considered. The log_2FC was calculated comparing KO to WT so the genes with a log_2FC >0 are overexpressed in KO myoblasts and the genes with a log_2FC <0 are overexpressed in WT myoblasts.

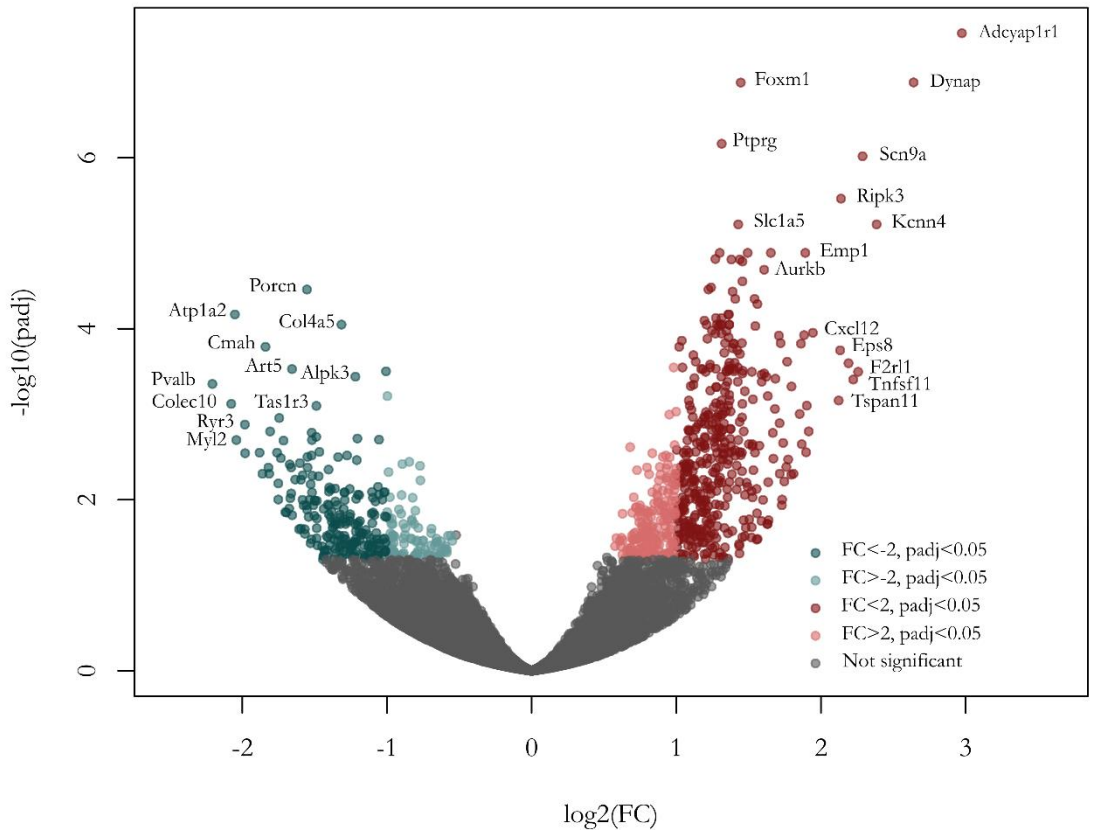

5.4.1. Gene ontology of genes overexpressed in HDAC11 deficient differentiating myoblasts

The Gene Ontology (GO) results obtained for the genes overexpressed in HDAC11 deficient myoblasts are shown on Table 26. As presented, all Biological process terms refer to cell cycle categories suggesting that the principal process affected upon HDAC11 silence would be cell cycle process.

Term	Overlap	Adjusted P-value	Z-score	Combined Score
GO Biological process				
mitotic cell cycle (GO:0000278)	89//404	9.05889E-52	-2.305	270.9
nuclear division (GO:0000280)	65//298	1.84489E-36	-2.313	190.3
organelle fission (GO:0048285)	66//325	1.3821E-35	-2.343	188.1
mitotic nuclear division (GO:0007067)	57//240	1.52021E-33	-2.272	171.7
chromosome organization (GO:0051276)	46//204	8.34535E-26	-2.288	132.1
cell cycle phase transition (GO:0044770)	46//280	9.04003E-21	-2.311	106.7
chromosome segregation (GO:0007059)	30//89	1.61148E-20	-2.164	98.6
mitotic cell cycle phase transition (GO:0044772)	45//277	3.19382E-20	-2.308	103.6
DNA repair (GO:0006281)	52//403	1.30794E-19	-2.443	106.2
DNA replication (GO:0006260)	37//186	5.06176E-19	-2.244	94.5
regulation of cell cycle process (GO:0010564)	52//481	1.34638E-16	-2.433	88.9
regulation of mitotic cell cycle (GO:0007346)	45//391	4.31295E-15	-2.436	80.6

cell cycle G1//S phase transition (GO:0044843)	29//152	2.55063E-14	-2.208	69.1
G1//S transition of mitotic cell cycle (GO:0000082)	29//152	2.55063E-14	-2.205	69.0
GO celular component				
nucleoplasm (GO:0005654)	91//1051	1.7335E-23	-2.259	118.4
chromosome, centromeric region (GO:0000775)	23//64	5.1462E-16	-2.188	77.0
chromosomal region (GO:0098687)	28//124	2.243E-15	-2.121	71.5
kinetochore (GO:0000776)	25//98	7.9156E-15	-2.177	70.7
chromosome (GO:0005694)	28//166	9.2576E-13	-2.260	62.6
spindle (GO:0005819)	22//93	1.4361E-12	-2.098	57.2
nuclear chromosome part (GO:0044454)	34//327	2.9598E-10	-2.306	50.6
GO Molecular function				
ATP binding (GO:0005524)	71//1494	2.09025E-07	-2.400	36.9
chromatin binding (GO:0003682)	32//420	7.25211E-07	-2.459	34.8

Table 26. GO terms for genes upregulated in HDAC11 deficient myoblasts.

Of the total of 89 genes included in the first GO category "Mitotic cell cycle", in Table 27 are shown some of the most known genes grouped by gene families. Most notably, we found changes in microsome maintenance complex (5 genes out of 6 with helicase functions), 2 out of the three Aurora kinase proteins, 4 cycline genes and 14/45 kinesines transcripts.

Family	Function	Gene	FC(KO/WT)	p adj val
	Unknown	KI67	2.31	0.0009
	DNA replication	PCNA	2.08	0.01
	Mitosis	BIRC5	2.33	0.0013
Cyclins	Cell cycle progression	CCNA2	2.44	0.001
		CCNB1	2.74	0.0001
		CCNB2	2.42	0.001
		CCNF	2.52	0.0002
Cyclin dependent kinases	Cell cycle progression	CDK1	2.47	0.0048
		CDKN3	2.28	0.0101
Aurora serine/threonine protein kinases	Chromatid segregation	AURKA	2.58	0.0007
		AURKB	3.05	0.00002
	Initiation of replication	CDT1	2.76	0.0016
		GMNN	2.31	0.0131
Minichormosome maintenance complex	Replicative helicase complex	MCM3	2.59	0.0019
		MCM4	2.19	0.0151
		MCM5	2.89	0.0007
		MCM6	2.2	0.0098
		MCM7	2.15	0.0233
	HRR	MCM8	2.1	0.0026

	Unknown	MCMD2	1.8	0.0439
Constitutive centromere associated network (CCAN)	Kinetochore formation	CENPA	2.58	0.0006
		CENPH	2.68	0.0004
		CENPI	2.71	0.0002
		CENPK	2.15	0.0186
		CENPL	1.99	0.0149
		CENPN	2.08	0.0209
		CENPQ	2.25	0.0003
		CENPU	2.25	0.0101
		CENPW	1.97	0.0091
Other proteins associated to kinetochore	Kinetochore formation	CENPE	2.53	0.0001
		CENPF	2.17	0.0005
		INCENP	2.29	0.0023
Kinesins	Mitosis	KIF2C	2.57	0.0003
		KIF4	2.71	0.00002
		KIF7	1.68	0.0126
		KIF11	2.25	0.0024
		KIF14	2.32	0.0001
		KIF15	2.59	0.0009
		KIF18A	2.59	0.0015
		KIF18B	2.91	0.00004
		KIF20A	2.47	0.0001
		KIF20B	2.29	0.0013
		KIF22	2.48	0.0007
		KIF23	2.62	0.0002
		KIFC1	2.57	0.0003
		KIFC5B	2.07	0.0028
Shugosin-like proteins	Chromatids cohesion	SGOL1	2.54	0.0009
		SGOL2A	2.36	0.00003
Condensin	Chromosome assembly/segregation	SMC2	2.06	0.0063
		SMC4	2.19	0.0002

Table 27. Selected genes from mitotic cell cycle GO category upregulated in HDAC11 deficient myoblasts. HRR: Homologous recombination repair. (Kushwaha et al. 2016; Juríková et al. 2016; Bell & Botchan 2013; Reinhold et al. 2011; Llano et al. 2008; Hirokawa et al. 2009).

5.4.2. Gene ontology of genes overexpressed in WT differentiating myoblasts

The Gene Ontology (GO) results obtained for the genes overexpressed in WT cells are shown on Table 28. As presented, the top represented terms correspond to genes involved in muscle contraction, suggesting an involvement of HDAC11 in muscle function.

Term	Overlap	Adjusted P-value	Z-score	Combined Score
GO Biological process				
muscle system process (GO:0003012)	28//237	3.759E-17	-2.321	87.8
muscle contraction (GO:0006936)	25//195	4.1429E-16	-2.286	81.0
actin filament-based process (GO:0030029)	26//303	4.3189E-13	-2.326	66.2
muscle filament sliding (GO:0030049)	12//38	3.4171E-11	-2.437	58.7
actin-myosin filament sliding (GO:0033275)	12//38	3.4171E-11	-2.431	58.6
striated muscle contraction (GO:0006941)	14//71	6.2191E-11	-2.087	49.0
actin-mediated cell contraction (GO:0070252)	12//46	1.6682E-10	-2.307	51.9
GO celular component				
contractile fiber part (GO:0044449)	29//167	2.9116E-23	-2.284	118.5
I band (GO:0031674)	8//19	2.2448E-08	-2.569	45.2
sarcoplasmic reticulum membrane (GO:0033017)	8//23	5.1351E-08	-2.445	41.0
GO Molecular function				
structural constituent of muscle (GO:0008307)	15//41	1.1692E-14	-2.494	80.0
actin binding (GO:0003779)	21//386	1.0202E-06	-2.383	32.9

Table 28. GO terms for upregulated genes in WT myoblasts.

Taking into account the high degree of specialization of contractile proteins expression in fiber types and that we found by GSEA enrichment analysis a category corresponding to fiber type specific genes (C2 MSigDB enriched category RNAseq, Chemello_soleus_vs_EDL_myofibers_up) we wondered if our changing genes where specifically or more abundantly expressed in fast or slow muscle types. As can be seen on Table 29, the downregulated contractile genes in HDAC11 deficient myoblasts did not seem to fall into a specific muscle type category but both fast and slow muscle type categories were represented by a similar number of genes.

Noteworthy, two specific cardiac genes, MYL4 and TNNT2, were also downregulated. Both striated muscle types have common features in their differentiation programs, evidenced by the fact that their terminal function is contraction and therefore need to induce the expression of contractile genes to fulfill their differentiation program. For these reasons, we explored the expression of HDAC11 in public datasets of cardiomyocytes differentiation observing that as for skeletal muscle, HDAC11 expression is upregulated through cardiac differentiation (Supplementary Figure 3 and 4). By now, we have not gone deeper into the characterization of HDAC11 in cardiomyocytes differentiation but our RNA-seq results may suggest an additional role of HDAC11 in the regulation of cardiac contraction genes.

	Gene	Name	FC (KO/WT)	P adj val
Fast	ACTN3	α-actinin type 3	-2.51	0.0147
	ATP2A1	Ca^{2+} ATPase	-2.44	0.0317
	MYL1	Myosin light chain 1	-2.76	0.0182
	MYLPF	Myosin light chain, phosphorylable	-2.43	0.0234
	MYOM2	Myomesin2	-2.49	0.0352
	TNNT3	Troponin T type 3	-2.14	0.0442
	PVALB	Parvalbumin	-4.41	0.0004
Slow	MYL2	Myosin light chain 2	-4.08	0.0020
	MYOM1	Skelemin	-2.52	0.0347
	MYOM3	Myomesin3	-2.23	0.0286
	MYL4	Myosin light chain 4 (atrial, cardiac)	-2.59	0.0167
	TNNI1	Troponin I type 1	-2.80	0.0072
Cardiac	TNNT2	Troponin T type 2	-1.90	0.0420
Other	MYH3	Embryonic	-2.71	0.0194
	MYL6B	Myosin light chain B	-2.51	0.0075

Table 29. Contraction-related genes upregulated in wild-type HDAC11 myoblast that had been described to be enriched in fast or slow muscle types.

5.5. Validation of HDAC11 targets

To validate HDAC11 target genes found by RNA-seq, we used additional primary myoblasts cultures from wild-type and HDAC11 deficient myoblasts, as well as an alternative loss of function system through shRNA mediated HDAC11 downregulation levels, and a gain of function system through overexpression of HDAC11.

First of all, we examined the expression of the most changing targets in the RNA-seq in additional primary myoblasts lines at day 1 of differentiation and as shown in Figure 39, the expression of the analyzed targets goes according to the RNA-seq results: DYNAP, KCNN4 and SNC9A are upregulated in HDAC11 deficient cells (Figure 39 A) and TRDN and PVALB are upregulated in wild-type myoblasts (Figure 39 B).

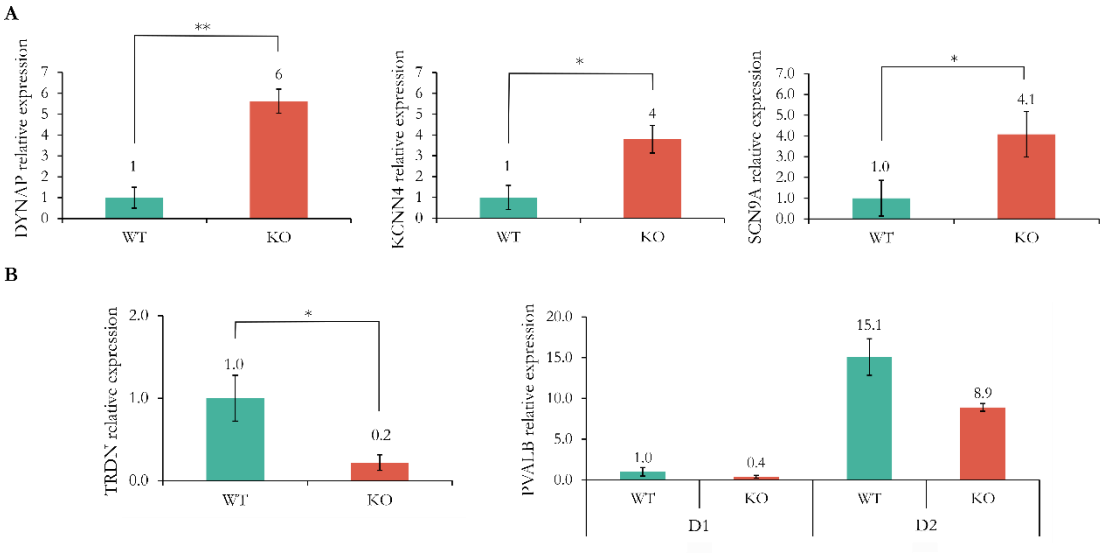

Figure 39. RNA-seq validation analysis at day 1 differentiating primary myoblasts. qPCR analyses of top changing RNA-seq genes upregulated in KO myoblasts (**A**) and in WT myoblasts (**B**). Data represents the average values of at least three WT and three KO samples ± SEM. **: p val <0.001, *: pval < 0.05, two tail t-test.

To further confirm these results, we bought a shRNA library from Mission Sigma-Aldrich, we generated lentivirus particles containing the shRNA and performed infection in C2C12 cells. Unfortunately, no shRNA achieved a downregulation less than 50% acceptable and all shRNA were discarded for further analyses. To circumvent this, we searched in the literature for shRNA's already used for HDAC11 downregulation in other mouse systems (when we bought the library no publication enlisting them had already came) and we selected three shRNA's: shRNA24, shRNA25 and shRNA28 ("Materials and methods" section). This time, we cloned them and after generating lentiviral particles, we assayed their capacity to downregulate HDAC11 expression in C2C12 cells, observing that only shRNA28 provided suitable levels of downregulation (Figure 40 A). As observed in Figure 40 B, the expression levels of the new set of genes analyzed also validated the RNA-seq results.

Figure 40. Upregulated targets in HDAC11 KO myoblasts are also upregulated in HDAC11 downregulated C2C12 cells. A Downregulation efficiency of shRNA 28 on HDAC11 endogenous levels. **B** qPCR analysis of proliferation related genes that were upregulated in HDAC11 deficient myoblasts at day 1 of differentiation. Data represents in all cases the average levels of two independent experiments at day 1 of differentiation relative to TBP1 reference gene ± SD. *: pval<0.05, t-test two tails.

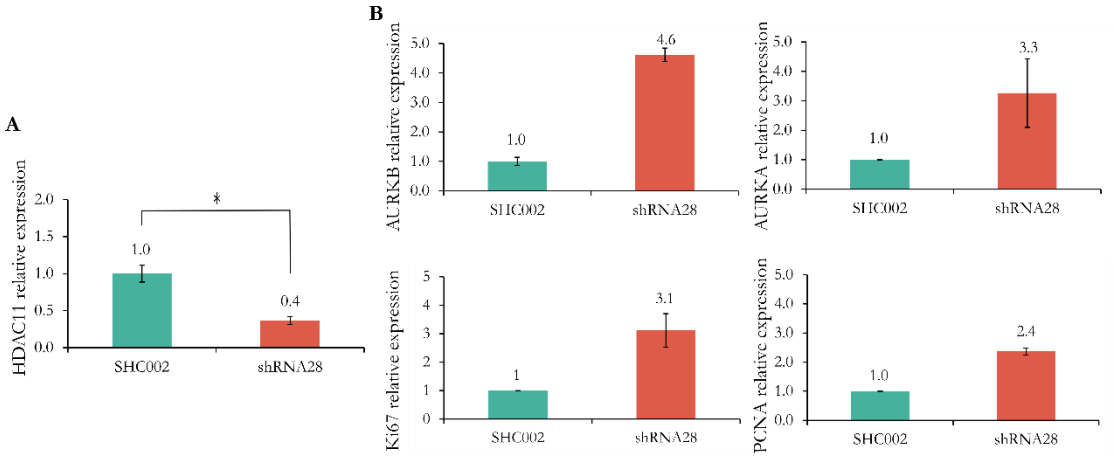

We next ascertain the expression of a third set of genes in the opposite gain of function system, overexpressing HDAC11 in C2C12 cells. As shown in Figure 41 B, the expression levels of the new set of genes analyzed were also validating RNA-seq results.

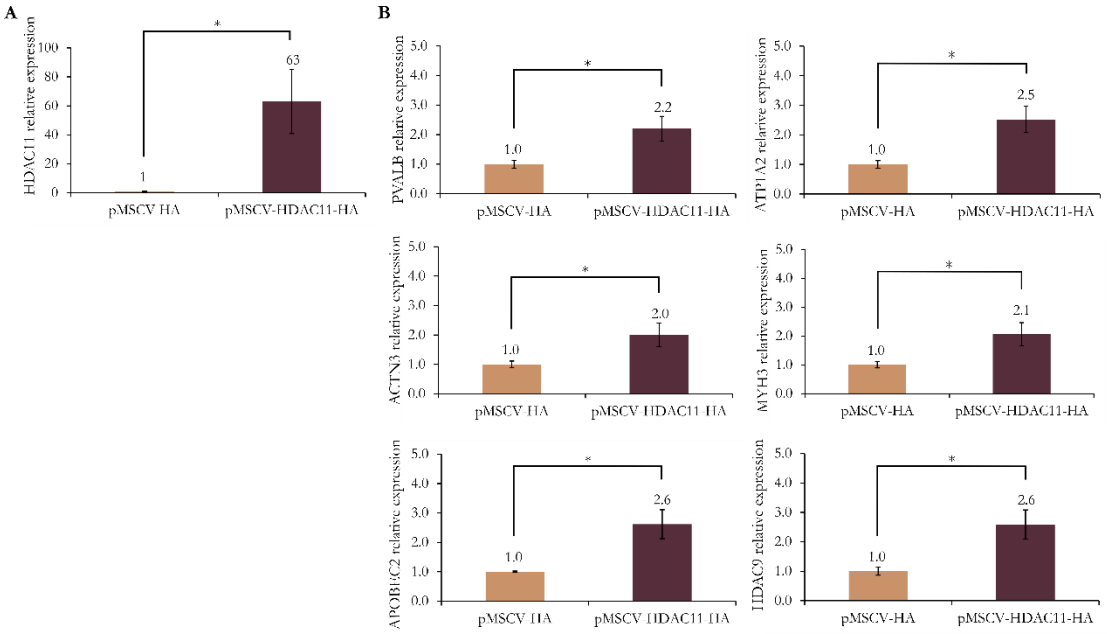

Figure 41. Downregulated targets in HDAC11 KO myoblasts are overexpressed in C2C12 HDAC11 overexpressing cells. A HDAC11 mRNA quantification levels in pMSCV-HA empty vector overexpressing cells and pMSCV-HDAC11-HA overexpressing cells. **B** qPCR quantification of most-changing targets identified by RNA-seq analysis and additional changing targets. In all cases data represent the average value of the indicated genes relative to TBP1 reference gene in three independent replicates ± SD. *: p val <0.05, t-test, two tails.

5.6. Up-regulation of proliferation genes in HDAC11 KO myoblasts is associated with the presence of higher levels of H3 acetylation in their promoters

To ascertain if the differences observed in gene expression are directly dependent on HDAC11 HDAC activity, we performed chromatin immunoprecipitation (ChIP) with α-H3 acetylation and H3K9ac antibodies, and analyzed the relative abundance of these marks in the promoter regions of selected genes that were up-regulated in HDAC11 KO myoblasts. We did not analyze the downregulated targets as their decrease in expression levels could not be directly linked to an increase on their H3ac promoter levels. The results have to be considered preliminary since they have been performed only once. In Figure 42 B are shown the positive and negative controls of the ChIP experiment. As expected, the studied H3ac marks are only present in the positive control region, the ACTB1 promoter, and are absent in the negative control region, a gene desert of chromosome 6. In Figure 42 C are represented the expression change values of the genes analyzed (in the same samples than those in which ChIP was performed) and the H3ac and H3K9ac levels present in their promoter regions upon HDAC11 knock-down compared to the non-targeting shRNA (SHC002) values. Notably, the levels of H3 acetylation on the promoter regions analyzed are higher in HDAC11 knock-down C2C12 cells and these results preliminarily suggest that the genes found up-regulated in HDAC11 deficient myoblasts present higher histone acetylation levels at day 1 of differentiation.

Figure 42. Proliferation genes up-regulated upon HDAC11 knock-down present higher levels of H3 acetylation marks on their promoter regions. A Relative qPCR quantification of HDAC11 expression to TBP1 gene in C2C12 overexpressing a non-targeting shRNA (SHC002) and shRNA28 against HDAC11 (sh28). **B** Negative and positive controls of ChIP. Data represent the fold change enrichment of H3 acetylation marks in a negative control region (gene desert on Chr6) and a positive control region (ACTB1 promoter). Values correspond to the indicated histone marks' values obtained by qPCR after ChIP, normalized to H3. **C** For each indicated gene are illustrated, in the left part, its relative expression value normalized by TBP1 gene in C2C12 cells at day 1 of differentiation, and in the right part, the relative histone marks (H3ac (pan-H3) and H3K9ac) enrichment to SCH002 pan-H3ac in the same samples. IgG is shown as a negative immunoprecipitation control. All the values are normalized to H3 levels and correspond only to one replicate.

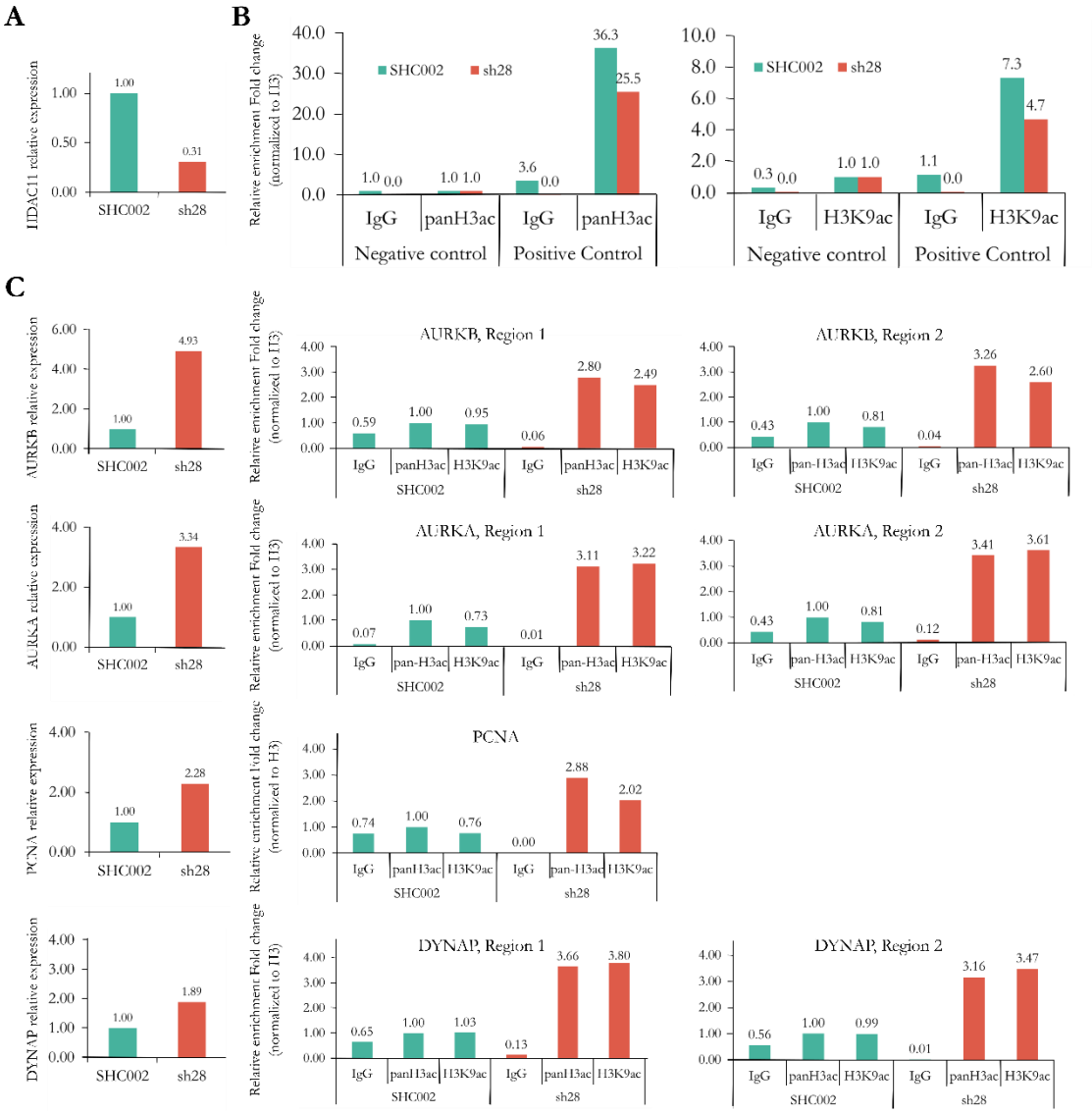
A
HDAC11 relative expression
1.00
0.31
SHC002
sh28
B
Relative enrichment Fold change (normalized to H3)
SHC002
sh28
1.0 0.0
1.0 1.0
3.6
0.0
36.3
25.5
IgG
panH3ac
IgG
panH3ac
Negative control
Positive Control
0.3 0.0
1.0 1.0
1.1
0.0
7.3
4.7
IgG
H3K9ac
IgG
H3K9ac
Negative control
Positive Control
C
AURKB relative expression
1.00
4.93
AURKB, Region 1
0.59
1.00
0.95
0.06
2.80
2.49
AURKB, Region 2
0.43
1.00
0.81
0.04
3.26
2.60
AURKA relative expression
1.00
3.34
AURKA, Region 1
0.07
1.00
0.73
0.01
3.11
3.22
AURKA, Region 2
0.43
1.00
0.81
0.12
3.41
3.61
PCNA relative expression
1.00
2.28
PCNA
0.74
1.00
0.76
0.00
2.88
2.02
DYNAP relative expression
1.00
1.89
DYNAP, Region 1
0.65
1.00
1.03
0.13
3.66
3.80
DYNAP, Region 2
0.56
1.00
0.99
0.01
3.16
3.47
IgG
panH3ac
H3K9ac
pan-H3ac
SHC002
sh28

6. HDAC11 expression in G0 arrested conditions

As our results indicated a role of HDAC11 in the repression of the expression of cell cycle genes, we wondered if HDAC11 was also expressed in other types of cell cycle arrest, where it may also contribute to the silencing of cell cycle genes. For that, we followed a method to induce C2C12 G0 cell cycle arrest independent of cell differentiation based on the resuspension of cells in methylcellulose containing medium, which results in loss of cell anchorage and G0 reversible cell cycle arrest entrance (Sachidanandan et al. 2002; Sambasivan et al. 2008). Although this experiment has been done only once, as shown in Figure 43 A, HDAC11 is upregulated in G0 arrested cells and gets rapidly downregulated upon cell re-plating and cell cycle reentry. As controls of cell cycle arrest are shown Ki67 and MYOD, whose expression is known to be down-regulated in G0 phase (Figure 43 B).

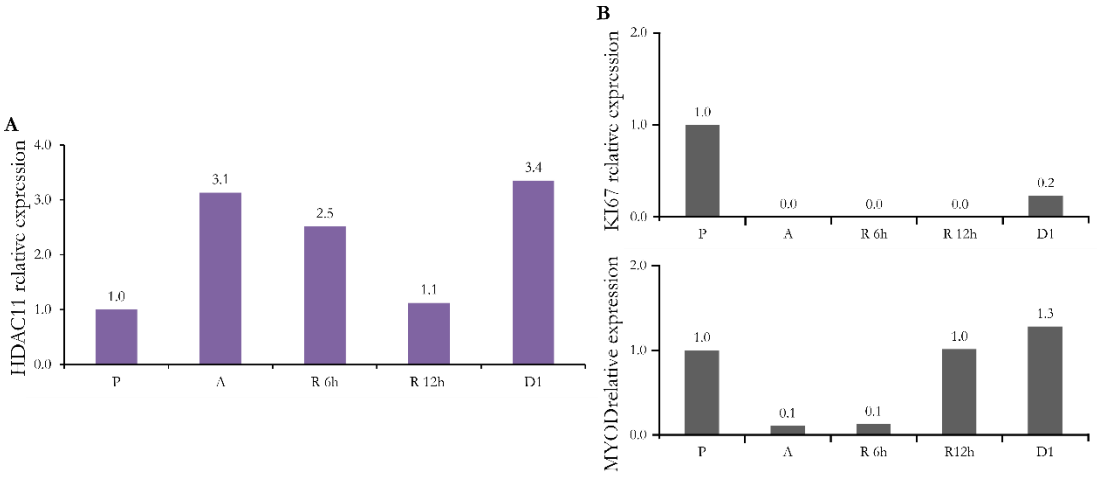

Figure 43. HDAC11 expression is upregulated in methylcellulose G0 arrested cells. A qPCR analysis of HDAC11 expression in a time course of cell cycle arrested C2C12 culture relative to SDHA reference gene. Briefly, C2C12 proliferating cells (P) were resuspended in methylcellulose medium which causes loss of cell anchorage and arrests the cells in G0 phase. The point of arrested (A) corresponds to directly isolated cell from the matrix after 48h of incubation. An aliquot of the recovered cells was replated again in conventional proliferation conditions and these were allowed to reenter to cell cycle (R) for 6 and 12 h. Finally, they were allowed to differentiate for 24 h (D1) to ascertain that their differentiation capacity has not been compromised. **B** KI67 and MYOD levels were quantified in the same experiment to assess cell cycle arrest and reenter.

Furthermore, we explored the expression of HDAC11 in another system of cell cycle arrest induction taking advantage of reserve cells. It has been described that when muscle cell differentiation takes place in *in vitro* conditions, not all cells actually differentiate but

some of them are able to downregulate MYOD expression avoiding cell differentiation and remaining mononucleated in a G0 reversible arrest state that resembles satellite cells *in vivo* (Yoshida et al. 1998; Kitzmann et al. 1998). Reserve cells can be isolated from differentiated myoblasts cultures (Figure 44 A 1) by mild trypsinization conditions with 0.5 % trypsin without EDTA, which selectively induces myotube detachment from the plates (Figure 44 A 2) while leaves reserve cells, which are round and undifferentiated (Figure 44 A 3), attached to the plates. After intensive washes, these cells can be recovered by normal trypsinization conditions. We analyzed the expression of HDAC11 in these purified fractions of reserve cells from primary myoblasts differentiated cultures, including the recovered detached myotubes and proliferating MPC's as controls. As observed on Figure 44 B, HDAC11 is highly expressed in this G0 arrested population compared to proliferative myoblasts and it is expressed at similar levels than in the purified myotubes.

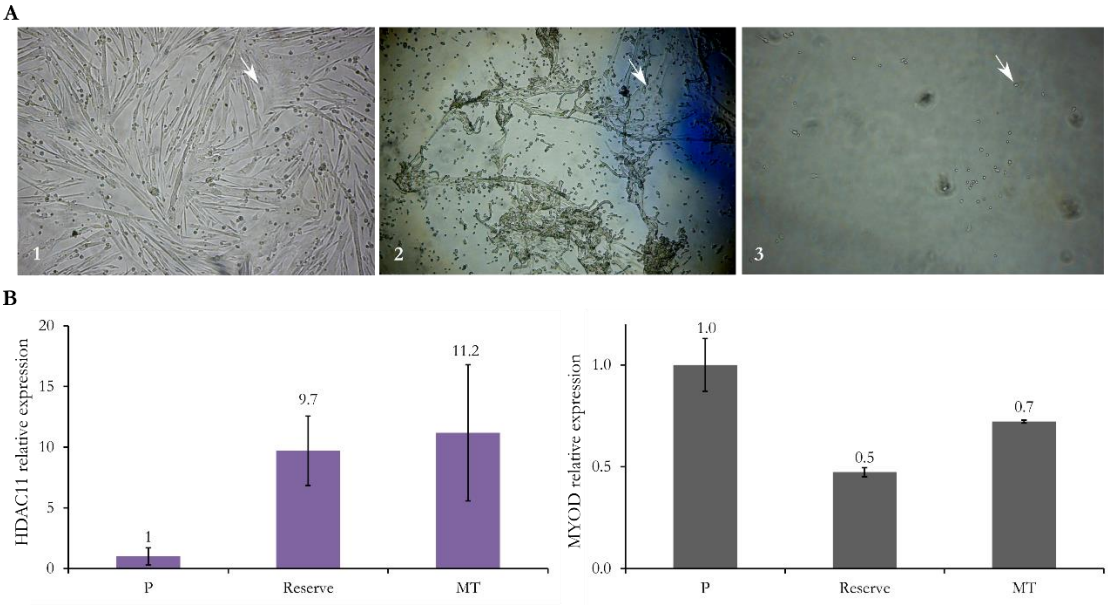

Figure 44. HDAC11 is upregulated in G0 arrested reserve cells compared to proliferating myoblasts. **A** Strategy to isolate reserve cells. D3 differentiated cultures of primary myoblasts (1) were washed with PBS+ (modified recipe containing cations) and trypsinyzed with 0.025% trypsin without EDTA, which allows the specific detachment of myotubes (2). After intensive washes, only single round cells remained attached to the plates. These cells were finally trypsinized and analyzed as the point of reserve cells. **B** qPCR analysis of HDAC11 expression relative to SDHA reference genes in proliferating myoblasts (P), purified reserve cells (Reserve) and detached myotubes (MT). MYOD expression is included as a control of reserve cells, which present MYOD downregulated expression levels compared to proliferating cells. Data correspond to the average of two independent experiments ± SEM.

These two *in vitro* experiments indicate that HDAC11 is not only expressed in differentiating myoblasts but its expression is also upregulated in G0 arrested phase conditions compared to the proliferation state. For this reason, we decided to broaden HDAC11 expression analysis in *in vivo* isolated G0 quiescent satellite cells (SCs). For that, we took advantage of a microarray data previously generated in our laboratory (Carrió 2015) that compared quiescent cells directly isolated from skeletal muscle (Q), isolated satellite cells activated *in vivo* after 6h of cardiotoxin injection (A 6h) and isolated proliferating MPC's after 72h of cardiotoxin injury (A 72h) (Figure 45 A). Cardiotoxin is a myotoxin that destroys specifically myofibers and thus induces SC's' activation to heal the injured muscle region.

With this microarray, we wanted to study the earliest transcriptomic changes occurring through SC activation and for that, the point of 6 h was selected to be previously reported as the earliest point where MYOD is expressed and the cells can be considered activated (Mahdy et al. 2016). In Figure 45 B are shown as controls of the activation process PAX7, which is a marker of quiescent SCs that is downregulated through SC activation, and MYOD, the best studied marker of SC activation. Indicated are also the expression fold changes of HDAC members in this early activation transition between quiescent and activated satellite cells at 6 h. Interestingly, HDAC11 was the HDAC family member that changed the most its expression in the process of satellite cell activation. In Figure 45 C is presented the validation by qPCR in four independent sets of cells: quiescent SCs, activated at 6 h and activated proliferating cells at 72 h. Notably, HDAC11 levels drop down immediately after SC activation to comparable levels in proliferating SCs, suggesting a role of HDAC11 in the maintenance of the quiescence state.

Figure 45. HDAC11 is the HDAC member that changes the most its expression upon *in vivo* SC activation from quiescence. A Schematic representation of the strategy followed to study early transcriptomic changes through SC's' activation. Quiescent SCs were obtained from four 3-months old mice by SC isolation followed by FACS sorting as explained in "Materials and methods" section. The points of SC activation correspond to SC isolated after 6h and 72 h after cardiotoxin injury. **B** In the left part are shown classical HDAC members organized by classes and in the right part are shown class III sirtuin members and the markers to monitor SC's' activation process, PAX7 and MYOD. For each gene it is indicated its fold change expression (FC), calculated by dividing the average value of three biological independent replicates at 6 h after cardiotoxin injury activation (A 6h) and quiescent SC (Q). To facilitate visual comparison the log2 FC value has been assigned to a color scale (Legend). P values were adjusted for multiple testing and in bold are highlight the genes whose expression change was statistically significant. For the genes represented by more than one probe in the microarray platform, representative probes are

indicated. **C** HDAC11 qPCR analysis in analogous samples as the used for microarray analysis. Data correspond to the average values of four biological independent samples in each case normalized to SDHA reference gene ± SD. *: p val <0.05, **: p val<0.001, t-test, two tails.

A

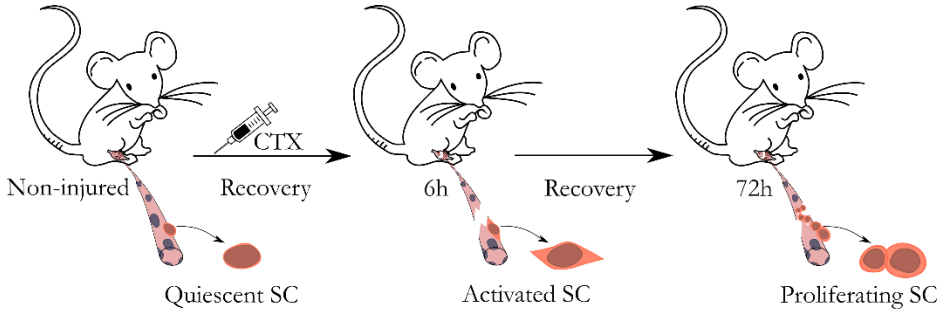

B

Log$_2$ratio (A 6h/Q)	Gene name	FC(A 6h/Q)	Padj val
	HDAC11	**-9.10**	**0.000001**
	HDAC10	**-3.14**	**0.000002**
	HDAC5	**-1.67**	**0.005972**
	HDAC6	**-1.51**	**0.001722**
	HDAC9	-1.30	0.128578
	HDAC8	-1.42	0.104502
	HDAC1	-1.19	0.200598
	HDAC3	1.00	0.992301
	HDAC7	1.10	0.534657
	HDAC2	1.30	0.210630
	HDAC4	**2.10**	**0.001863**

Log$_2$ratio (A 6h/Q)	Gene name	FC(A 6h/Q)	Padj val
	SIRT4	**-3.30**	**0.000007**
	SIRT2	**-2.50**	**0.000044**
	SIRT3	**-1.63**	**0.001819**
	SIRT6	**-1.98**	**0.016442**
	SIRT5	**-1.59**	**0.024906**
	SIRT7	-1.06	0.736209
	SIRT1	1.37	0.074932

Legend

Log$_2$ratio (A 6h/Q)	Gene name	FC(A 6h/Q)	Padj val
	PAX7	**-2.83**	**0.000016**
	MYOD1	**10.11**	**0.000000**

C

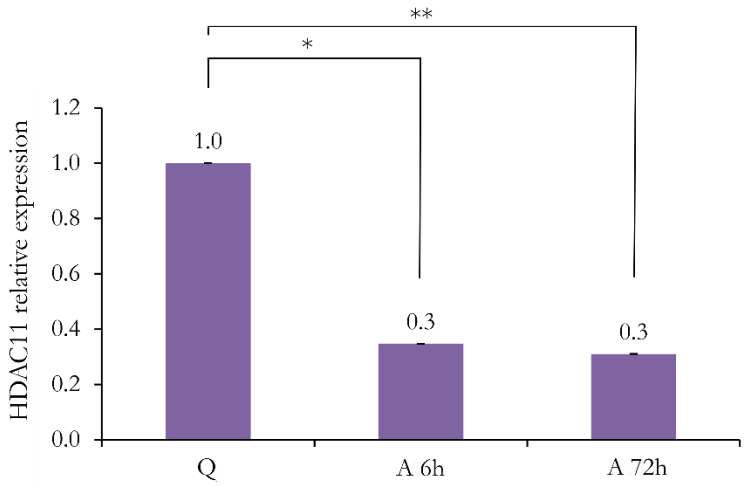

7. Skeletal muscle analysis of HDAC11 KO mice

After the *in vitro* analysis of primary myoblasts cultures, we decided to extend our studies to the whole HDAC11 KO mice. As illustrated in Figure 46 A, HDAC11 KO mice were viable and did not present apparent phenotypical differences. They were also fertile and born at the expected mendelian ratios (Gutiérrez 2012).

Taking into account our *in vitro* results, we wondered whether HDAC11 deficient mice showed differences in muscle growth. First of all, we compared HDAC11 expression in neonatal 10 days old mice muscles, and 3 months old adult mice muscles. As observed in Figure 46 C, HDAC11 was more expressed in neonatal muscles than in adult ones. As explained in the Introduction, the neonatal stage is a period of intense muscle growth where SCs fuse to preexisting fibers resulting in an increase in muscle size. The higher HDAC11 expression in neonatal mice coincides with the high number of differentiating myoblasts which have completely finished their differentiation in the adult. To envision if HDAC11 has a major effect in muscle growth, we weighted HDAC11 KO and WT mice through their first month of life (the more intense of muscle growth) and in three month adults. As shown on Figure 46 D, HDAC11 KO mice did not present differences in total body weight. As half of the mice weight at this stage corresponds to skeletal muscle (Gokhin et al. 2008), this measurements discard a major role for HDAC11 in muscle growth. By now, we have been mostly devoted to the analysis of HDAC11 absence consequences in adult mice as they are easier to manipulate, but we are pending on analyzing HDAC11 absence effect into more detail in developing skeletal and cardiac muscles (motivated by the repression of light cardiac myosins observed in the RNA-seq) of neonatal mice in a near future.

Figure 46. HDAC11 KO mice. A Adult HDAC11 KO mice do not present apparent morphological differences with WT littermates. Photographs showing HDAC11 WT and KO mice. **B** Genotyping results of a WT, heterozygote (Het) and KO samples. PCR was performed as described in Materials and methods using as templates 10 ng of DNA extracted from the corresponding mice tails. Primers anneal to the flanking intronic regions of HDAC11 exon 3 and the observed differences of amplicon lengths observed in Het and KO mice correspond to the floxed region. **C** HDAC11 is more expressed in growing muscles than adult resting ones. qPCR analysis of HDAC11 expression in two legs from 10 days old WT mice and three gastrocnemius from 90 days old mice (tissues were kindly by Dr. Roser López). Bars correspond to ± SEM. **D** HDAC11 KO mice do not present differences of total body weight through growth. Data represents the average weights of at least three male WT and three male KO mice in grams (g) at the indicated days after birth. Bars correspond to ± SEM.

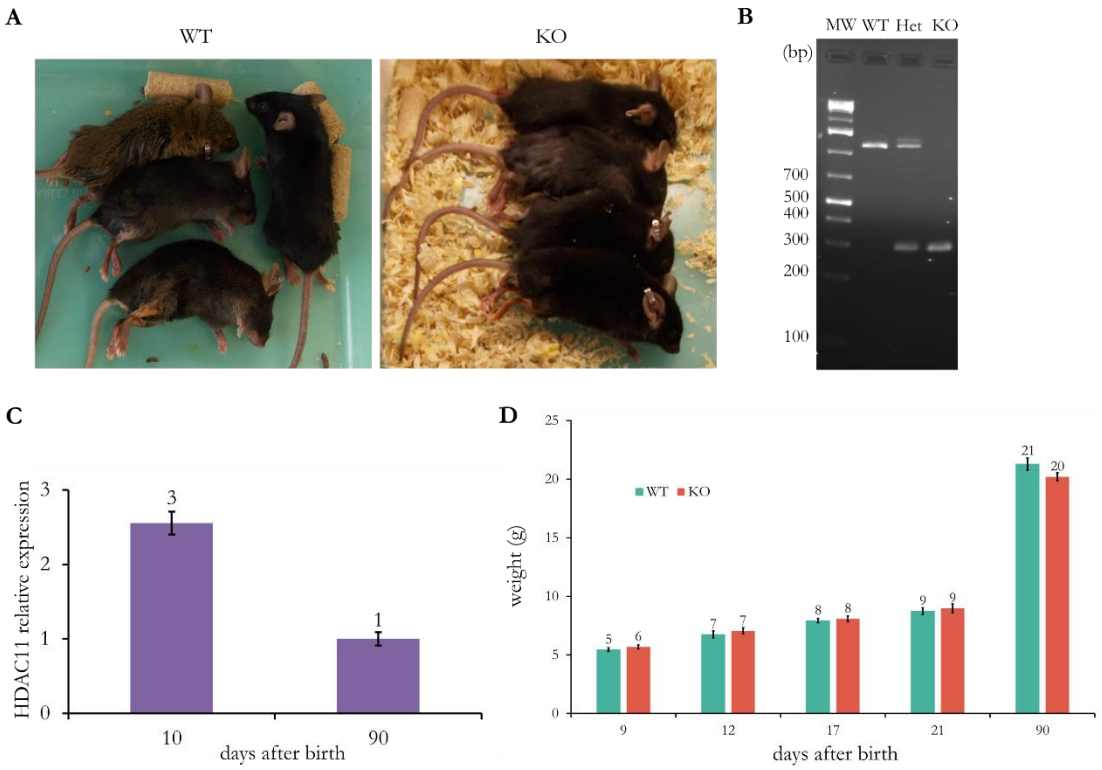

As it was already described that HDAC11 could have gender specific roles (Kim et al. 2013) and that our RNA-seq results suggested differences between slow and fast muscles expression, we examined HDAC11 expression in different adult muscle types of both genders. As representatives of fast muscles, we selected tibialis (TB) and EDL. Soleus (Sol) was selected as a slow muscle and gastrocnemius (GC) was included as a mixed-fiber type muscle. We also included heart in the quantification analyses and brain extracts as a reference tissue where HDAC11 is highly expressed (Gao et al. 2002; Liu et al. 2007). The results of HDAC11 quantification in these tissues are shown in Figure 47 A. As observed, the tissue expressing the highest HDAC11 levels is brain. Regarding muscle types, HDAC11 is higher expressed in fast muscles than slow or mixed ones. It is not observed a gender differential expression in brain or heart but in skeletal muscle HDAC11 is higher expressed in males and in fast muscles. Regarding HDAC11 protein, it could be detected only in brain (Figure 47 B), where it is 6 to 60 folds more expressed by RNA levels than in muscles. This fact could explain our previous failed attempts to detect protein expression in primary myoblasts and C2C12 cells, as the endogenous antibodies tried only are sensitive to high expression levels.

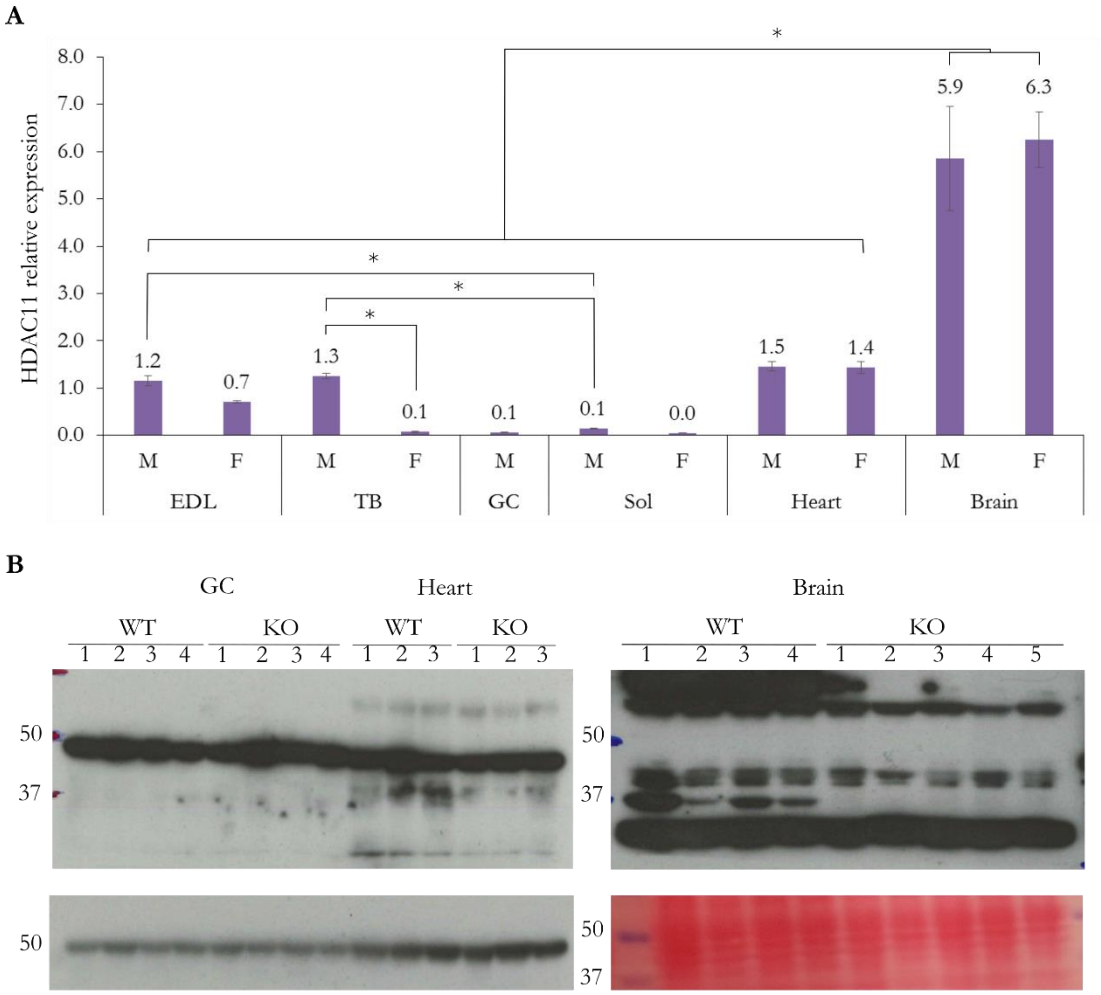

Figure 47. HDAC11 is highly expressed in brain, heart and fast male skeletal muscles. A HDAC11 qPCR quantification in male (M) and female (F) tissues. Data represents the average of at least three samples in each case ± SEM. *: p val<0.05, ttest two tails. **B** Western blot detection of HDAC11 in male gastrocnemius (GC), heart and brain. 50 μg of total RIPA extracted protein were ran into 8%acrylamide gels and detected with α-HDAC11 (Ref. H4539, Sigma-Aldrich) (upper panels). Above are indicated as loading controls, tubulin for GC and heart and Ponceau-S for brain.

We next addressed whether HDAC11 deficient mice presented any defects in adult muscles. For that, we analyzed morphologically the myofiber size of tibialis as a representative of fast muscle, soleus as a slow muscle and gastrocnemius as a mixed type, both in male and female mice. As shown in Figure 48, HDAC11 deficient mice did not present alterations in myofiber numbers or their cross-sectional area values in any type of muscle analyzed and regardless of mice gender.

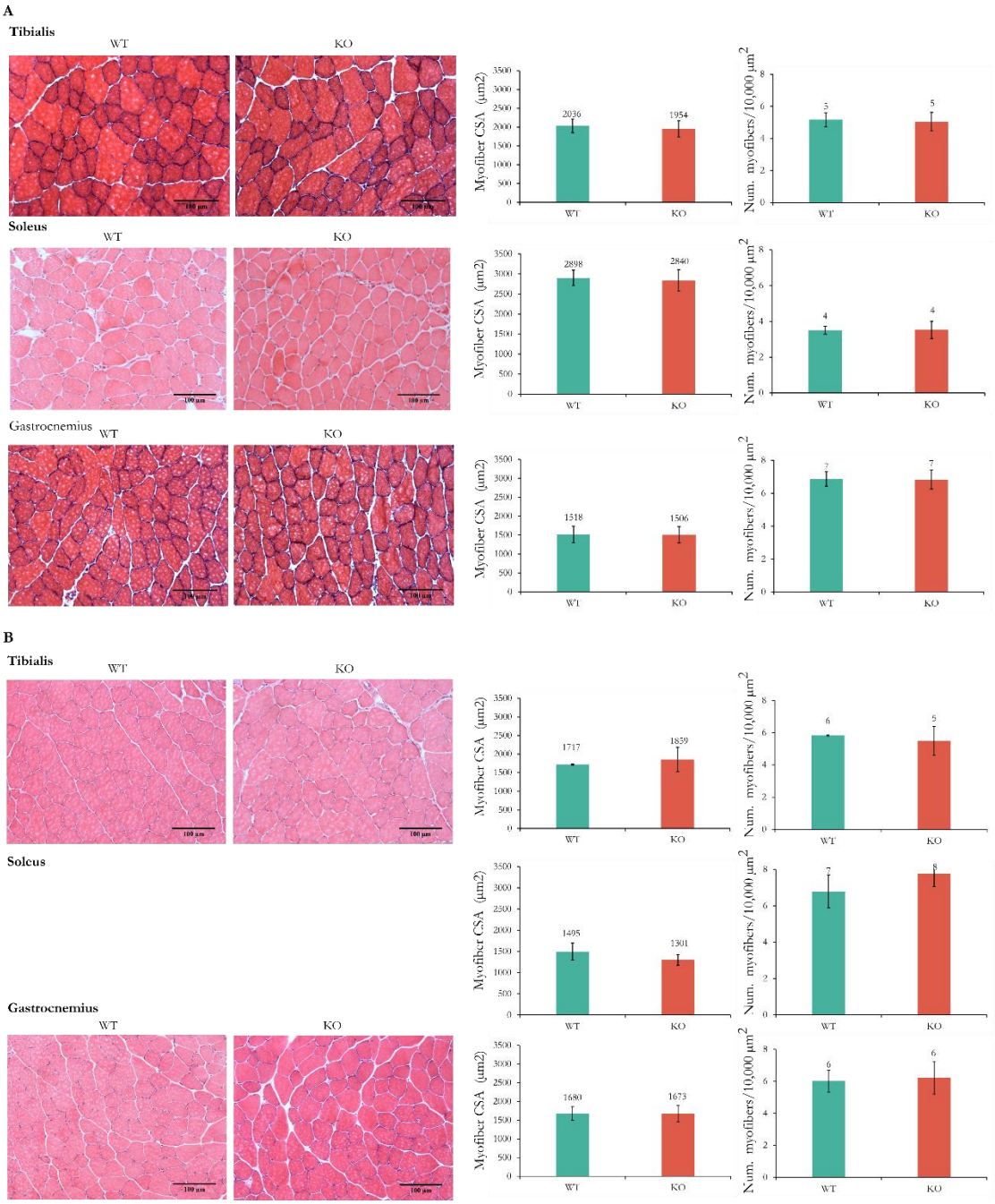

Figure 48. HDAC11 KO mice did not present alterations in myofiber numbers or cross-sectional area. A Male muscles. **B** Female muscles. Left: Hematoxylin/eosin representative sections of WT and KO three month old mice of tibialis, soleus and gastrocnemius muscles. Right: Average values of myofiber size and numbers. For each muscle, the average cross-sectional area (CSA) of at least 400 myofibers per muscle and animal was determined. Values represent the average values of the mean cross-sectional myofiber area of four mice ± SD. In the right part is shown the number of myofibers per 10,000 µm². For at least 4 microscopy fields, the total area of muscle and the number of myofibers present were calculated. Then, the number of myofibers per µm² was calculated and extrapolated to 10,000 µm².

Moreover, we analyzed by real time PCR the expression of myosin heavy chain genes (MyHC) that determine fiber type composition in the aforementioned muscle types in both males and females and we did not find any differences in gene expression regardless muscle type or mice gender (Figure 49), suggesting that HDAC11 deficient muscles did not present differences in fiber type composition.

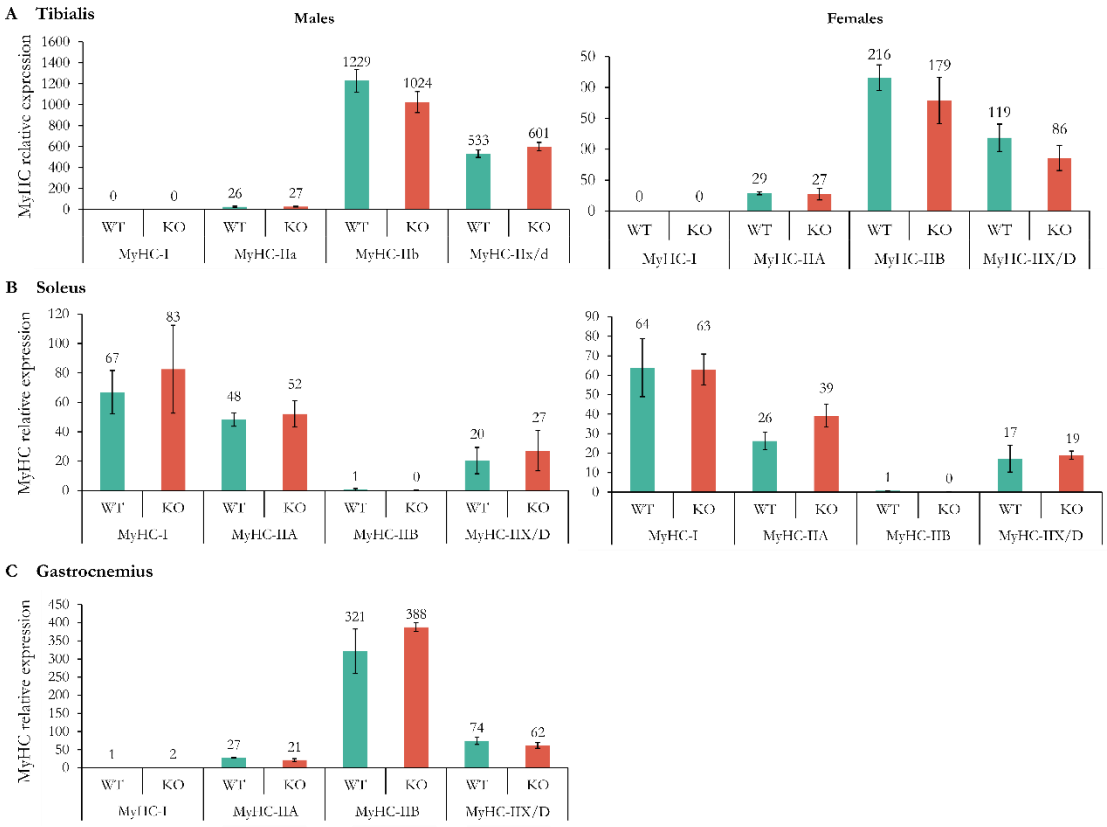

Figure 49. HDAC11 KO mice muscles did not present differences in MHC gene expression. qPCR analysis in tibialis (**A**), soleus (**B**) and gastrocnemius (**C**) muscles of myosin heavy chain genes: MYH7 (MyHC-I), MYH2 (MyHC-IIA), MYH4 (MyHC-IIB) and MYH1 (MyHC-IIX/D). Data correspond to the average values on the indicated genes relative to TBP1 reference gene expression in at least three WT and three KO mice ± SEM.

8. Characterization of HDAC11 functions during skeletal muscle regeneration

Taking into account our *in vitro* results, we further wanted to assess if the regenerative capacity of HDAC11 deficient mice was preserved or if they presented any defects in muscle regeneration *in vivo*. As adult skeletal muscle is mostly a quiescent tissue, to study postnatal muscle regeneration is necessary to induce some insult to stimulate SCs to exit their quiescent state, proliferate, differentiate, fuse and maturate to reconstitute the damaged tissue. Among the different existing methods to induce muscle injury, we selected cardiotoxin intramuscular injection, a venom isolated from the snake *Naja pallida* that specifically produces myolisis without affecting the basal lamina, nerves or blood vessels. Indeed, it is a widely used method to study muscle regeneration because it induces a reproducible muscle destruction required for regeneration studies.

To assess HDAC11 deficient mice regeneration capacity, we decided to investigate four time points of regeneration which are represented in Figure 50 A. All mice were injured by intramuscular cardioxin injection in gastrocnemius and tibialis muscles. We selected these muscles because they are the ones of the hind limbs the most accessible for performing an injection without the need of operation. In the panel 50 B are shown representative images from cross-sectional stains of WT tibialis muscles at the indicated regeneration time points. First, we decided to examine the early point of 6 hours post injury (6 hpi) to assess the activation capacity of HDAC11 deficient mice SCs. As we had observed that HDAC11 was expressed in quiescent SC and its expression was dramatically downregulated after SC activation, we decided to investigate whether HDAC11 deficient mice SCs presented the same activation capacity after muscle injury. As can be observed in the Figure, at 6 hpi is evident an extended muscle damage compared to the non-injured (NI) tissue; the muscle architecture is altered, with changes in myofiber shape and intense inflammatory infiltration even to myofibers, which are mainly necrotic in the injected regions. Second, we decided to look to 4 dpi muscles as an early point of SC differentiation. As can be observed in the corresponding section, at this point small regenerating fibers are already present. Some of them present more than one nuclei because they had already started to fuse to replenish the damaged area and an intense inflammatory infiltration is still present. Third, we included 7 dpi as a latter point to assess differentiation capacity of SCs. As it will be explained later on, these point was performed and analyzed in two independent experiments. As can be observed in the sections, the size of regenerating fibers is higher

than at 4 dpi and the damaged area had recuperated more the architectural appearance with the presence of less inflammatory infiltrates. Finally, we looked at 21 dpi as a latter point of regeneration to assess the maturation capacity of myofibers and determine if the changes observed, if any, are preserved or not through time. As can be observed, the muscle architecture at this point is mostly recovered and resembles very much to the non-injured muscle except for the remaining central nuclei of the regenerating myofibers, will at latter points will recover its peripheral location.

Using this time course of regeneration in tibialis muscles from HDAC11 wild-type mice, we quantified the expression of HDAC11 through muscle differentiation. As observed in Figure 50 C, the expression of HDAC11 drops immediately after induced muscle damage and then recovers the non-injured levels for all the additional analyzed points.

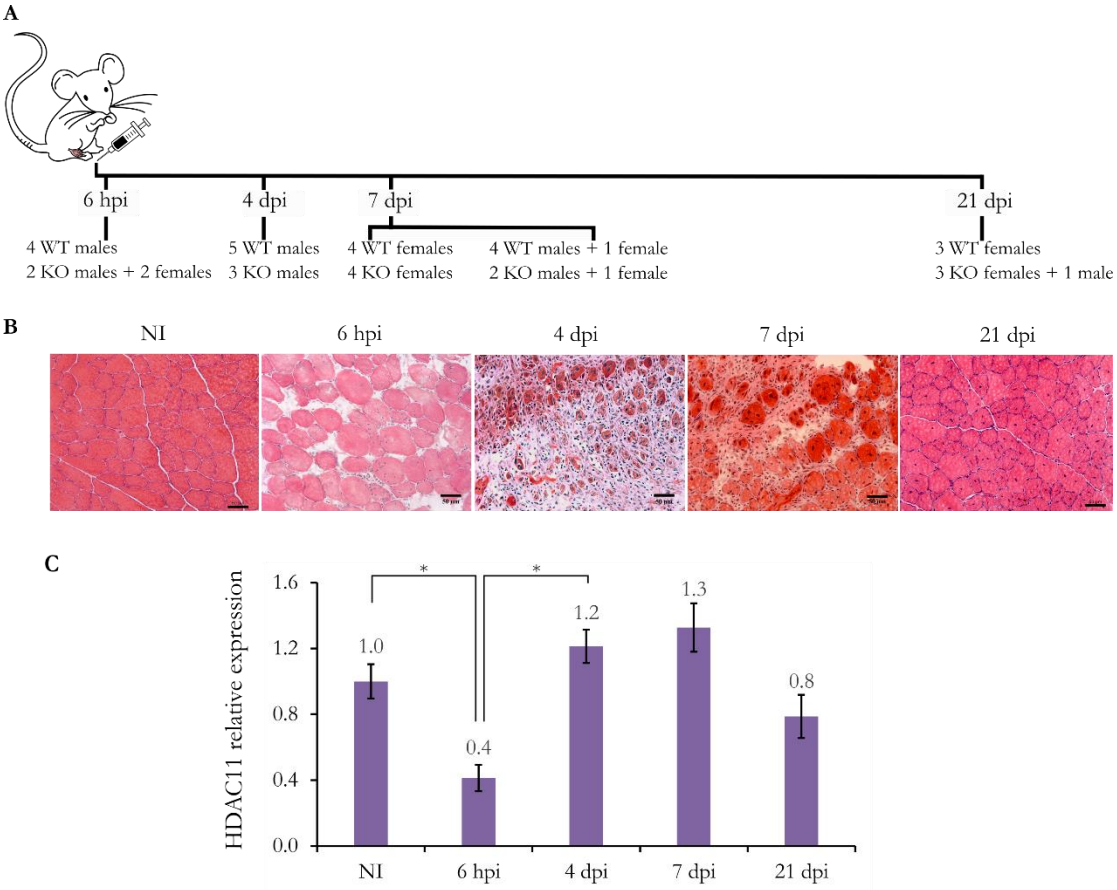

Figure 50. Regeneration experiments' overview. A Scheme representation of induced regeneration experiments. The indicated WT and KO animals in each case were injured at day 0 and collected at the indicated time points. **B** Microscopy images of tibialis muscle cross-sectional areas stained with hematoxylin-eosin at the indicated time points of regeneration at 20X augments. **C** qPCR analysis of HDAC11 expression in WT tibialis muscles at the indicated time points normalized to TBP1 gene expression. * p val < 0.05 (t-test, two tails). NI: non-injured, hpi: hours post injury, dpi: days post injury.

8.1. SCs from HDAC11 deficient mice are activated up to the same extent than WT ones at 6 hpi

As can be observed in Figure 51 A both HDAC11 wild-type (WT) and deficient (KO) mice present the expected extensive muscle degeneration at this point with the arrival of the first inflammatory cells. We specifically focused on the state of SCs at this point. For that, we performed immunofluorescence staining using PAX7 antibody, to identify SCs, and MYOD, which is the most used marker of SC activation. As illustrated on Figure 51 B, SCs from both WT and KO tibialis muscles are already activated at this point. To get into detail, we quantified the expression of these markers together with MYF5, a commitment marker, in the same muscles both by qPCR and WB analysis and as can observed, the levels of MYOD are the same in WT and KO muscles. We also assayed CALR, a marker of cell quiescence, but it was undetectable in all the samples suggesting that SCs from both genotypes had left the quiescent state. Moreover, we also tested the expression of KI67 gene as a marker of cell proliferation but it was also undetectable at any point, suggesting that SCs from both genotypes had not still entered to cell cycle. It was intriguing why the expression of PAX7 was significantly upregulated in KO mice because, as explained in the previous section, the number of SCs was not different between these two genotypes. It is possible that HDAC11 absence interferes with the PAX7 downregulation that occurs through cell activation but further experiments are needed to address this point.

Altogether, we conclude that SCs from KO mice are activated up to the same extent at 6 hpi.

Figure 51. HDAC11 KO mice did not present alterations in SCs activation. A Hematoxylin/eosin staining of representative transversal sections of tibialis muscles from WT and KO mice at 6 hours post injury showed no difference between the two genotypes, both presenting extensive tissue damage and inflammatory cell infiltrates. **B** Immunofluorescence staining of the mentioned sections with α-PAX7 (recognizing SCs) and α-MYOD antibodies, showing the presence of activated SCs characterized by MYOD expression. **C** Expression analysis by qPCR of PAX7 as a marker of SCs, MYF5 as a marker of cell commitment and MYOD as a marker of cell activation in RNA extracts of the aforementioned tissues. Data represents the average of 3 WT and 4 KO animals relative to SDHA reference gene expression ± SEM. **D** Western blot quantification of total RIPA protein extracts of the aforementioned tissues. 50 μg of protein for each mouse were loaded into 10% acrylamide gels and probed with the specified antibodies. In the right panel are shown MYOD and PAX7 optical densities (OD) quantification relative to tubulin OD and normalized by WT average value. Error bars represent ± SEM. *: p val<0.05, two tail t-test.

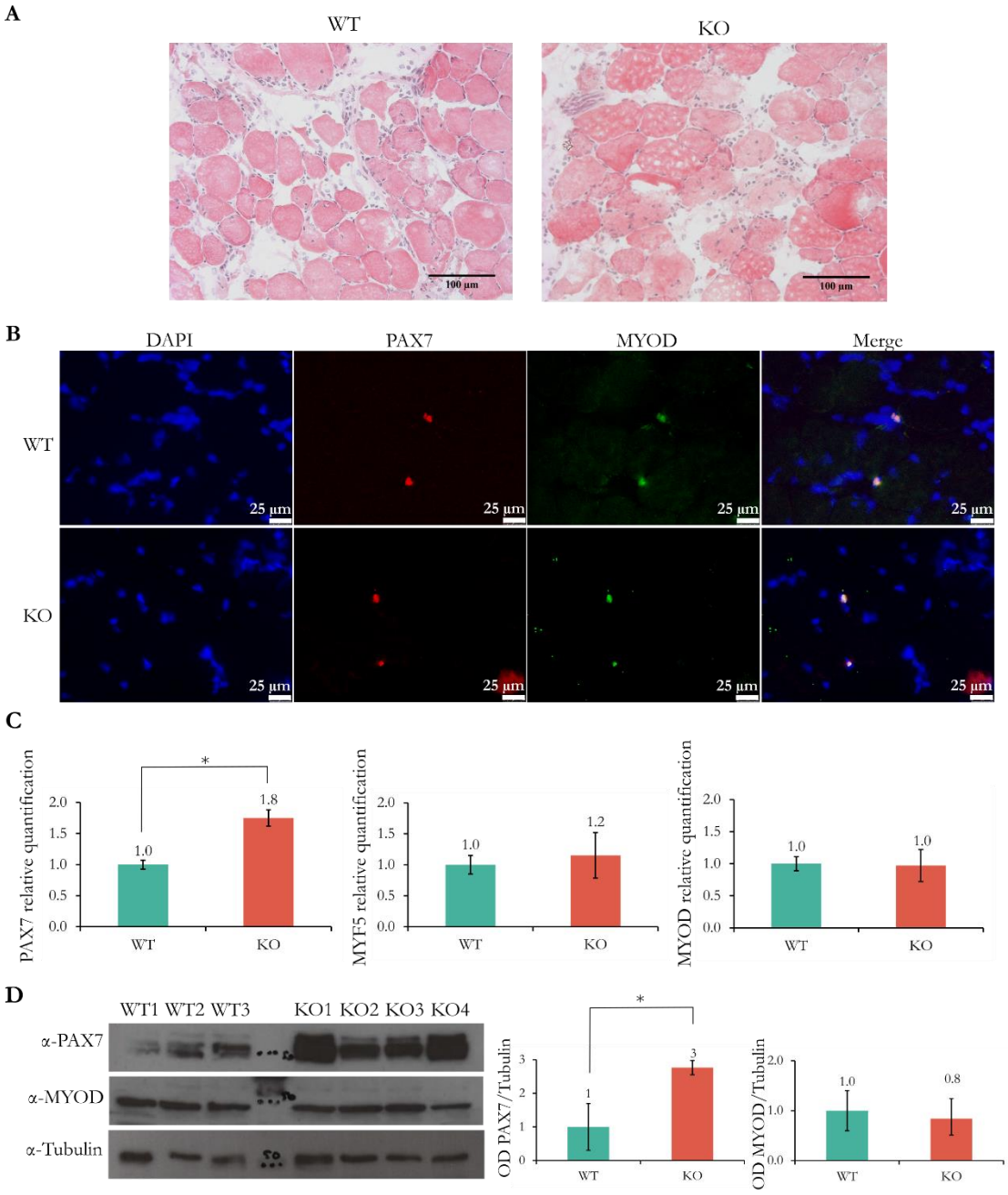

8.2. HDAC11 deficient mice did not present alterations in muscle regeneration at 4 dpi

As observed in Figure 52 A, both HDAC11 wild-type and knock-out mice presented regenerating fibers, characterized by their presence of central nuclei and basophilic staining, at this time point. To ascertain the regeneration abilities of both genotypes, we quantified the number of cells presented per regenerating area of tibialis muscle (Figure 52 B), concluding that it was not different between WT and KO mice. Moreover, the average

number of nuclei per regenerating fiber (Figure 52 C), the average area of each myofiber (Figure 52 D) and the distribution of regenerating myofibers by size (Figure 52 E) did not present differences between both conditions genotypes.

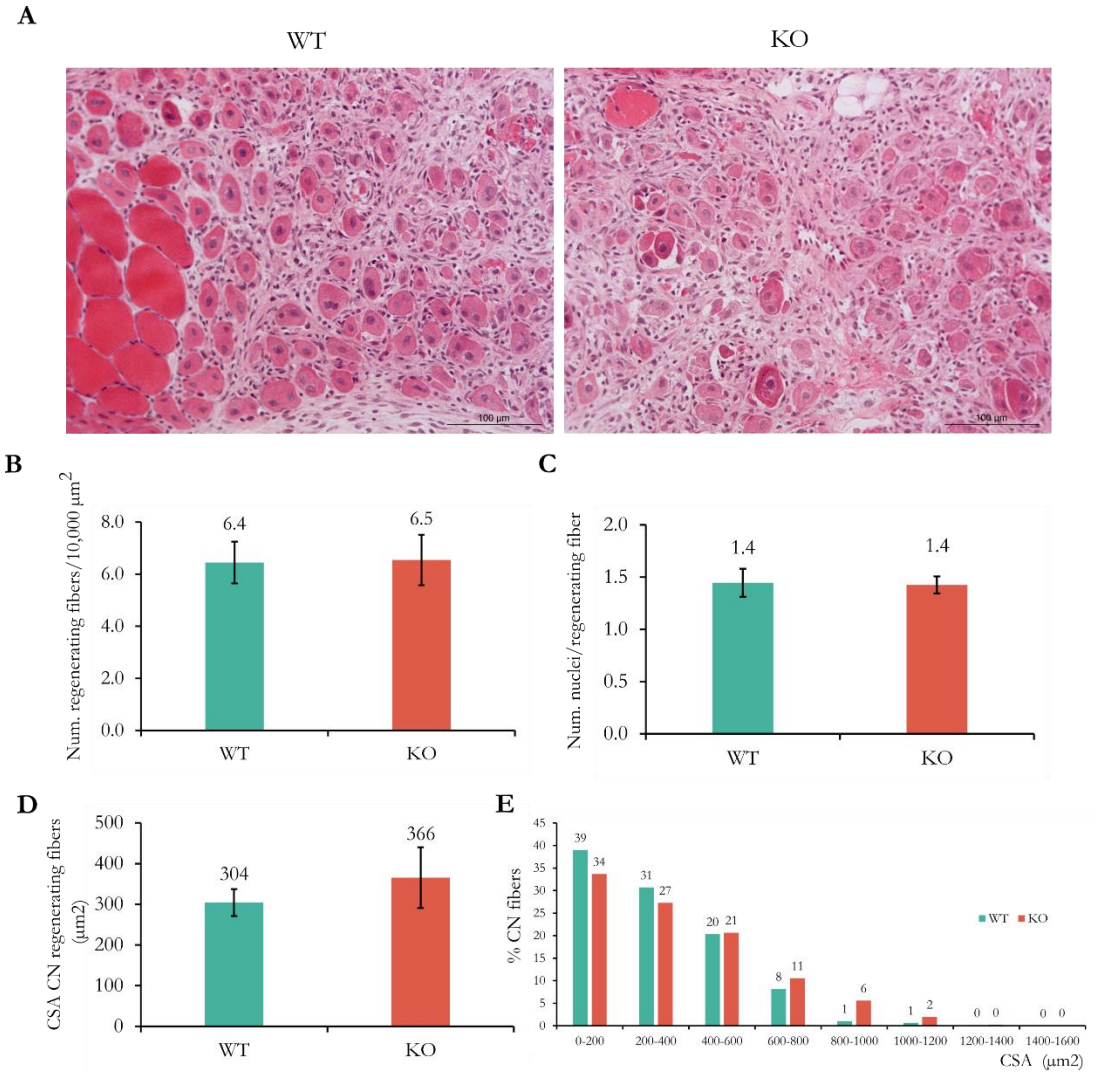

Figure 52. HDAC11 KO mice present equal regeneration capacity than WT mice at 4dpi. A. Representative hematoxylin-eosin stained transversal sections of regenerating regions from tibialis muscles of WT and KO mice at 4 days after injury at 20 augments magnification. In both genotypes can appreciated the abundant presence of inflammatory cells (small and violet) and regenerating fibers, characterized by the presence of central nuclei. **B** Number of regenerating fibers (central-nucleated) per 10,000 µm^2 of regenerating area. The number of central nucleated cells were counted in at least 5 random images per condition taken from regenerating regions of 3 WT and 3 KO mice. The number was normalized to the regenerating area region of the image. Values correspond to the average value of 3 WT and 3 KO male mice ± SEM. **C** Number of nuclei per regenerating fiber in WT and KO mice. The number of nuclei from regenerating fibers of the aforementioned images was counted and normalized to the number of regenerating fibers in the region. Data correspond to the average values of at least 4 image counts per condition of 4 WT and 3 KO mice ± SEM. **D** Average value of cross-sectional area (CSA) of central nucleated (CN) regenerating

fibers. The area of regenerating fibers was measured in at least 4 of the aforementioned images. Data correspond to the average values of 3 WT and 3 KO mice ± SD. **E** Regenerating fiber size distribution. For the measured fibers in C are represented their size distribution as a percentage of total cells having an area in the indicated intervals.

We also quantified by qPCR the expression of PAX7 as an indicative of the number of SCs present, to address if HDAC11 KO 4 dpi muscles presented more proliferating SCs at this point. As shown on Figure 53 A, the expression of PAX7 was identical in both conditions. Moreover, we also quantified the expression of the muscle differentiation markers, MYOD, MYOG and MCK, which remained also invariant in this condition between both genotypes.

As at 4dpi myoblasts are differentiating, we examined if the expression of HDAC11 targets according to by RNA-seq results were changing at this point. As shown in Figure 53 B, all the markers showed the same tendency than in the RNA-seq, although the expression of none of them resulted statistically different (probably because we need to increase the number of analyzed animals or the differences are not enough to be determined in whole muscle extracts).

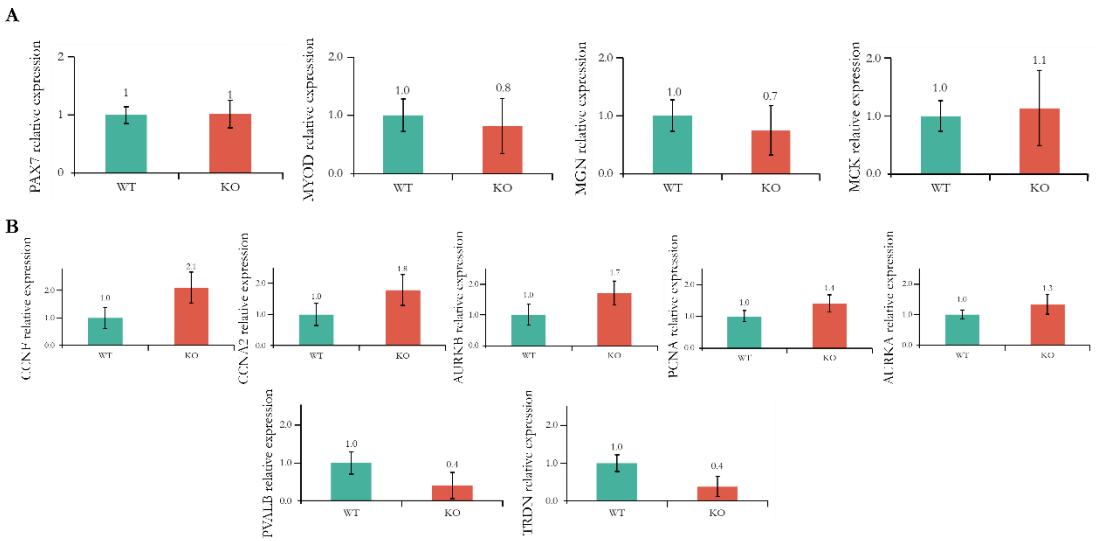

Figure 53. HDAC11 KO mice at 4 dpi did not show differences in MRFs expression but the expression of HDAC11 selected targets, followed the same patterns than in isolated primary cells. **A** qPCR quantification of PAX7 SC marker and the muscle differentiation markers MYOD, MGN and MCK. **B** qPCR quantification of proliferation markers whose expression was upregulated in HDAC11 KO primary myoblasts at D1 of differentiation (upper lane) and most changing differentiation markers whose expression was downregulated in the same conditions (lane below). Data correspond in all cases to the average values obtained in 3 WT and 3 KO tibialis muscles relative to SDHA reference gene ± SEM.

8.3. HDAC11 deficient male and female mice presented an advanced muscle regeneration at 7 dpi

To ascertain the regeneration capacity at 7dpi, we first chose to analyze HDAC11 male mice, as in non-injured conditions presented higher expression of HDAC11 in skeletal muscles compared to females ones. The quantification of the average of cross-sectional area and the distribution of regenerating myofibers by size, showed that HDAC11 deficient male mice presented an advance regeneration capacity at this point, both in tibialis and gastrocnemius muscles (Figure 54 A and B). There are also shown representative images of hematoxylin/eosin regenerating sections, in which is presented that central-nucleated fibers from HDAC11 deficient muscles possessed increased areas than wild-type ones. The staining of equivalent sections with embryonic myosin heavy chain (eMHC), which specifically stains regenerating myofibers, also provided the same result. The quantification of MRFs expression in the same muscles showed no differences between both genotypes and the expression of myosin heavy chains expressed during regeneration (MYH3 and MYH8) was neither different (Figure 54 C). We also quantified the expression of adult myosin heavy chains' expression to ascertain if HDAC11 could be involved in fiber type reestablishment after injury but the expression of the four genes remained unchanged between both genotypes (data not shown).

As HDAC11 had been described to mediate gender specific functions in kidney (Kim et al. 2013), we wondered whether the increase in regenerating fiber size was also observed in female mice. For that, we repeated the explained experiment analyzing this time female injured tibialis and gastrocnemius muscles and as shown in Figure 55, HDAC11 deficient females also presented an advance muscle regeneration capacity at 7 dpi.

Figure 54. HDAC11 deficient male mice present higher regenerating myofibers' cross-sectional areas than wild-type mice at 7dpi. Left panel: **A** Tibialis and **B** gastrocnemius representative 20X microscopy images of hematoxylin/eosin (H/E) and embryonic myosin heavy chain (eMHC) stained muscle transversal sections. Right: Upper panel: Average of cross-sectional area (CSA) of central-nucleated (CN) regenerating fibers. Data represent the average of at least three male mice ± SEM. **: p val < 0.001, one-way ANOVA. Lower panel: percentage of central-nucleated regenerating fibers. For both measures, at least were considered 5 random images at 20X, and counted at least 300 regenerating myofibers per mice. **C** qPCR quantification of muscle differentiation markers. Data correspond in all cases to the average values of 3 WT and 3 KO gastrocnemius male muscles relative to SDHA reference gene ± SEM.

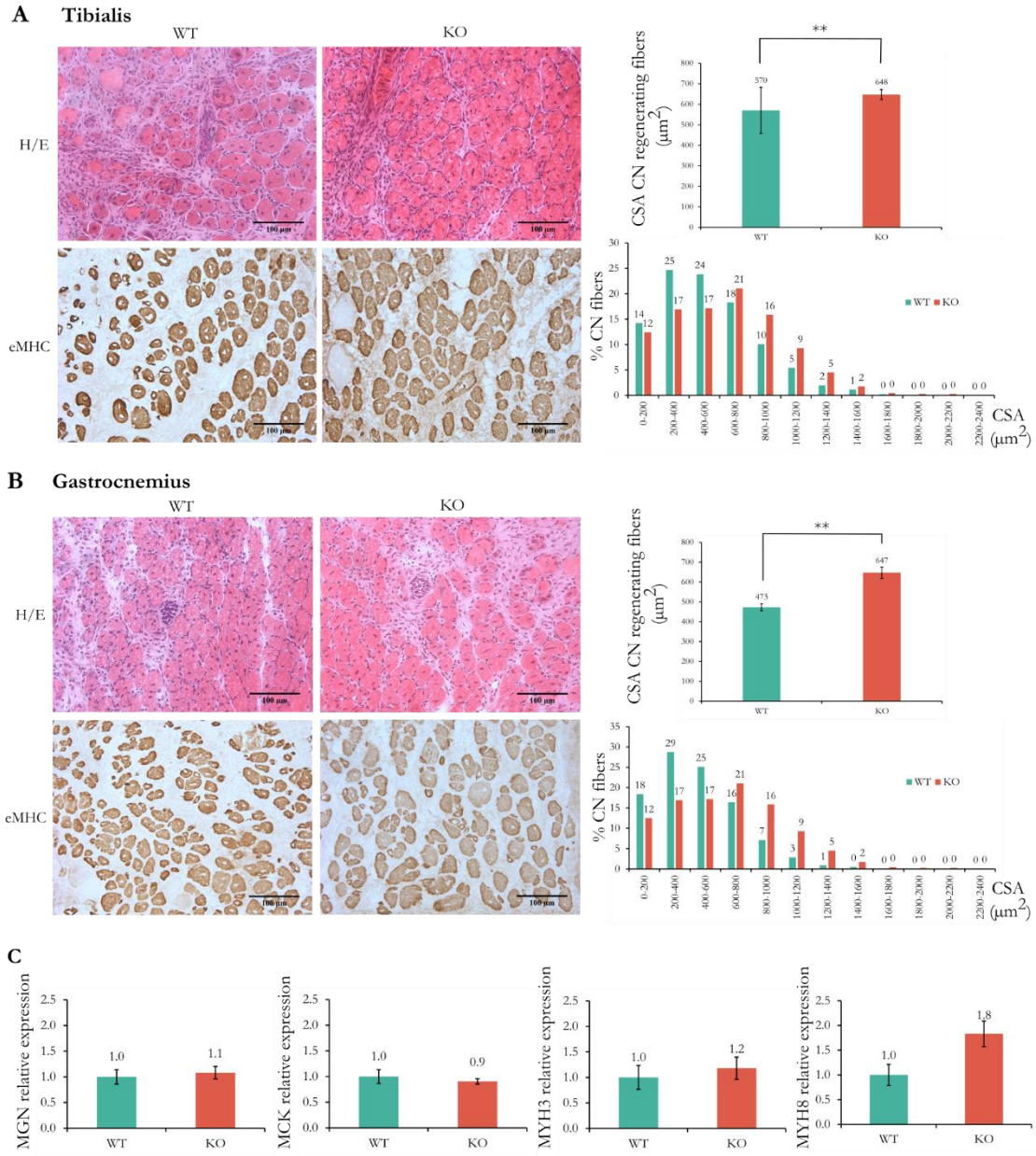

Figure 55. HDAC11 deficient female mice present higher regenerating myofibers' cross-sectional areas than wild-type mice at 7dpi. Left panel: **A** Tibialis and **B** gastrocnemius representative 20X microscopy images of hematoxylin/eosin (H/E) and embryonic myosin heavy chain (eMHC) stained muscle transversal sections. Right: Upper panel: Average of cross-sectional area (CSA) of central-nucleated (CN) regenerating fibers. Data represent the average of at least three female mice ± SEM. **: p val < 0.001, one-way ANOVA. Lower panel: percentage of central-nucleated regenerating fibers. For both measures, at least were considered 5 random images at 20X, and counted at least 300 regenerating myofibers per mice.

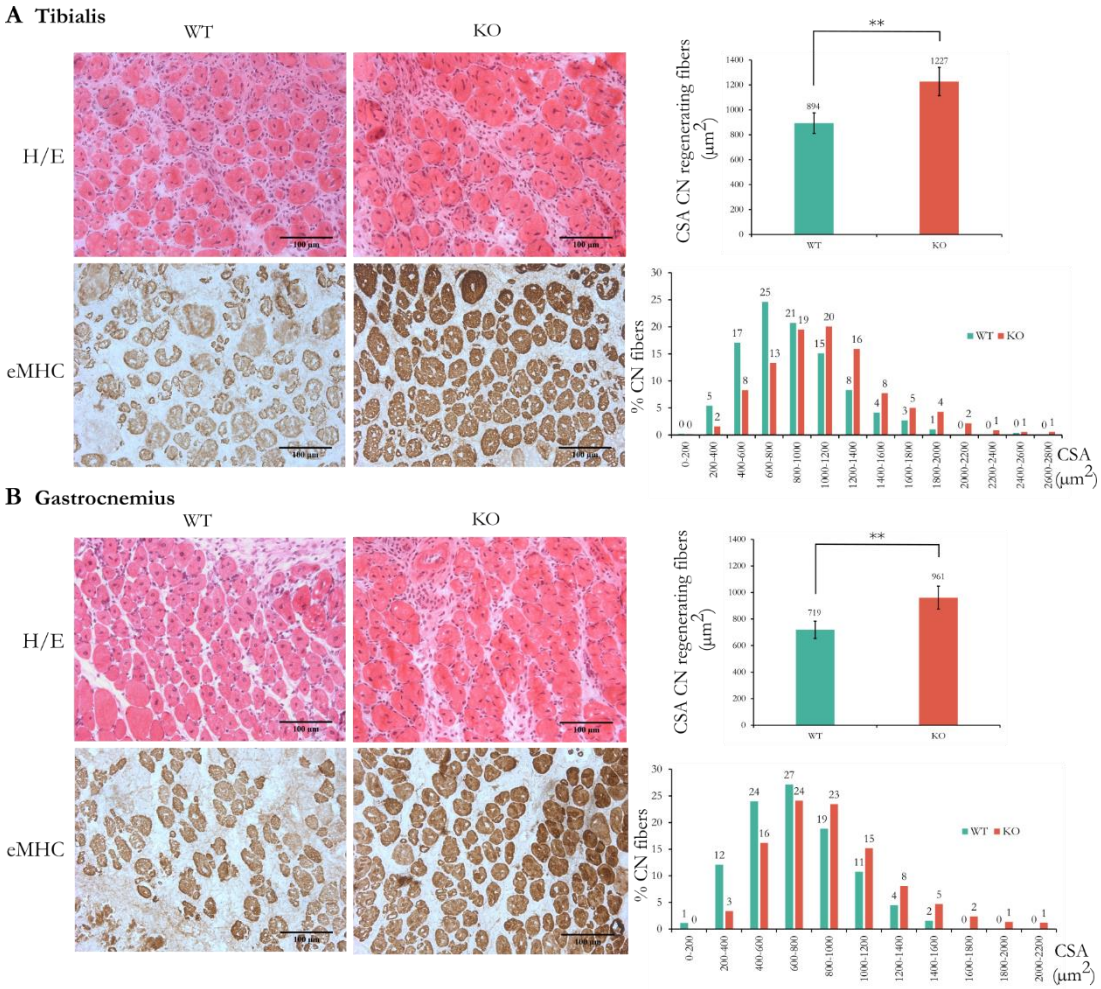

8.4. HDAC11 deficient mice shown equal regeneration capacity than wild-type mice at late regeneration time point

To ascertain whether the observed phenotype was maintained al late time points of muscle regeneration we analyzed tibialis and gastrocnemius sections of female HDAC11 wild-type and deficient mice at 21 dpi. As observed in Figure 56 A, hematoxylin/eosin staining of transversal regenerating muscles presented the same appearance. Moreover, quantification of the CSA of CN regenerating fibers and their distribution by size in tibialis muscles was not different between both genotypes (Figure 56 C), suggesting that the observed phenotype at 7dpi is compensated at late differentiation time points.

Figure 56. HDAC11 deficient males present equal regeneration capacity than wild-type mice at 21 dpi. A Tibialis and **B** gastrocnemius representative 20X microscopy images of hematoxylin/eosin (H/E) stained muscle transversal sections. **C** Upper panel: Average of cross-sectional area (CSA) of central-nucleated (CN) regenerating fibers. Data represent the average of three tibialis female mice ± SEM. Lower

panel: percentage of central-nucleated regenerating fibers. For both measures, at least were considered 5 random images at 20X, and counted at least 300 regenerating myofibers per mice.

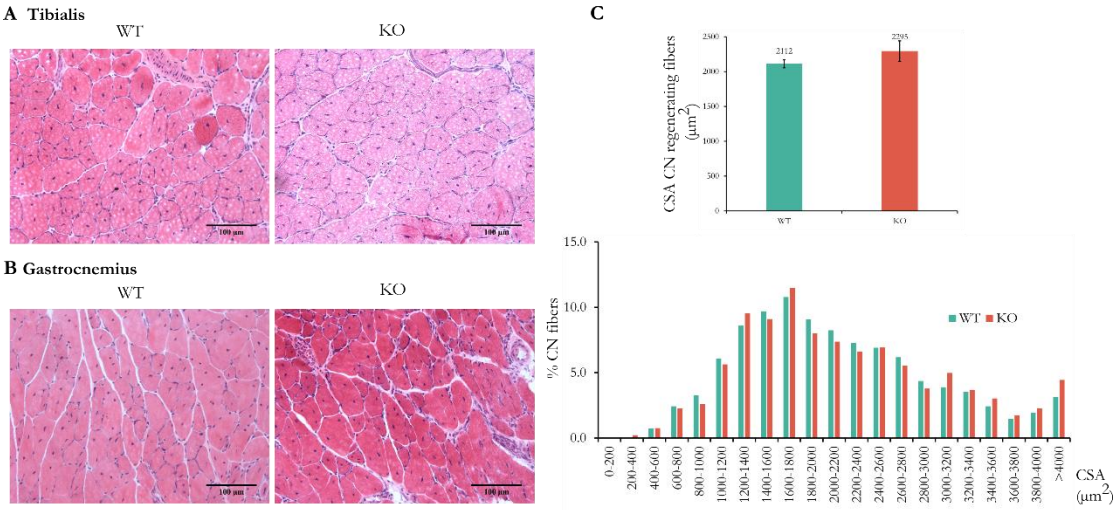

At this moment, we were intrigued by the observed phenotype at 7dpi which cannot be anticipated by our previously obtained results in isolated differentiating myoblasts, which suggest a delayed reenter in differentiation and expression of myosin genes. Nevertheless, we considered if any target regulated by HDAC11 could be responsible of the advanced regeneration capabilities of HDAC11 KO mice observed at 7 dpi. In that moment, CXCL12 (upregulated in KO myoblasts) caught our attention for being previously described to promote SCs migration to injured skeletal muscle (Brzoska et al. 2015; Bobadilla et al. 2014) and promote skeletal muscle regeneration (Hunger et al. 2012; Kowalski et al. 2015; Rybalko et al. 2015). Unfortunately, we quantified CXCL12 expression at 4 dpi and 7 dpi injured mice but we did not observe an increase in their expression levels neither at 4 nor 7 dpi (data not shown). Although it cannot be completely ruled out that CXCL12 plays a role in increasing HDAC11 KO regeneration capabilities, we discarded CXCL12 as the main HDAC11 effector in muscle regeneration and we started to consider alternative possibilities.

Given the previously described roles of HDAC11 in the immune system (Villagra et al. 2009; Woods et al. 2013; Sahakian et al. 2015; Cheng et al. 2014) and taking into account the crucial contribution of the immune response in muscle regeneration, we decided to explore the inflammatory response of HDAC11 KO myoblasts during muscle regeneration.

8.5 Inflammatory response depending processes

We first investigated if HDAC11 deficient muscles presented alterations in the numbers of recruited macrophages at 4 dpi. We choose 4dpi because it is a time point where M1 and M2 populations coexist, while at 7 dpi the main macrophage population are M2 macrophages and we specifically aimed to address if the balance of pro-inflammatory and anti-inflammatory macrophages was affected in HDAC11 KO mice.

For that, we isolated and quantified by FACS neutrophils, M1 and M2 macrophage populations in the injured muscles. As observed on Figure 57 A and B, the number of isolated inflammatory populations was not different in HDAC11 deficient mice, suggesting that the balance between pro-inflammatory and anti-inflammatory macrophage populations at this point was not affected.

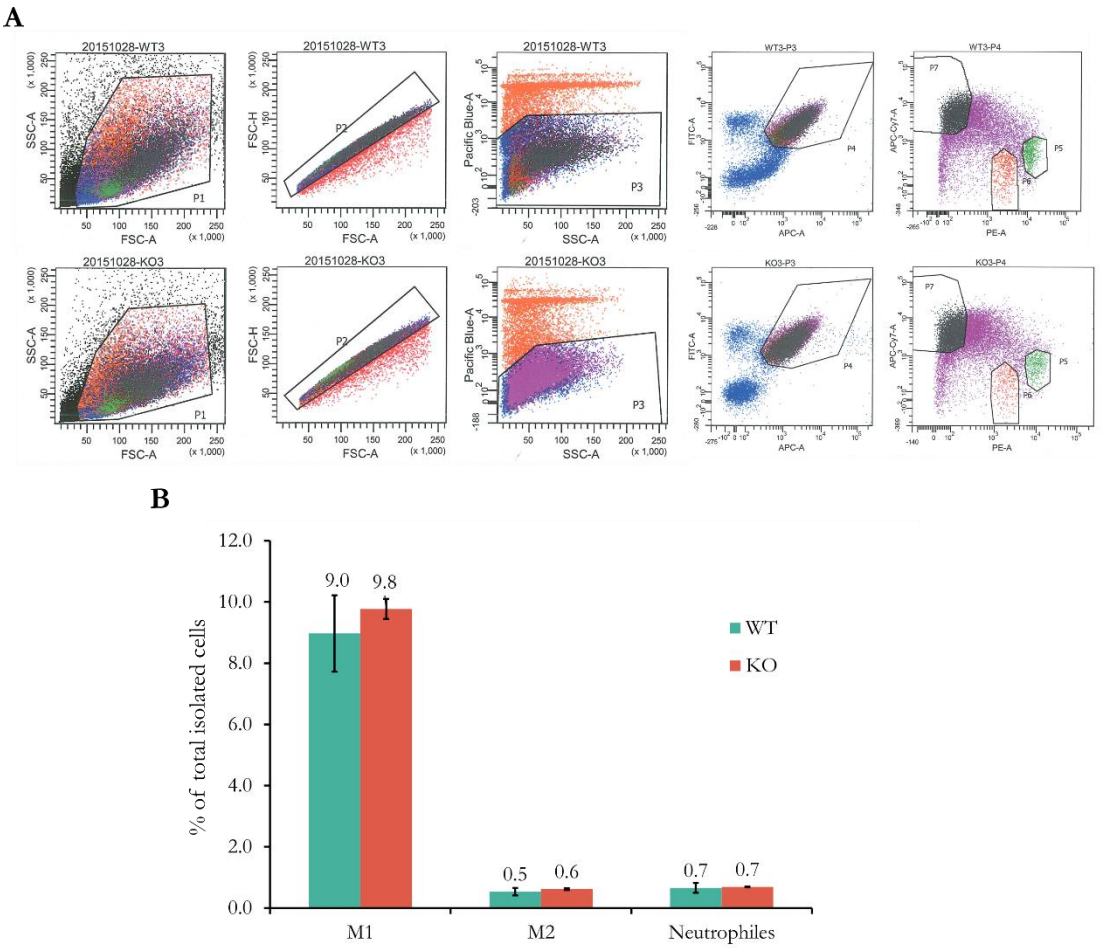

Figure 57. HDAC11 KO mice present the same number of recruited inflammatory cells at 4 dpi. A Gating strategy for FACS isolation of inflammatory cell populations. Cells were extracted from injured gastrocnemius and tibialis mice at 4dpi following "Muscle bulk preparation". To separate the three main populations recruited to regenerating muscles, the cell extracts where sorted. First, cells (P1 population) were separated from debris using forward-scattered light (FSC) an side-scattered light (SSC) parameters. Living

cells (P3) were separated from death cells using Pacific blue staining (DAPI) and then myeloid cells (P4 population) were selected as followed: neutrophils: F4/80$^-$, Ly6C$^+$ (intermediate levels), CD11b$^+$; M1 macrophages: F4/80$^+$, Ly6C$^+$ (higher levels), CD11b$^+$; M2 macrophages: F4/80$^+$, Ly6C$^-$ (very low levels), CD11b$^+$. FACS gates had already been set-up by Pura Muñoz's laboratory (Perdiguero et al. 2011). **B** Relative abundance of myeloid populations in WT and KO 4 dpi injured muscles. Data represent the average values of the indicated populations versus the total number of total living isolated cells (N= 5 WT and 3 KO) ± SEM.

We next investigated if the expression of inflammatory cytokines was different in HDAC11 deficient macrophage populations. We centered on Il-10, whose expression had been previously described to be controlled by HDAC11 (Villagra et al. 2009; Cheng et al. 2014). Interestingly, as observed on Figure 58 A, M1 HDAC11 deficient macrophages expressed higher levels of Il-10. In addition, also M2 HDAC11 deficient macrophages expressed higher levels of Il-10, although this result was not statistically significant, maybe because of the reduced number of samples analyzed.

For M1 isolated macrophages, we also quantified the expression levels of the typical M1 inflammatory markers CD68, CCL2 and Il6 (Figure 58 B), but unfortunately we have observed a high variability in HDAC11 deficient samples that impairs to conclude if there are changes in the expression levels of pro-inflammatory cytokines. In addition, as the amount of RNA isolated for M2 macrophages was scarce (the cell number isolated at this point was much lower than M1 ones, Figure 57 B) we could not assess the expression of other M2 cytokines in these samples. To try to bypass these limitations, we are planning to increase the sample number at 4 dpi and also extend the quantification of macrophage populations and their secreted cytokines in 7 dpi animals.

Figure 58. Cytokine' expression in HDAC11 KO mice. A Il-10 expression qPCR quantification in M1 (left) and M2 (right) isolated macrophages by FACS. **B** M1 representative cytokines qPCR quantification in M1 isolated macrophages. Data correspond in all cases to the average values of 5 WT and 3 KO macrophage populations isolated from tibialis and gastrocnemius muscles at 4 dpi normalized to 18S reference gene values. *: pval<0.05, ttest two tails.

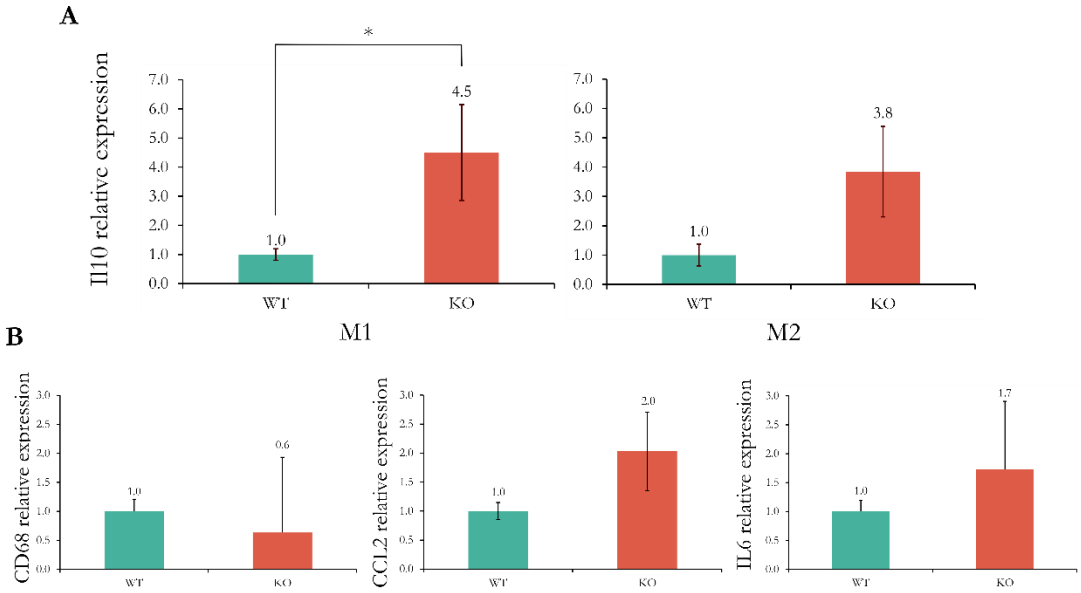
A
*
Il10 relative expression
7.0
6.0
5.0
4.0
3.0
2.0
1.0
0.0
4.5
1.0
WT
KO
M1
3.8
1.0
WT
KO
M2
B
CD68 relative expression
1.0
0.6
WT
KO
CCL2 relative expression
1.0
2.0
WT
KO
IL6 relative expression
1.0
1.7
WT
KO

9. Characterization of HDAC11 expression in physiological and pathological muscles

9.1. Human muscle differentiation

To ascertain whether the changes observed in HDAC11 expression through murine muscle differentiation occurred also in humans, we took advantage of two human primary myoblast cell lines kindly provided by Dr. Eduard Gallardo (Institut de Recerca de Sant Pau, Universitat Autònoma de Barcelona) and analyzed HDAC11 expression at proliferation and day 1 and 4 differentiation points. As observed on Figure 59 A, HDAC11 levels are also upregulated at day 1 and 4 of muscle differentiation, indicating that the expression changes observed in mouse are shared in humans. In Figure 59 B are shown two classical differentiation markers that allow the monitor of the differentiation process, MYOD, whose expression increased transiently at day 1 and decreased through differentiation, and MGN, that increased through differentiation (Owens et al. 2013). As for mouse samples, we tried to detect human HDAC11 by western blot analysis but our attempts were also unsuccessful.

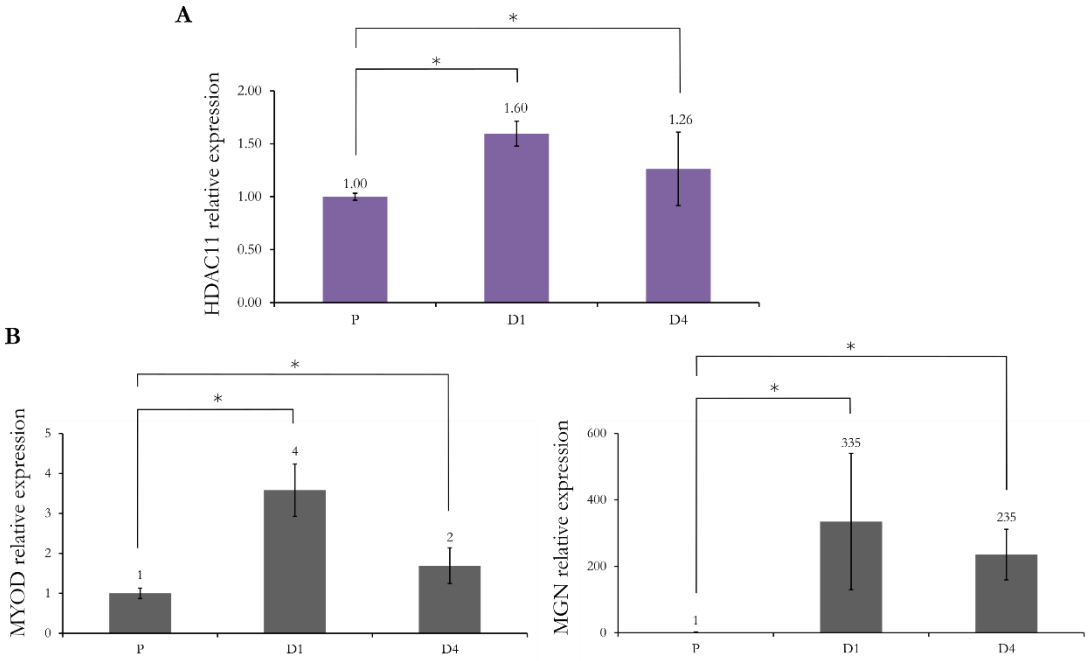

Figure 59. HDAC11 expression through human primary myoblast differentiation. A HDAC11 expression in two human primary myoblasts cell lines assayed in duplicate. **B** MYOD and myogenin (MGN) qPCR quantification in the same time courses to monitor the differentiation process. Data represent in all cases the average values normalized to RPO reference gene ± SD.

9.2. HDAC11 expression in human myopathies

As many genes involved in muscle differentiation have been reported to be affected in human myopathies and thanks to the availability of human samples and cells lines from our collaborators, we decided to explore the putative dysregulation of HDAC11 expression in human myopathies.

9.2.1. Rhabdomyosarcoma

Rhabdomyosarcoma (RMS) tumors, as other types of cancer, are characterized by an imbalance between proliferation and differentiation processes. Given our identified roles of HDAC11 in G0 entry and differentiation, we wondered if HDAC11 expression, as many other factors involved in cell differentiation, may be altered in rhabdomyosarcoma subtypes.

Notably, two significantly enriched C2 curated GSEA categories identified with our generated RNA-seq data, suggested that the downregulated targets in HDAC11 deficient myoblasts overlap with rhabdomyosarcoma processes. In Figure 60 A are illustrated the plots for these categories: Ebauer_myogenic_targets_of_PAX3_FOXO1_fusion which analyzes PAX3:FOXO1 targets comparing aRMS cell line Rh4 with eRMS Rd (Ebauer et al. 2007) and Ren_alveolar_rhabdomyosarcoma_up, which ascertains the gens commonly down-regulated in aRMS and PAX3:FOXO1 derived murine models (Ren et al. 2008).

For all these reasons, we decided to examine the expression of HDAC11 in our available human rhabdomyosarcoma cell lines, kindly provided by Drs. Óscar Martínez Tirado and Roser López-Alemany (IDIBELL, Barcelona), Eduard Gallardo (Institut de Recerca de Sant Pau, Universitat Autònoma de Barcelona) and Josep Roma (Hospital Vall d'Hebron Research Institute). As observed in Figure 60 B, HDAC11 expression is higher in PAX3:FOXO1 alveolar rhabdomyosarcoma cell lines (aRMS) than embryonal ones. Two fetal and two adult muscles (kindly provided by Dr. Eduard Gallardo) were included as references for HDAC11 expression in normal tissues. Taking into account the adult normal reference tissues, HDAC11 is downregulated in all rhabdomyosarcoma cell lines except for Rh4, albeit this downregulation is higher for eRMS cell lines, as mentioned. To increase the number of cell lines and further validate these results, we screened available data from GSE8840, that included the same analyzed cell lines plus 3 additional aRMS, 2 eRMS and one pleomorphic cell lines (Missiaglia et al. 2009). These results, which go according to our observations, are presented on Supplementary Figure 5.

With the same purpose, we additionally evaluated HDAC11 expression in primary mouse derived cell lines from induced rhabdomyosarcoma by PAX3:FOXO1 translocation under the control of MYF6 promoter, highly expressed during muscle development (cell line U23674, resembling aRMS subtype) or PAX7 inducible promoter, expressed upon tamoxifen administration in 1 month-old mice (U29415, resembling eRMS subtype) (Abraham et al. 2014). As observed on Figure 60 C, HDAC11 expression was again lower in eRMS origin cell line.

Next, we evaluated HDAC11 expression in RMS tumors from public transcriptomic datasets. In Figure 60 D, is represented HDAC11 probe data for GSE66533 in 33 aRMS (26 PAX3:FOXO1 and 7 PAX7:FOXO1 positives) and 25 eRMS human rhabdomyosarcoma samples (Sun et al. 2015). The statistical analysis with Geo2R revealed a $\log_2$FC 4.95 with a p adjusted value of 1.66×10^{-7}(Benjamini and Hochberg) of HDAC11 upregulation in aRMS compared to eRMS primary samples. Notably, another independent dataset comprising a total of 102 samples also revealed an up-regulation of HDAC11 in aRMS subtype versus eRMS (FDR: 0.003853) (Davicioni et al. 2006; Romualdi et al. 2006) (data not shown). Altogether, these analysis shown a reduction of HDAC11 levels in embryonal RMS tumors.

To bring light to the putative mechanisms of HDAC11 silencing in eRMS subtype, we analyzed by bisulphite sequencing selected regulatory regions of HDAC11 locus in the aforementioned rhabdomyosarcoma cell lines and one fetal and two adult muscles as controls. As shown in Figure 61 A, we did not observe differences in the DNA methylation levels of the studied regions. Moreover, we observed that HDAC11 locus contained an antisense HDAC11 transcript in its promoter region. We tried to detect the expression of this antisense transcript in normal and rhabdomyosarcoma cell lines performing retrotranscription with poly-dT, random hexamer and specific primers to retrotranscribe the antisense transcript but we were not able to detect its presence in these cell lines in any condition.

Figure 60. HDAC11 is downregulated in embryonal rhabdomyosarcoma subtype. A C2 curated GSEA significantly enriched categories from HDAC11 murine KO differentiating myoblasts RNA-seq. **B** Human HDAC11 expression relative to RPO reference gene in two fetal and two adult muscles and the indicated rhabdomyosarcoma cell lines. **C** HDAC11 qPCR expression of proliferating aRMS U23674 and eRMS U29415 cell lines derived from murine rhabdomyosarcoma models (Abraham et al. 2014). Data represents

the average of two experiments relative to GAPDH reference gene ± SD. **D** HDAC11 227679_at probe intensity values in GSE66533 dataset (Sun et al. 2015).

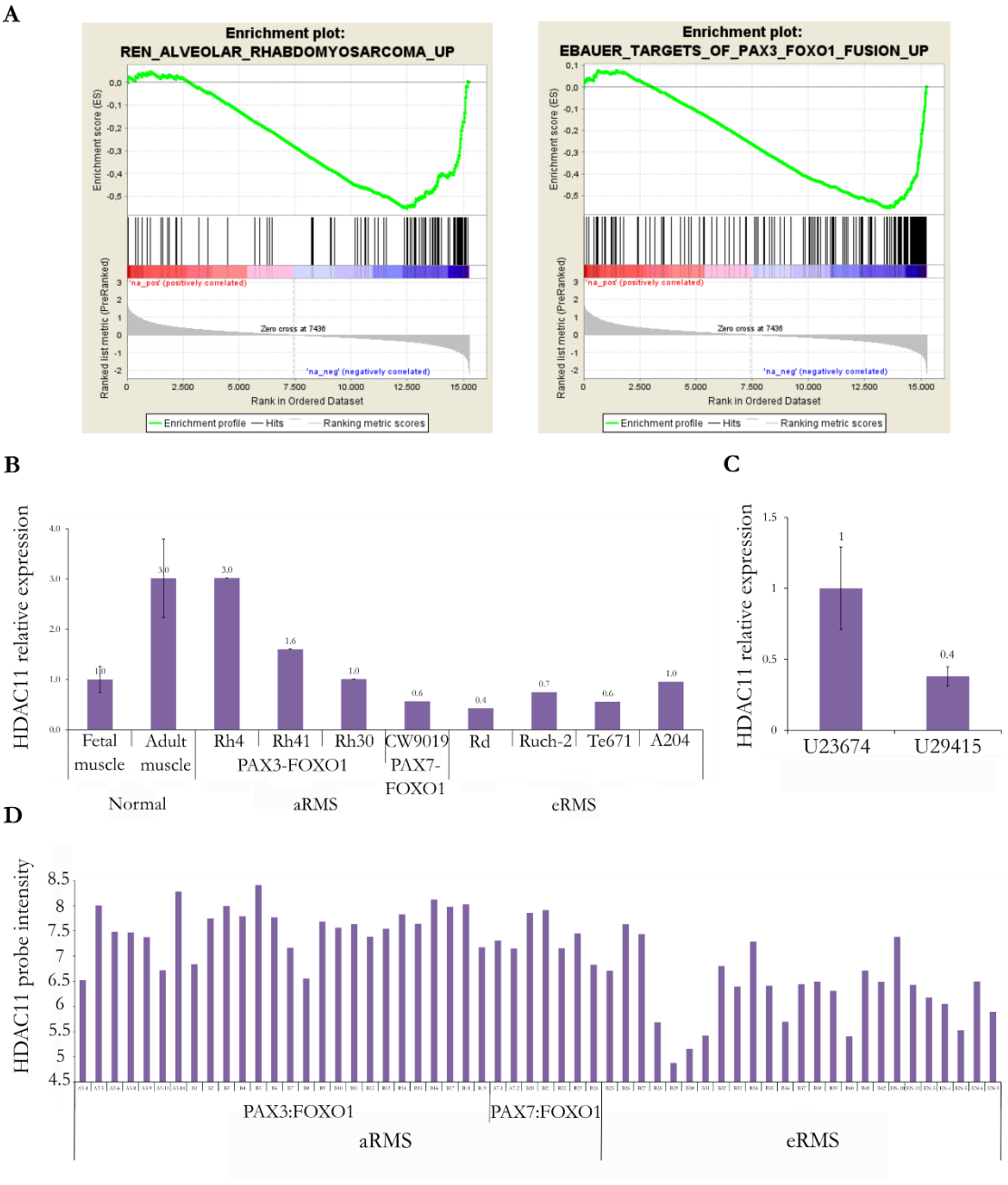

Due to a previous collaboration with Dr. Charles Keller (Children's Cancer Theraphy Development Institute, Portland, USA), we had treated the two aforementioned primary derived RMS cell lines (U23674 with aRMS origin and U29415 with eRMS origin) with the class I specific HDACi Entinostat (Ent) and the pan-HDACi SAHA (suberoylanilide hydroxamic acid). Notably, as shown in Figure 61 B, HDACi treatment in eRMS origin cell line induced HDAC11 expression while had minor effects in HDAC11 expression in aRMS cell line. We are currently addressing specifically in eRMS cell lines if HDAC

mediated acetylation of MYOD, as occurred in normal murine proliferating myoblasts, could restore HDAC11 expression in eRMS cell lines and the putative benefits of HDAC11 reexpression in eRMS cell differentiation.

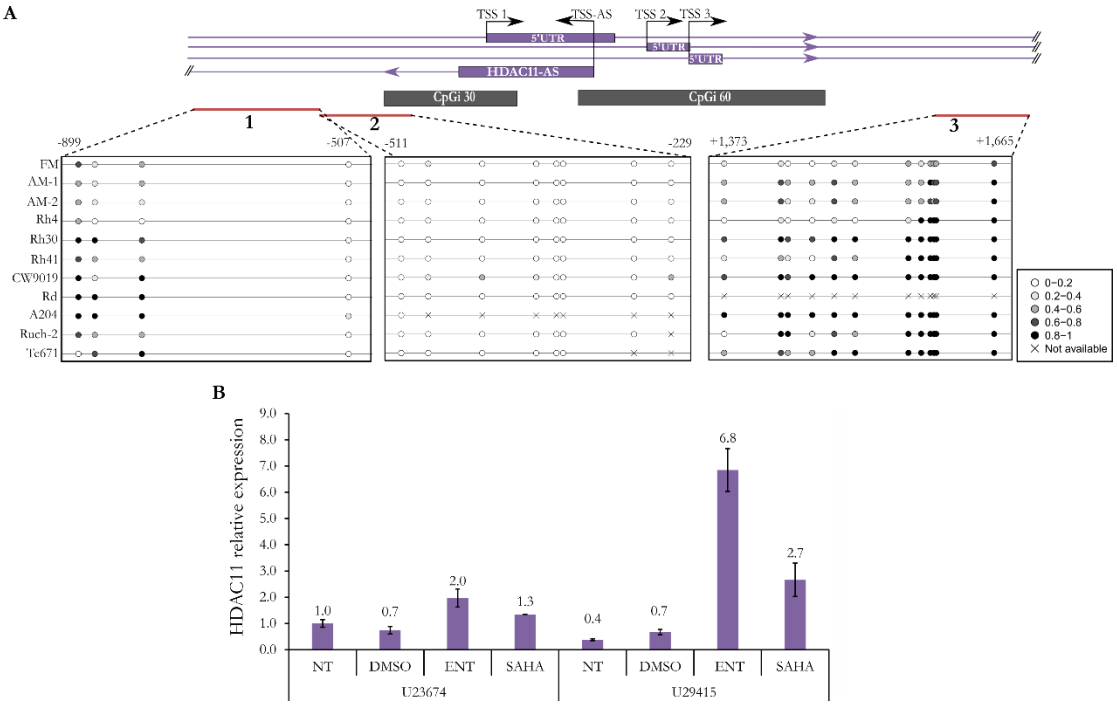

Figure 61. HDAC11 silencing in eRMS cell lines is released by HDACi treatment. A Scheme of HDAC11 human genomic locus. Indicated are the transcription start sites for the different HDAC11 isoforms (TSS) and antisense transcript (AS). In red lines are indicated the regions analyzed by bisulphite sequencing with their relative position to TSS1 indicated in numbers above the boxes. Each dot within the boxes represent a cytosine of a CpG dinucleotide and their relative separation are proportional to their genomic position. Their color indicates the percentage of methylation, as showed on the legend. **B** HDAC11 relative expression in proliferating cell lines of aRMS origin (U23674) and eRMS (U29415) treated for 24 h with the indicated HDACi. Data correspond to the average values of HDAC11 qPCR quantification in two independent experiments relative to GAPDH reference gene expression ± SD.

9.2.2. Other myopathies

It has been previously described that Il-10 expression is elevated in mdx (most used murine model of Duchenne muscular dystrophy) muscles in comparison with wild-type ones (Villalta et al. 2011). Given the described role of HDAC11 in controlling Il-10 expression in macrophages (Villagra et al. 2009), we wondered whether HDAC11 expression could be decreased in mdx muscles. For that, we quantified HDAC11 expression in 3 months old mdx quadriceps (kindly provided by Dr. Roser-López-Alemany, IDIBELL, Barcelona).

As observed in Figure 62 A, HDAC11 expression did not change in these dystrophic muscles.

Another putative involvement of HDAC11 in muscle dystrophies that we had explored, began with the publication that HDAC11, through protein binding to SMN1, GEMIN3 and GEMIN4, contributes to U12-type intron splicing (Joshi et al. 2013). In this work, Joshi and colleagues demonstrated that upon HDAC11 silencing, ATXN10, albeit not THOC2, was aberrantly spliced and retained its U12 intron as occurred in lymphoblasts from spinal muscular atrophy (SMA) patients presenting homozygous SMN1 deletion. Spinal muscular atrophy is a neurodegenerative disease characterized by muscle weakness and atrophy derived from motor neurons degeneration (Zhang et al. 2008). Although from a neuronal causative origin, pioneer works pointed out the contribution of skeletal muscle to atrophy (Boyer et al. 2014), although their specific mechanisms are far from being completely understood. In that sense, we wondered if HDAC11 deficiency could cause U12 intron retaining in skeletal muscle tissue as occurs in SMN1 deficiency.
To tackle this, we took advantage again of our RNA-seq generated data and we performed transcript differential expression, finding that the statistically changing transcripts corresponded to changing genes and not to specifically mis-spliced transcripts. To further address this question, we decided to search in the literature for murine known U12 type introns whose splicing is altered in SMN mouse model of SMA (U12 intron is not conserved in murine ATXN10 and U12 introns are poorly conserved between mouse and human http://genome.crg.es/cgi-bin/u12db/u12db.cgi (Alioto 2007)). Although scarce information is available about this topic, we found a work from Zhang and colleagues that specifically addressed the effects of SMN deficiency in several mice tissues including skeletal muscle (Zhang et al. 2008). We selected the exon junctions whose expression was most affected in skeletal muscle, and we assessed their expression in non-injured HDAC11 WT and KO male gastrocnemius. As observed on Figure 62 B, none studied junction changed statistically its expression, discarding a role for HDAC11 in the splicing of these particular SMN murine splicing sites.

To further address the putative dysregulation of HDAC11 expression in human myopathies, we screened public available data about muscle diseases. As observed in Figure 62 C, HDAC11 expression was downregulated in muscle infiltrated leukocytes from body inclusion myopathy patients FC:-1.89, p adj val: 0.0016 (Geo2R) (Zhu et al. 2012), although

the functional implications of this downregulation are totally unknown.

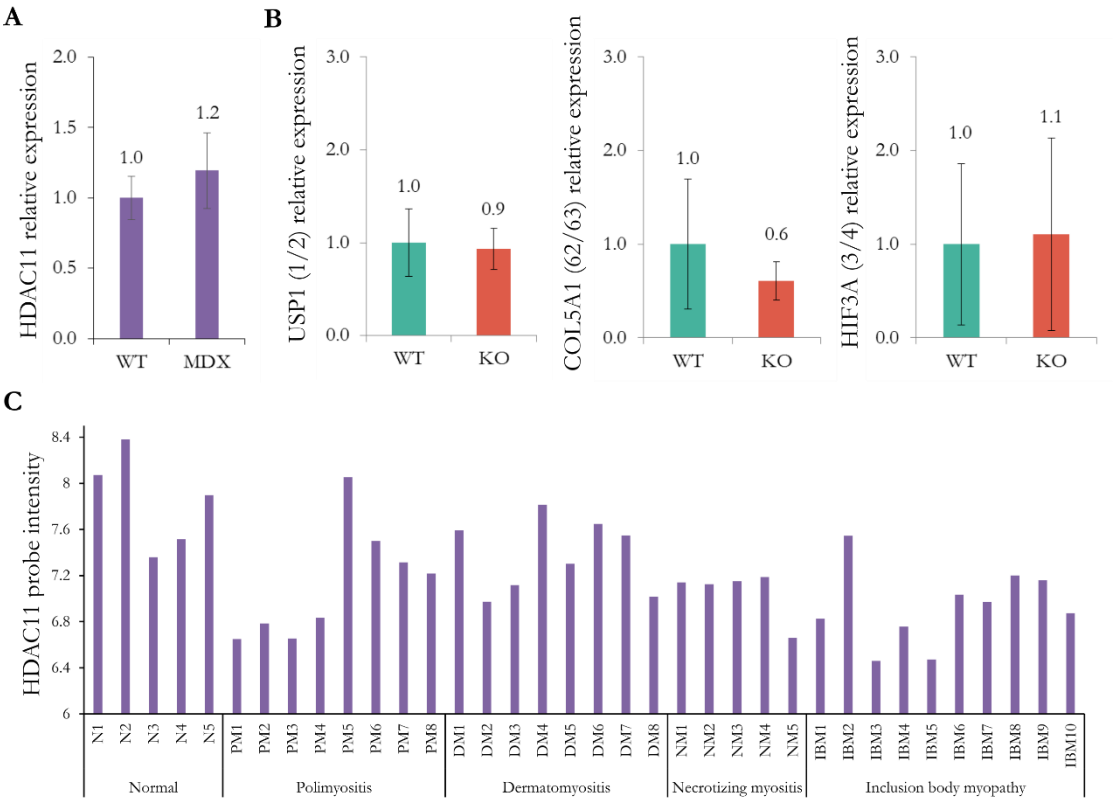

Figure 62. HDAC11 expression in myopathies. A HDAC11 relative expression quantification in 3 WT and 3 mdx quadriceps muscles. Data correspond to the average values of HDAC11 relative expression to TBP1 reference gene ± SD. **B** qPCR analysis of the indicated exons flanking U12 introns of changing genes in SMN1 mice muscles according to (Zhang et al. 2008). Data represent the average values of 7 WT and 8 KO gastrocnemius and tibialis muscles from 3 month adult WT and HDAC11 KO mice ± SD. **C** HDAC11 227679_at probe intensity in GSE39454 in purified leukocytes infiltrated in normal and the indicated myositis affected muscles (Zhu et al. 2012).

DISCUSSION

HDAC11, after 15 years

At the beginning of this PhD in September of 2011, only 20 hits appeared when searching "HDAC11" on Pubmed. Now, at the moment of finishing this thesis, the knowledge about this protein has quadruplicated to 92 research articles (1st June, 2017). Nevertheless, the number of publications addressing HDAC11 functions is still vastly lower than for all other classical HDAC members except for HDAC10.

In its very first describing article, HDAC11 was reported to be highly expressed in kidney, brain, testis heart and skeletal muscle (Gao et al. 2002). Since that moment, the knowledge of HDAC11 expression and functions has increased mainly in brain (Yu et al. 2015; Kizuka et al. 2014; Watanabe et al. 2014; Takase et al. 2013; Liu et al. 2009; Liu et al. 2007; Broide et al. 2007) and also in kidney (Kim et al. 2013) and testis (Gutiérrez 2012, unpublished data). By now, its expression has also been extended to other systems like the immune system (Villagra et al. 2009; Cheng et al. 2014; Zhang et al. 2015; Sahakian et al. 2015; Sahakian et al. 2017), while its expression and functions in striated muscles remains completelly unsolved. Although scratching the first layers of HDAC11 functions in skeletal muscle, this PhD has tried to bring some light in this unexplored tissue.

HDAC members as players in myogenesis

To our knowledge, we have performed the first integrative analysis of all classical HDAC members' expression through the muscle differentiation process although, certainly, the expression of most of them has been already investigated independently.

Class I members' expression and functions account for the most well described through literature. HDAC1 and HDAC3 are the HDAC members the highest expressed in all the muscle differentiation processes analyzed (proliferation, and days 1 and 3 of differentiation). The expression of HDAC1 is downregulated through differentiation, as it had been previously described by Puri and coworkers (Puri et al. 2001). In proliferation conditions, HDAC1 prevents expression of differentiation genes by binding to MYOD and preventing its acetylation (Puri et al. 2001) and by direct histone deacetylation of MYOD targets' promoters (Mal & Harter 2003). At the early points of differentiation, HDAC1 binds to CLP-1 and MYOD to silence proliferation genes (Galatioto et al. 2010). The specific roles of HDAC1 in differentiated myotubes, where it is mainly associated with Rb, are still elusive (Puri et al. 2001).

HDAC3 expression, at its turn, remains constant in the transition from proliferation to differentiation conditions and its expression increases at day 3. We have not found any work addressing HDAC3 expression through muscle differentiation although its inhibition has been reported to block myotube formation but not cell cycle exit, which goes according its increased expression at late differentiation points (Collins et al. 2017).

HDAC2 expression was not detected by qPCR or microarray probes at any point analyzed although it was previously described to be downregulated by northern and western blots though differentiation (Puri et al. 2001). This divergence of results is probably explained by the sensitivity of northern blots and the different probes used in both studies. HDAC8 was low expressed and invariant though all the process (not literature available).

Among class IIa HDAC members, the HDAC expression that changed the most was HDAC9, which had already described by Zhang and coworkers (Zhang et al. 2001). The other class IIa HDAC members that undergo lesser extent changes through this process, HDAC5 and 7, have only been evaluated at the protein levels, which resulted unchanged through the process (Puri et al. 2001) and (Gao et al. 2010), respectively. HDAC4 did not change its expression in this process and neither did at the protein level as described by (Puri et al. 2001). The most studied function of class IIa members in the muscle differentiation process is MEF2 repression in proliferation conditions, which is released during differentiation by HDAC nuclear export to allow the differentiation process to proceed. Subsequently, this level of regulation by protein compartmentalization may suggest that their total transcript or protein levels present in the cell is not as crucial as for class I members.

Both class IIb members, HDAC6 and HDAC10, remain invariant through this process. To our knowledge, HDAC10 has not been addressed in skeletal muscle differentiation and HDAC6 expression in human muscle differentiation remained mostly constant (Balasubramanian et al. 2014).

As far as we know, the expression of the sole member of class IV, HDAC11, is the first time to be addressed in myogenesis and that is why we have evaluated it in murine and human muscle differentiation processes and compared it with public RNA-seq data (Wold 2012). In all these comparisons, we found HDAC11 highly induced at the onset of differentiation (day 1). Nevertheless, while we observed that HDAC11 expression in primary myoblasts remains constant at day 3, in C2C12 cells this upregulation of expression is higher at later differentiation points. This divergence can be explained because primary myoblasts are more

prone to differentiate and behave more homogeneously than C2C12 cell line (Asp et al. 2011).

Regulated by the regulators

Regarding the mechanisms that could explain HDAC11 expression changes during muscle differentiation, we decided to study first epigenetic mechanisms, as they had been described to play a major role in the regulation of myogenesis (Segalés et al. 2015). As HDAC11 possesses a CpGi in its promoter region, we first investigated if HDAC11 repression in proliferation conditions could be mediated by DNA methylation of the CpG dinucleotides present in this region. Bisulphite analysis in proliferating and differentiated cells revealed that this region was completely unmethylated in both conditions, discarding a role for CpGi methylation in the control of HDAC11 expression in this process, as also happens for important muscle regulators such as MYF5, MCK and myosines (Carrió et al. 2015).

The analysis of the public available chromatin marks in the regulatory regions of HDAC11 (Wold 2012), revealed the absence of the negative transcriptional associated histone mark (H3K27me3) and the presence already in proliferation conditions of positive associated transcriptional histone marks (H3ac and H3K4me3). This result goes according the genome-wide study of the epigenetic landscape through muscle differentiation (Asp et al. 2011). In this work, Asp and colleagues identified that the genes whose expression increased in myotubes, already presented polymerase II and positive associated with transcription histone marks in their promoter regions and the absence of negative histone marks, adopting an active chromatin conformation prior to transcription. Interestingly, in the dataset from Wold's laboratory (Wold 2012), we observed that the marks deposited as a consequence of gene transcription (H3K79me2 and H3K36 me3), were increased in differentiating cells, suggesting that HDAC11 mRNA upregulation was a consequence of an increased transcription of the gene.

As MYOD and MGN are the master regulators that trigger the muscle differentiation program and HDAC11 expression coincides with the onset of this process, we investigated the binding of these MRFs to HDAC11 promoter region, finding that both are bound to HDAC11 regulatory regions exclusively in differentiating conditions. This result has already been reported in several publications addressing MRFs' targets. A chip-on-chip performed with MYOD and MGN antibodies revealed that MYOD and MGN were exclusively bound

to HDAC11 promoter in day 4 differentiated myotubes compared to proliferating myoblasts although they did not ascertain HDAC11 expression changes (Blais et al. 2005). Moreover, the depletion of BAF60C, which facilitates MYOD transcription, caused a 4 fold reduction of HDAC11 expression in 18 h differentiating C2C12 cells compared to the scrambled control (Forcales et al. 2011). Regarding myogenin control of HDAC11 expression, myogenin deficient myoblasts at day 2 of differentiation presented a 50% decrease in HDAC11 expression (Meadows et al. 2008).

Taking this information into account, some questions came to our mind. Which MRF is the principal responsible for HDAC11 induction in differentiation conditions? Or is the cooperative binding of both indispensable for HDAC11 induction? Thanks to the work of Cao and coworkers addressing MYOD and MGN overlapping and individual targets through myoblast differentiation, we could compared HDAC11 expression induction only in MGN or MYOD overexpressing cells and both overexpressing MYOD and MGN ones, with the result that neither MYOD nor MGN alone are sufficient to trigger HDAC11 expression in proliferation conditions up to the same extent that the reached in differentiation (Cao et al. 2006). At the 12 h post differentiation induction point (the only one where MYOD and MGN targets can be separated as later on MYOD activates MGN endogenous expression), the full HDAC11 induction is reached by combined overexpression of MRFs, while at day 1 and 2 of differentiation, this effect is maintained and MGN alone cannot induce HDAC11 expression. We hypothesized that when MGN is exogenously expressed alone in proliferation or differentiation conditions, it cannot activate HDAC11 expression because it requires a prior MYOD binding to the E-box or the presence of some additional factors whose expression is induced by MYOD. On the contrary, MYOD when expressed alone can slightly but significantly increase HDAC11 expression at 12 h of differentiation, albeit to a much lesser extent than the combined MRF expression, but this increase is not observed in proliferation conditions. We were curious about this incapability of MYOD to induce HDAC11 expression in proliferation conditions and we searched for a mechanism that may keep MYOD repressed albeit overexpressed. One of the known mechanisms that could mediate this effect is MYOD acetylation, as MYOD needs to be acetylated in three conserved arginine residues to fully activate the transcription of its targets. For that, we took advantage of the data generated by (Di Padova et al. 2007), to further explore MYOD induction activation mechanism of HDAC11 transcription. As expected, non-acetylable MYOD is incapable of inducing HDAC11 expression up to the same extent than wild-type one at any point of differentiation. The increase of HDAC11 expression in the mutated MYOD form

with respect to the control levels, can be explained because non-acetylable MYOD may still have some remaining transactivation potential. Also, it cannot be discarded that additional factors further participate in the control of HDAC11 expression. For example, SOX6, a transcription factor involved in skeletal muscle differentiation, was reported to bind to HDAC11 promoter in fetal myotubes differentiated for 48 hours and induce its expression (An et al. 2011).

To further address the acetylation mediated activation of HDAC11 expression capability of MYOD, we performed class I and pan-HDAC inhibition in proliferating C2C12 cells, which resulted in the same levels of HDAC11 induction than day 1 differentiation conditions, suggesting that HDAC11 expression is repressed in proliferation conditions mainly by class I mediated MYOD deacetylation (probably HDAC1). It had been previously described that both pan-HDACi (TSA and SAHA) and class I specific HDACi (valproic acid and butyrate), strongly induced HDAC11 expression in acute myeloid leukemia cell lines and patient samples (Bradbury et al. 2005), probably in this case mediated by other mechanisms rather than MYOD acetylation.

This acetylation mediated capacity of MYOD to activate the expression of HDAC11 when HDAC1 is downregulated and detached from MYOD, further extends the fine-tuning balance between acetylation and deacetylation in myogenesis.

The smallest plays better hide-and-seek game

HDAC11 is the smallest classical HDAC known (Gao et al. 2002). One apparent consequence of this fact is that it contains less epitopes than other bigger ones. We had tried, without success, to detect endogenous HDAC11 protein through differentiation conditions in primary and C2C12 cells in murine and human skeletal muscle tissues by different detection methods (western blot using commercial and custom-made antibodies, immunoprecipitation followed by western blot detection, acrylamide band excision followed by MALDI-TOF detection and immunofluorescence on HDAC11 wild-type and deficient mice muscles).

The antibodies that we had available could detect overexpressed HDAC11 in endogenous brain levels, which are about 6 (male EDL and tibialis) to 60 (male gastrocnemius) folds more expressed by qPRC analysis. Indeed, little information about HDAC11 is available in literature if not for brain tissue and immune system cells. As an example, no protein

information is available for any tissue in the Protein atlas, version 16.1 (Uhlen et al. 2015; Uhlen et al. 2010). In testis, another high HDAC11 expressing murine tissue, it has also been described the incapability to detect HDAC11 protein levels with endogenous antibodies (Gutiérrez 2012, unpublished data). Indeed, CRISPR tagging of endogenous HDAC11 with the strong immunogenic epitope hemagglutinin, only achieved HDAC11 detection prior immunoprecipitation with 10 mg of total protein. This fact could be explained in part because, unfortunately, we did not obtain any clone tagged in both alleles which could have facilitated epitope detection. The efficiencies obtained by CRISPR/Cas9 of the generated monoallelic knock-in clones (6%) are in the range of the current published literature for diploid cell lines, with depend very much on the sgRNA and the cell type used, ranging between 0.5 and 20% of efficiency (Maruyama et al. 2016; Mali et al. 2013). Actually, this is not the first described CRISPR mediated tagging experiment that cannot be directly detected by western blot without a prior immunoprecipitation against tag enrichment (K. Li et al. 2014).

This CRISPR/Cas 9 mediated tagging system of detection, finally allowed us to confirm that HDAC11 protein is absent in proliferating cells and that its expression is induced at day 1 and 3 of differentiation, confirming at the protein level the results obtained by mRNA analysis. This result may be of special relevance as it was previously described that at P30 developing murine optical nerve, HDAC11 protein levels were anti-correlated with mRNA levels (Tiwari et al. 2014).

Altogether, these results suggest that HDAC11 protein levels are low in skeletal muscle cells and this may be a limitation to detect them compared to other tissues and that this has to been taken into account for further works. For all these reasons, we had not been able to validate the location experiments done with overexpressed HDAC11 with the endogenous protein. As these experiments suggest, overexpressed HDAC11 is located both in nucleus and cytoplasm of proliferating (albeit in proliferation the endogenous protein may be absent) and differentiating cells. We wanted to address the location of HDAC11 in our cells because of the divergent locations described for HDAC11 in different of cell types ("Introduction" section) and also to further ascertain if it may be possible that HDAC11 regulates its targets by direct binding to their promoters. The small size of HDAC11 agrees with their location in both nuclear and cytoplasmatic compartments as it may allow the protein to passively diffuse through nuclear pores (Wang & Brattain 2007). Moreover, HDAC11 lacks the two conserved phosphorylable serines present in shuttling class IIa HDACs, discarding this mechanism of subcellular relocation (de Ruijter et al. 2003).

HDAC11 acts downstream MYOD and MGN in the myogenic differentiation cascade

A very first experiment treating C2C12 cells at the moment of performing serum withdrawal with the pan-HDAC inhibitor Trichostatin (TSA), which inhibits class I, II and IV HDACs, and class I specific inhibitor Valproic acid (VPA) (Lozada et al. 2016), showed a further impairment of myotube formation in TSA treated cells than those that received the class I specific HDAC inhibitor. This first exploratory experiment gave us the clue that HDAC11 may be involved in the muscle differentiation process.

Observing this and considering that HDAC11 is activated by MRF factors, the responsible to trigger the differentiation process, and that HDAC11 is expressed specifically in differentiating cells, we investigated whether increased levels of HDAC11 could advance muscle differentiation. In this sense, we observed that the overexpression of HDAC11 is not sufficient to trigger the muscle differentiation program in proliferation or to accelerate it in differentiation conditions, evidenced by the fact that HDAC11 does not affect the expression of MRFs, which allow to monitor the differentiation progress. Indeed, HDAC11 deficient myoblasts are capable of differentiate up to the same differentiation indexes and with the same levels of MRF factors expressed as wild-type myoblasts. Altogether, these results suggest that HDAC11 acts downstream MYOD and MGN factors when the myogenic differentiation program has already started without performing any feedback loop affecting MRFs' levels.

The clue of the contribution of HDAC11 to the muscle differentiation process was brought up by the RNA-seq transcriptomic analysis of HDAC11 wild-type and deficient at day 1 differentiating myoblasts. To our knowledge, this is the first and more complete analysis of HDAC11 targets in any system. As far as we know, up to date, only one microarray has been performed in non-disease cells, with one wild-type and one HDAC11 deficient macrophage samples (GSE563669, unpublished data).

We decided to assess HDAC11 RNA-seq targets with deficient myoblasts rather than with C2C12 overexpressing HDAC11 to ascertain its endogenous functions. As we had not generated an inducible expression construct, we were unsure if HDAC11 overexpression in proliferation (where it is absent in endogenous systems) could difficult or change the interpretation of the results in differentiating conditions. Moreover, as the levels of the protein obtained by overexpression were very much higher than the endogenous ones (they

were detected by HDAC11 antibodies and the endogenous ones were not) we were concerned about if these higher levels could confer spurious off-targets. For these reasons, we decided to keep the overexpressing cell lines as a validation tool and we determined that the best approach to assess physiological HDAC11 functions was to analyze the primary MPCs cultures from wild-type and HDAC11 deficient mice. We validated the most changing targets in additional differentiation time courses, including more primary myoblasts cell lines. In addition, we extended our validation to an alternative loss of function system using a shRNA targeting HDAC11 to ascertain that our results were a consequence of HDAC11 downregulation and not the system used. Finally, we extended the analysis to the opposite gain of function system through HDAC11 retrovirus mediated overexpression finding the opposite expected results.

Overall, we identified 918 genes that changed its expression between wild-type and deficient HDAC11 myoblast at day 1 of differentiation with a p adj value <0.05. To perform data mining of these genes, we did gene ontology and GSEA analysis. Of the 609 upregulated genes in HDAC11 deficient myoblasts, 89 were included in the category of mitosis and cell cycle, comprising genes of many families involved in DNA replication, helicases, cell cycle progression genes and mitosis and chromatids segregation. Among the already published results of genome-wide studies about HDAC11 targets, the results available in literature are hardly comparable as all of them, besides being performed in different cell types (testis and macrophages), were done in terminal differentiated cells, so the expression of proliferating genes cannot be compared. Notably, in a microarray performed with HDAC11 knock-down by siRNA and wild-type human neuroblastoma cell lines, the authors found that these cells depended on HDAC11 for cell progression and survival and the genes they found the most upregulated upon HDAC11 silencing were also found in our RNA-seq: CCNE1, CENPA, CENPE, DLGAP5, KIF14, KIF23, UHRF1 and RACGAP1 (Thole et al. 2017), suggesting that these targets of HDAC11 may be shared between different cell lines and in murine and human models. Indeed, it is not the first time that HDAC11 function is related to cell proliferation processes, although these works analyzed HDAC11 protein-protein interactions rather than gene expression control, but curiously these HDAC11 described partners are also upregulated at mRNA levels in our RNA-seq: CDC25 (Lozada et al. 2016) and CDT1 and MCM (minichromosome maintenance complex) proteins (Wong et al. 2010).

Regarding the functional implications of the overexpression of proliferation genes in HDAC11 deficient myoblasts, we propose that this will be affecting only cells in the transition between proliferation and G0. Indeed, both deficient and overexpressing

myoblasts did not present alterations in cell cycle progress in proliferating conditions. This goes according previous studies with normal epithelial types, in which HDAC11 down-regulation did neither affect its proliferation capabilities (Deubzer et al. 2013) and HDAC11 deficient spermatozoid precursors, which did not show alterations in meiosis (Gutiérrez 2012). To further ascertain HDAC11 functions in G0 entry in differentiation conditions, we are currently analyzing if HDAC11 deficient myoblasts present a delayed entry in G0 and an increased number of cells present in S phase after differentiation conditions induction.

Regarding the genes down-regulated upon HDAC11 silence, we found 309 differentially expressed genes, with a p adj val <0.05, identifying as their most enriched gene ontology category, muscle system processes and muscle contraction. Being contractile genes very specialized families with differential expression between slow and fast type muscles (Drexler et al. 2012; Reggiani & Kronnie 2006), we examined if the downregulated genes upon HDAC11 silence were preferentially expressed in fast or slow muscles, finding that these genes belonged indistinctly to both speed contraction muscle types. Indeed, none adult myosin heavy chain isoform, the genes most widely used to determine muscle types, were not found differentially expressed. Indeed, only MYH3, involved in muscle embryogenesis and regeneration, was differentially expressed suggesting that the downregulation of the expression of contractile genes observed upon HDAC11 silence was more related to a specific regulation in contractile genes rather than to a specific fiber type gene regulation. Interestingly, two genes described as having a preferential expression in cardiac muscles, TNNT2 and MYL4 (England & Loughna 2013), were also downregulated in HDAC11 deficient myoblasts. We explored published time courses of cardiomyocyte's differentiation transcriptomic datasets, finding also HDAC11 expression up-regulated in this process (Gan et al. 2014; Wamstad et al. 2012). By now, we have not gone deeper into the role of HDAC11 in this other striated muscle but in the future we aim to explore the putative regulation by HDAC11 of cardiac contractile genes and heart formation in HDAC11 deficient mice.

Regarding the decreased fusion index and number of nuclei per myotube observed in HDAC11 deficient cells and its opposing phenotype in overexpressing cells, it had been described that pan-HDACi and class I specific inhibitors enhanced myoblast fusion and increased their size by induction of follistatin expression (Iezzi et al. 2004). In our RNA-seq, we observed that follistatin gene was 2.26 folds (p adj value: 0.04) downregulated in

HDAC11 deficient myoblasts, so the downregulation of this crucial gene for myoblast fusion could explain the decreased fusion capacity of HDAC11 deficient myoblasts. Follistatin is a tightly regulated gene, since it is a potent inhibitor of the myostatin pathway (Yaden et al. 2014) and interestingly our results showed that HDAC11 may also regulate its expression levels during early differentiation.

Moreover, we have also found downregulated Caveolin-2 gene member of the caveolae family, whose deficient mice presented abnormal fusion capabilities (Schubert et al. 2007). Furthermore, Dysferlin gene was also down-regulated in HDAC11 deficient myoblasts. Dysferlin has been described to promote α-tubulin acetylation through HDAC6 binding (Di Fulvio et al. 2011). Proper posttranslational modifications are essential for microtubule stability and myoblast fusion (Gundersen et al. 1989) and indeed, dysferlin knock-out mice had alterations in myoblast fusion, which could further explain the phenotype observed in HDAC11 deficient myoblasts (Cohen et al. 2012). Moreover, HDAC6 inhibition also impaired myotube formation (Di Fulvio et al. 2011). As HDAC11 itself has been described to interact with HDAC6 at the protein level in other cell types (Gao et al. 2002; Cheng et al. 2014), it is also possible that HDAC11 absence modifies HDAC6-mediated fusion by protein interaction. We are currently elucidating the specific mechanisms by which HDAC11 mediates myoblast fusion capabilities.

How HDAC11 mediates RNA expression changes?

To discuss HDAC11 putative regulation mechanisms of their target genes expression, these should be divided into two groups: targets anti-correlated with HDAC11 expression (up-regulated in HDAC11 deficient cells) and correlated with HDAC11 expression (down-regulated expression in HDAC11 deficient cells).

The first category of genes is the easiest to explain, taking into account the traditional view of HDAC members as repressors of gene transcription. HDAC members received their name in a first moment because of their capacity to deacetylate histones (Dokmanovic et al. 2007). According to this, they are classified as epigenetic factors, in the category of erasers of histone marks. As the histone acetylation mark has been traditionally seen as an activation mark, HDAC enzymes were considered mainly as repressors of gene expression. Indeed, in our RNA-seq we found almost twice more down-regulated genes than upregulated ones

upon HDAC11 silence, according to this traditional view of HDACs as transcriptional repressors.

As for all HDAC members when discovered, the first experiment that was done with HDAC11 was to test their deacetylation activity towards purified histones *in vitro* (Gao et al. 2002). In this first assay, HDAC11 showed deacetylase activity towards H4 acetylated residues. In later works, it was demonstrated that HDAC11 also shown deacetylation capacity towards H3ac and H4ac histone residues in Il-10 promoter (Villagra et al. 2009), H3ac in PAI-1 promoter (Kim et al. 2013) and H3K9ac and H3K14ac in MBP and PLP promoters (Liu et al. 2009).

Our ChIP experiment after shRNA mediated downregulation of HDAC11, resulted in increased H3K9ac and pan-H3 acetylation levels in the promoter regions of selected targets whose expression was upregulated upon HDAC11 downregulation. Although this experiment needs to be repeated, it suggests that in early differentiating myoblasts HDAC11 is involved in the silencing of proliferation-related genes by deacetylation of H3 residues located in their promoter regions. To our knowledge, there is not any published study addressing HDAC11 genome-wide binding to DNA. Current literature suggests that HDAC11 may present intrinsic histone deacetylase activity, opposing to class IIa HDACs that are considered catalytically inactive and exert its deacetylase activities through class I HDACs recruitment (Schuetz et al. 2008; Fischle et al. 2002). Nevertheless, little is known about HDAC11 mechanism of deacetylation as it has not been identified in any corepressor complex as class I and class II HDAC's (Gao et al. 2002; Seto & Yoshida 2014). In this sense, it would be very interesting to explore if in differentiating myoblasts, HDAC11 catalyzes the deacetylation of H3 residues itself or if it recruits another HDAC, for example, by α-H3ac ChIP of overexpressing catalytically inactive HDAC11 (Deubzer et al. 2013) myoblasts cells compared with ones overexpressing wild-type HDAC11.

Regarding the HDAC11-mediated mechanism to downregulate the expression of the muscle contractile category, HDAC11 mechanism of gene expression regulation is more indirect to address and we could point out several possibilities. The first one, is that one or more up-regulated target(s) may negatively regulate the expression of these down-regulated targets. To our knowledge, none of the up-regulated targets could explain this subset of targets as they have mainly proliferation functions, although this hypothesis cannot be completely rejected as the functions and targets of all of them are not known.

The second possibility may be that HDAC11 could deacetylate a "repressive" acetylated histone mark and thus the expression of this target may correlate with HDAC11 expression one. As mentioned, until very recently, histone acetylation has been seen as an activation mark that correlated with actively gene transcription both in H3 and H4 histones. Nevertheless, a year ago was identified the first histone acetylation residue with transcriptional repressive associated capacities (Kaimori et al. 2016). Although the eraser for this mark has not yet been identified to our knowledge, this revolutionary fact changed the view of HDAC's as (only) repressors of transcription and maybe additional acetylation repressive marks would be discovered. In this sense, it would be possible that HDAC11 silencing causes repression of these genes because of the decreased deacetylation levels of some repressive histone marks in their promoter regions. This possibility is merely speculative as no repressive acetylation mark has been described for HDAC11, but since the histone acetylome of HDAC11 is unknown, it could not be completely discarded.

The third possibility is that HDAC11 deacetylates residues of transcriptional regulators, modulating their activities. To explore this possibility, we analyzed the consensus transcription binding motifs present in the downregulated target genes, and we found an enrichment in E-boxes that can be bound by MEF2, MYOD and MGN by GSEA analysis (Supplementary Table 2) (Kuleshov et al. 2016; Chen et al. 2013). Indeed, we analyzed the binding of MYOD and MGN to HDAC11 by co-immunoprecipitation followed by western blot analysis, but we did not see any positive band in the enriched extract fractions. To explore deeper this possibility, we started the analysis of HDAC11 binding proteins by MASS-spectrometry of the co-immunoprecipitated fractions, we have no results yet. To our knowledge, only one protein interactome for HDAC11 has been published in T–cells, but as is a cell type very different than ours, the results are very different to be compared (Joshi et al. 2013).

Finally and regarding the published interaction between HDAC11 and HDAC6 (Gao et al. 2002) and their opposite effects controlling Il-10 gene expression (Cheng et al. 2014), it would also be very interesting to find out the histone and non-histone deacetylation targets of both HDAC members in myogenesis.

HDAC11 is the HDAC family member the most upregulated during (and not only) muscle differentiation

We found HDAC11 as the HDAC family member the most upregulated through the skeletal muscle differentiation process. But, is HDAC11 specific of skeletal muscle differentiation or it is a common hallmark of cell differentiation? In fact, this is not the first time that HDAC11 upregulation has been described through cell differentiation. The first reports about this topic appeared in brain development (Liu et al. 2007), oligodendrocyte differentiation (Liu et al. 2009) and post-natal neuron formation (Watanabe et al. 2014). Although brain and muscle differentiation may seem very distinct processes, both depend on master regulators that trigger the differentiation cascade, respectively, NEUROD2 and MYOD. These transcription factors bind to "shared" consensus E-box sequences, so it is possible to speculate that during neuronal differentiation HDAC11 expression is upregulated by the same equivalent mechanisms than in skeletal muscle differentiation. Notably, we have observed that HDAC11 upregulation also occurs during cardiomyocyte differentiation (Gan et al. 2014; Wamstad et al. 2012).

In addition, HDAC11 expression has also been described to be upregulated through differentiation in other cell types, such as plasma cells (Brayer et al. 2013) and neutrophils (Sahakian et al. 2013; Sahakian et al. 2017).

Finally, the work of Bagui and colleagues revealed that serum deprivation or cell density cell cycle arrest of fibroblast resulted in an increase of HDAC11 expression independent of cell differentiation conditions (Bagui et al. 2013). This interesting work, made us wonder if the upregulation of HDAC11 expression could be beyond cell differentiation conditions and if its expression could be also induced as a result of G0 cell cycle entry.

HDAC11 expression is upregulated in G0 cell cycle arrested conditions

As mentioned above, the first paper describing HDAC11 described it highest expression in human tissues in brain, skeletal and cardiac muscles and kidney (Gao et al. 2002). These tissues are characterized by being mostly quiescence, opposing to others like skin or colon that have a high cell turn over. Our results highlight HDAC11 as the HDAC that changes the most its expression in G0 arrested state in comparison to the proliferative one: it is the HDAC that changes the most its expression between proliferative myoblasts and irreversible arrested G0 differentiating myocytes and also between reversible arrested G0 quiescent SCs

and the very early activated cells at 6 h post-injury, even before the induction of the proliferation genes. Indeed, during neuronal differentiation, it has been previously described that HDAC11 and KI67 proteins rarely colocalize in the same cell (Liu et al. 2007).

In the myogenic process, there are three different transitions to/from cell cycle from/to G0 state. The first one, is the transition from reversible G0 arrested quiescent satellite cells to the activated state. The second, is the cell cycle exit of proliferating myoblasts to G0 irreversible arrested myocytes that will fuse to myotubes. And the third one is the return to quiescence after injury or after growth, to reconstitute the G0 arrested SC' pool. Among all these three transitions, in this thesis we have mainly addressed the second one, but we would like also to discuss the other two.

Regarding the first transition from quiescent to activated SCs, we have analyzed the expression of all HDAC members in a microarray previously generated in our laboratory that addressed the expression changes between directly isolated quiescent SCs, 6h activated SCs purified after cardiotoxin injury, and proliferating SCs after 3 days post-injury. HDAC11 was the HDAC that changed the most its expression in the early transition from quiescent to 6h activated SCs and the most downregulated during this transition. Indeed, this result was reproduced in cardiotoxin injured muscles time courses, where HDAC11 expression was also downregulated after 6 hours post injury compared to non-injured muscles.

We consider that our approach to study the transcriptome of SC' activation is the most physiological up to date, as the precedent genome-wide published transcriptomes considered the activation point in different manners. The first genome-wide study that addressed the expression changes occurring through SC' activation, compared directly isolated SCs with SCs activated after plating them in culture (Fukada et al. 2007). This study had the limitation, in our opinion, that the cells were activated outside their niche in *in vitro* conditions. However, HDAC11 was upregulated in this study 10 folds in the *in vitro* activated SCs versus the quiescent ones, suggesting that HDAC11 downregulation may represent an intrinsic process of cell activation not depending on the activation conditions. The second work addressing SCs activation transcriptional changes, considered *in vitro* activation of SCs and also *in vivo* activation using SCs from 1 month old mice, when SCs are activated due to the intense period of muscle growth; and SCs from adult mdx mice, which as a consequence of their pathology are constantly activated (Pallafacchina et al. 2010). In their comparisons, HDAC11 is found downregulated 17.45 folds in *in vitro* activated SC compared to quiescent ones, but not changing with the other two systems, suggesting that HDAC11 downregulation could

be present in short term activation but not in permanently activated SCs. Finally, the transcriptomic analysis from Farina and colleagues, which investigated the transcriptomic changes between quiescent and 12 h activated *in vivo* SCs neither found HDAC11 changing (Farina et al. 2012). Nevertheless, in this case only two biological replicates were analyzed and the results for HDAC11 probe were very variable (GSE38870).

To really check the presence of HDAC11 upregulation in cell cycle arrested cells independently of differentiation conditions, we induced G0 by loss of cell anchorage capacity by culturing C2C12 myoblasts in methylcellulose containing medium. In this experiment, HDAC11 levels were upregulated up to the same levels reached in differentiation conditions, compared to proliferation mRNA levels. Moreover, isolated reserve cells, which are cells that down-regulate MYOD and escape differentiation, from differentiated primary cultures also presented increased HDAC11 levels compared with the levels presented in primary proliferating myoblasts.

In these two G0 arrested states, HDAC11 expression is antagonic with MYOD expression, condition that differs with G0 cell cycle entry in differentiation conditions, where MYOD triggers HDAC11 expression. In these reversible quiescent G0 states, HDAC11 upregulation may be induced by additional mechanisms which would be very interesting to explore in the future. Interestingly, the higher expression of HDAC11 in quiescent SCs reinforces the idea that quiescence state is not a passive state but an active maintained one, with the specific expression of selected genes that would contribute to actively maintain this state, protecting the cells from stress and premature activation (Montarras et al. 2013). In the future, it would be very interesting to address the transcriptomic changes between quiescent wild-type and HDAC11 deficient SCs. Taking into account our results, it is possible to suggest that HDAC11 contributes to maintain the quiescence state by maintaining repressed the expression of proliferation-related genes.

Regarding the consequences of HDAC11 deficiency in SCs activation process, we found that after 6 hpi of cardiotoxin injection HDAC11 deficient SCs were activated up to the same extent than wild-type ones, according to MYOD mRNA and protein expression levels. Interestingly, in this point PAX7 expression was upregulated in HDAC11 KO muscles. As the number of SCs was not different in basal conditions between both genotypes, we propose that HDAC11-mediated deacetylation could contribute to PAX7 regulation in SCs. It had been described that PAX7 upregulation promotes SCs' self-renewal (Wen et al. 2012) and cell cycle exit towards the quiescent state preventing MYOD and MYOG expression (Olguin

& Olwin 2012). In HDAC11 deficient cells, presumably, the levels of induction of PAX7 were not sufficient to prevent MYOD upregulation and SCs activation. It would be very interesting in the future to investigate if activated HDAC11 deficient SCs present the same cell fate patterns of if they preferentially generate cells that return to quiescence, for example, by isolation of myofibers and *in vitro* single cell monitoring at different points of the fate of SCs daughter cells by immunofluorescence against PAX7, MYOD and KI67 markers. It would be also very interesting to compare the transcriptomic changes between HDAC11 wild-type and deficient cells to ascertain whether the expression of other activation genes is equivalent in HDAC11 deficient cells.

Regarding the third type of cell cycle to G0 transition, the exit from cell cycle to G0 quiescent state, we presume that HDAC11 deficient cells have no major alterations to return to the quiescent state as HDAC11 WT and KO mice presented the same number of SCs by FACS isolation and that after isolation, both SCs genotypes were negative for MYOD expression. Nevertheless, it would be very interesting in the future to address immediately after mice juvenile growth if HDAC11 deficient cells can return to quiescence or if at longer points after regeneration (for example, 50 dpi), SCs can return to quiescence up to the same extent than wild-type ones.

HDAC11 is dispensable for life: is a redundant HDAC?

HDAC11 is conserved in evolution in vertebrates and invertebrates (like *Drosophila* and *C. elegans*) and even plants (NCBI n.d.), although it is absent in other organisms, for example in parasites (ex. *Toxoplasma* sp.). This fact may imply that is not a universally required HDAC for life, as may be HDAC1, but that it would have acquired specific functions through evolution.

HDAC11 deficiency does not compromise cell viability. Indeed, our mice is the second one to be described as HDAC11 knock-out. The first one was generated by Dr. Sotomayor's laboratory (Villagra et al. 2009; Cheng et al. 2014; Sahakian et al. 2017). In these publications, they did not specifically comment anything about mice appearance or phenotypes besides the macrophage's and neutrophil's ones. As they performed macrophage's and neutrophils' extraction from the mice, we assumed that they are born and growth normally and that they did not present major apparent phenotypes like in our case. Moreover, no human diseases have been described up to date to be caused by HDAC11 mutations or silencing, suggesting

that HDAC11 lack does not compromise life or cause major alterations. Regarding the role of HDAC11 in muscle growth, we found that HDAC11 was higher expressed in 10 days old mice than 3 months adult ones. This observation goes according the higher expression observed in HDAC11 differentiating myoblasts compared to terminal differentiated myotubes. To ascertain whether HDAC11 deficiency affects muscle growth, we weighted HDAC11 wild-type and deficient male mice through postnatal growth, not finding differences in total body mice weight between both genotypes. As postnatal stage is a very intense period of muscle growth, were the weight of mice can increase up to 7-8 folds, half on them corresponding to skeletal muscle weight (Gokhin et al. 2008), we assumed that HDAC11 did not caused major alterations in muscle growth. Nevertheless, to further this issue, we are currently analyzing the myofiber cross-sectional area and fiber type composition in 10 days old mice.

The HDAC domain of HDAC11 presents homology to both class I and class II HDAC's but neither enough to be classified in none of them (Gao et al. 2002; Seto & Yoshida 2014). We took into account whether HDAC11 deficiency could be compensated by other HDAC members, as occurs for HDAC1 and 2 or class IIb proteins. In this case, they were two options, or HDAC11 was so different than class I and II members that cannot be compensated at all by any of them, or that as is homologous to both, both HDAC classes could compensate their effects. We explored our RNA-seq data for other HDAC member upregulation as a transcriptional mechanism of compensation, finding none HDAC member expression induced in HDAC11 deficient myoblasts. Nevertheless, it cannot be discarded some kind of compensation at protein level without the need to induce mRNA upregulation, although this topic has not been addressed for HDAC11 in the literature to our knowledge.

On the contrary, we observed HDAC9 downregulation upon HDAC11 deficiency. This is quite interesting as by now it has not been described a regulation of any class IIa member by class IV HDAC, besides that HDAC11 and HDAC9 downregulation did not occur in kidney of orchiectomized mice (Kim et al. 2013) and that upon HDAC11 expression after HDACi treatment in acute myeloid leukemia cells, HDAC9 expression was also induced up to a lesser extent (Bradbury et al. 2005). We interpret that in these works, HDAC9 changes of expression could be mediated by HDAC11 expression, although the authors did not address this regulation issues. As described in the analysis of HDAC members' expression through myoblast differentiation, HDAC9 expression is induced following the same pattern as

HDAC11 but up to a lesser extent, which matches with our observation by RNA-seq. Moreover, HDAC9 has also been described to be involved in the muscle differentiation process by antagonizing MEF2 activity and limiting differentiation, probably to shut the process off when it is already accomplished (Haberland et al. 2007). HDAC9 it has also been described to prevent differentiation in proliferation conditions by repressing MEF2 dependent transcription in (Zhang et al. 2001). In that sense, HDAC11, through regulation of HDAC9 expression, would further contribute to the regulation of the muscle differentiation program.

HDAC11 has male gender

Skeletal muscle is a tissue with an apparent sexual dimorphism trait: their higher size in males. Many works have addressed more specific sexual differences mediated mainly by testosterone induction in males: higher cross-sectional myofiber area, increased SC numbers and different behavior (Neal et al. 2012) and differential gene expression (Welle et al. 2008; Yang et al. 2006), among others. For this reason, is essential to include both male and female individuals when analyzing muscle characteristics, if a differential expression or behavior of a given factor is suspected. In the case of HDAC11, this clue came from an interesting work that revealed that during kidney ischemia/reperfusion induced injury, which is a disease more frequently affecting male individuals, testosterone hormone mediated HDAC11 detachment from PAI-1 promoter (plasminogen activator inhibitor type 1), causing an increase of H3 acetylation in PAI-1 promoter region, which was correlated with an increase in PAI-1 expression and enhanced kidney damage (Kim et al. 2013). For this reason, we decided to include both genders in the analysis of non-injured muscles and in 7 days post injury regeneration experiments to ascertain whether HDAC11 deficient mice could present sexual dimorphism phenotypes.

We first considered whether HDAC11 could be differentially expressed depending on gender and muscle types. For that, we analyzed its expression in the predominantly fast muscles EDL and tibialis, the slow muscle for excellence, soleus; and gastrocnemius, as an example of mixed type muscle. In all cases, we observed that HDAC11 was more expressed in male muscles, but this effect was more evidenced in tibialis muscle. This result is no surprising, since the first paper describing HDAC11 already pointed a higher expression of HDAC11 in testis and not in ovarian tissues, already indicating a gender preferential expression of HDAC11 in male tissues (Gao et al. 2002). Without taking gender into account, we did

observe a higher HDAC11 expression in fast EDL and tibialis muscles compared to soleus and gastrocnemius in both males and females. The expression of HDAC11 has already been examined in the same muscle types by Ann and coworkers. Unfortunately, in this work the authors did not specify the gender of mice used for the study (An et al. 2011). According to our results, we suspect that they may be females, as when we analyzed the expression of HDAC11 exclusively in female muscles types, we saw the same 20% increased HDAC11 expression as these authors in fast type muscles compared to soleus. Instead, when analyzing only male muscles, this increase is higher up to 8 folds in EDL and tibialis fast muscles compared to soleus. This differences cannot be explained by the presence of different SCs numbers in these muscles (HDAC11 is highly expressed in quiescent SCs) as soleus muscles contain higher numbers of SCs than fast ones (Shefer et al. 2006; Keefe et al. 2015), suggesting that HDAC11 may be higher expressed specifically in fast myofibers.

We then addressed if HDAC11 deficiency could affect myofiber size in adult HDAC11 deficient mice, observing the same myofiber cross-sectional areas as wild-type muscles, regardless of muscle type and mice gender. Moreover, the quantification of myosin heavy chain transcripts, the genes widely used to assess fiber type, were equally expressed in both genotypes, indicating that HDAC11 is dispensable for fiber type establishment in the adult and myofiber size maintenance in basal conditions.

The summary of skeletal muscle analysis of HDAC11 wild-type and deficient mice is schematized in Figure 63. It would be very interesting in the future to address the consequences of HDAC11 in the fiber type transitions and hypertrophy induced by exercise or also through postnatal growth.

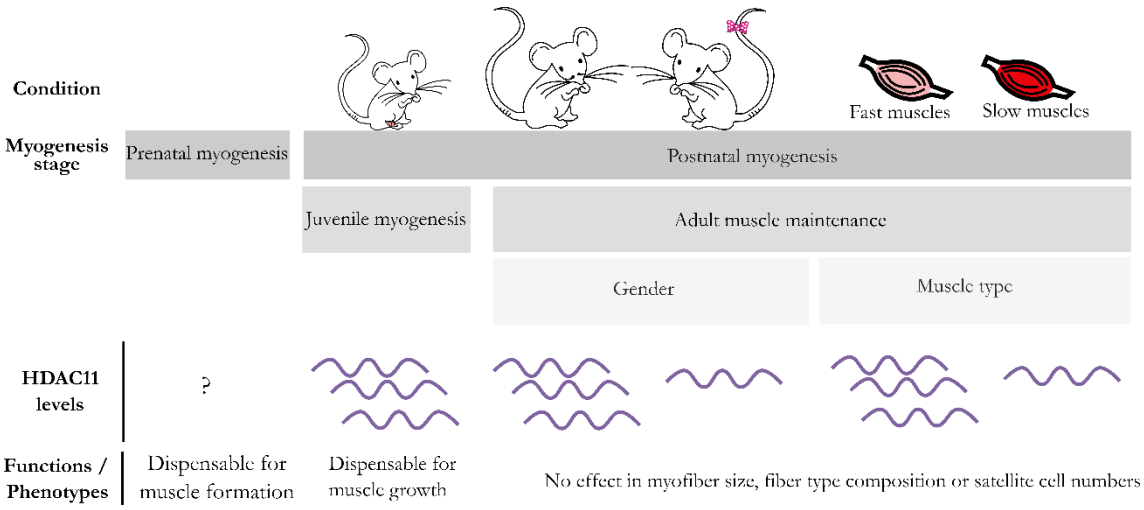

Figure 63. Summary of HDAC11 levels during mice' myogenesis and the observed phenotypes in HDAC11 deficiency mice. Three violet lines represent high HDAC11 levels while one line indicates low HDAC11 expression levels.

HDAC11 deficiency accelerates muscle regeneration

As adult muscle is mostly a quiescent tissue and satellite cells only activate to repair focal damages induced by contraction (Ceafalan et al. 2014; Charge 2004), to assess HDAC11 functions *in vivo* we decided to performed muscle injury to induce extensive *de novo* myogenesis in adult mice. Cardiotoxin injection is one of the best methods to perform a reproducible injury as only destroys myofibers without affecting blood vessels, basal lamina and motoneurons' innervation (Plant et al. 2006; Czerwinska et al. 2012).

The analysis of regenerating regions in HDAC11 wild-type and deficient muscles at 4 days post-injury revealed that HDAC11 deficient mice did not present alterations in the cross-sectional areas of regenerating fibers, their numbers or the expression levels of muscle differentiation factors. These results are in accordance to our *in vitro* results, except that we did not observe a reduced number of nuclei in regenerating myofibers. Interestingly, the expression analysis of some proliferation-related genes (HDAC11 targets found by RNA-seq analysis of differentiating myoblasts), showed the same tendency to be higher expressed at this regeneration point, although we need to increase the number of analyzed animals.

The analysis of HDAC11 deficient regenerating muscles at 7 dpi, revealed that HDAC11 deficient mice presented an increased cross-sectional area of regenerating fibers at this point. This experiment was repeated twice, in one cohort of male mice and in another with female ones, both showing the same increased areas in regenerating myofibers, in both gastrocnemius and tibialis muscles. Just as we observed at 4 dpi, the expression of muscle differentiation factors remained unchanged at this point, and we did not address the expression of proliferation genes because at 7 dpi supposedly most of the myoblasts were differentiating.

Taking into account that our *in vitro* analysis of primary myoblasts showed reduced fusion abilities instead of increasing of their size and the previously described role of HDAC11 in the control of Il-10 expression, we decided to study the immune response in regenerating mice. For that, we chose the point of 4 days post injury as in this point, M1 pro-inflammatory macrophages and M2 anti-inflammatory populations coexist (Tidball 2017). We are currently extending our studies also to the point of 7 dpi.

At 4dpi, we did not find differences in neutrophils or M1 or M2 macrophage numbers between both genotypes. A very recent study that examined blood cell types' numbers in peripheral blood of HDAC11 deficient mice, did neither find different numbers of lymphocytes, monocytes, granulocytes or white blood cells compared to wild-type controls, further indicating that HDAC11 deficiency does not cause alterations in blood cell types' numbers (Sahakian et al. 2017). We quantified Il-10 expression in M1 and M2 macrophages isolated by FACS, observing higher expression of Il-10 in M1 and M2 , according to the previously published results by (Villagra et al. 2009).

Importantly, Il-10 is considered a crucial cytokine that deactivates the M1 phenotype inhibiting the expression of pro-inflammatory cytokines and promoting skeletal muscle regeneration. A study in mdx mice, revealed that ablation of Il-10 increased muscle damage, while treatment with Il-10 reduced the damage extent (Villalta et al. 2011). Moreover, another study of ablation of Il-10 expression in mice after overloading showed a slower regeneration due to amplification of M1 response and myoblast treatment treated with Il-10 showed enhance proliferation capacity without affecting the levels of MYOD or myogenin expression (Deng et al. 2012). Indeed, in *in vivo* time courses, Il-10 expression already starts to increase at day 1, but the peak of higher expression is at day 3 after injury, which coincides with the peak of M2 macrophages present (Tidball 2017). This observation goes in agreement with our results, as at 7 dpi, myoblasts had already been exposed to higher levels of Il-10 while at 4 dpi M1 response is already present (Deng et al. 2012). Moreover, at 21 dpi, when M2 macrophage response has declined, the observed increase in myofiber size is compensated, which also goes in agreement that the observed phenotype is mediated by Il-10 increased expression in HDAC11 deficient macrophages. The levels of HDAC11 during regeneration and observed effects in HDAC11 deficient mice and myoblasts are summarized in Figure 64.

Unfortunately, by now, we had not been able to demonstrate that the advanced regeneration capacity of HDAC11 deficient mice is mediated by Il-10 expression. To determine that, it would be very interesting to transplant to bone marrow of wild-type mice to irradiated deficient mice to see if the increase in regenerating fiber size is lost, and the other way around, to transplant bone marrow from HDAC11 deficient mice to irradiated wild-type mice, to see if the increase in fiber size is maintained. It would be also possible to perform cardiotoxin injury while transducing regenerating muscles of HDAC11 deficient mice with a shRNA against Il-10, perform a knock-out with Cre-lox expression driven by PAX7 promoter to

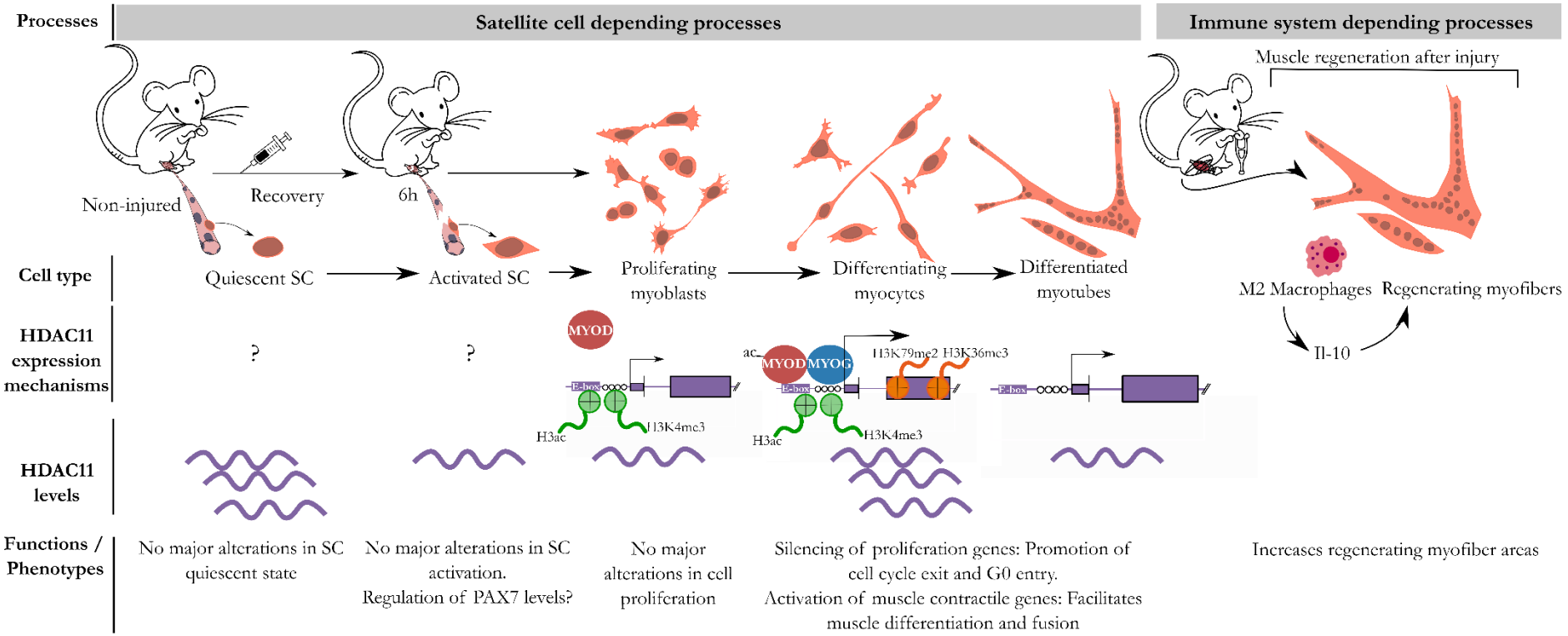

Figure 64. Summary of HDAC11 levels and effects through skeletal muscle regeneration. Three violet lines represent high HDAC11 levels while one line indicates low HDAC11 expression levels.

obtain a HDAC11 knock-out specific of skeletal muscle cells or to perform a double knock-out of HDAC11 and Il-10.

HDAC11 expression in reduced in impaired differentiation conditions

In the very first paper describing HDAC11 (Gao et al. 2002), it was already announced that Sjrh30, a rhabdomyosarcoma cell line, was the cell line which possessed the highest expression of HDAC11 among all tissues and cell types screened. Although for some other cancer types HDAC11 expression and roles has already been ascertained, no further works had brought light to the putative roles of HDAC11 in this pediatric cancer.

Taking into account our results regarding the increase of HDAC11 in murine and human myoblasts through cell differentiation and its involvement in G0 exit and terminal contractile genes expression, we wondered if its expression may be impaired in rhabdomyosarcoma cell lines and samples, which possess an imbalance between proliferation and differentiation capabilities. According to our predictions, HDAC11 is underexpressed in aRMS and eRMS cell lines with respect to normal human muscle tissues, being its expression mostly reduced in eRMS subtype. A recent study has also identified HDAC11 significantly upregulated in 2 aRMS cell lines (Rh28 and Rh30) compared to 4 eRMS (Rh36, Rd, CCA and SMS-CTR) (Tombolan et al. 2017). We investigated if this downregulation of expression might be mediated by DNA hypermethylation of HDAC11 CpGi as had already been reported for many differentiation factors (such in (Huertas-Martínez et al. 2014)). Although our studies need to be extended to further regulatory regions, for example CpGi 60, our results suggest that HDAC11 may not be silenced by DNA methylation. Indeed, we searched for HDAC11 methylation in genome-wide studies with aRMS and eRMS cell lines, not finding differences in HDAC11 probes (Sun et al. 2015).

To exclude that HDAC11 increased expression in aRMS subtype versus eRMS one was driven by PAX3:FOXO1 oncoprotein, we evaluated HDAC11 expression in GSE73483 dataset, which studied the transcriptomic changes after siRNA silencing of PAX3:FOXO1 in Rh4 aRMS cell line at different time points (Ebauer et al. 2007; Bhöm et al. 2016). In all conditions, the expression of HDAC11 remained invariant. Moreover, we examined the expression of HDAC11 in a cohort of 13 PAX3:FOXO1 positive and 14 negative aRMS samples with the result that HDAC11 levels did not change between both conditions (GSE2787, probe ID's 7005 and 700r) (De Pittà et al. 2006).

Another putative mechanism of HDAC11 silencing in aRMS and specifically in eRMS cell lines, derived from our observations of HDAC11 control of expression by MRF binding, can be mediated through impaired MRF binding to HDAC11 regulatory regions or a decrease in MRF transactivation potential. We explored the genome-wide binding profiles of MYOD in normal and Rd eRMS cell line but we did not find a decrease in MYOD binding (MacQuarrie et al. 2013), although a reduction in its transactivation potential could not be discarded. Regarding MYOG binding, it was reported that aRMS samples are mainly positive for myogenin expression while eRMS ones are mostly negative. This fact suggest that aRMS may present a cell differentiation impairment downstream MYOG expression, while eRMS cell lines may be blocked upstream MYOG (Dias et al. 2000). Even more studies are needed about this topic, we hypothesized that aRMS may express higher levels of HDAC11 due to MYOG expression, which may be available to bind to HDAC11 promoter regions and activate its expression, although to a lesser extent than in normal tissues, while the lower or absent MYOG expression in eRMS, may be associated to lower HDAC11 levels. Our results with HDACi treatments in primary murine derived rhabdomyosarcoma cell lines, revealed that only in eRMS subtype the expression of HDAC11 could be increased through inhibition of protein deacetylation. It is possible that HDACi treatment enhances MYOD transactivation potential in eRMS cell line and/or increases MGN expresion, resulting in the upregulation of HDAC11 expression levels. Unfortunately, we have not been able to ascertain by now the effects mediated by HDAC11 in eRMS subtypes. It would be very interesting in the future to investigate if HDAC11 expression restitution in eRMS cell lines may facilitate G0 entry and cell differentiation as it occurs in normal myoblasts, or if its silencing constitutes a passenger event.

Putative involvement of HDAC11 in myopathies

As Il-10 expression was described to be up-regulated in mdx mice (Villalta et al. 2011) and HDAC11 controls Il-10 expression (Villagra et al. 2009), we investigated whether HDAC11 expression was decreased in mdx muscles, finding no differences in muscles from three months old mice. However, as Il-10 treatment has been reported to ameliorate mdx pathology, it would be interesting to address in the future the potential benefit of HDAC11 inhibition to try to increase endogenous Il-10 levels.

To try to identify the putative involvement of HDAC11 in myopathies, we searched for public data of transcriptome analysis of muscle dystrophies, finding HDAC11

downregulated in leukocytes isolated from patients of inclusion body myopathy (Zhu et al. 2012). It is remarkable that HDAC11 expression is dysregulated in inflammatory myopathies and this would be a very interesting field of research to explore in the future, as HDAC11 inhibition has been described for other inflammatory diseases involving HDAC11 and Ill-10 (Lai et al. 2011; Li et al. 2016).

Final thoughts

HDAC11 targets, not only in differentiating myoblasts but also in cancer cells (Thole et al. 2017), comprise crucial genes involved in cell proliferation processes. Thus, HDAC11 has become a promising druggable target altered in many cancer types since the description that its inhibition specifically caused apoptosis in tumoral cells but not in any normal assayed one, considering as normal cells actively dividing cells (Deubzer et al. 2013).

Our results, together with many previous ones, revealed that HDAC11 may be enriched in normal conditions not in proliferation states but in G0 arrested cells from the immune system, heart, brain, muscle and probably most quiescent stem cells. In this sense, more efforts are necessary to further address HDAC11 roles in physiological conditions to assess the benefits of inhibiting HDAC11 in pathological states and try to predict possible adverse effects of class IV specific inhibitors for clinical use when discovered.

CONCLUSIONS

1. HDAC11 is the HDAC member that changes the most its expression at the onset of skeletal muscle differentiation and is the most induced HDAC member at day 1 after induction of differentiation. CRISPR/Cas9 endogenous HDAC11 tagging revealed that HDAC11 RNA levels correlated with protein ones, being HDAC11 protein absent in proliferation conditions and expressed through differentiation.

2. HDAC11 silencing in proliferating conditions is not controlled by CpGi methylation but by MRFs binding. The induction of HDAC11 expression at day 1 of differentiation takes place upon MYOD and MYOG binding to its promoter and is accompanied by an increase in the levels of the active transcription marks H3K4me3, H3K79me2 and H3K36me3. In proliferation conditions, HDAC11 expression is repressed by Class I HDAC mediated deacetylation of MYOD conserved lysines. At day 1 of differentiation, acetylated MYOD and later on, MYOG, bind to the E-boxes present in HDA11 promoter and induce its expression.

3. HDAC11 is not only upregulated in differentiation conditions but in reversible quiescence G0 arrested states and is the HDAC member that changes the most its expression between quiescent and activated satellite cells.

4. Overexpressed HDAC11 is located both in nucleus and cytoplasm of proliferating and differentiating cells. HDAC11 overexpression does not affect cell proliferation or differentiation capabilities but facilitates myoblast fusion. Conversely, HDAC11 deficient myotubes contain fewer nuclei per myotube.

5. Day 1 differentiating HDAC11 deficient myoblasts showed higher expression of proliferation genes and a reduced expression of terminal differentiation genes involved in muscle contraction. The upregulation of proliferation genes correlates with an increase of H3ac levels in their promoter regions.

6. HDAC11 deficient mice are viable, fertile and apparently do not present phenotypic alterations. HDAC11 expression is significantly higher in fast muscles of male mice. Male and female HDAC11 deficient adult muscle mice do not present alterations in growth, their number of satellite cells, myofiber cross-sectional areas or specific slow/fast myosins expression.

7. HDAC11 accelerates muscle regenetation, being the cross-sectional areas of regenerating myofibers bigger in HDAC11 deficient muscles. The analysis of the immune response in regenerating muscles show no differences in the number of neutrophils or macrophages recruited at 4 dpi but at this point, the levels of the anti-inflammatory cytokine Il-10 are significantly higher in HDAC11 deficient muscles.

8. The upregulation of HDAC11 expression through muscle differentiation is conserved in human muscle differentiation. In rhabdomyosarcoma tumors, its expression is significantly downregulated in eRMS subtype.

BIBLIOGRAPHY

Abraham, J. et al., 2014. Lineage of origin in rhabdomyosarcoma informs pharmacological response. *Genes and Development*, 28(14), pp.1578–1591.

Alberts, B. et al., 2002. *Molecular Biology of the Cell*. 4th ed., Garland Science. Available at: https://www.ncbi.nlm.nih.gov/books/NBK21054/.

Alioto, T.S., 2007. U12DB: a database of orthologous U12-type spliceosomal introns. *Nucleic Acids Research*, 35, pp.110–115.

Almada, A.E. & Wagers, A.J., 2016. Molecular circuitry of stem cell fate in skeletal muscle regeneration, ageing and disease. *Nature Reviews Molecular Cell Biology*, 17(5), pp.267–279.

An, C.-I., Dong, Y. & Hagiwara, N., 2011. Genome-wide mapping of Sox6 binding sites in skeletal muscle reveals both direct and indirect regulation of muscle terminal differentiation by Sox6. *BMC Developmental Biology*, 11(1), p.59. Available at: http://bmcdevbiol.biomedcentral.com/articles/10.1186/1471-213X-11-59.

Andrews, S., 2010. FastQC: a quality control tool for high throughput sequence data. Available at: http://www.bioinformatics.babraham.ac.uk/projects/fastqc.

Arányi, T. et al., 2006. The BiSearch web server. *BMC Bioinformatics*, 7(1), p.431. Available at: http://bmcbioinformatics.biomedcentral.com/articles/10.1186/1471-2105-7-431.

Asp, P. et al., 2011. Genome-wide remodeling of the epigenetic landscape during myogenic differentiation. *Proceedings of the National Academy of Sciences of the United States of America*, 108(22), pp.E149-58. Available at: http://www.pubmedcentral.nih.gov/articlerender.fcgi?artid=3107312&tool=pmcentrez&rendertype=abstract.

Bagui, T.K. et al., 2013. Proliferative status regulates HDAC11 mRNA abundance in nontransformed fibroblasts. *Cell Cycle*, 12(21), pp.3433–3441.

Balasubramanian, A. et al., 2014. Fam65b is important for formation of the HDAC6-dysferlin protein complex during myogenic cell differentiation. *FASEB Journal*, 28(7), pp.2955–2969.

Bannister, A.J. & Kouzarides, T., 2011. Regulation of chromatin by histone modifications. *Cell research*, 21(3), pp.381–395. Available at: http://www.pubmedcentral.nih.gov/articlerender.fcgi?artid=3193420&tool=pmcentrez&rendertype=abstract.

Barth, T.K. & Imhof, A., 2010. Fast signals and slow marks: the dynamics of histone modifications. *Trends in Biochemical Sciences*, 35(11), pp.618–626. Available at: http://dx.doi.org/10.1016/j.tibs.2010.05.006.

Beharry, A.W. et al., 2014. HDAC1 activates FoxO and is both sufficient and required for

skeletal muscle atrophy. *Journal of cell science*, 127(Pt 7), pp.1441–53. Available at: http://www.ncbi.nlm.nih.gov/pubmed/24463822.

Bell, S.D. & Botchan, M.R., 2013. The minichromosome maintenance replicative helicase. *Cold Spring Harbor Perspectives in Biology*, 5(11), pp.1–12.

Bentzinger, C.F. et al., 2012. Building Muscle : Molecular Regulation of Myogenesis Building Muscle : Molecular Regulation of Myogenesis.

Berkes, C.A. & Tapscott, S.J., 2005. MyoD and the transcriptional control of myogenesis. *Seminars in Cell and Developmental Biology*, 16(4–5), pp.585–595.

Bettica, P. et al., 2016. Histological effects of givinostat in boys with Duchenne muscular dystrophy. *Neuromuscular disorders : NMD*, 26(10), pp.643–649. Available at: http://www.sciencedirect.com/science/article/pii/S0960896616300694.

Bharathy, N. et al., 2013. Epigenetics: Development and Disease. , 61, pp.139–150. Available at: http://link.springer.com/10.1007/978-94-007-4525-4.

Bharathy, N. et al., 2016. P/CAF mediates PAX3-FOXO1-dependent oncogenesis in alveolar rhabdomyosarcoma. *The Journal of Pathology*, 240(3), pp.269–281. Available at: http://doi.wiley.com/10.1002/path.4773.

Bhöm, M. et al., 2016. Helicase CHD4 is an epigenetic coregulator of PAX3-FOXO1 in alveolar rhabdomyosarcoma. *Journal of Clinical Investigation*, 126(11), pp.4237–4249.

Bird, A. et al., 1985. A fraction of the mouse genome that is derived from islands of nonmethylated, CpG-rich DNA. *Cell*, 40(1), pp.91–99.

Biressi, S. & Rando, T.A., 2010. Heterogeneity in the muscle satellite cell population. *Seminars in Cell and Developmental Biology*, 21(8), pp.845–854. Available at: http://dx.doi.org/10.1016/j.semcdb.2010.09.003.

Black, B.L. & Olson, E.N., 1998. Transcriptional Control of Muscle Development By Myocyte Enhancer Factor-2 (Mef2) Proteins. *Annu. Rev. Cell Dev. Biol*, 14, pp.167–96.

Blais, A. et al., 2005. An initial blueprint for myogenic differentiation An initial blueprint for myogenic differentiation. , pp.553–569.

Blau, H.M. & Epstein, C.J., 1979. Manipulation of myogenesis in vitro: Reversible inhibition by DMSO. *Cell*, 17(1), pp.95–108.

Bobadilla, M. et al., 2014. The CXCR4/SDF1 axis improves muscle regeneration through MMP-10 activity. *Stem cells and development*, 23(12), pp.1417–27. Available at: http://www.pubmedcentral.nih.gov/articlerender.fcgi?artid=4046222&tool=pmcentrez&rendertype=abstract.

Bolden, J.E., Peart, M.J. & Johnstone, R.W., 2006. Anticancer activities of histone deacetylase

inhibitors. *Nat Rev Drug Discov*, 5(9), pp.769–784. Available at: http://www.ncbi.nlm.nih.gov/pubmed/16955068.

Bolger, A.M., Lohse, M. & Usadel, B., 2014. Trimmomatic: a flexible trimmer for Illumina sequence data. *Bioinformatics*, 30(15), pp.2114–2120. Available at: http://dx.doi.org/10.1093/bioinformatics/btu170.

Boyer, J.G. et al., 2014. Myogenic program dysregulation is contributory to disease pathogenesis in spinal muscular atrophy. *Human Molecular Genetics*, 23(16), pp.4249–4259.

Brack, A.S. & Rando, T.A., 2012. Tissue-specific stem cells: Lessons from the skeletal muscle satellite cell. *Cell Stem Cell*, 10(5), pp.504–514. Available at: http://dx.doi.org/10.1016/j.stem.2012.04.001.

Bradbury, C. a et al., 2005. Histone deacetylases in acute myeloid leukaemia show a distinctive pattern of expression that changes selectively in response to deacetylase inhibitors. *Leukemia*, 19(10), pp.1751–1759.

Braun, T. & Arnold, H.H., 1995. Inactivation of Myf-6 and Myf-5 genes in mice leads to alterations in skeletal muscle development. *The EMBO journal*, 14(6), pp.1176–1186.

Braun, T. & Gautel, M., 2011. Transcriptional mechanisms regulating skeletal muscle differentiation, growth and homeostasis. *Nature Reviews Molecular Cell Biology*, 12(6), pp.349–361. Available at: http://www.nature.com/doifinder/10.1038/nrm3118.

Brayer, J.B. et al., 2013. A Novel Role For Histone Deacetylase 11 (HDAC11) In Plasma Cell Differentation and Survival E. Sahakian, ed. *Blood*, 122(21), p.1907 LP-1907. Available at: http://www.bloodjournal.org/content/122/21/1907.abstract.

Broide, R. et al., 2007. Distribution of histone deacetylases 1-11 in the rat brain. *Journal of Molecular Neuroscience*, 31, pp.47–58.

Brzoska, E. et al., 2015. Sdf-1 (CXCL12) induces CD9 expression in stem cells engaged in muscle regeneration. *Stem cell research & therapy*, 6(1), p.46. Available at: http://www.pubmedcentral.nih.gov/articlerender.fcgi?artid=4445299&tool=pmcentrez&rendertype=abstract.

Buckingham, M. & Relaix, F., 2015. PAX3 and PAX7 as upstream regulators of myogenesis. *Seminars in Cell and Developmental Biology*, 44, pp.115–125. Available at: http://dx.doi.org/10.1016/j.semcdb.2015.09.017.

Buglio, D. et al., 2011. HDAC11 plays an essential role in regulating OX40 ligand expression in Hodgkin lymphoma. , 117(10), pp.2910–2917.

Calandra, P. et al., 2016. Allele-specific DNA hypomethylation characterises FSHD1 and

FSHD2. *Journal of Medical Genetics*, p.jmedgenet-2015-103436. Available at: http://jmg.bmj.com/lookup/doi/10.1136/jmedgenet-2015-103436.

Cao, Y. et al., 2010. Genome-wide MyoD Binding in Skeletal Muscle Cells: A Potential for Broad Cellular Reprogramming. *Developmental Cell*, 18(4), pp.662–674. Available at: http://dx.doi.org/10.1016/j.devcel.2010.02.014.

Cao, Y. et al., 2006. Global and gene-specific analyses show distinct roles for Myod and Myog at a common set of promoters. *The EMBO journal*, 25(3), pp.502–11. Available at: http://www.ncbi.nlm.nih.gov/pubmed/16437161%5Cnhttp://www.pubmedcentral.nih.gov/articlerender.fcgi?artid=PMC1383539.

Capecchi, M.R., 2005. Gene targeting in mice: functional analysis of the mammalian genome for the twenty-first century. *Nature reviews. Genetics*, 6(6), pp.507–512.

Carlberg, C. & Molnár, F., 2014. Chapter 2. The impact of chromatin. In *Mechanisms of gene regulation*. Springer, p. 23.

Carrió, E. et al., 2015. Deconstruction of DNA methylation patterns during myogenesis reveals specific epigenetic events in the establishment of the skeletal muscle lineage. *Stem Cells*, 33(6), pp.2025–2036.

Carrió, E., 2015. *DNA Methylation Dynamics during Myogenesis*. University of Barcelona. Available at: http://diposit.ub.edu/dspace/handle/2445/65983.

Casar, J.C. et al., 2004. Transient up-regulation of biglycan during skeletal muscle regeneration: Delayed fiber growth along with decorin increase in biglycan-deficient mice. *Developmental Biology*, 268(2), pp.358–371.

Ceafalan, L.C., Popescu, B.O. & Hinescu, M.E., 2014. Cellular players in skeletal muscle regeneration. *BioMed Research International*, 2014.

Chang, S. et al., 2006. Histone Deacetylase 7 Maintains Vascular Integrity by Repressing Matrix Metalloproteinase 10. *Cell*, 126(2), pp.321–334.

Chang, S. et al., 2004. Histone Deacetylases 5 and 9 Govern Responsiveness of the Heart to a Subset of Stress Signals and Play Redundant Roles in Heart Development. *Molecular and Cellular Biology*, 24(19), pp.8467–8476.

Charge, S.B.P.R.M.A., 2004. Cellular and molecular regulation of muscle regeneration. *Physiol. Rev.*, 84(1), pp.209–238.

Chazaud, B. et al., 2009. Dual and beneficial roles of macrophages during skeletal muscle regeneration. *Exercise and sport sciences reviews*, 37(1), pp.18–22.

Chazaud, B. et al., 2003. Satellite cells attract monocytes and use macrophages as a support to escape apoptosis and enhance muscle growth. *Journal of Cell Biology*, 163(5), pp.1133–

1143.

Chen, E.Y. et al., 2013. Enrichr: interactive and collaborative HTML5 gene list enrichment analysis tool. *BMC bioinformatics*, 14(1), p.128. Available at: http://bmcbioinformatics.biomedcentral.com/articles/10.1186/1471-2105-14-128.

Cheng, F. et al., 2014. Divergent roles of histone deacetylase 6 (HDAC6) and histone deacetylase 11 (HDAC11) on the transcriptional regulation of IL10 in antigen presenting cells. *Molecular Immunology*, 60(1), pp.44–53. Available at: http://dx.doi.org/10.1016/j.molimm.2014.02.019.

Cheung, T.H. et al., 2013. Molecular regulation of stem cell quiescence. *Nature reviews. Molecular cell biology*, 14(6), pp.329–40. Available at: http://www.ncbi.nlm.nih.gov/pubmed/23698583%5Cnhttp://www.pubmedcentral.nih.gov/articlerender.fcgi?artid=PMC3808888.

Cho, O.H. et al., 2015. Contrasting roles for MyoD in organizing myogenic promoter structures during embryonic skeletal muscle development. *Developmental Dynamics*, 244(1), pp.43–55.

Choudhary, C. et al., 2009. Lysine acetylation targets protein complexes and co-regulates major cellular functions. *Science (New York, N.Y.)*, 325(5942), pp.834–40. Available at: http://www.ncbi.nlm.nih.gov/pubmed/19608861.

Christov, C. et al., 2007. Muscle Satellite Cells and Endothelial Cells: Close Neighbors and Privileged Partners. *Molecular biology of the cell*, 18(April), pp.1397–1409.

Ciciliot, S. & Schiaffino, S., 2010. Regeneration of Mammalian Skeletal Muscle : Basic Mechanisms and Clinical Implications. *Current Pharmaceutical Design*, 16, pp.906–914.

Cieśla, M., Dulak, J. & Józkowicz, A., 2014. MicroRNAs and epigenetic mechanisms of rhabdomyosarcoma development. *International Journal of Biochemistry and Cell Biology*, 53, pp.482–492.

Clark, S.J. et al., 2006. DNA methylation: Bisulphite modification and analysis. *Nature Protocols*, 1(5), pp.2353–2364. Available at: http://www.nature.com/doifinder/10.1038/nprot.2006.324.

Cohen, T. V., Cohen, J.E. & Partridge, T.A., 2012. Myogenesis in dysferlin-deficient myoblasts is inhibited by an intrinsic inflammatory response. *Neuromuscular Disorders*, 22(7), pp.648–658.

Collins, C.M., Ellis, J. & Holaska, J.M., 2017. MAPK signaling pathways and HDAC3 activity are disrupted during emerin-null myogenic progenitor differentiation. *Disease Models & Mechanisms*, p.dmm.028787. Available at:

http://dmm.biologists.org/lookup/doi/10.1242/dmm.028787.

Cong, L. & Addgene, 2013. Zhang Lab's CRISPR Frequently Asked Questions. Available at: https://www.addgene.org/crispr/zhang/faq/ [Accessed May 29, 2017].

Consalvi, S. et al., 2011. Histone Deacetylase Inhibitors in the Treatment of Muscular Dystrophies: Epigenetic Drugs for Genetic Diseases. *Molecular Medicine*, 17(5–6), p.1. Available at: http://www.molmed.org/content/pdfstore/11_49_Consalvi.pdf.

Consalvi, S. et al., 2013. Preclinical Studies in the mdx Mouse Model of Duchenne Muscular Dystrophy with the Histone Deacetylase Inhibitor Givinostat Silvia. *Molecular Medicine*, 19(1), pp.79–87. Available at: http://www.molmed.org/content/pdfstore/13_011_Consalvi.pdf.

Constantinides, P., Jones, P. & Gevers, W., 1977. Functional striated muscle cells from non-myoblast precursors following 5-azacytidine treatment. *Nature*, 267, pp.364–366.

Cooper, G., 2000. *The Cell: A Molecular Approach. 2nd edition. Cell Walls and the Extracellular Matrix.*, Sunderland (MA): Sinauer Associates. Available at: https://www.ncbi.nlm.nih.gov/books/NBK9961/.

Corrales-Berjano, M. et al., 2017. Clustering of Drosophila housekeeping promoters facilitates their expression. *Genome research*, p.gr.211433.116. Available at: http://www.ncbi.nlm.nih.gov/pubmed/28420691.

Coulondre, C. et al., 1978. Molecular basis of base substitution hotspots in Escherichia coli. *Nature*, 274(5673), pp.775–780.

Czerwinska, A.M. et al., 2012. Mouse gastrocnemius muscle regeneration after mechanical or cardiotoxin injury. *Folia Histochemica et Cytobiologica*, 50(1), pp.144–153.

Davicioni, E. et al., 2006. Identification of a PAX-FKHR gene expression signature that defines molecular classes and determines the prognosis of alveolar rhabdomyosarcomas. *Cancer Research*, 66(14), pp.6936–6946.

Davis, R., Weintraub, H. & Lassar, A., 1987. Transfection of a DNA locus that mediates the conversion of 10T1 2 fibroblasts to myoblasts. *Cell*, 51(6), pp.987–1000. Available at: http://dx.doi.org/10.1016/0092-8674(86)90507-6.

Daxinger, L., Tapscott, S.J. & van der Maarel, S.M., 2015. Genetic and epigenetic contributors to FSHD. *Current Opinion in Genetics and Development*, 33, pp.56–61.

Deaton, A. & Bird, A., 2011. CpG islands and the regulation of transcription. *Genes & development*, 25(10), pp.1010–1022. Available at: http://genesdev.cshlp.org/content/25/10/1010.short.

Deng, B. et al., 2012. IL-10 Triggers Changes in Macrophage Phenotype That Promote

Muscle Growth and Regeneration. *The Journal of Immunology*, 189(7), pp.3669–3680. Available at: http://www.jimmunol.org/content/189/7/3669.short%5Cnhttp://www.pubmedcentral.nih.gov/articlerender.fcgi?artid=3448810&tool=pmcentrez&rendertype=abstract%5Cnhttp://www.jimmunol.org/cgi/doi/10.4049/jimmunol.1103180.

Deubzer, H.E. et al., 2013. HDAC11 is a novel drug target in carcinomas. *International Journal of Cancer*, 132(9), pp.2200–2208.

Dias, P. et al., 2000. Strong immunostaining for myogenin in rhabdomyosarcoma is significantly associated with tumors of the alveolar subclass. *The American journal of pathology*, 156(2), pp.399–408. Available at: http://www.pubmedcentral.nih.gov/articlerender.fcgi?artid=1850049&tool=pmcentrez&rendertype=abstract.

Dokmanovic, M., Clarke, C. & Marks, P.A., 2007. Histone deacetylase inhibitors: overview and perspectives. *Molecular Cancer Research*, 5(10), pp.981–989. Available at: http://mcr.aacrjournals.org/content/5/10/981%5Cnhttp://mcr.aacrjournals.org/content/5/10/981.full%5Cnhttp://mcr.aacrjournals.org/content/5/10/981.full.pdf%5Cnhttp://www.ncbi.nlm.nih.gov/pubmed/17951399.

Dressel, U. et al., 2001. A Dynamic Role for HDAC7 in MEF2-mediated Muscle Differentiation. *Journal of Biological Chemistry*, 276(20), pp.17007–17013.

Drexler, H.C. a. et al., 2012. On Marathons and Sprints: An Integrated Quantitative Proteomics and Transcriptomics Analysis of Differences Between Slow and Fast Muscle Fibers. *Molecular & Cellular Proteomics*, 11(4), p.M111.010801-M111.010801.

Dumont, N.A., Wang, Y.X. & Rudnicki, M.A., 2015. Intrinsic and extrinsic mechanisms regulating satellite cell function. *Development (Cambridge, England)*, 142(9), pp.1572–1581. Available at: http://www.ncbi.nlm.nih.gov/pubmed/25922523.

Ebauer, M. et al., 2007. Comparative expression profiling identifies an in vivo target gene signature with TFAP2B as a mediator of the survival function of PAX3/FKHR. *Oncogene*, 26(51), pp.7267–81. Available at: http://www.ncbi.nlm.nih.gov/pubmed/17525748.

Eden, E. et al., 2009. GOrilla: a tool for discovery and visualization of enriched GO terms in ranked gene lists. *BMC bioinformatics*, 10(1), p.48. Available at: http://bmcbioinformatics.biomedcentral.com/articles/10.1186/1471-2105-10-48.

Engelhardt, K.R. & Grimbacher, B., 2014. *Interleukin-10 in Health and Disease*, Available at: http://link.springer.com/10.1007/978-3-662-43492-5.

England, J. & Loughna, S., 2013. Heavy and light roles: Myosin in the morphogenesis of the heart. *Cellular and Molecular Life Sciences*, 70(7), pp.1221–1239.

Falkenberg, K.J. & Johnstone, R.W., 2014. Histone deacetylases and their inhibitors in cancer, neurological diseases and immune disorders. *Nature reviews. Drug discovery*, 13(9), pp.673–91. Available at: http://dx.doi.org/10.1038/nrd4360.

Farina, N.H. et al., 2012. A role for RNA post-transcriptional regulation in satellite cell activation. *Skeletal muscle*, 2(1), p.21. Available at: http://www.pubmedcentral.nih.gov/articlerender.fcgi?artid=3563611&tool=pmcentrez&rendertype=abstract.

Fischle, W. et al., 2002. Enzymatic activity associated with class II HDACs is dependent on a multiprotein complex containing HDAC3 and SMRT/N-CoR. *Molecular Cell*, 9(1), pp.45–57.

Fiszman, M. et al., 1980. Expression of myogenic differentiation and myotube dormation of chick myoblasts in the presence of sodium butyrate. , 126, pp.31–37.

Forcales, S. V et al., 2011. Signal-dependent incorporation of MyoD–BAF60c into Brg1-based SWI/SNF chromatin-remodelling complex. *The EMBO Journal*, 31(June), pp.301–316. Available at: http://dx.doi.org/10.1038/emboj.2011.391.

Fraga, M.F. et al., 2005. Loss of acetylation at Lys16 and trimethylation at Lys20 of histone H4 is a common hallmark of human cancer. *Nature genetics*, 37(4), pp.391–400.

Frontera, W.R. & Ochala, J., 2015. Skeletal muscle: a brief review of structure and function. *Calcified tissue international*, 96(3), pp.183–195.

Fukada, S. et al., 2007. Molecular signature of quiescent satellite cells in adult skeletal muscle. *Stem Cells*, 25(10), pp.2448–2459. Available at: http://www.ncbi.nlm.nih.gov/pubmed/17600112.

Di Fulvio, S. et al., 2011. Dysferlin interacts with histone deacetylase 6 and increases alpha-tubulin acetylation. *PLoS ONE*, 6(12).

Gaj, T., 2014. ZFN, TALEN and CRISPR/Cas based methods for genome engineering. *2013*, 31(7), pp.397–405.

Galatioto, J., Mascareno, E. & Siddiqui, M.A.Q., 2010. CLP-1 associates with MyoD and HDAC to restore skeletal muscle cell regeneration. *Journal of Cell Science*, 123(21), pp.3789–3795. Available at: http://jcs.biologists.org/cgi/doi/10.1242/jcs.073387.

Gan, L., Schwengberg, S. & Denecke, B., 2014. Transcriptome analysis in cardiomyocyte-specific differentiation of murine embryonic stem cells reveals transcriptional regulation network. *Gene Expression Patterns*, 16(1), pp.8–22. Available at:

http://dx.doi.org/10.1016/j.gep.2014.07.002.

Gao, C. et al., 2010. Histone deacetylase 7 (HDAC7) regulates myocyte migration and differentiation. *Biochimica et Biophysica Acta - Molecular Cell Research*, 1803(10), pp.1186–1197. Available at: http://dx.doi.org/10.1016/j.bbamcr.2010.06.008.

Gao, L. et al., 2002. Cloning and functional characterization of HDAC11, a novel member of the human histone deacetylase family. *Journal of Biological Chemistry*, 277(28), pp.25748–25755.

García-Alcalde, F. et al., 2012. Qualimap: evaluating next-generation sequencing alignment data. *Bioinformatics*, 28(20), pp.2678–2679. Available at: http://dx.doi.org/10.1093/bioinformatics/bts503.

Gautel, M. & Djinović-Carugo, K., 2016. The sarcomeric cytoskeleton: from molecules to motion. *The Journal of experimental biology*, 219(Pt 2), pp.135–45. Available at: http://www.ncbi.nlm.nih.gov/pubmed/26792323.

Gayraud-Morel, B. et al., 2012. Myf5 haploinsufficiency reveals distinct cell fate potentials for adult skeletal muscle stem cells. *Journal of cell science*, 125(Pt 7), pp.1738–49. Available at: http://www.ncbi.nlm.nih.gov/pubmed/22366456.

Gehlert, S., Bloch, W. & Suhr, F., 2015. Ca2+-dependent regulations and signaling in skeletal muscle: From electro-mechanical coupling to adaptation. *International Journal of Molecular Sciences*, 16(1), pp.1066–1095.

Gilbert, J. et al., 2004. The clinical application of targeting cancer through histone acetylation and hypomethylation. *Clinical Cancer Research*, 10(14), pp.4589–4596.

Gillies, A.R. & Lieber, R.L., 2012. Structure and function of the skeletal muscle extracellular matrix. *Muscle nerve*, 44(3), pp.318–331.

Gokhin, D.S. et al., 2008. Quantitative analysis of neonatal skeletal muscle functional improvement in the mouse. *The Journal of experimental biology*, 211(Pt 6), pp.837–43. Available at: http://www.ncbi.nlm.nih.gov/pubmed/18310108.

Gregoretti, I. V., Lee, Y.M. & Goodson, H. V., 2004. Molecular evolution of the histone deacetylase family: Functional implications of phylogenetic analysis. *Journal of Molecular Biology*, 338(1), pp.17–31.

Greising, S.M. et al., 2013. Systems biology of skeletal muscle: fiber type as an organizing principle. *Wiley Interdiscip Rev Syst Biol Med*, 4(5), pp.1–26.

Grozinger, C.M., Hassig, C. a & Schreiber, S.L., 1999. Three proteins define a class of human histone deacetylases related to yeast Hda1p. *Proceedings of the National Academy of Sciences of the United States of America*, 96(9), pp.4868–4873.

Gryder, B.E., Sodji, Q.H. & Oyelere, A.K., 2012. Targeted cancer therapy: giving histone deacetylase inhibitors all they need to succeed. , 4(4), pp.505–524.

Gundersen, G.G., Khawaja, S. & Bulinski, J.C., 1989. Generation of a stable, posttranslationally modified microtubule array is an early event in myogenic differentiation. *Journal of Cell Biology*, 109(5), pp.2275–2288.

Gundersen, K., Bruusgaard, J.C. & Gundersen, K., 2008. Nuclear domains during muscle atrophy: nuclei lost or paradigm lost? *J Physiol*, 58611, pp.2675–2681.

Gutiérrez, C., 2012. *Análisis funcional de proteínas implicadas en el mantenimiento de la estabilidad cromosómuca en mamíferos*. Universidad de Salamanca. Available at: https://digital.csic.es/handle/10261/135886.

Haberland, M., Mokalled, M.H., et al., 2009. Epigenetic control of skull morphogenesis by histone deacetylase 8 service Epigenetic control of skull morphogenesis by histone deacetylase 8. , pp.1625–1630.

Haberland, M. et al., 2007. Regulation of HDAC9 gene expression by MEF2 establishes a negative-feedback loop in the transcriptional circuitry of muscle differentiation. *Molecular and cellular biology*, 27(2), pp.518–525.

Haberland, M., Montgomery, R.L. & Olson, E.N., 2009. The many roles of histone deacetylases in development and physiology: implications for disease and therapy. *Nature reviews. Genetics*, 10(1), pp.32–42. Available at: http://www.nature.com/nrg/journal/v10/n1/full/nrg2485.html#B4%5Cnhttp://www.ncbi.nlm.nih.gov/pubmed/19065135%5Cnhttp://www.pubmedcentral.nih.gov/articlerender.fcgi?artid=PMC3215088.

Hagiwara, H. et al., 2011. Histone deacetylase inhibitor trichostatin A enhances myogenesis by coordinating muscle regulatory factors and myogenic repressors. *Biochemical and Biophysical Research Communications*, 414(4), pp.826–831. Available at: http://dx.doi.org/10.1016/j.bbrc.2011.10.036.

Han, P. et al., 2011. Chromatin remodeling in cardiovascular development and physiology. *Circulation Research*, 108(3), pp.378–396.

Hansol, L., Habas, R. & Abate-Shen, C., 2004. Msx1 Cooperates with Histone H1b for Inhibition of Transcription and Myogenesis. *Science*, 304(5677), pp.1675–1678. Available at: http://science.sciencemag.org/content/304/5677/1675.abstract%5Cnhttp://www.sciencemag.org/cgi/doi/10.1126/science.1098096.

Harada, A. et al., 2012. Chd2 interacts with H3.3 to determine myogenic cell fate. *The EMBO*

journal, 31(13), pp.2994–3007. Available at: http://dx.doi.org/10.1038/emboj.2012.136%5Cnhttp://www.pubmedcentral.nih.gov/articlerender.fcgi?artid=3395093&tool=pmcentrez&rendertype=abstract.

Henikoff, S., 2005. Histone modifications: combinatorial complexity or cumulative simplicity? *Proceedings of the National Academy of Sciences of the United States of America*, 102(15), pp.5308–5309.

Hettmer, S. et al., 2014. Rhabdomyosarcoma: current challenges and their implications for developing therapies. *Cold Spring Harb Perspect Med*, 4(11), p.a025650. Available at: http://www.ncbi.nlm.nih.gov/pubmed/25368019%5Cnhttp://perspectivesinmedicine.cshlp.org/content/4/11/a025650.full.pdf.

Hirokawa, N. et al., 2009. Kinesin superfamily motor proteins and intracellular transport. *Nature Reviews Molecular Cell Biology*, 10(10), pp.682–696. Available at: http://www.nature.com/doifinder/10.1038/nrm2774.

Hotchkiss, R., 1948. The quantitative separation of purines, pyrimidines, and nucleosides by paper chromatography. *The Journal of biological chemistry*, 175(1), pp.315–332.

Huertas-Martínez, J. et al., 2014. Caveolin-1 is down-regulated in alveolar rhabdomyosarcomas and negatively regulates tumor growth. *Oncotarget*, 5(20), pp.9744–55. Available at: http://www.pubmedcentral.nih.gov/articlerender.fcgi?artid=4259434&tool=pmcentrez&rendertype=abstract.

Hunger, C., Ödemis, V. & Engele, J., 2012. Expression and function of the SDF-1 chemokine receptors CXCR4 and CXCR7 during mouse limb muscle development and regeneration. *Experimental Cell Research*, 318(17), pp.2178–2190.

Iezzi, S. et al., 2004. Deacetylase inhibitors increase muscle cell size by promoting myoblast recruitment and fusion through induction of follistatin. *Developmental Cell*, 6(5), pp.673–684.

Iezzi, S. et al., 2002. Stage-specific modulation of skeletal myogenesis by inhibitors of nuclear deacetylases. *Proceedings of the National Academy of Sciences of the United States of America*, 99(11), pp.7757–62. Available at: http://www.pubmedcentral.nih.gov/articlerender.fcgi?artid=124343&tool=pmcentrez&rendertype=abstract.

Inoue, A. & Fujimoto, D., 1969. Enzymatic deacetylation of histone. *Biochemical and Biophysical Research Communications*, 36, pp.146–150.

Irizarry, R.A. et al., 2009. The human colon cancer methylome shows similar hypo- and

hypermethylation at conserved tissue-specific CpG island shores. *Nat Genet*, 41(2), pp.178–186. Available at: http://www.ncbi.nlm.nih.gov/entrez/query.fcgi?cmd=Retrieve&db=PubMed&dopt=Citation&list_uids=19151715.

Johnston, L., Tapscott, S. & Eisen, H., 1992. Sodium butyrate inhibits myogenesis by interfering with the transcriptional activation of MyoD and Myogenin. *Molecular and Cellular Biology*, 12(11), pp.5123–5130.

Jones, P.A., 2012. Functions of DNA methylation: islands, start sites, gene bodies and beyond. *Nature Reviews Genetics*, 13(7), pp.484–492. Available at: http://dx.doi.org/10.1038/nrg3230.

Joshi, P. et al., 2013. The functional interactome landscape of the human histone deacetylase family. *Molecular systems biology*, 9(672), p.672. Available at: /Users/yurikoharigaya/Documents/ReadCube Media/joshi2013.pdf%5Cnhttp://dx.doi.org/10.1038/msb.2013.26%5Cnhttp://www.ncbi.nlm.nih.gov/pubmed/23752268%5Cnhttp://www.pubmedcentral.nih.gov/articlerender.fcgi?artid=PMC3964310.

Jung, M.O. & Bakin, R.E., 2008. HDAC2 Cytoplasmic Sequestration Potentiates Keratinocyte Terminal Differentiation. *The Open Cell Development & Biology Journal*, 1, pp.1–9.

Juríková, M. et al., 2016. Ki67, PCNA, and MCM proteins: Markers of proliferation in the diagnosis of breast cancer. *Acta Histochemica*, 118(5), pp.544–552.

Kablar, B. et al., 2003. Myf5 and MyoD activation define independent myogenic compartments during embryonic development. *Developmental Biology*, 258(2), pp.307–318.

Kagey, M.H. et al., 2010. Mediator and Cohesin Connect Gene Expression and Chromatin Architecture. *Young*, 467(7314), pp.430–435.

Kaimori, J. et al., 2016. Histone H4 lysine 20 acetylation is associated with gene repression in human cells. *Nature Publishing Group*, (April), pp.1–10. Available at: http://dx.doi.org/10.1038/srep24318.

Karalaki, M. et al., 2009. Muscle regeneration: cellular and molecular events. *In vivo (Athens, Greece)*, 23(5), pp.779–96. Available at: http://www.ncbi.nlm.nih.gov/pubmed/19779115.

Kassar-Duchossoy, L. et al., 2004. Letters To Nature. *Nature*, 431(September), pp.466–471.

Keedy, K.S. et al., 2009. A limited group of class I histone deacetylases acts to repress human

immunodeficiency virus type 1 expression. *Journal of virology*, 83(10), pp.4749–56. Available at: http://jvi.asm.org/content/83/10/4749.full.

Keefe, A.C. et al., 2015. Muscle stem cells contribute to myofibres in sedentary adult mice. *Nature communications*, 6(May), p.7087. Available at: http://www.nature.com/ncomms/2015/150514/ncomms8087/full/ncomms8087.html.

Keller, C. & Guttridge, D.C., 2013. Mechanisms of impaired differentiation in rhabdomyosarcoma. *FEBS Journal*, 280(17), pp.4323–4334.

Kelly, R.D.W. & Cowley, S.M., 2013. The physiological roles of histone deacetylase (HDAC) 1 and 2: complex co-stars with multiple leading parts. *Biochemical Society transactions*, 41(3), pp.741–9. Available at: http://www.biochemsoctrans.org/bst/041/0741/bst0410741.htm.

Kim, H.J. & Bae, S.C., 2011. Histone deacetylase inhibitors: molecular mechanisms of action and clinical trials as anti-cancer drugs. *Am J Transl Res*, 3(2), pp.166–179. Available at: http://www.ncbi.nlm.nih.gov/pubmed/21416059.

Kim, J.I. et al., 2013. Gender-specific role of HDAC11 in kidney ischemia- and reperfusion-induced PAI-1 expression and injury. *American journal of physiology. Renal physiology*, 305(1), pp.F61-70. Available at: http://www.ncbi.nlm.nih.gov/pubmed/23657855.

Kim, J.Y. & Casaccia, P., 2010. HDAC1 in axonal degeneration: A matter of subcellular localization. *Cell Cycle*, 9(18), pp.3680–3684.

Kitzmann, M. et al., 1998. The muscle regulatory factors MyoD and Myf-5 undergo distinct cell cycle-specific expression in muscle cells. *Journal of Cell Biology*, 142(6), pp.1447–1459.

Kizuka, Y. et al., 2014. Epigenetic regulation of a brain-specific glycosyltransferase N-acetylglucosaminyltransferase-IX (GnT-IX) by specific chromatin modifiers. *Journal of Biological Chemistry*, 289(16), pp.11253–11261.

Knapp, J.R. et al., 2006. Loss of myogenin in postnatal life leads to normal skeletal muscle but reduced body size. *Development (Cambridge, England)*, 133, pp.601–610.

Kooistra, S.M. & Helin, K., 2012. Molecular mechanisms and potential functions of histone demethylases. *Nature Reviews Molecular Cell Biology*, 13(5), pp.297–311. Available at: http://www.nature.com/doifinder/10.1038/nrm3327.

Koressaar, T. & Remm, M., 2007. Enhancements and modifications of primer design program Primer3. *Bioinformatics*, 23(10), pp.1289–1291. Available at: http://dx.doi.org/10.1093/bioinformatics/btm091.

Kowalski, K. et al., 2015. Stromal derived factor-1 and granulocyte-colony stimulating factor

treatment improves regeneration of *Pax7* −/− mice skeletal muscles. *Journal of Cachexia, Sarcopenia and Muscle*, (November 2015), p.n/a-n/a. Available at: http://doi.wiley.com/10.1002/jcsm.12092.

Kuang, S. et al., 2009. Asymmetric self-renewal and commitment of satellite stem cells in muscle. *Cell*, 129(5), pp.999–1010.

Kuang, S. & Rudnicki, M.A., 2008. The emerging biology of satellite cells and their therapeutic potential. *Trends in Molecular Medicine*, 14(2), pp.82–91.

Kuleshov, M. V et al., 2016. Enrichr: a comprehensive gene set enrichment analysis web server 2016 update. *Nucleic Acids Research*, 44(W1), pp.W90–W97. Available at: http://dx.doi.org/10.1093/nar/gkw377.

Kushwaha, P.P., Rapalli, K.C. & Kumar, S., 2016. Geminin a multi task protein involved in cancer pathophysiology and developmental process: A review. *Biochimie*, 131, pp.115–127. Available at: http://www.sciencedirect.com/science/article/pii/S0300908416302206 [Accessed May 31, 2017].

Lagger, G. et al., 2002. Essential function of histone deacetylase 1 in proliferation control and CDK inhibitor repression. *EMBO Journal*, 21(11), pp.2672–2681.

Lahm, A. et al., 2007. Unraveling the hidden catalytic activity of vertebrate class IIa histone deacetylases. *Proceedings of the National Academy of Sciences of the United States of America*, 104(44), pp.17335–40. Available at: http://www.pubmedcentral.nih.gov/articlerender.fcgi?artid=2077257&tool=pmcentrez&rendertype=abstract.

Lai, X. et al., 2011. Advantages of Promoting Interleukin-10 by Silence of Histone Deacetylase 11 in Inducing Tolerance in Orthotopic Liver Transplantation in Rats. *Transplantation proceedings*, 43(7), pp.2728–2732. Available at: http://www.transplantation-proceedings.org/article/S0041-1345(11)00842-6/pdf.

Laing, N.G. & Nowak, K.J., 2005. When contractile proteins go bad: The sarcomere and skeletal muscle disease. *BioEssays*, 27(8), pp.809–822.

Lassar, A. et al., 1991. Functional activity of myogenic HLH proteins requires hetero-oligomerization with E12/E47-like proteins in vivo. *Cell*, 66(2), pp.305–315.

Laumonier, T. & Menetrey, J., 2016. Muscle injuries and strategies for improving their repair. *Journal of Experimental Orthopaedics*, 3(1), p.15. Available at: http://jeo-esska.springeropen.com/articles/10.1186/s40634-016-0051-7.

Lee, M.H. et al., 2011. Histone methyltransferase KMT1A restrains entry of alveolar

rhabdomyosarcoma cells into a myogenic differentiated state. *Cancer Research*, 71(11), pp.3921–3931.

de Lera, A.R. & Ganesan, A., 2016. Epigenetic polypharmacology: from combination therapy to multitargeted drugs. *Clinical Epigenetics*, 8(1), p.105. Available at: http://clinicalepigeneticsjournal.biomedcentral.com/articles/10.1186/s13148-016-0271-9.

Li, K. et al., 2014. Optimization of genome engineering approaches with the CRISPR/Cas9 system. *PLoS ONE*, 9(8).

Li, L.-C. & Dahiya, R., 2002. MethPrimer: designing primers for methylation PCRs. *Bioinformatics (Oxford, England)*, 18(11), pp.1427–1431.

Li, M. et al., 2016. Interleukin-13 suppresses interleukin-10 via inhibiting A20 in peripheral B cells of patients with food allergy. , pp.1–11.

Li, Q., Foote, M. & Chen, J., 2014. Effects of histone deacetylase inhibitor valproic acid on skeletal myocyte development. *Scientific Reports*, 4, p.7207. Available at: http://www.nature.com/doifinder/10.1038/srep07207.

Liao, Y., Smyth, G.K. & Shi, W., 2014. featureCounts: an efficient general purpose program for assigning sequence reads to genomic features. *Bioinformatics*, 30(7), pp.923–930. Available at: http://dx.doi.org/10.1093/bioinformatics/btt656.

Lin, L. et al., 2013. Type I IFN inhibits innate IL-10 production in macrophages through histone deacetylase 11 by downregulating microRNA-145. *Journal of immunology (Baltimore, Md.: 1950)*, 191(7), pp.3896–904. Available at: http://www.ncbi.nlm.nih.gov/pubmed/23980205.

Lindberg, D., Åkerström, G. & Westin, G., 2007. Mutational analyses of WNT7A and HDAC11 as candidate tumour suppressor genes in sporadic malignant pancreatic endocrine tumours. *Clinical Endocrinology*, 66(1), pp.110–114.

Liu, F. et al., 2017. Vitamin D3 induces vitamin D receptor and HDAC11 binding to relieve the promoter of the tight junction proteins. , pp.1–9.

Liu, H. et al., 2007. Developmental Expression of Histone Deacetylase 11 in the Murine Brain. *Journal of neuroscience research*, 86, pp.537–543.

Liu, H. et al., 2009. Histone deacetylase 11 regulates oligodendrocyte-specific gene expression and cell development in OL-1 oligodendroglia cells. *Glia*, 57(1), pp.1–12.

Liu, X.S. et al., 2016. Editing DNA Methylation in the Mammalian Genome. *Cell*, 167(1), pp.233–247. Available at: http://dx.doi.org/10.1016/j.cell.2016.08.056.

Llano, E. et al., 2008. Shugoshin-2 is essential for the completion of meiosis but not for

mitotic cell division in mice. *Genes and Development*, 22(17), pp.2400–2413.

Long, C. et al., 2014. Prevention of muscular dystrophy in mice by CRISPR/Cas9-mediated editing of germline DNA. *Science (New York, N.Y.)*, 345(6201), pp.1184–8. Available at: http://www.pubmedcentral.nih.gov/articlerender.fcgi?artid=4398027&tool=pmcentrez&rendertype=abstract.

Love, M.I., Huber, W. & Anders, S., 2014. Moderated estimation of fold change and dispersion for RNA-seq data with DESeq2. *Genome biology*, 15(12), p.550. Available at: http://genomebiology.biomedcentral.com/articles/10.1186/s13059-014-0550-8.

Lozada, E.M. et al., 2016. Acetylation and deacetylation of Cdc25A constitutes a novel mechanism for modulating Cdc25A functions with implications for cancer. *Oncotarget*, 7(15). Available at: http://www.oncotarget.com/abstract/7966.

Lu, J. et al., 2000. Regulation of Skeletal Myogenesis by Association of the MEF2 Transcription Factor with Class II Histone Deacetylases. *Molecular Cell*, 6(2), pp.233–244.

Luo, W. & Brouwer, C., 2013. Pathview: An R/Bioconductor package for pathway-based data integration and visualization. *Bioinformatics*, 29(14), pp.1830–1831.

MacQuarrie, K.L. et al., 2013. Comparison of genome-wide binding of MyoD in normal human myogenic cells and rhabdomyosarcomas identifies regional and local suppression of promyogenic transcription factors. *Molecular and cellular biology*, 33(4), pp.773–84. Available at: http://mcb.asm.org/content/33/4/773.full.

Mahdy, M.A.A., Waritaa, K. & Hosaka, Y.Z., 2016. Early ultrastructural events of skeletal muscle damage following cardiotoxin-induced injury and glycerol-induced injury. *Micron*, 91, pp.29–40. Available at: http://dx.doi.org/10.1016/j.micron.2016.09.009.

Mahoney, S.E. et al., 2012. Genome-wide DNA methylation studies suggest distinct DNA methylation patterns in pediatric embryonal and alveolar rhabdomyosarcomas. *Epigenetics*, 7(4), pp.400–408.

Mal, A. et al., 2001. A role for histone deacetylase HDAC1 in modulating the ... *The EMBO journal*, 20(7), pp.1739–1753.

Mal, A. & Harter, M.L., 2003. MyoD is functionally linked to the silencing of a muscle-specific regulatory gene prior to skeletal myogenesis. *Proceedings of the National Academy of Sciences of the United States of America*, 100(4), pp.1735–1739.

Malam, Z. & Cohn, R.D., 2014. Stem cells on alert: Priming quiescent stem cells after remote injury. *Cell Stem Cell*, 15(1), pp.7–8. Available at: http://dx.doi.org/10.1016/j.stem.2014.06.012.

Mali, P. et al., 2013. RNA-Guided Human Genome. , (February), pp.823–827. Available at: file:///E:/papers/823.full.pdf.

Mallona, I. et al., 2017. Chainy, an universal tool for standardized relative quantification in real-time PCR. *Bioinformatics*, p.btw839. Available at: http://bioinformatics.oxfordjournals.org/lookup/doi/10.1093/bioinformatics/btw839.

Mallona, I., Díez-Villanueva, A. & Peinado, M.A., 2014. Methylation plotter: a web tool for dynamic visualization of DNA methylation data. *Source code for biology and medicine*, 9(1), p.11. Available at: http://www.scfbm.org/content/9/1/11.

Mann, C.J. et al., 2011. Aberrant repair and fibrosis development in skeletal muscle. *Skeletal muscle*, 1(1), p.21. Available at: http://www.pubmedcentral.nih.gov/articlerender.fcgi?artid=3156644&tool=pmcentrez&rendertype=abstract.

Marshall, A.D. & Grosveld, G.C., 2012. Alveolar rhabdomyosarcoma - The molecular drivers of PAX3/7-FOXO1-induced tumorigenesis. *Skeletal muscle*, 2(1), p.25. Available at: http://www.pubmedcentral.nih.gov/articlerender.fcgi?artid=3564712&tool=pmcentrez&rendertype=abstract.

Maruyama, T. et al., 2016. Increasing the efficiency of precise genome editing with CRISPR-Cas9 by inhibition of nonhomologous end joining. *Nature Biotechnology*, 34(2), pp.210–210. Available at: http://www.nature.com/doifinder/10.1038/nbt0216-210c.

Marx, V., 2012. Epigenetics: Reading the second genomic code. *Nature*, 491, pp.143–147.

Matsakas, A. & Patel, K., 2009. Skeletal muscle fibre plasticity in response to. *Histology & Histopathology*, pp.611–629.

Maunakea, A.K. et al., 2013. Intragenic DNA methylation modulates alternative splicing by recruiting MeCP2 to promote exon recognition. *Cell research*, 23(11), pp.1256–69. Available at: http://www.pubmedcentral.nih.gov/articlerender.fcgi?artid=3817542&tool=pmcentrez&rendertype=abstract.

Mauro, A., 1961. Satellite cell of skeletal muscle fibers. *The Journal of biophysical and biochemical cytology*, 9, pp.493–495.

Meadows, E. et al., 2008. Myogenin regulates a distinct genetic program in adult muscle stem cells. *Developmental Biology*, 322(2), pp.406–414. Available at: http://dx.doi.org/10.1016/j.ydbio.2008.07.024.

van der Meer, S., Jaspers, R. & Degens, H., 2011. Is the myonuclear domain size fixed? *Journal*

of Musculoskeletal Neuronal Interactions, 11(4), pp.286–297.

Megeney, L.A. et al., 1996. MyoD is required for myogenic stem cell function in adult skeletal muscle. *Genes and Development*, 10(10), pp.1173–1183.

Minetti, G.C. et al., 2006. Functional and morphological recovery of dystrophic muscles in mice treated with deacetylase inhibitors. *Nature medicine*, 12(10), pp.1147–1150.

Missiaglia, E. et al., 2009. Genomic imbalances in rhabdomyosarcoma cell lines affect expression of genes frequently altered in primary tumors: an approach to identify candidate genes involved in tumor development. *Genes, chromosomes & cancer*, 48, pp.455–467.

Montarras, D., L'Honoré, A. & Buckingham, M., 2013. Lying low but ready for action: The quiescent muscle satellite cell. *FEBS Journal*, 280(17), pp.4036–4050.

Montgomery, R.L. et al., 2007. Histone deacetylases 1 and 2 redundantly regulate cardiac morphogenesis, growth, and contractility. *Genes and Development*, 21(14), pp.1790–1802.

Montgomery, R.L. et al., 2008. Maintenance of cardiac energy metabolism by histone deacetylase 3 in mice. *Journal of Clinical Investigation*, 118(11), pp.3588–3597.

Moore, L.D., Le, T. & Fan, G., 2013. DNA methylation and its basic function. *Neuropsychopharmacology : official publication of the American College of Neuropsychopharmacology*, 38(1), pp.23–38. Available at: http://www.pubmedcentral.nih.gov/articlerender.fcgi?artid=3521964&tool=pmcentrez&rendertype=abstract.

Moresi, V. et al., 2012. Histone deacetylases 1 and 2 regulate autophagy flux and skeletal muscle homeostasis in mice. *Proceedings of the National Academy of Sciences*, 109(5), pp.1649–1654.

Morrison, B.E. & D'Mello, S.R., 2008. Polydactyly in mice lacking HDAC9/HDRP. *Experimental biology and medicine (Maywood, N.J.)*, 233(8), pp.980–8. Available at: http://www.pubmedcentral.nih.gov/articlerender.fcgi?artid=2656257&tool=pmcentrez&rendertype=abstract.

Mukherjee, S. et al., 2014. Imipramine Exploits Histone Deacetylase 11 To Increase the IL-12/IL-10 Ratio in Macrophages Infected with Antimony-Resistant Leishmania donovani and Clears Organ Parasites in Experimental Infection. *Journal of Immunology*, 193(8), pp.4083–4094. Available at: http://www.jimmunol.org/content/193/8/4083.full.pdf.

Munshi, N. V., 2016. CRISPR (Clustered Regularly Interspaced Palindromic Repeat)/Cas9 System. *Circulation*, 134(11), pp.777–779. Available at:

http://circ.ahajournals.org/lookup/doi/10.1161/CIRCULATIONAHA.116.024007.

Musarò, A., 2014. The Basis of Muscle Regeneration. *Advances in biology*, 2014(Table 1), pp.1–16.

NCBI, Homologene. Available at: https://www.ncbi.nlm.nih.gov/homologene/11743.

Neal, A., Boldrin, L. & Morgan, J.E., 2012. The satellite cell in male and female, developing and adult mouse muscle: Distinct stem cells for growth and regeneration. *PLoS ONE*, 7(5), pp.1–11.

Nebbioso, A. et al., 2009. Selective class II HDAC inhibitors impair myogenesis by modulating the stability and activity of HDAC-MEF2 complexes. *EMBO Rep*, 10(7), pp.776–782. Available at: http://www.ncbi.nlm.nih.gov/pubmed/19498465.

Nervi, C. et al., 2001. Inhibition of Histone Deacetylase Activity by Trichostatin A Modulates Gene Expression during Mouse Embryogenesis without Apparent Toxicity 1. *Cell Research*, pp.1247–1249.

Ngo, T.T.M. et al., 2016. Effects of cytosine modifications on DNA flexibility and nucleosome mechanical stability. *Nature communications*, 7, p.10813. Available at: http://www.nature.com/doifinder/10.1038/ncomms10813%5Cnhttp://www.ncbi.nlm.nih.gov/pubmed/26905257.

Novak, M.L., Weinheimer-Haus, E.M. & Koh, T.J., 2014. Macrophage activation and skeletal muscle healing following traumatic injury. *The Journal of pathology*, 232(3), pp.344–55. Available at: http://www.ncbi.nlm.nih.gov/pubmed/24255005.

Oberdoerffer, P. & Sinclair, D.A., 2007. The role of nuclear architecture in genomic instability and ageing. *Nat Rev Mol Cell Biol*, 8(9), pp.692–702. Available at: http://www.ncbi.nlm.nih.gov/pubmed/17700626.

Ohkawa, Y., Marfella, C.G.A. & Imbalzano, A.N., 2006. Skeletal muscle specification by myogenin and Mef2D via the SWI/SNF ATPase Brg1. *The EMBO journal*, 25(3), pp.490–501.

Olguin, H. & Olwin, B., 2012. Pax-7 up-regulation inhibits myogenesis and cell cycle progression in satellite cells: a potential mechanism for self- renewal. *Developmental biology*, 275(2), pp.375–388.

Owens, J., Moreira, K. & Bain, G., 2013. Characterization of primary human skeletal muscle cells from multiple commercial sources. *In vitro cellular & developmental biology. Animal*, 49(9), pp.695–705. Available at: http://www.pubmedcentral.nih.gov/articlerender.fcgi?artid=3824271&tool=pmcentrez&rendertype=abstract.

Di Padova, M. et al., 2007. MyoD acetylation influences temporal patterns of skeletal muscle gene expression. *Journal of Biological Chemistry*, 282(52), pp.37650–37659.

Paix, A. et al., 2014. Scalable and versatile genome editing using linear DNAs with microhomology to Cas9 sites in Caenorhabditis elegans. *Genetics*, 198(4), pp.1347–1356.

Pallafacchina, G. et al., 2010. An adult tissue-specific stem cell in its niche: A gene profiling analysis of in vivo quiescent and activated muscle satellite cells. *Stem Cell Research*, 4(2), pp.77–91. Available at: http://dx.doi.org/10.1016/j.scr.2009.10.003.

Pasut, A., Jones, A.E. & Rudnicki, M.A., 2013. Isolation and culture of individual myofibers and their satellite cells from adult skeletal muscle. *Journal of visualized experiments : JoVE*, (73), p.e50074. Available at: http://www.pubmedcentral.nih.gov/articlerender.fcgi?artid=3639710&tool=pmcentrez&rendertype=abstract.

Perdiguero, E. et al., 2011. p38/MKP-1-regulated AKT coordinates macrophage transitions and resolution of inflammation during tissue repair. *Journal of Cell Biology*, 195(2), pp.307–322.

Petrie, K. et al., 2003. The histone deacetylase 9 gene encodes multiple protein isoforms. *Journal of Biological Chemistry*, 278(18), pp.16059–16072.

Pette, D. & Staron, R.S., 2000. Myosin isoforms, muscle fiber types, and transitions1. *Microsc.Res.Tech.*, 50(6), pp.500–509.

De Pittà, C. et al., 2006. Gene expression profiling identifies potential relevant genes in alveolar rhabdomyosarcoma pathogenesis and discriminates PAX3-FKHR positive and negative tumors. *International Journal of Cancer*, 118(11), pp.2772–2781.

Plant, D.R., Colarossi, F.E. & Lynch, G.S., 2006. Notexin causes greater myotoxic damage and slower functional repair in mouse skeletal muscles than bupivacaine. *Muscle and Nerve*, 34(5), pp.577–585.

Potthoff, M.J. et al., 2007. Histone deacetylase degradation and MEF2 activation promote the formation of slow-twitch myofibers. *Journal of Clinical Investigation*, 117(9), pp.2459–2467.

Puri, P.L. et al., 2001. Class I histone deacetylases sequentially interact with MyoD and pRb during skeletal myogenesis. *Molecular Cell*, 8(4), pp.885–897.

Rahimov, F. & Kunkel, L.M., 2013. The cell biology of disease: cellular and molecular mechanisms underlying muscular dystrophy. *The Journal of cell biology*, 201(4), pp.499–510. Available at: http://www.pubmedcentral.nih.gov/articlerender.fcgi?artid=3653356&tool=pmcentr

ez&rendertype=abstract.

Ran, F.A. et al., 2013. Genome engineering using the CRISPR-Cas9 system. *Nature protocols*, 8(11), pp.2281–308. Available at: http://www.ncbi.nlm.nih.gov/pubmed/24157548%5Cnhttp://www.pubmedcentral.nih.gov/articlerender.fcgi?artid=3969860&tool=pmcentrez&rendertype=abstract%5Cnhttp://www.ncbi.nlm.nih.gov/pubmed/24157548%5Cnhttp://www.nature.com/nprot/journal/v8/n11/abs/nprot.2013.143.h.

Reardon, S., 2016. First CRISPR clinical trial gets green light from US panel. *Nature News*. Available at: http://www.nature.com/news/first-crispr-clinical-trial-gets-green-light-from-us-panel-1.20137.

Reardon, S., 2014. Gene-editing method tackles HIV in first clinical test. *Nature News*. Available at: http://www.nature.com/news/gene-editing-method-tackles-hiv-in-first-clinical-test-1.14813.

Reardon, S., 2015. Leukaemia success heralds wave of gene-editing therapies. *Nature*, 527(7577), pp.146–147. Available at: http://www.nature.com/doifinder/10.1038/nature.2015.18737.

Reggiani, C. & Kronnie, T. Te, 2006. RyR isoforms and fibre type-specific expression of proteins controlling intracellular calcium concentration in skeletal muscles. *Journal of Muscle Research and Cell Motility*, 27(5–7), pp.327–335.

Reinhold, W.C. et al., 2011. Identification of a predominant co-regulation among kinetochore genes, prospective regulatory elements, and association with genomic instability. *PLoS ONE*, 6(10), pp.1–11.

Relaix, F. et al., 2005. A Pax3/Pax7-dependent population of skeletal muscle progenitor cells. *Nature*, 435(7044), pp.948–53. Available at: http://www.ncbi.nlm.nih.gov/pubmed/15843801.

Relaix, F. & Zammit, P.S., 2012. Satellite cells are essential for skeletal muscle regeneration: the cell on the edge returns centre stage. *Development*, 139(16), pp.2845–56. Available at: http://www.ncbi.nlm.nih.gov/pubmed/22833472.

Ren, Y.X. et al., 2008. Mouse mesenchymal stem cells expressing PAX-FKHR form alveolar rhabdomyosarcomas by cooperating with secondary mutations. *Cancer Research*, 68(16), pp.6587–6597.

Rigamonti, E. et al., 2014. Macrophage plasticity in skeletal muscle repair. *BioMed Research International*, 2014.

Riggs, A.D., Martienssen, R.A. & Russo, V.E., 1996. Introduction. *Epigenetic mechanisms of gene*

regulation, pp.0–4. Available at: https://cshmonographs.org/index.php/monographs/issue/view/087969490.32.

Rios, A.C. & Marcelle, C., 2009. Head Muscles: Aliens Who Came in from the Cold? *Developmental Cell*, 16(6), pp.779–780. Available at: http://dx.doi.org/10.1016/j.devcel.2009.06.004.

Rocheteau, P. et al., 2012. A subpopulation of adult skeletal muscle stem cells retains all template DNA strands after cell division. *Cell*, 148(1–2), pp.112–125. Available at: http://dx.doi.org/10.1016/j.cell.2011.11.049.

Rodgers, J.T. et al., 2014. mTORC1 controls the adaptive transition of quiescent stem cells from G0 to G(Alert). *Nature*, 509(7505), pp.393–6. Available at: http://www.ncbi.nlm.nih.gov/pubmed/24870234.

Rokach, O. et al., 2015. Epigenetic changes as a common trigger of muscle weakness in congenital myopathies. *Human Molecular Genetics*, 24(16), pp.4636–4647.

Romualdi, C. et al., 2006. Defining the gene expression signature of rhabdomyosarcoma by meta-analysis. *BMC Genomics*, 7(1), p.287. Available at: http://bmcgenomics.biomedcentral.com/articles/10.1186/1471-2164-7-287.

de Ruijter, A.J.M. et al., 2003. Histone deacetylases (HDACs): characterization of the classical HDAC family. *The Biochemical journal*, 370(Pt 3), pp.737–49. Available at: http://www.pubmedcentral.nih.gov/articlerender.fcgi?artid=1223209&tool=pmcentrez&rendertype=abstract.

Rumman, M., Dhawan, J. & Kassem, M., 2015. Concise Review: Quiescence in Adult Stem Cells: Biological Significance and Relevance to Tissue Regeneration. *Stem cells (Dayton, Ohio)*, 33, pp.2903–2912. Available at: http://www.ncbi.nlm.nih.gov/pubmed/17690176.

Rybalko, V.Y. et al., 2015. Controlled delivery of SDF-1α and IGF-1: CXCR4 $^{+}$ cell recruitment and functional skeletal muscle recovery. *Biomater. Sci.*, 3(11), pp.1475–1486. Available at: http://xlink.rsc.org/?DOI=C5BM00233H.

Saade, E. & Ogryzko, V. V, 2014. Epigenetics: What It Is About? , 30, pp.3–9.

Sachidanandan, C., Sambasivan, R. & Dhawan, J., 2002. Tristetraprolin and LPS-inducible CXC chemokine are rapidly induced in presumptive satellite cells in response to skeletal muscle injury. *J Cell Sci*, 115(Pt 13), pp.2701–2712. Available at: http://www.ncbi.nlm.nih.gov/entrez/query.fcgi?cmd=Retrieve&db=PubMed&dopt=Citation&list_uids=12077361.

Saclier, M. et al., 2013. Monocyte/macrophage interactions with myogenic precursor cells

during skeletal muscle regeneration. *FEBS Journal*, 280(17), pp.4118–4130.

Sahakian, E. et al., 2013. A Novel Role For Histone Deacetylase 11 (HDAC11) As a Regulator Of Neutrophil Function and Differentiation In Normal and Malignant Hematopoesis E. Sahakian, ed. *Blood*, 122(21), p.2267 LP-2267. Available at: http://www.bloodjournal.org/content/122/21/2267.abstract.

Sahakian, E. et al., 2017. Essential role for histone deacetylase 11 (HDAC11) in neutrophil biology. *Journal of Leukocyte Biology*, 102(August), p.jlb.1A0415-176RRR. Available at: http://www.jleukbio.org/lookup/doi/10.1189/jlb.1A0415-176RRR.

Sahakian, E. et al., 2015. Histone deacetylase 11: A novel epigenetic regulator of myeloid derived suppressor cell expansion and function. *Molecular Immunology*, 63(2), pp.579–585.

Sambasivan, R., Pavlath, G.K. & Dhawan, J., 2008. A gene-trap strategy identifies quiescence-induced genes in synchronized myoblasts. *Journal of Biosciences*, 33(1), pp.27–44.

Sanjana, N.E., Shalem, O. & Zhang, F., 2014. Improved vectors and genome-wide libraries for CRISPR screening. *Nature Methods*, 11(8), pp.783–784. Available at: http://biorxiv.org/content/early/2014/06/28/006726.abstract%5Cnhttp://www.nature.com/doifinder/10.1038/nmeth.3047.

Saxonov, S., Berg, P. & Brutlag, D.L., 2006. A genome-wide analysis of CpG dinucleotides in the human genome distinguishes two distinct classes of promoters. *Proceedings of the National Academy of Sciences of the United States of America*, 103(5), pp.1412–1417. Available at: http://www.pnas.org/content/103/5/1412.full.pdf.

Schiaffino, S. et al., 2015. Developmental myosins: expression patterns and functional significance. *Skeletal Muscle*, pp.1–14. Available at: http://dx.doi.org/10.1186/s13395-015-0046-6.

Schiaffino, S. et al., 2016. Regulatory T cells and skeletal muscle regeneration. *The FEBS journal*, (Vimm), pp.1–8. Available at: http://www.ncbi.nlm.nih.gov/pubmed/27479876.

Schiaffino, S. & Reggiani, C., 2011. Fiber types in mammalian skeletal muscles. *Physiological reviews*, 91(4), pp.1447–531. Available at: http://www.ncbi.nlm.nih.gov/pubmed/22013216.

Schnyder, S. & Handschin, C., 2015. Skeletal muscle as an endocrine organ: PGC-1??, myokines and exercise. *Bone*, 80, pp.115–125.

Schubert, W. et al., 2007. Caveolin-1(−/−)- and Caveolin-2(−/−)-Deficient Mice Both Display Numerous Skeletal Muscle Abnormalities, with Tubular Aggregate Formation.

The American Journal of Pathology, 170(1), pp.316–333. Available at: http://linkinghub.elsevier.com/retrieve/pii/S0002944010608565.

Schuetz, A. et al., 2008. Human HDAC7 harbors a class IIa histone deacetylase-specific zinc binding motif and cryptic deacetylase activity. *Journal of Biological Chemistry*, 283(17), pp.11355–11363.

Segalés, J., Perdiguero, E. & Muñoz-Cánoves, P., 2015. Epigenetic control of adult skeletal muscle stem cell functions. *FEBS Journal*, 282(9), pp.1571–1588.

Servier, 2017. Servier Medicat Art. Available at: http://www.servier.com/slidekit/?item=40 [Accessed June 3, 2017].

Seto, E. & Yoshida, M., 2014. Erasers of Histone Acetylation : The Histone Deacetylase Enzymes Erasers of Histone Acetylation : The Histone Deacetylase Enzymes. *Cold Spring Harbor Perspectives in Biology*, 1, pp.1–26.

Shapiro, J.A., 2014. Epigenetic control of mobile DNA as an interface between experience and genome change. *Frontiers in Genetics*, 5(APR), pp.1–16.

Sharma, S., Kelly, T.K. & Jones, P.A., 2009. Epigenetics in cancer. *Carcinogenesis*, 31(1), pp.27–36.

Shefer, G. et al., 2006. Satellite-cell pool size does matter: Defining the myogenic potency of aging skeletal muscle. *Developmental Biology*, 294(1), pp.50–66.

Shi, X. & Garry, D.J., 2006. Muscle stem cells in development, regeneration, and disease. *Genes & Development*, 20(13), pp.1692–1708. Available at: http://www.genesdev.org/cgi/doi/10.1101/gad.1419406.

Simmons, B.J. et al., 2011. Histone Deacetylases: the Biology and Clinical Implication. *Handbook of Experimental Pharmacology 206*, 206, pp.79–101. Available at: http://www.springerlink.com/index/10.1007/978-3-642-21631-2.

Sincennes, M., Brun, C. & Rudnicky, M., 2016. Concise Review: Epigenetic Regulation of Myogenesis in Health and Disease. *Stem Cells Translational Medicine*, 5, pp.1–9.

Snijders, T. et al., 2015. Satellite cells in human skeletal muscle plasticity. *Frontiers in Physiology*, 6(OCT), pp.1–21.

Song, S.Y. et al., 2010. Mutational analysis of mononucleotide repeats in dual specificity tyrosine phosphatase genes in gastric and colon carcinomas with microsatellite instability. *Apmis*, 118(5), pp.389–393.

Sousa-Victor, P., Muñoz-Cánoves, P. & Perdiguero, E., 2011. Regulation of skeletal muscle stem cells through epigenetic mechanisms. *Toxicology mechanisms and methods*, 21(4), pp.334–342.

Sparrow, D.B. et al., 1999. MEF-2 function is modified by a novel co-repressor, MITR. *EMBO Journal*, 18(18), pp.5085–5098.

Steinbac, O.C., Wolffe, A.P. & Rupp, R.A., 2000. Histone deacetylase activity is required for the induction of the MyoD muscle cell lineage in Xenopus. *Biological chemistry*, 381(9–10), pp.1013–1016.

Strahl, B.D. & Allis, C.D., 2000. The language of covalent histone modifications. *Nature*, 403(6765), pp.41–45.

Subramanian, A. et al., 2005. Gene set enrichment analysis: a knowledge-based approach for interpreting genome-wide expression profiles. *Proceedings of the National Academy of Sciences of the United States of America*, 102(43), pp.15545–50. Available at: http://www.ncbi.nlm.nih.gov/pubmed/16199517.

Sun, W. et al., 2015. Distinct methylation profiles characterize fusion-positive and fusion-negative rhabdomyosarcoma. *Modern Pathology*, 28(9), pp.1214–1224. Available at: http://www.ncbi.nlm.nih.gov/pubmed/26226845.

Sun, Z. et al., 2011. Diet-induced lethality due to deletion of the Hdac3 gene in heart and skeletal muscle. *Journal of Biological Chemistry*, 286(38), pp.33301–33309.

Tajbakhsh, S., 2009. Skeletal muscle stem cells in developmental versus regenerative myogenesis. *Journal of Internal Medicine*, 266(4), pp.372–389.

Takase, K. et al., 2013. Monoaminergic and Neuropeptidergic Neurons Have Distinct Expression Profiles of Histone Deacetylases. *PLoS ONE*, 8(3).

Tapscott, S.J., Thayer, M.J. & Weintraub, H., 1993. Deficiency in rhabdomyosarcomas of a factor required for MyoD activity and myogenesis. *Science*, 259(5100), pp.1450–1453. Available at: http://www.ncbi.nlm.nih.gov/pubmed/8383879.

Tedesco, F.S. et al., 2010. Review series Repairing skeletal muscle : regenerative potential of skeletal muscle stem cells. *Journal of Clinical Investigation*, 120(1), pp.11–19.

Terranova, R. et al., 2005. The reorganisation of constitutive heterochromatin in differentiating muscle requires HDAC activity. *Experimental Cell Research*, 310(2), pp.344–356.

Tessarz, P. & Kouzarides, T., 2014. Histone core modifications regulating nucleosome structure and dynamics. *Nature reviews. Molecular cell biology*, 15(11), pp.703–708. Available at: http://dx.doi.org/10.1038/nrm3890.

Thole, T.M. et al., 2017. Neuroblastoma cells depend on HDAC11 for mitotic cell cycle progression and survival. *Cell Death and Disease*, 8(3), p.e2635. Available at: http://www.nature.com/doifinder/10.1038/cddis.2017.49.

Tidball, J.G., 2017. Regulation of muscle growth and regeneration by the immune system. *Nature Reviews Immunology*, 17(3), pp.165–178. Available at: http://www.nature.com/doifinder/10.1038/nri.2016.150.

Tidball, J.G. & Villalta, S.A., 2010. Regulatory interactions between muscle and the immune system during muscle regeneration. *Am J Physiol Regul Integr Comp Physiol*, 298(5), pp.R1173-87. Available at: http://www.ncbi.nlm.nih.gov/pubmed/20219869.

Timp, W. et al., 2014. Large hypomethylated blocks as a universal defining epigenetic alteration in human solid tumors. *Genome medicine*, 6(8), p.61. Available at: http://www.pubmedcentral.nih.gov/articlerender.fcgi?artid=4154522&tool=pmcentrez&rendertype=abstract.

Tiwari, S. et al., 2014. Histone deacetylase expression patterns in developing murine optic nerve. *BMC developmental biology*, 14(1), p.30. Available at: http://www.pubmedcentral.nih.gov/articlerender.fcgi?artid=4099093&tool=pmcentrez&rendertype=abstract.

Tombolan, L. et al., 2017. NELL1 , whose high expression correlates with negative outcomes , has different methylation patterns in alveolar and embryonal rhabdomyosarcoma.

Toropainen, S. et al., 2010. The Down-regulation of the Human MYC Gene by the Nuclear Hormone 1??,25-dihydroxyvitamin D3 is Associated with Cycling of Corepressors and Histone Deacetylases. *Journal of Molecular Biology*, 400(3), pp.284–294.

Trapnell, C., Pachter, L. & Salzberg, S.L., 2009. TopHat: discovering splice junctions with RNA-Seq. *Bioinformatics*, 25(9), pp.1105–1111. Available at: http://dx.doi.org/10.1093/bioinformatics/btp120.

Trivedi, C.M. et al., 2007. Hdac2 regulates the cardiac hypertrophic response by modulating Gsk3 beta activity. *Nature medicine*, 13(3), pp.324–31. Available at: http://www.ncbi.nlm.nih.gov/pubmed/17322895.

Tronick, E. & Hunter, R.G., 2016. Waddington, Dynamic Systems, and Epigenetics. *Frontiers in Behavioral Neuroscience*, 10(June), pp.1–6. Available at: http://journal.frontiersin.org/Article/10.3389/fnbeh.2016.00107/abstract.

Trybus, K.M., 1994. Role of myosin light chains. *Journal of Muscle Research and Cell Motility*, 15, pp.587–594.

Tsumagari, K. et al., 2013. Early de novo DNA methylation and prolonged demethylation in the muscle lineage. *Epigenetics*, 8(3), pp.317–332.

Tusnády, G.E. et al., 2005. BiSearch: primer-design and search tool for PCR on bisulfite-treated genomes. *Nucleic Acids Research*, 33(1), pp.e9–e9. Available at:

http://dx.doi.org/10.1093/nar/gni012.

Uhlen, M. et al., 2015. Tissue-based map of the human proteome. *Science*, 347(6220), pp.1260419–1260419. Available at: http://www.sciencemag.org/cgi/doi/10.1126/science.1260419.

Uhlen, M. et al., 2010. Towards a knowledge-based Human Protein Atlas. *Nature Biotechnology*, 28(12), pp.1248–1250. Available at: http://www.nature.com/doifinder/10.1038/nbt1210-1248.

Untergasser, A. et al., 2012. Primer3-new capabilities and interfaces. *Nucleic Acids Research*, 40(15), pp.1–12.

Vega, R.B. et al., 2004. Histone deacetylase 4 controls chondrocyte hypertrophy during skeletogenesis. *Cell*, 119(4), pp.555–566.

Venuti, J.M. et al., 1995. Myogenin is required for late but not early aspects of myogenesis during mouse development. *Journal of Cell Biology*, 128(4), pp.563–576.

Villagra, A. et al., 2009. The histone deacetylase HDAC11 regulates the expression of interleukin 10 and immune tolerance. *Nature immunology*, 10(1), pp.92–100. Available at: http://www.ncbi.nlm.nih.gov/pubmed/19011628.

Villalta, S.A. et al., 2011. Interleukin-10 reduces the pathology of mdx muscular dystrophy by deactivating M1 macrophages and modulating macrophage phenotype. *Human Molecular Genetics*, 20(4), pp.790–805.

Voelter-Mahlknecht, S., Ho, A.D. & Mahlknecht, U., 2005. Chromosomal organization and localization of the novel class IV human histone deacetylase 11 gene. *International journal of molecular medicine.*, 16(4), pp.589–598.

Waddington, C.H., 1942. The epigenotype. *Endeavour*, 1, pp.18–20.

Walters, Z.S. et al., 2014. JARID2 is a direct target of the PAX3-FOXO1 fusion protein and inhibits myogenic differentiation of rhabdomyosarcoma cells. *Oncogene*, 33(9), pp.1148–57. Available at: http://www.pubmedcentral.nih.gov/articlerender.fcgi?artid=3982124&tool=pmcentrez&rendertype=abstract.

Wamstad, J.A. et al., 2012. Dynamic and coordinated epigenetic regulation of developmental transitions in the cardiac lineage. *Cell*, 151(1), pp.206–220. Available at: http://dx.doi.org/10.1016/j.cell.2012.07.035.

Wang, M., Glass, Z.A. & Xu, Q., 2016. Non-viral delivery of genome-editing nucleases for gene therapy. *Gene Therapy*, (October). Available at: http://www.nature.com/doifinder/10.1038/gt.2016.72.

Wang, R. & Brattain, M.G., 2007. The maximal size of protein to diffuse through the nuclear pore is larger than 60 kDa. *FEBS Letters*, 581(17), pp.3164–3170.

Watanabe, Y., Khodosevich, K. & Monyer, H., 2014. Dendrite Development Regulated by the Schizophrenia-Associated Gene FEZ1 Involves the Ubiquitin Proteasome System. *Cell Reports*, 7(2), pp.552–564. Available at: http://dx.doi.org/10.1016/j.celrep.2014.03.022.

Weintraub, H., 1993. The MyoD family and myogenesis: redundancy, networks, and thresholds. *Cell*, 75(7), pp.1241–1244.

Welle, S., Tawil, R. & Thornton, C.A., 2008. Sex-related differences in gene expression in human skeletal muscle. *PLoS ONE*, 3(1).

Wen, Y. et al., 2012. Constitutive Notch Activation Upregulates Pax7 and Promotes the Self-Renewal of Skeletal Muscle Satellite Cells. *Molecular and Cellular Biology*, 32(12), pp.2300–2311. Available at: http://mcb.asm.org/cgi/doi/10.1128/MCB.06753-11.

Wold, B., 2012. ENCODE, Caltech. Available at: https://www.encodeproject.org/biosamples/ENCBS124ENC/ [Accessed May 29, 2017].

Wolfson, N.A., Ann Pitcairn, C. & Fierke, C.A., 2013. HDAC8 substrates: Histones and beyond. *Biopolymers*, 99(2), pp.112–126.

Wong, P.G. et al., 2010. Chromatin unfolding by Cdt1 regulates MCM loading via opposing functions of HBO1 and HDAC11-geminin. *Cell Cycle*, 9(21), pp.4351–4363.

Woods, D. et al., 2013. Histone deacetylase 11 is an epigenetic regulator of cytotoxic T-lymphocyte effector function and memory formation (P1404). *The Journal of Immunology*, 190(1 Supplement), p.117.2. Available at: http://www.jimmunol.org/content/190/1_Supplement/117.2.

Woods, D.M. et al., 2017. T-cells lacking HDAC11 have increased effector functions and mediate enhanced alloreactivity in a murine model. *Blood*, p.blood-2016-08-731505. Available at: http://www.bloodjournal.org/lookup/doi/10.1182/blood-2016-08-731505.

Workman, J.L., 2006. Nucleosome displacement in transcription. *Genes and Development*, 20(15), pp.2009–2017.

Workman, J.L. & Kingston, R.E., 1998. Alteration of nucleosome structure as a mechanism of transcriptional regulation. *Annual review of biochemistry*, 67, pp.545–579.

Xu, W.S., Parmigiani, R.B. & Marks, P.A., 2007. Histone deacetylase inhibitors: molecular mechanisms of action. *Oncogene*, 26(37), pp.5541–5552. Available at:

http://www.nature.com/doifinder/10.1038/sj.onc.1210620.

Yablonka-Reuveni, Z., 2011. The Skeletal Muscle Satellite Cell: Still Young and Fascinating at 50. *Journal of Histochemistry & Cytochemistry*, 59(12), pp.1041–1059. Available at: http://jhc.sagepub.com/lookup/doi/10.1369/0022155411426780.

Yaden, B.C. et al., 2014. Follistatin: A Novel Therapeutic for the Improvement of Muscle Regeneration. *Journal of Pharmacology and Experimental Therapeutics*, 349(2), pp.355–371. Available at: http://jpet.aspetjournals.org/cgi/doi/10.1124/jpet.113.211169.

Yaffe, D. & Saxel, O.R.A., 1977. Serial passaging and differentiation of myogenic cells isolated from dystrophic mouse muscle. *Nature*, 270(5639), pp.725–727. Available at: http://dx.doi.org/10.1038/270725a0.

Yang, W.M. & Yao, Y.L., 2011. Beyond histone and deacetylase: An overview of cytoplasmic histone deacetylases and their nonhistone substrates. *Journal of Biomedicine and Biotechnology*, 2011.

Yang, X. et al., 2006. Tissue-specific expression and regulation of sexually dimorphic genes in mice\r10.1101/gr.5217506. *Genome Research*, p.gr.5217506. Available at: http://www.genome.org/cgi/content/abstract/gr.5217506v1%5Cninternal-pdf://2328-1563060736/2328.pdf.

Yang, X.-J. & Seto, E., 2008. The Rpd3/Hda1 family of lysine deacetylases: from bacteria and yeast to mice and men. *Nature reviews. Molecular cell biology*, 9(3), pp.206–218.

Yang, X.J. et al., 2010. Dietary, metabolic, and potentially environmental modulation of the lysine acetylation machinery. *International Journal of Cell Biology*, (November 2016).

Yang, Z. et al., 2009. MyoD and E-protein heterodimers switch rhabdomyosarcoma cells from an arrested myoblast phase to a differentiated state. *Genes and Development*, 23(6), pp.694–707.

Yoshida, N. et al., 1998. Cell heterogeneity upon myogenic differentiation: down-regulation of MyoD and Myf-5 generates "reserve cells". *Journal of cell science*, 111, pp.769–779.

Yu, G. et al., 2012. clusterProfiler: an R package for comparing biological themes among gene clusters. *Omics : a journal of integrative biology*, 16(5), pp.284–7. Available at: http://www.pubmedcentral.nih.gov/articlerender.fcgi?artid=3339379&tool=pmcentrez&rendertype=abstract.

Yu, P. et al., 2015. Characterization of brain cell nuclei with decondensed chromatin. *Developmental Neurobiology*, 75(7), pp.738–756.

Yun, K. & Wold, B., 1996. Skeletal muscle determination and differentiation: Story of a core regulatory network and its context. *Current Opinion in Cell Biology*, 8(6), pp.877–889.

Yun, M. et al., 2011. Readers of histone modifications. *Cell research*, 21(4), pp.564–78. Available at: http://www.pubmedcentral.nih.gov/articlerender.fcgi?artid=3131977&tool=pmcentrez&rendertype=abstract.

Zanou, N. & Gailly, P., 2013. Skeletal muscle hypertrophy and regeneration: Interplay between the myogenic regulatory factors (MRFs) and insulin-like growth factors (IGFs) pathways. *Cellular and Molecular Life Sciences*, 70(21), pp.4117–4130.

Zhang, C.L., McKinsey, T.A., Chang, S., et al., 2002. Class II histone deacetylases act as signal-responsive repressors of cardiac hypertrophy. *Cell*, 110(4), pp.479–488.

Zhang, C.L., McKinsey, T.A. & Olson, E.N., 2002. Association of class II histone deacetylases with heterochromatin protein 1: potential role for histone methylation in control of muscle differentiation. *Molecular and cellular biology*, 22(20), pp.7302–12. Available at: http://www.pubmedcentral.nih.gov/articlerender.fcgi?artid=139799&tool=pmcentrez&rendertype=abstract.

Zhang, C.L., McKinsey, T.A. & Olson, E.N., 2001. The transcriptional corepressor MITR is a signal-responsive inhibitor of myogenesis. *Proceedings of the National Academy of Sciences of the United States of America*, 98(13), pp.7354–9. Available at: http://www.pubmedcentral.nih.gov/articlerender.fcgi?artid=34672&tool=pmcentrez&rendertype=abstract.

Zhang, H.P. et al., 2015. Histone deacetylation of memory T lymphocytes by You-Gui-Wan alleviates allergen-induced eosinophilic airway inflammation in asthma. *Chinese Medicine*, 10(1), p.9. Available at: http://www.cmjournal.org/content/10/1/9.

Zhang, Y. et al., 2008. Mice Lacking Histone Deacetylase 6 Have Hyperacetylated Tubulin but Are Viable and Develop Normally. *Molecular and Cellular Biology*, 28(5), pp.1688–1701. Available at: http://mcb.asm.org/cgi/doi/10.1128/MCB.01154-06.

Zhang, Z. et al., 2008. SMN Deficiency Causes Tissue-Specific Perturbations in the Repertoire of snRNAs and Widespread Defects in Splicing. *Cell*, 133(4), pp.585–600.

Zhou, H. et al., 2006. Epigenetic Allele Silencing Unveils Recessive RYR1 Mutations in Core Myopathies. *The American Journal of Human Genetics*, 79(5), pp.859–868. Available at: http://www.sciencedirect.com/science/article/pii/S0002929707608295.

Zhou, X. & Wang, T., 2002. Using the Wash U Epigenome Browser to Examine Genome-Wide Sequencing Data. In *Current Protocols in Bioinformatics*. John Wiley & Sons, Inc. Available at: http://dx.doi.org/10.1002/0471250953.bi1010s40.

Zhu, W. et al., 2012. Genomic signatures characterize leukocyte infiltration in myositis muscles. , pp.1–12.

Zupkovitz, G. et al., 2010. The cyclin-dependent kinase inhibitor p21 is a crucial target for histone deacetylase 1 as a regulator of cellular proliferation. *Mol Cell Biol*, 30(5), pp.1171–1181. Available at: http://www.ncbi.nlm.nih.gov/pubmed/20028735.

APPENDIX 1

Supplementary Figure 1. CRISPR HDAC11-HA clone screening.

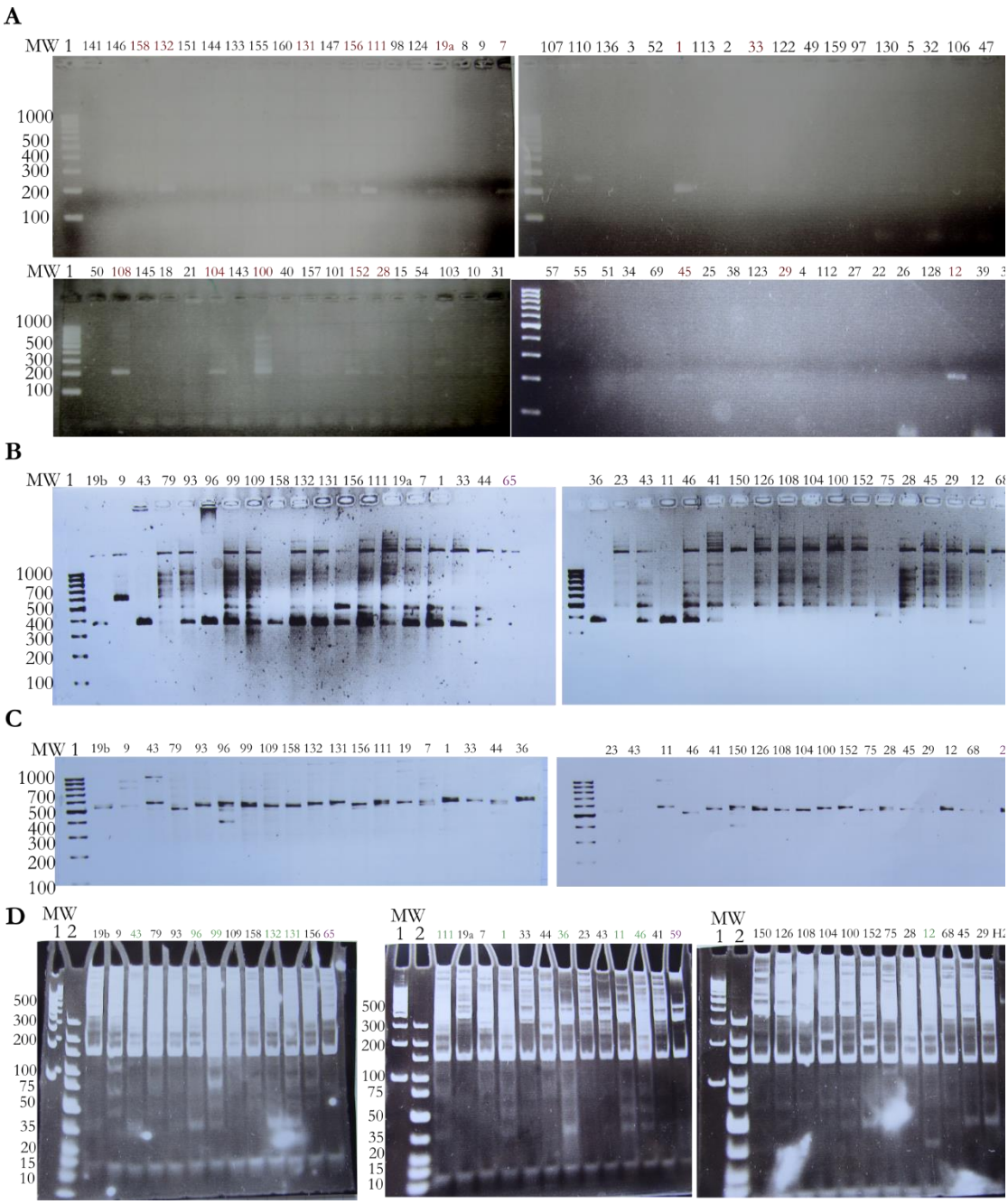

To validate HA knock-in insertion in derived clones from pool of sgRNA_1, PCR amplification of their extracted DNA was performed using primers directly annealing on HA. Thus, amplification of the designed amplicons was only expected in KI clones and no amplification in the ones without editing. In **A** and **B** are shown the resulting PCR reactions ran into 2% agarose gels stained with ethidium bromide for the amplification with 5'UTR_F and HA_R (expected band 200 bp) (**A**). After this first, screening the positive clones (red) were further analyzed with HA_F and 5'_UTR_R (expected band 372 bp) (**B**). In violet are shown clones that had already been validated as non-edited as negative controls. In **C** is shown an aliquot (3 µl) of the PCR 5'UTR ran into 2% agarose gel of all the clones from PCR validation with HA_F. As a

difference with the PCR product of the pools, some clones that were later on validated as positive (as clone 7), showed two band pattern compatible with the amplification of the edited and non-edited alleles. **D** Restriction products by NdeI of the amplicons in **C** ran into 8% acrylamide gels. Green labelled clones presented the expected 34 bp band and were considered as edited. The ones showing more intense bands (clones 11, 36, 43, 96, 99 139 and 12) were further screened by DNA Sanger sequencing. MW: Molecular weight ladder. 1: GeneRuler 100 bp DNA ladder (Ref.SM0241, Thermo Scientific). 2: GeneRuler ultra low range DNA ladder (Ref. SM1211, ThermoFisher).

Supplementary Figure 2. Set-up of HDAC11-HA Co-IP.

A Western blot detection of overexpressed HDAC11-HA with α-HA (Ref. ab91110, Abcam). 50 μg of RIPA extracted proteins for pMSCV-HA (Empty) and pMSCV-HDAC11-HA (HA) were ran into 8% acrylamide gels. HDAC11-HA corresponds to the upper band indicated with an arrow and the lower band marked with an asterisk was detected as unspecific. **B** Western blot analysis of endogenous HDAC11-HA from day 1 differentiating clone 19 after immunoprecipitation. Immunoprecipitation was performed with 5 μg of protein. RIPA extracted overexpressing HDAC11-HA C2C12 (same sample than A) was ran as control (HA). KI HDAC11-HA was detected only after o/n exposure of the film. **C** Western blot analysis of HDAC11-HA co-immunoprecipitation. Co-IP was performed as described on "Materials and methods" section starting with 500 μg of total protein. The samples were ran into 8% acrylamide gels. Input fractions correspond to 50 μg of sample (10% of the amount immunoprecipitated). The unbound HA corresponds to 50 μg of the extract after incubation with the beads for 6h. The beads were included to ensure that the immunoprecipitated fraction was efficiently eluted. The upper image corresponds to 10 min exposition and the lower to 5 min exposition both after Luminata Crescendo developing.

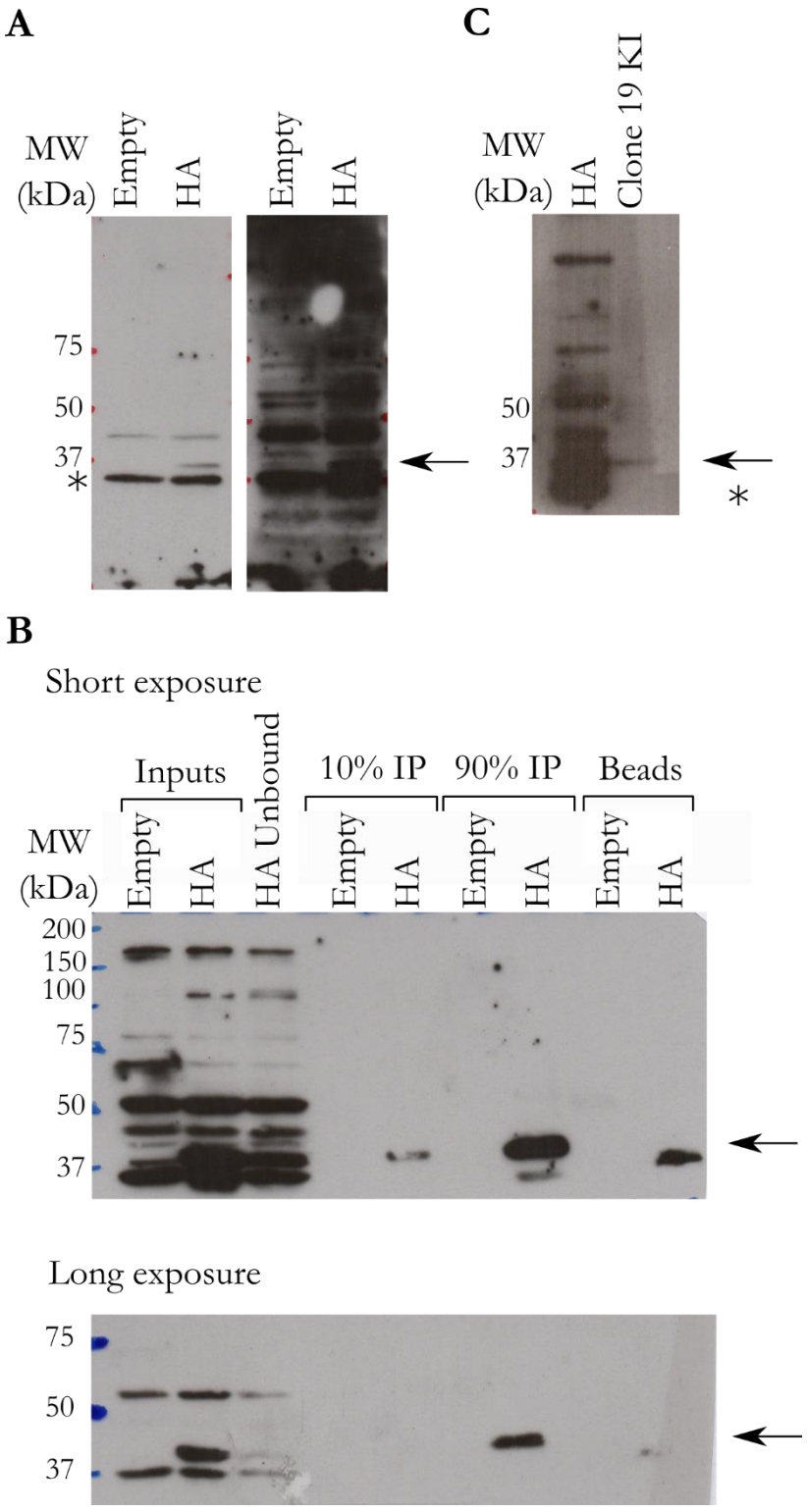
A
MW (kDa)
Empty
HA
Empty
HA
75
50
37
*
C
MW (kDa)
HA
Clone 19 KI
50
37
*
B
Short exposure
Inputs
10% IP
90% IP
Beads
MW (kDa)
Empty
HA
HA Unbound
Empty
HA
Empty
HA
Empty
HA
200
150
100
75
50
37
Long exposure
75
50
37

Supplementary Figure 3. HDAC11 is upregulated through cardiomyocyte differentiation of mESC.

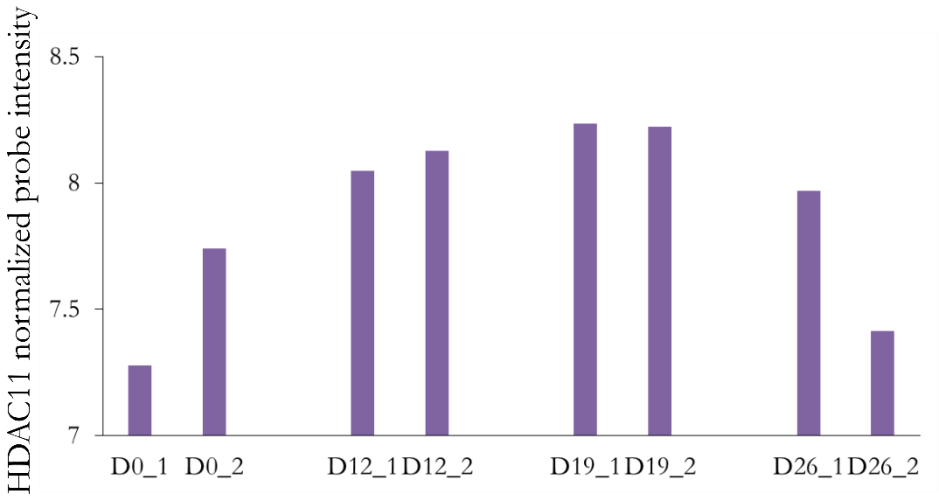

Values correspond to the average normalized probe intensity of HDAC11 (ENSMUSG00000034245), Affymetrix Mouse Exon 1.0 S7 Array. The names refer to the days of mESC differentiation. For each time point, two replicates are represented. Data was extracted from GSE8300 (Gan et al. 2014). As occurred in skeletal muscle differentiation, at the beginning of differentiation HDAC11 mRNA levels increase and after cardiomyocytes maturation (D19), HDAC11 levels decrease again.

Supplementary Figure 4. HDAC11 is expressed the most in functional cardiomyocytes through the cardiac lineage development.

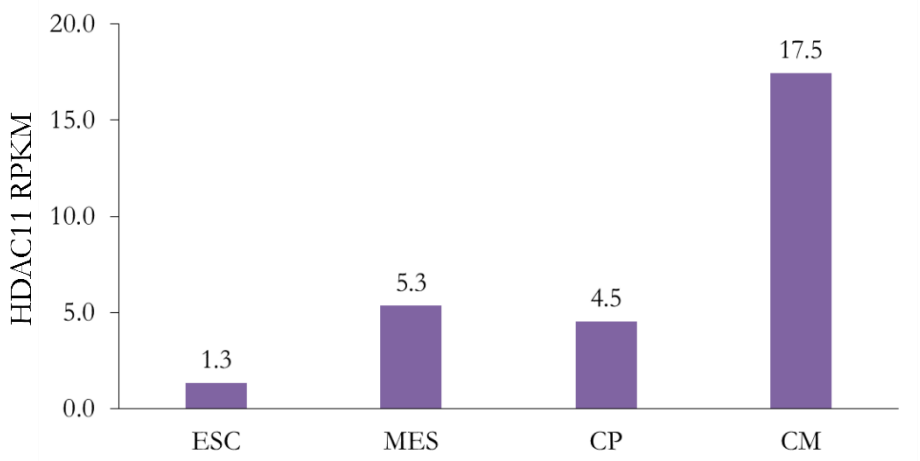

Sample names correspond to Embryonic stem cells (ESC), mesodermal stem cells (MSC), cardiac precursors (CP) and cardiomyocytes (CM). Data correspond to RNA-seq normalized average of two biological replicates for each sample expressed in reads per million mapped reads (RPKM). Data was downloaded from GSE47948 (Wamstad et al. 2012).

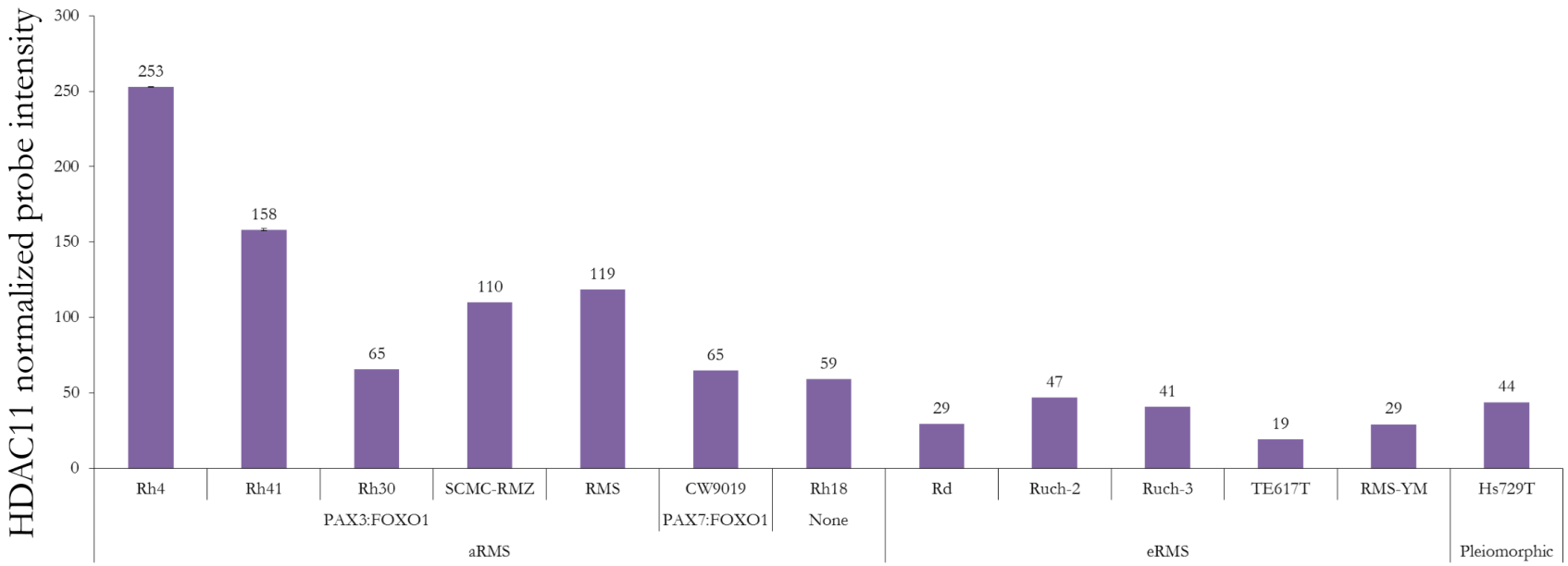

Supplementary Figure 5. HDAC11 expression in extended rhabdomyosarcoma cell lines. HDAC11 227679_at probe intensity values in a microarray normalized data (GSE8840). Data was downloaded from GSE8840. (Missiaglia et al. 2009).

Supplementary Table 1. Differentially expressed genes between WT and KO myoblasts at day 1 of differentiation. Listed are the differentially expressed genes by RNA seq with a p adjusted value ≤ 0.05 and absolute fold change (FC) value >/2/. Fold change (FC) represents the ratio between KO and WT average values.

Number	Gene	FC (KO vs WT)	p adj value	Number	Gene	FC (KO vs WT)	p adj value
1399	Adcyap1r1	7.86	3.5E-08	2927	Camk1g	3.10	6.1E-04
4973	Dynap	6.23	1.3E-07	17964	Serpina6	3.10	1.9E-02
12432	Kcnn4	5.22	6.0E-06	2405	B4galnt3	3.09	1.9E-02
17807	Scn9a	4.88	9.6E-07	18445	Slc5a3	3.08	3.6E-04
5510	F2rl1	4.78	3.2E-04	20972	Wdhd1	3.05	3.3E-04
20044	Tnfsf11	4.67	3.9E-04	2322	Aurkb	3.05	2.0E-05
13432	Mertk	4.56	2.5E-04	11690	Hmga1	3.03	1.0E-02
16972	Ripk3	4.40	3.0E-06	20123	Tpbg	3.01	4.2E-04
5365	Eps8	4.38	1.8E-04	16839	Rem1	3.01	3.4E-04
20364	Tspan11	4.35	6.9E-04	19176	Styk1	3.01	1.8E-02
4264	Cxcl12	3.85	1.1E-04	14171	Mybl2	2.98	2.3E-03
11813	Hrh1	3.77	1.6E-03	11358	Gsta1	2.95	2.9E-02
5453	Etv4	3.74	7.9E-04	20299	Troap	2.95	5.1E-05
19618	Thbs4	3.73	2.8E-03	764	5031415H12Rik	2.94	1.4E-02
5278	Emp1	3.71	1.3E-05	5422	Esm1	2.94	2.9E-02
16399	Ptgs2	3.69	1.2E-04	19614	Thbd	2.94	7.5E-03
3292	Cd34	3.65	2.2E-03	15396	Pdlim2	2.92	9.3E-05
1920	Aqp1	3.63	1.5E-04	4720	Dlx1	2.92	2.8E-03
4841	Dock8	3.61	9.9E-04	12505	Kif18b	2.91	4.5E-05
12648	Krt18	3.51	5.0E-03	3355	Cdc6	2.89	4.5E-03
11266	Gprc5a	3.47	4.7E-04	13337	Mcm5	2.89	6.7E-04
13347	Mcpt8	3.47	5.1E-03	3232	Ccnjl	2.88	9.4E-03
11436	Gzme	3.42	3.4E-03	445	2810429I04Rik	2.88	2.2E-03
5581	Fam131b	3.40	2.4E-04	1965	Arhgap22	2.88	2.4E-03
1872	Apcdd1	3.39	4.1E-03	17720	Sapcd2	2.87	3.2E-04
11603	Hhip	3.36	6.1E-03	13227	Mapk13	2.87	2.1E-02
6248	Gas7	3.34	2.2E-03	3278	Cd24a	2.87	7.9E-03
21107	Xlr3a	3.32	9.9E-03	5500	Eya2	2.87	2.8E-02
6400	Gli1	3.32	1.2E-02	10926	Gm8773	2.84	1.7E-02
15694	Pla2g4a	3.30	1.5E-04	18956	Srd5a1	2.83	2.2E-03
11886	Htr1b	3.28	5.0E-03	3362	Cdca7	2.82	7.1E-03
14414	Ndst3	3.28	1.3E-03	13309	Mboat1	2.82	1.3E-05
19564	Tfap4	3.27	1.2E-04	4722	Dlx2	2.80	6.3E-03
2516	BC030867	3.22	3.8E-04	6286	Gchfr	2.79	2.1E-02
12976	Lrrc4	3.21	8.7E-04	19124	Stmn2	2.78	8.8E-03
16703	Rasl11a	3.18	3.3E-03	15355	Pde1a	2.78	2.7E-02
18173	Ska3	3.15	1.3E-05	5419	Esco2	2.78	5.4E-04
6434	Glyat	3.11	1.7E-02	3441	Cdt1	2.76	1.6E-03
1531	AI504432	3.11	6.2E-03	15279	Pcdhga12	2.76	1.7E-02

3507	Cep55	2.75	3.1E-04	2320	Aurka	2.58	6.9E-04
1153	Abcb1b	2.75	1.6E-05	1742	Ankle1	2.58	2.5E-04
1925	Aqp5	2.75	2.7E-02	11564	Hells	2.58	6.2E-03
18834	Spag5	2.75	2.8E-05	3467	Cenpa	2.58	5.9E-04
18437	Slc4a8	2.74	3.3E-04	3358	Cdca2	2.58	8.9E-05
18171	Ska1	2.74	7.6E-04	3364	Cdca8	2.58	8.9E-05
20668	Uhrf1	2.74	1.1E-03	5651	Fam19a5	2.58	3.0E-04
12951	Lrr1	2.74	4.6E-03	12534	Kifc1	2.57	3.0E-04
3213	Ccnb1	2.74	1.5E-04	3359	Cdca3	2.57	6.8E-05
452	2810468N07Rik	2.74	2.8E-03	12522	Kif2c	2.57	2.7E-04
20271	Trip13	2.72	3.0E-03	5712	Fam64a	2.57	2.8E-03
6050	Foxm1	2.72	1.3E-07	4677	Diaph3	2.57	1.3E-04
3473	Cenpi	2.71	2.0E-04	5385	Ercc6l	2.57	3.4E-03
12526	Kif4	2.71	1.5E-05	11410	Gtse1	2.57	7.9E-04
441	2810417H13Rik	2.71	2.8E-03	15590	Pif1	2.57	6.8E-05
13426	Melk	2.71	1.2E-03	19866	Tmem200b	2.56	4.9E-02
18247	Slc1a6	2.71	4.2E-02	438	2810408I11Rik	2.56	2.5E-02
4137	Csf1	2.71	6.2E-03	19036	St14	2.56	9.3E-03
16089	Ppp4r4	2.70	3.5E-02	15790	Plk1	2.56	4.2E-04
5458	Eva1c	2.70	3.3E-02	4521	Ddias	2.55	3.8E-03
19654	Ticrr	2.69	2.0E-03	11692	Hmga2	2.55	7.5E-03
18246	Slc1a5	2.69	6.0E-06	4452	Dbf4	2.55	3.2E-04
14962	Oip5	2.69	2.8E-04	3334	Cdc25c	2.54	1.1E-04
3472	Cenph	2.68	4.2E-04	3705	Ckap2l	2.54	3.1E-04
11699	Hmgb3	2.68	1.8E-04	18054	Sgol1	2.54	9.3E-04
5850	Fbxo5	2.67	4.0E-03	20449	Ttk	2.54	4.7E-04
21103	Xkr5	2.67	7.6E-03	3470	Cenpe	2.53	1.5E-04
11262	Gpr85	2.65	3.1E-03	4600	Depdc1a	2.53	5.5E-04
14364	Ncapg	2.65	4.5E-05	4198	Cth	2.53	3.6E-02
16779	Rbp1	2.65	2.6E-03	12813	Lig1	2.53	2.1E-03
15223	Pbk	2.65	2.5E-04	20708	Upp1	2.52	1.2E-02
11682	Hlx	2.64	3.0E-04	16237	Prr11	2.52	2.5E-03
3363	Cdca7l	2.64	3.1E-04	1728	Angptl4	2.52	2.1E-02
15895	Pole	2.63	1.5E-04	3226	Ccnf	2.52	1.9E-04
11465	H2afx	2.63	1.5E-04	2763	Bub1	2.51	1.3E-03
6377	Gja1	2.62	3.7E-05	3531	Cers4	2.51	8.3E-04
12516	Kif23	2.62	1.7E-04	5029	E2f7	2.51	3.0E-03
12422	Kcnk5	2.62	2.3E-02	14168	Myb	2.51	4.6E-02
3585	Chaf1b	2.61	5.0E-03	16626	Rad54l	2.50	2.9E-03
3792	Clspn	2.61	2.8E-03	19097	Stil	2.50	1.5E-03
3004	Casc5	2.60	1.5E-05	3361	Cdca5	2.50	3.4E-03
16141	Prim1	2.60	2.4E-03	15907	Polq	2.50	1.0E-03
12504	Kif18a	2.59	1.5E-03	7104	Gm13232	2.49	4.7E-02
12501	Kif15	2.59	9.3E-04	16439	Ptprg	2.49	6.9E-07
3778	Clmp	2.59	1.5E-03	5761	Fanci	2.49	8.9E-05
13334	Mcm3	2.59	1.9E-03	5753	Fanca	2.49	7.5E-05

13281	Mastl	2.48	1.1E-04	15862	Pnp	2.40	1.9E-03
12515	Kif22	2.48	6.9E-04	5103	Efcab11	2.40	1.5E-02
1263	Acot1	2.48	6.3E-03	15359	Pde3b	2.40	2.5E-02
5124	Efna5	2.48	2.5E-03	2158	Atad2	2.40	2.1E-03
12628	Knstrn	2.48	1.6E-03	5147	Ehd2	2.39	8.2E-04
15333	Pcsk9	2.48	3.6E-04	11783	Hoxc8	2.39	4.4E-02
4714	Dlgap5	2.48	1.9E-03	16618	Rad51	2.38	4.7E-03
13808	Mms22l	2.48	1.0E-03	1162	Abcc4	2.38	1.3E-03
12511	Kif20a	2.47	8.9E-05	18903	Spn	2.38	3.7E-02
3387	Cdk1	2.47	7.8E-04	14362	Ncapd2	2.37	1.1E-04
21415	Zfp36l2	2.47	5.5E-03	61	1500009L16Rik	2.37	6.9E-03
3584	Chaf1a	2.47	3.3E-03	2764	Bub1b	2.37	1.5E-03
6031	Fosl1	2.46	4.1E-02	15814	Plscr1	2.37	1.7E-02
2145	Aspm	2.46	1.3E-05	18055	Sgol2a	2.36	3.3E-05
18101	Shank3	2.46	4.7E-02	14781	Nrp2	2.36	2.4E-02
5469	Exo1	2.46	1.2E-02	5560	Fam111a	2.36	3.3E-03
15793	Plk4	2.46	1.8E-03	20595	Ube2t	2.36	8.5E-03
1962	Arhgap19	2.46	1.5E-03	12302	Jade2	2.35	3.4E-02
18871	Spdl1	2.45	6.3E-03	5423	Espl1	2.35	5.3E-04
5265	Eme1	2.45	5.9E-03	569	4930427A07Rik	2.35	2.8E-04
3674	Chtf18	2.45	1.4E-03	16823	Recql4	2.35	2.6E-04
5541	Fah	2.45	9.3E-05	10593	Gm6104	2.35	1.9E-02
5126	Efnb2	2.45	4.2E-03	4959	Dusp5	2.35	2.6E-02
3212	Ccna2	2.44	1.0E-03	17577	Rrm2	2.35	7.5E-03
3667	Chst2	2.44	1.5E-02	2635	Birc5	2.33	1.3E-03
19465	Tcf19	2.43	1.1E-03	5792	Fbln1	2.33	3.5E-05
5890	Fen1	2.43	2.0E-02	15896	Pole2	2.33	1.2E-02
14398	Ndc80	2.43	2.8E-03	14366	Ncaph	2.33	1.0E-03
3704	Ckap2	2.43	8.9E-05	3330	Cdc20	2.33	1.0E-03
20106	Top2a	2.43	4.8E-04	273	1810059H22Rik	2.33	1.9E-02
11347	Gsg2	2.43	1.9E-03	13441	Metrn	2.33	2.8E-02
20831	Vcam1	2.43	7.9E-03	12500	Kif14	2.32	1.3E-04
8130	Gm20667	2.42	2.8E-02	1793	Anln	2.32	6.2E-03
6129	Fut4	2.42	1.5E-03	4601	Depdc1b	2.32	7.4E-03
5072	Ect2	2.42	4.8E-04	13747	Mis18bp1	2.32	3.3E-03
15016	Orc1	2.42	4.2E-03	14745	Nr2f1	2.32	4.2E-02
14865	Nuf2	2.42	1.1E-03	12291	Itpripl1	2.32	3.8E-03
3215	Ccnb2	2.42	7.5E-05	5136	Egfr	2.31	2.3E-02
20160	Tpx2	2.42	7.4E-04	11467	H2afy2	2.31	8.9E-05
5756	Fancd2	2.42	2.9E-04	11098	Gmnn	2.31	1.3E-02
2318	Aunip	2.41	1.1E-02	4261	Cxadr	2.31	1.8E-02
11199	Gpc6	2.41	1.5E-05	13752	Mki67	2.31	9.4E-04
14487	Nek2	2.41	1.1E-04	20247	Trim47	2.30	1.0E-02
14483	Neil3	2.41	2.4E-03	5734	Fam83d	2.30	3.2E-04
4908	Dscc1	2.41	3.5E-02	5717	Fam69b	2.30	1.4E-02
20208	Trerf1	2.41	4.8E-03	2448	Bambi	2.30	4.9E-02

2686	Bora	2.30	6.9E-03	18551	Smc4	2.19	2.4E-04
14824	Ntn4	2.30	1.9E-03	14176	Myc	2.19	2.7E-02
6455	Gm10075	2.30	1.1E-02	4482	Dchs1	2.19	1.5E-03
18415	Slc43a3	2.30	2.5E-03	13336	Mcm4	2.19	1.5E-02
4803	Dnajc9	2.30	1.1E-03	21771	Zwilch	2.19	8.5E-03
11698	Hmgb2	2.29	1.8E-03	2127	Asf1b	2.19	4.0E-03
12123	Incenp	2.29	2.3E-03	3713	Cks1b	2.19	8.5E-03
16609	Racgap1	2.29	8.0E-05	3881	Cobll1	2.18	6.1E-03
6324	Gen1	2.29	2.3E-03	14532	Nfib	2.18	3.8E-04
19892	Tmem238	2.29	4.3E-02	2699	Brca1	2.18	1.6E-02
12512	Kif20b	2.29	1.3E-03	6384	Gjc1	2.18	5.7E-03
13746	Mis18a	2.29	1.1E-03	20697	Ung	2.18	4.6E-02
3128	Ccdc18	2.29	3.2E-02	11124	Gnb4	2.17	5.8E-03
3429	Cdkn3	2.28	1.0E-02	3471	Cenpf	2.17	4.5E-04
13332	Mcm10	2.28	1.4E-02	21037	Wee1	2.17	2.0E-04
2717	Brip1	2.28	5.8E-03	19390	Tbc1d2	2.17	7.1E-03
5785	Fat4	2.27	3.0E-04	15322	Pcolce2	2.17	4.4E-02
12947	Lrp8	2.27	3.1E-02	19311	Tacc3	2.17	1.9E-03
4919	Dtl	2.27	2.4E-02	19617	Thbs3	2.17	2.5E-02
6368	Gins2	2.27	1.1E-02	12731	Lbh	2.17	2.1E-02
13117	Mad2l1	2.26	3.8E-03	4434	Dagla	2.16	1.1E-03
14795	Nsl1	2.26	1.4E-02	14092	Mtfr2	2.16	4.6E-03
2453	Bard1	2.26	2.2E-02	6075	Frem1	2.16	3.6E-02
19535	Tert	2.26	2.7E-02	3475	Cenpk	2.15	1.9E-02
16828	Reep4	2.26	1.2E-03	13339	Mcm7	2.15	2.3E-02
12497	Kif11	2.25	2.4E-03	15874	Poc1a	2.15	5.8E-03
3481	Cenpq	2.25	3.0E-04	3607	Chek2	2.15	6.2E-03
3483	Cenpu	2.25	1.0E-02	11442	H1fx	2.15	8.9E-04
5531	Fabp5	2.25	2.6E-02	5436	Etaa1	2.15	2.2E-02
18108	Shcbp1	2.25	8.5E-03	17702	Samd14	2.14	4.7E-04
13313	Mbp	2.25	1.2E-02	16234	Prps2	2.14	1.6E-03
19662	Timeless	2.25	2.1E-03	19403	Tbc1d4	2.14	3.0E-02
19693	Tk1	2.24	3.6E-03	20253	Trim59	2.13	3.9E-03
2540	BC055324	2.24	1.1E-02	18865	Spc25	2.13	9.8E-03
15143	Palb2	2.23	2.3E-02	4640	Dhfr	2.13	2.9E-02
7106	Gm13237	2.22	3.1E-02	14898	Nusap1	2.13	7.9E-04
2832	C330027C09Rik	2.22	1.3E-03	5754	Fancb	2.13	2.5E-02
14921	Oaf	2.22	2.6E-02	20533	Tyms	2.13	2.0E-02
11693	Hmgb1	2.21	7.9E-03	15202	Parpbp	2.13	3.8E-03
4964	Dut	2.21	9.2E-03	18323	Slc27a3	2.13	2.8E-03
2004	Arhgef39	2.21	2.2E-03	15886	Pola1	2.13	8.2E-03
16996	Rnase4	2.20	2.2E-02	2700	Brca2	2.12	1.6E-03
16258	Prrg1	2.20	3.6E-02	4822	Dnmt1	2.12	6.9E-04
15889	Pold1	2.20	1.4E-03	6167	G6pdx	2.12	1.5E-03
13338	Mcm6	2.20	9.8E-03	1791	Anks6	2.12	1.8E-02
11712	Hmmr	2.19	2.8E-03	611	4930503L19Rik	2.12	3.4E-02

2403	B4galnt1	2.11	4.7E-03	18864	Spc24	2.03	1.6E-04
14751	Nr4a2	2.11	4.3E-03	19123	Stmn1	2.03	6.2E-03
3034	Cav2	2.11	2.0E-03	14008	Msh6	2.02	1.4E-02
13355	Mdc1	2.11	4.6E-03	670	4930579G24Rik	2.02	1.3E-02
13340	Mcm8	2.10	2.6E-03	5504	Ezh2	2.02	1.8E-02
14170	Mybl1	2.10	4.1E-03	19119	Stk39	2.02	2.2E-02
15677	Pkmyt1	2.10	3.9E-03	2381	B3galnt1	2.02	1.2E-02
14365	Ncapg2	2.09	3.0E-03	3055	Cbx2	2.01	2.6E-02
4740	Dna2	2.09	4.4E-02	11221	Gpr137b	2.01	3.1E-02
15432	Peg12	2.09	2.4E-02	21192	Zbed3	2.01	1.3E-02
16861	Rfc5	2.09	1.1E-02	11507	Haus4	2.01	1.7E-02
18926	Spry2	2.09	4.3E-03	6223	Galnt7	2.01	3.6E-02
419	2700099C18Rik	2.08	1.9E-02	6519	Gm10357	2.01	4.9E-02
18289	Slc25a30	2.08	2.1E-02	5930	Fgfr4	2.00	2.6E-03
16142	Prim2	2.08	7.3E-03	20567	Ube2c	2.00	5.1E-03
15313	Pcna	2.08	1.0E-02	2075	Arpp21	-2.01	1.6E-02
3478	Cenpn	2.08	2.1E-02	13544	Mid1	-2.01	3.1E-04
2443	Baiap2	2.08	1.3E-02	900	9230112E08Rik	-2.02	4.0E-02
19225	Suv39h2	2.08	2.7E-02	11850	Hsp25-ps1	-2.02	3.2E-02
5951	Fignl1	2.07	2.3E-02	4706	Dlg2	-2.03	4.1E-02
12275	Itgb8	2.07	4.0E-03	19098	Stim1	-2.03	1.6E-02
2718	Brip1os	2.07	1.2E-02	14078	Mtcl1	-2.03	3.9E-02
20110	Topbp1	2.07	6.2E-03	17900	Sema3b	-2.03	8.1E-03
12537	Kifc5b	2.07	2.8E-03	2869	Cables1	-2.04	2.8E-02
2073	Arpin	2.07	3.8E-03	3659	Chrng	-2.04	4.0E-02
20660	Ugdh	2.07	4.9E-03	13112	Macf1	-2.04	8.2E-03
20178	Traip	2.07	4.3E-02	3039	Cbfa2t3	-2.06	2.9E-02
20785	Usp6nl	2.07	4.9E-02	18735	Sntb1	-2.06	9.9E-03
20355	Tshz1	2.07	1.1E-02	15837	Pmepa1	-2.11	3.2E-02
16666	Rap2a	2.06	1.7E-02	5145	Ehbp1l1	-2.11	8.7E-03
5280	Emp3	2.06	1.3E-02	12665	Ksr1	-2.11	2.0E-03
1355	Adamts10	2.06	2.8E-04	4517	Ddc	-2.11	5.0E-02
18548	Smc2	2.06	6.3E-03	12974	Lrrc39	-2.11	3.9E-02
15587	Pidd1	2.06	9.4E-03	20461	Ttn	-2.12	4.2E-02
21029	Wdr90	2.05	1.4E-04	15364	Pde4dip	-2.12	7.1E-03
13581	Mir17hg	2.04	2.9E-02	368	2500002B13Rik	-2.13	4.5E-02
3715	Cks2	2.04	1.4E-02	20071	Tnnt3	-2.14	4.4E-02
21426	Zfp395	2.04	4.1E-03	2888	Cacnb1	-2.14	2.9E-02
18118	Shmt1	2.04	4.3E-02	4996	Dysf	-2.14	4.6E-02
20480	Tubb5	2.04	1.2E-02	15091	P2rx5	-2.15	2.4E-02
13054	Ltbp4	2.04	5.5E-03	5953	Filip1	-2.15	3.4E-02
17938	Sept6	2.03	1.2E-02	18980	Srpk3	-2.16	4.5E-02
15839	Pmf1	2.03	1.1E-02	20749	Usp2	-2.16	1.0E-02
11580	Hes1	2.03	4.9E-03	2810	C230012O17Rik	-2.16	4.4E-02
16891	Rgs10	2.03	2.9E-02	14146	Murc	-2.17	1.5E-02
4844	Dok1	2.03	2.6E-02	14252	Mypn	-2.18	3.1E-02

4323	Cyp46a1	-2.19	1.4E-02	14246	Myom2	-2.49	3.5E-02
6929	Gm12439	-2.19	9.5E-03	15120	Pacsin3	-2.49	3.3E-02
18074	Sh3bgr	-2.20	1.9E-02	20511	Txlnb	-2.50	3.7E-02
11041	Gm9821	-2.21	3.5E-02	1310	Actn3	-2.51	1.5E-02
17566	Rrad	-2.21	8.1E-03	11268	Gprc5c	-2.51	4.2E-02
11593	Hfe2	-2.21	4.8E-02	12882	Lmod3	-2.51	1.6E-02
4017	Cp	-2.21	1.5E-02	14210	Myl6b	-2.51	7.5E-03
5905	Fgd3	-2.22	3.7E-02	13900	Mrln	-2.52	1.8E-02
14247	Myom3	-2.23	2.9E-02	14245	Myom1	-2.52	3.5E-02
6661	Gm11361	-2.24	4.1E-02	17668	Ryr1	-2.55	3.0E-03
1527	AI464131	-2.25	4.4E-02	9474	Gm3830	-2.57	1.8E-02
12603	Klhl41	-2.25	4.8E-02	18788	Sorbs2os	-2.57	4.3E-02
17901	Sema3c	-2.25	3.3E-02	1773	Ankrd44	-2.57	2.9E-02
15951	Popdc2	-2.26	3.5E-02	19987	Tmod1	-2.57	1.9E-02
1469	Aff2	-2.28	2.5E-02	3710	Ckm	-2.58	3.3E-02
11538	Hdac9	-2.29	2.3E-02	12142	Inpp4b	-2.58	1.0E-02
15691	Pla2g16	-2.30	4.8E-02	14462	Neb	-2.58	8.2E-03
16364	Pstpip1	-2.30	4.7E-02	5234	Elmo1	-2.59	8.2E-03
6072	Fras1	-2.31	4.5E-02	19586	Tgfb2	-2.59	2.6E-02
2894	Cacng6	-2.32	3.4E-02	1905	Apol9b	-2.59	4.0E-02
12328	Jph1	-2.34	2.5E-02	14208	Myl4	-2.59	1.7E-02
19587	Tgfb3	-2.35	2.5E-02	11810	Hrc	-2.60	2.9E-02
13125	Mafa	-2.36	2.6E-02	16137	Prickle1	-2.60	1.3E-02
6103	Fst	-2.36	4.4E-02	18094	Sh3rf2	-2.62	4.7E-02
6007	Fn3k	-2.37	1.8E-02	1195	Abhd3	-2.63	3.3E-02
14175	Mybph	-2.38	3.0E-02	3920	Col4a5	-2.63	8.9E-05
2109	Asb16	-2.38	2.4E-02	11321	Grin3b	-2.64	3.5E-02
16494	Pygm	-2.38	8.8E-03	12579	Klhl13	-2.65	1.9E-02
16155	Prkag3	-2.40	1.9E-02	2112	Asb2	-2.65	1.6E-02
15479	Pfkm	-2.40	8.7E-03	3117	Ccdc162	-2.65	1.5E-02
18786	Sorbs1	-2.41	2.0E-02	19633	Thpo	-2.65	4.7E-02
20053	Tnik	-2.41	1.9E-03	20743	Usp13	-2.66	2.6E-02
4713	Dlgap4	-2.42	3.4E-03	13178	Maob	-2.66	3.7E-02
4483	Dchs2	-2.42	3.1E-02	11544	Hdgfrp3	-2.68	3.2E-03
1759	Ankrd23	-2.42	4.0E-02	4425	Daam2	-2.68	3.0E-02
14148	Musk	-2.43	9.8E-03	7807	Gm16574	-2.69	1.2E-02
2607	Best1	-2.43	2.9E-02	20264	Trim72	-2.70	1.9E-02
14217	Mylpf	-2.43	2.3E-02	2884	Cacna1s	-2.70	2.5E-02
1672	Alpk3	-2.44	3.6E-04	19368	Tas1r1	-2.71	4.2E-02
2226	Atp2a1	-2.44	3.2E-02	14195	Myh3	-2.71	1.9E-02
1584	Akap6	-2.44	1.9E-02	11575	Herc3	-2.71	1.0E-02
1892	Apobec2	-2.45	4.6E-02	13870	Mpp3	-2.71	3.8E-02
11644	Hist1h2be	-2.46	3.2E-02	21280	Zdhhc14	-2.72	1.8E-02
2802	C1qtnf3	-2.46	3.1E-02	18787	Sorbs2	-2.72	7.4E-03
570	4930429F24Rik	-2.47	4.6E-02	12172	Ip6k3	-2.73	2.9E-02
15487	Pgam2	-2.48	3.9E-02	18127	Shroom3	-2.74	2.0E-02

15757	Plekha6	-2.74	4.9E-02	17208	RP23-423B21.6	-3.07	1.0E-02
3104	Ccdc148	-2.75	2.1E-02	2955	Capn11	-3.08	1.6E-02
14202	Myl1	-2.76	1.8E-02	11201	Gpd1	-3.10	4.2E-03
14960	Ogn	-2.76	1.4E-02	16146	Prkaa2	-3.10	3.1E-03
14350	Nav2	-2.77	7.6E-03	15149	Palmd	-3.11	1.3E-02
16792	Rcan2	-2.78	1.6E-02	15954	Porcn	-3.11	3.5E-05
11871	Hspb3	-2.78	2.5E-02	13771	Mlip	-3.11	1.2E-02
19446	Tcap	-2.79	3.4E-02	15747	Pld5	-3.14	2.5E-02
20065	Tnni1	-2.80	7.2E-03	1397	Adcy8	-3.14	2.2E-02
4016	Cox8b	-2.80	1.2E-02	14260	Myzap	-3.15	1.2E-02
14302	Nacad	-2.80	8.0E-03	507	4632404M16Rik	-3.16	5.2E-03
1208	Ablim3	-2.81	1.5E-02	18938	Sptb	-3.17	1.0E-02
12410	Kcnj11	-2.81	4.4E-03	18227	Slc16a8	-3.19	2.2E-02
2384	B3galt2	-2.82	2.8E-02	19455	Tceal7	-3.19	5.8E-03
12594	Klhl30	-2.82	1.1E-02	20206	Trdn	-3.20	3.7E-03
4429	Dact1	-2.82	4.6E-02	2968	Caps2	-3.22	2.2E-02
5923	Fgfbp1	-2.83	3.9E-02	2608	Best3	-3.27	5.8E-03
4569	Ddx60	-2.83	2.7E-02	7911	Gm17224	-3.31	1.5E-02
1210	Abra	-2.86	3.9E-02	2091	Art5	-3.31	3.0E-04
16429	Ptpn5	-2.86	4.0E-02	10486	Gm5532	-3.32	4.2E-03
6020	Fndc9	-2.87	4.6E-02	19252	Syn2	-3.32	8.4E-03
4170	Csrp3	-2.87	1.3E-02	3807	Cmbl	-3.34	9.6E-03
3712	Ckmt2	-2.88	4.6E-02	15671	Pkhd1	-3.34	3.9E-03
16580	Rab44	-2.88	5.0E-02	2231	Atp2b3	-3.35	1.3E-02
15356	Pde1b	-2.90	3.5E-02	10098	Gm44220	-3.39	1.4E-02
1386	Adck3	-2.93	2.8E-03	9674	Gm42837	-3.40	1.4E-02
5637	Fam189a1	-2.94	5.3E-03	15758	Plekha7	-3.43	2.0E-03
20312	Trp63	-2.96	3.4E-02	1165	Abcc9	-3.47	3.3E-03
5728	Fam78a	-2.97	1.7E-02	15169	Pappa2	-3.49	1.1E-03
16176	Prkg1	-2.97	1.0E-02	1363	Adamts20	-3.50	9.9E-03
13294	Mb	-2.97	2.1E-02	2923	Calr4	-3.50	6.4E-03
12698	Lamc3	-2.97	2.8E-02	141	1700024P16Rik	-3.52	2.8E-03
19369	Tas1r3	-2.98	8.0E-04	18942	Sptbn5	-3.62	1.6E-03
1294	Acsl6	-2.98	1.8E-03	8761	Gm2694	-3.63	5.0E-03
4453	Dbh	-3.00	1.0E-02	710	4933403O08Rik	-3.64	4.2E-03
14938	Obscn	-3.00	1.0E-02	3805	Cmah	-3.68	1.6E-04
7388	Gm14635	-3.00	1.5E-02	15095	P2ry14	-3.72	5.0E-03
1207	Ablim2	-3.02	1.2E-02	14378	Nckap1l	-3.76	2.8E-03
19729	Tm6sf1	-3.03	5.2E-03	20316	Trpc3	-3.96	2.9E-03
6136	Fxyd1	-3.04	8.2E-03	17669	Ryr3	-3.96	1.3E-03
1799	Ano5	-3.04	2.0E-03	14206	Myl2	-4.08	2.0E-03
19453	Tceal5	-3.04	1.6E-03	2219	Atp1a2	-4.10	6.8E-05
329	2310015K22Rik	-3.04	2.9E-02	3937	Colec10	-4.15	7.6E-04
2089	Art1	-3.04	3.0E-03	16472	Pvalb	-4.41	4.4E-04
12697	Lamc2	-3.05	6.6E-03				
1100	A930030B08Rik	-3.06	3.2E-02				

Supplementary Table 2. C3 (Motifs) MSigDB enriched genesets by GSEA analysis. Positive normalized enrichment score (NES) correspond to the genes overexpressed in KO vs WT MPC's and negative NES correspond to the genes overexpressed in WT vs KO MPC's. Abbreviations: Enrichment score (ES), false discovery rate (FDR), familywise-error rate (FWER). **Note**: RSRFC4: alternative name of MEF2A.

GENESET	ES	NES	FDR	FWER	Rank_at_ES	Rank_score_at_ES
SGCGSSAAA_V$E2F1DP2_01	0.650	2.742	0	0	2703	0.370
V$E2F1DP1_01	0.590	2.618	0	0	2508	0.398
V$E2F4DP2_01	0.590	2.600	0	0	2508	0.398
V$E2F1_Q6	0.590	2.589	0	0	2733	0.367
V$E2F_02	0.590	2.588	0	0	2508	0.398
V$E2F1DP2_01	0.590	2.572	0	0	2508	0.398
V$E2F4DP1_01	0.588	2.556	0	0	2508	0.398
V$E2F_Q6	0.572	2.500	0	0	2380	0.417
V$E2F_Q4	0.570	2.489	0	0	2380	0.417
V$E2F1DP1RB_01	0.566	2.476	0	0	2380	0.417
V$E2F_Q4_01	0.544	2.409	0	0	1589	0.559
V$E2F1_Q3	0.542	2.391	0	0	2380	0.417
V$E2F_Q3_01	0.541	2.386	0	0	2662	0.376
V$E2F1_Q4_01	0.543	2.386	0	0	2662	0.376
V$E2F_03	0.527	2.320	0	0	1668	0.542
V$E2F_Q6_01	0.531	2.319	0	0	2662	0.376
V$E2F_Q3	0.527	2.279	0	0	1817	0.511
V$E2F1_Q6_01	0.518	2.267	0	0	2662	0.376
V$E2F_01	0.608	2.164	0	0	2371	0.419
KTGGYRSGAA_UNKNOWN	0.560	2.140	0	0	1152	0.687
V$E2F1_Q4	0.451	2.007	0.0001	0.002	3035	0.330
V$E2F1_Q3_01	0.386	1.690	0.0073	0.168	2408	0.413
GCGSCMNTTT_UNKNOWN	0.449	1.651	0.0116	0.264	3412	0.288
V$MYCMAX_B	0.363	1.607	0.0192	0.415	3040	0.329
V$NFY_01	0.369	1.605	0.0188	0.421	2518	0.396
V$ZF5_01	0.355	1.565	0.029	0.588	4039	0.225
CTAWWWATA_V$RSRFC4_Q2	-0.500	-2.366	0	0	13004	-0.430
V$MEF2_02	-0.523	-2.348	0	0	13055	-0.437
V$MYOD_Q6	-0.517	-2.325	0	0	12550	-0.370
V$RSRFC4_Q2	-0.515	-2.285	0	0	13055	-0.437
V$RSRFC4_01	-0.500	-2.236	0	0	13312	-0.480
V$MEF2_Q6_01	-0.478	-2.177	0	0	13005	-0.430

V$HMEF2_Q6	-0.503	-2.094	0.0002	0.001	12739	-0.396
V$TBP_01	-0.463	-2.082	0.0001	0.001	12936	-0.420
V$AMEF2_Q6	-0.455	-2.055	0.0001	0.001	12333	-0.344
V$E2A_Q2	-0.451	-2.025	0.0001	0.001	13045	-0.435
V$E12_Q6	-0.437	-1.984	0.0002	0.002	13072	-0.439
YTATTTTNR_V$MEF2_02	-0.399	-1.979	0.0002	0.002	13287	-0.475
V$MEF2_01	-0.475	-1.960	0.0002	0.002	12932	-0.420
V$MEF2_03	-0.432	-1.943	0.0002	0.002	13055	-0.437
TAAWWATAG_V$RSRFC 4_Q2	-0.438	-1.888	0.0007	0.009	12537	-0.368
CAGCTG_V$AP4_Q5	-0.360	-1.878	0.0007	0.01	12932	-0.420
V$MMEF2_Q6	-0.407	-1.837	0.0015	0.021	13465	-0.513
V$MYOD_01	-0.394	-1.807	0.0026	0.039	13117	-0.446
V$AP4_Q6_01	-0.399	-1.803	0.0027	0.041	13474	-0.515
V$MYOD_Q6_01	-0.399	-1.798	0.0027	0.043	13112	-0.445

APPENDIX 2

During the realization of this PhD I have had the opportunity to participate in another works related to the epigenetic state of normal and cancer cells.

Peer-reviewed publications:

- Fernández-Veledo S, Ejarque M, Ceperuelo-Mallafré V, Serena C Pachon G, **Núñez-Álvarez Y**, Terron-Puig M, Calvo E, Núñez-Roa C, Oliva-Olivera W, Tinahones FJ, Peinado MA, Vendrell J. (2017). Survivin, a key player in cancer progression, increases in obesity and protects adipose tissue stem cells from apoptosis. Cell Death and Disease, 8(5), e2802. http://doi.org/10.1038/cddis.2017.209

In this work I was responsible for the methylation analysis.

- Huertas-Martínez J, Rello-Varona S, Herrero-Martín D, Barrau I, García-Monclús S, Sáinz-Jaspeado M, Lagares-Tena L, **Núñez-Álvarez Y**, Mateo-Lozano S, Mora J, Roma J, Toran N, Moran S, López-Alemany R, Gallego S, Esteller M, Peinado MA, Del Muro XG, Tirado OM. (2014) Caveolin-1 is down-regulated in alveolar rhabdomyosarcomas and negatively regulates tumor growth. Oncotarget, 5(20), 9744-55. PMID: 25313138.

In this work I performed the CpGi methylation analysis of Caveolin-1 gene.

- Abraham, J., **Nuñez-Álvarez, Y.**, Hettmer, S., Carrió, E., Chen, H. I. H., Nishijo, K., Huang ET, Prajapati SI, Walker RL, Davis S, Rebeles J, Wiebush H, McCleish AT, Hampton ST, Bjornson CR, Brack AS, Wagers AJ, Rando TA, Capecchi MR, Marini FC, Ehler BR, Zarzabal LA, Goros MW, Michalek JE, Meltzer PS, Langenau DM, LeGallo RD, Mansoor A, Chen Y, Suelves M, Rubin BP, Keller, C. (2014). Lineage of origin in rhabdomyosarcoma informs pharmacological response. Genes and Development, 28(14), 1578–1591. http://doi.org/10.1101/gad.238733.114

In this work I was responsible for ChIP analysis of murine and human rhabdomyosarcoma cell lines.

- Gallardo, E., Ankala, A., **Núñez-Álvarez, Y.**, Hegde, M., Diaz-Manera, J., Luna, N. De, Pastoret A, Suelves M, Illa, I. (2014). Genetic and Epigenetic Determinants of Low Dysferlin Expression in Monocytes. Human Mutation, 35(8), 990–997. http://doi.org/10.1002/humu.22591

In this work I was responsible for the methylation analysis of promoter regions of Dysferlin gene.

Review article:

- Suelves, M., Carrió, E., **Núñez-Álvarez, Y.**, & Peinado, M. A. (2016). DNA methylation dynamics in cellular commitment and differentiation. *Briefings in Functional Genomics*, *15*(June), elw017. http://doi.org/10.1093/bfgp/elw017

In this work I was responsible for the section dedicated to methylation in diseases.

In preparation:

- Ejarque M, Victoria Ceperuelo-Mallafré V, Serena C, Duran X, Millan-Scheiding M, **Núñez-Álvarez Y**, Núñez-Roa C, Gama P, Garcia-Roves PM, Peinado MA, Gimble JM, Zorzano A, Vendrell J, Fernández-Veledo S. Obesity-driven methylation signature of adipose-derived stem cells determines mitochondrial phenotype in human adipose tissue. Expected submission: July 2017.

In this work I was responsible for DNA methylation analyses.

- **Núñez-Álvarez Y**, Muñoz M, Custodio J, Mallona I, Peinado MA. HDAC9 downregulation is an early event in colorectal adenomas and tumor progression. Submission expected: 2018.

In this work I participate in the genesis of the project, the TCGA analysis of HDAC members in COAD dataset and the design and execution of most part of experiments.